

博士論文 (要約)

Doctoral Dissertation

Studies on Unprecedented Catalytic Selective Molecular
Transformations through Rational Construction of
Systems Specific to Solid Catalysts

(固体触媒に特有な系の合理的構築による
新奇選択的分子変換に関する研究)

谷田部 孝文

Takafumi Yatabe

東京大学大学院工学系研究科応用化学専攻

Department of Applied Chemistry, School of Engineering

The University of Tokyo

2019

Contents

Chapter I General Introduction

1.1. Background	
1.1.1. Catalyst	2
1.1.2. Catalyst Classification	4
1.1.3. Catalyst Design and Preparation	6
1.1.3.1. Homogeneous Catalysts	6
1.1.3.2. Heterogeneous Catalysts (Solid Catalysts)	9
1.1.3.2.1. Support	9
1.1.3.2.2. Immobilization of Active Species	10
1.1.3.2.3. Nanoparticles	15
1.1.3.2.4. Bimetallic Nanoparticles	17
1.1.4. Systems Specific to Solid Catalysts	22
1.1.4.1. Chemical and Physical Properties of Bulk and Surface	22
1.1.4.2. Function-integrated Catalysts	26
1.1.4.3. Nanoparticles/Nanoclusters	29
1.1.4.4. Bimetallic Catalysts	34
1.1.5. Liquid-phase Organic Synthesis via Heterogeneous Catalysis	38
1.2. Purpose and Concept of This Dissertation	45
1.3. References	49

Chapter II Transition-Metal-Free Selective Formal Hydroacylation of Terminal Alkynes Catalyzed by Layered Double Hydroxide

2.1. Introduction	60
2.2. Experimental	64
2.2.1. Instruments and Reagents	64
2.2.2. Preparation of Catalysts	65
2.2.3. Reactions and Synthesis	66

2.2.4. Spectral Data of Products	68
2.3. Results and Discussion	77
2.3.1. Effect of Catalysts and Optimization of Reaction Conditions	77
2.3.2. Interaction between Alkynes and Layered Double Hydroxide	81
2.3.3. Heterogeneous Catalysis and Catalyst Reuse	87
2.3.4. Substrate Scope	91
2.3.5. Mechanistic Studies	94
2.4. Summary	100
2.5. References	101

Chapter III Selective Flavonoid Synthesis Enabled by Function-Integrated Solid Catalysts

3.1. Introduction of Flavonoids	106
---------------------------------	-----

3-1 One-Pot Selective Flavone Synthesis Catalyzed by Gold Nanoparticles Supported on Layered Double Hydroxide

3-1.1. Introduction	110
3-1.2. Experimental	114
3-1.2.1. Instruments and Reagents	114
3-1.2.2. Preparation of Catalysts	115
3-1.2.3. Reactions and Synthesis	116
3-1.2.4. Spectral Data of Products	118
3-1.3. Results and Discussion	123
3-1.3.1. Effect of Catalysts	123
3-1.3.2. Heterogeneous Catalysis and Catalyst Reuse	125
3-1.3.3. Substrate Scope	130
3-1.3.4. Mechanistic Studies	133
3-1.4. Summary	141

3-2 Selective Aurone Synthesis Catalyzed by Palladium-on-Gold Bimetallic Nanoparticles Supported on Ceria

3-2.1. Introduction	142
3-2.2. Experimental	146
3-2.2.1. Instruments and Reagents	147
3-2.2.2. Preparation of Catalysts	147
3-2.2.3. Reactions and Synthesis	149
3-2.2.4. Spectral Data of Products	156
3-2.3. Results and Discussion	161
3-2.3.1. Catalyst Characterization	161
3-2.3.2. Catalyst Design and Optimization of Reaction Conditions	165
3-2.3.3. Heterogeneous Catalysis and Catalyst Reuse	174
3-2.3.4. Substrate Scope	179
3-2.3.5. Mechanistic Studies	182
3-2.4. Summary	192
3.5. References	193

Chapter IV Selective Transformations of Secondary/Tertiary Amines Enabled by Supported Nanoparticle Catalysts

4.1. Introduction of Amine Transformations	200
---	------------

4-1 Selective Acceptorless Dehydrogenative Aromatization of Cyclic Secondary Amines Catalyzed by Supported Palladium Nanoparticles

4-1.1. Introduction	210
4-1.2. Experimental	213
4-1.2.1. Instruments and Reagents	213
4-1.2.2. Preparation of Catalysts	214
4-1.2.3. Reactions and Synthesis	215
4-1.2.4. Spectral Data of Products	217
4-1.3. Results and Discussion	219

4-1.3.1. Effect of Catalysts and Optimization of Reaction Conditions	219
4-1.3.2. Heterogeneous Catalysis and Catalyst Reuse	227
4-1.3.3. Substrate Scope	230
4-1.3.4. Mechanistic Studies	232
4-1.4. Summary	236

4-2 Selective Formal α -Oxygenation of Secondary/Tertiary Amines Catalyzed by Supported Gold Nanoparticles

4-2.1. Introduction	238
4-2.2. Experimental	241
4-2.2.1. Instruments and Reagents	241
4-2.2.2. Preparation of Catalysts	242
4-2.2.3. Reactions and Synthesis	243
4-2.2.4. Spectral Data of Products	244
4-2.3. Results and Discussion	250
4-2.3.1. Effect of Catalysts	250
4-2.3.2. Heterogeneous Catalysis and Catalyst Reuse	254
4-2.3.3. Substrate Scope	257
4-2.3.4. Mechanistic Studies	262
4-2.4. Summary	269

4-3 Unusual Regioselective α -Alkynylation of Tertiary Amines Afforded by a Hybrid Catalyst Comprising Gold Nanoparticles and a Zinc Salt

4-3.1. Introduction	270
4-3.2. Experimental	274
4-3.2.1. Instruments and Reagents	274
4-3.2.2. Preparation of Catalysts	275
4-3.2.3. Reactions and Synthesis	276
4-3.2.4. Spectral Data of Products	278
4-3.3. Results and Discussion	286
4-3.3.1. Effect of Catalysts and Optimization of Reaction Conditions	286
4-3.3.2. Heterogeneous Catalysis and Catalyst Reuse	293

4-3.3.3. Substrate Scope	297
4-3.3.4. Mechanistic Studies	301
4-3.4. Summary	304
4.5. References	305
<u>Chapter V General Conclusions and Future Perspectives</u>	317
<u>List of Publications</u>	333
<u>Acknowledgement</u>	337

Chapter I

General Introduction

1.1. Background

1.1.1. Catalyst

A “catalyst” is a material most frequently used for controlling chemical reactions, and “catalysis”, the typical activity of catalysts, was defined in 1894 as “the acceleration of a slow chemical process by the presence of a foreign material” by Wilhelm Ostwald,^[1] the 1909 Nobel laureate who received the award “in recognition for his work on catalysis and for his investigations into the fundamental principles governing chemical equilibria and rates of reaction.”^[1b] The above definition of catalysis implies that catalysts remain unchanged after a chemical reaction; however, no catalyst remains unchanged during a chemical reaction and catalyst deactivation occurs in majority of the cases.^[2] Currently, it is widely known that catalysts interact with reactant molecules to reduce the activation energies of chemical reactions, resulting in an acceleration of the said reactions.^[1c]

The fundamental functions that should be performed by the catalysts include i) an activity that promotes chemical reactions as per the catalyst definition; ii) a selectivity that enables users to access only the desired products; and iii) a durability to continuously produce products.^[2b,d,3] The sophisticated control of these catalytic functions has afforded a variety of benefits, including the development of novel chemical reactions that have changed our world, such as the Haber–Bosch process, the preservation of earth’s resources, and means to achieve environmental purification.^[4] Catalysts also play a central role in synthetic chemistry as key components of the processes that afford the production of most of the surrounding materials, including medicines, pesticides, plastics, fibers, and dyes.^[4] In short, without catalysts, our lives would be vastly different.

In addition, from the viewpoint of green and sustainable chemistry,^[5] catalytic reactions should be used for all the synthetic processes because, in contrast to stoichiometric reagents, ideal catalysts are hardly changed and consumed during the said processes. As for the atom economy, which is a central parameter of green chemistry indexes defined as the ratio of the desired products’ molecular weight to the total molecular weight of all the chemicals used in the reaction, except for the solvent and work-up reagents, the use of catalysts ensures high atom economy; for example, when the Dess–Martin reagent is used for alcohol oxidation (Figure 1-1), the atom

economy is 22%; if the same reaction is catalytically performed using molecular oxygen as the sole oxidant, the atom economy reaches 87%. In general, atom economy values are quite low in the production of fine chemicals and pharmaceuticals because stoichiometric redox reagents are frequently used to perform the relevant processes. In other words, the number of catalytic reactions that can be used in these fields is currently unsatisfactory, and the development of novel efficient catalytic systems that are applicable to precise organic syntheses remains a highly desirable research goal. By considering the issues that have recently become social concerns, such as environmental preservation, the importance of catalysts will only increase further in the future.

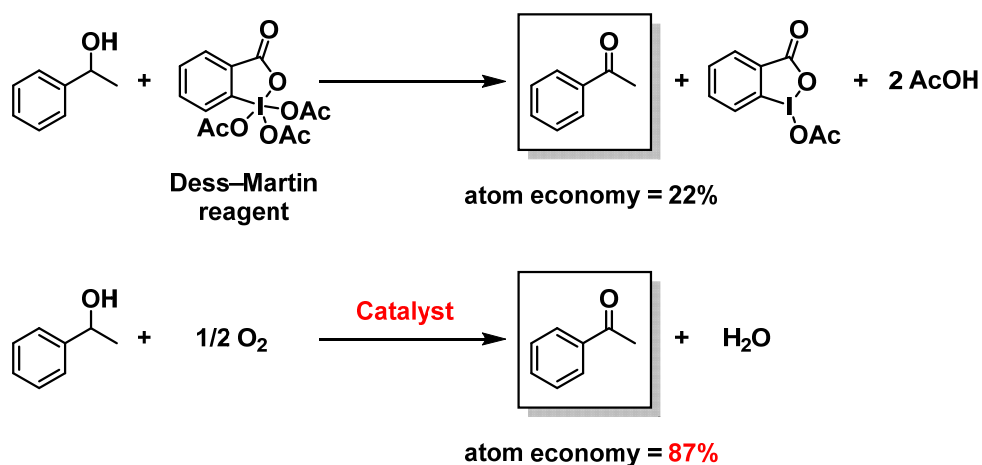


Figure 1-1. Comparison between the atom economies associated with a non-catalytic approach and a catalytic approach to alcohol oxidation.

1.1.2. Catalyst Classification

Many methods exist to classify catalysts, which depend on the characters being focused on; for instance, when concentrating on the identity of the main active species, catalysts can be classified into metal catalysts, metal oxides, molecular catalysts, and biocatalysts. In this section, however, I focus on the simplest and most widely used catalyst classification: homogeneous *versus* heterogeneous catalysts.^[3,6a,7a]

In a homogeneous catalytic reaction, catalysts and substrates are present in the same phase. In general, the activity and selectivity of homogeneous catalysts are higher than those of their heterogeneous counterparts, thanks to the homogeneous catalysts' easy access to substrates, high concentration of active species, and presence of uniform molecular active sites. As a consequence, most precise organic transformations are performed using homogeneous catalysts. The homogeneity of the reaction medium, furthermore, makes it comparatively easy to elucidate the reaction mechanisms using a number of analytical approaches, such as NMR spectrometry, Fourier-transform IR spectrometry, UV-Vis spectrometry, electron spin resonance, electrospray ionization mass spectrometry, and X-ray absorption fine structure spectrometry. On the flip side, homogeneous catalysts are difficult to separate from the reaction mixtures, retrieve, and reuse, leading them to be used only once, with a heavy environmental burden.

In heterogeneous catalytic reactions, catalysts and substrates are present in different phases; for instance, a catalytic reaction may take place between substrates dissolved in an organic solvent and insoluble solid materials. In the bulk chemical industry, heterogeneous catalysts, in particular solid catalysts for gas-phase reactions, are the ones used most widely, owing to their good stability in extreme reaction conditions, like high temperatures and high pressures, simple preparation procedures, and easy application to flow reactors. In the case of liquid-phase reactions, furthermore, heterogeneous catalysts can be easily separated from the reaction mixture and retrieved just by way of filtration; additionally, their reuse is also possible, making the choice of heterogeneous catalysts an environmentally-friendly one. However, the development of highly active and selective heterogeneous catalysts is comparatively difficult to realize, and so is the elucidation of the mechanisms of heterogeneous catalytic reactions, because these reactions occur only on the surface of the solid catalysts. As to the characterization techniques applicable to heterogeneous catalysts,^[6b] besides the

conventional ones already mentioned for the investigation of homogeneous catalysts, various advanced methods for more detailed and/or operando observation have been reported, including dynamic nuclear polarization surface-enhanced NMR spectroscopy (DNP SENS),^[6c] high-pressure scanning tunneling microscopy (HP-STM), and environmental transmission electron microscopy (ETEM)^[6d]. These techniques will contribute to solving the above-described difficulties associated with elucidating the mechanisms of heterogeneous catalysis.

Please note that in Table 1-1 I have synthetically reported the key characteristics of homogeneous *versus* heterogeneous catalysts. Be aware that these are just general trends. Some notable examples of these two classes of catalysts will be discussed throughout this dissertation.

Table 1-1. Comparison between the general characteristics of homogeneous *versus* heterogeneous catalysts.

	Homogeneous Catalyst	Heterogeneous Catalyst
Form	Molecule	Bulk
Reaction Phase	Liquid	Gas/Solid, Liquid/Solid
Mechanism Elucidation	Comparatively Easy	Difficult
Activity	High	Low
Selectivity	High	Low
Durability	Low	High
Separation	Difficult	Easy
Reuse	Difficult	Easy

1.1.3. Catalyst Design and Preparation

As mentioned in section 1.1.2., the characteristics of heterogeneous catalysts are quite different from those of their homogeneous counterparts. In this section, I will discuss how catalysts belonging to either category are designed and prepared.

1.1.3.1. Homogeneous Catalysts

Homogeneous catalysts can be subdivided into two classes: metal catalysts and organic catalysts.^[7a–d] Metal catalysts, particularly organometallic catalysts, have been actively studied since World War II, and they have had a big impact on organic chemistry and society at large; in fact, four Nobel Prizes in chemistry have been awarded for advances made in the field of metal-catalyzed reactions, including the development of Ziegler–Natta polymerizations,^[7e,f] asymmetric catalysis by Noyori, Knowles, and Sharpless,^[7g–i] olefin metathesis by Grubbs, Schrock, and Chauvin,^[7j–l] and cross-couplings by Suzuki, Negishi, and Heck.^[7m–q] By contrast, organic catalysts (organocatalysts) have attracted remarkable and exponentially growing attention only since the beginning of the 21st century, although their existence and potential were already known in the 1970s.^[7c,r]

Organometallic catalysts are generally composed of active metal species and ligands coordinating the metal center, thus forming organometallic complexes. The choice of metal species and the design of ligands *via* organic synthesis enable us to prepare structurally diverse organometallic catalysts and tune their electronic and/or steric properties precisely in accordance with, for instance, the 18-electron rule, the crystal field theory, and the ligand field theory (Figure 1-2).^[7a,b] Organometallic catalysts have played a pivotal role in the development of novel organic reactions, aside from those already mentioned introduced by Nobel laureates, including hydrofunctionalizations, carbonylations, and C–H functionalizations.^[7a,b] Recently, the computational design of catalysts based on the organometallic structure has also been attempted.^[7s]

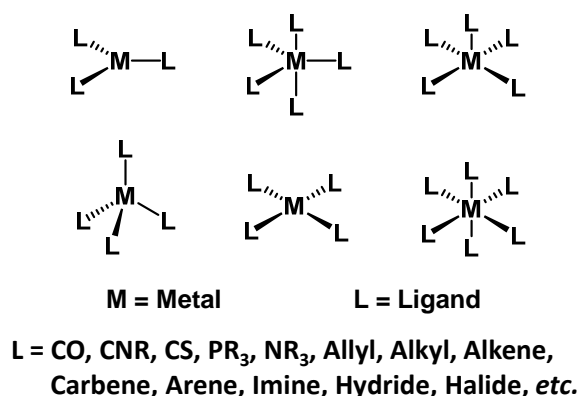


Figure 1-2. Generic structures of organometallic catalysts.

On the other hand, organic catalysts comprise no metallic species, although they too can be fine-tuned by organic synthetic methods as it is the case with the ligands of organometallic catalysts. As with the examples of proline and MacMillan's catalyst,^[7] aminocatalysts comprise a major class of organocatalysts. Various activation modes *via* enamines or iminium cations formed by condensation of aminocatalysts and carbonyl compounds are known, which afford diverse regioselective and/or stereoselective functionalizations (Figure 1-3).^[7c] Besides aminocatalysts, various other types of organocatalysts have been studied in depth, including asymmetric phase-transfer catalysts^[7u] and chiral Brønsted acid catalysts.^[7v,w]

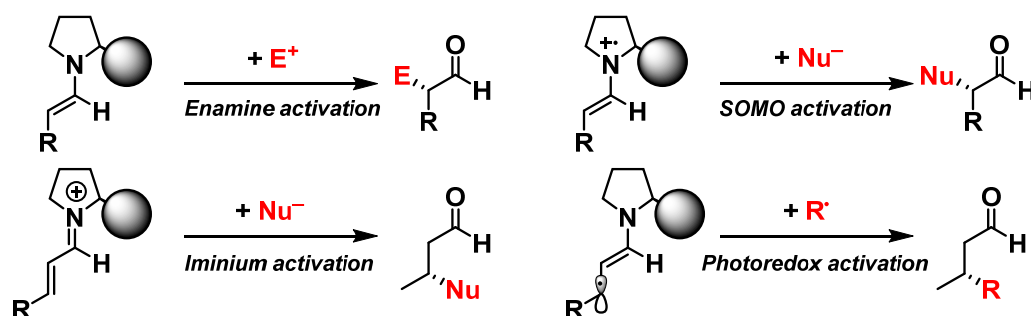


Figure 1-3. Various activation modes using aminocatalysts.

Recently, by utilizing combinations of metal catalysts and organocatalysts, different types of novel multicatalytic reactions have been developed.^[7c,d] Evidence

suggests, therefore, that many more homogeneous catalysis-based reactions are likely to be developed in the future; however, the chemistry of homogeneous catalysts aimed at organic synthesis appears to be gradually reaching maturity.

1.1.3.2. Heterogeneous Catalysts (Solid Catalysts)

In general, a heterogeneous catalyst consists of three components: i) a main active species that promotes a target reaction, ii) a promoter of the main catalytic activity, and iii) a support for dispersing and stabilizing active species and promoter.^[3a] In addition to them, it is important to see iv) a combined structure of the three parts. In this section, I will outline the approaches to designing and assembling the aforementioned components by introducing relevant preparation methods, including the preparation of nanoparticles as the typical main active species, and bimetallic nanoparticles as examples of promoters and structures.

1.1.3.2.1. Support

As supports, conventional metal oxides, such as SiO₂, Al₂O₃, SiO₂–Al₂O₃, zeolite, MgO, TiO₂, CeO₂, and ZnO, are usually used in both industrial processes and academic research,^[3a,4c] although other materials like polymers are also used.^[13,18] Herein, I describe the main methods for the preparation of inorganic materials like metal oxides to be used as catalyst supports.^[3a]

Co-precipitation Method^[12]

The co-precipitation method is usually the approach of choice to prepare mixed hydroxide–oxides like a layered double hydroxide (LDH, refer to section 1.1.4.1.). By adding bases into the solution containing more than two kinds of metal cations in order to excess the ionic products of OH[−] and the metal cations, a homogeneous mixed metal hydroxide is made to precipitate from an oversaturated solution. Instead of the addition of the base to the metal cation solution, the evaporation of the solvent is also effective as a way to reach oversaturation conditions, although bases like NaHCO₃ and NaOH are frequently used for LDH preparation.

Sol-gel Process^[8a,b]

The sol-gel process is an approach to obtaining the desired solid material, for instance mesoporous silica and nanomaterials, *via* formation of a gel from a colloidal sol dispersed in a solution. For example, a kind of mesoporous silica, MCM-41, can be prepared by calcination of aluminosilicate gels in the presence of surfactants.^[8a] The

group of Mizuno and Yamaguchi utilized a kind of sol-gel process to produce nanomaterials; in particular, ultra-small Li–Mn spinel oxides were successfully obtained by heating amorphous Li–Mn oxides produced at room temperature using alcohols as both solvents and reductants.^[8b]

Solvothermal Synthesis^[8c,d]

Solvothermal synthesis is carried out to prepare various solid materials, including zeolites and metal-organic framework (MOF) structures. In this approach, a mixture of solids and liquids or solution is heated in a sealed vessel up to a temperature near or above the liquid's or solvent's boiling point, resulting in the one-step crystallization of the desired materials. When the solvent is water, this approach is dubbed hydrothermal synthesis, which has been widely used for a very long time.

1.1.3.2.2. Immobilization of Active Species

The choice of the procedures for immobilizing the active species on the support has a great influence on the system's various properties, including stability, dispersion, and formation. In this section, I will describe impregnation, deposition–precipitation, ion-exchange, equilibrium deposition, selective deposition, supported homogeneous catalysis (SHC), and surface organometallic chemistry (SOMC) as the most widely used procedures for generating supported metal species. Additionally, methods for supporting nanoparticles will also be presented, including photo-assisted deposition and sol-immobilization (for the approaches to the preparation of nanoparticles themselves, see section 1.1.3.2.3.).

Impregnation^[3a,9a]

The impregnation method is one of the simplest approaches to obtaining metal species immobilized on a solid support. After dispersing a support in the solution containing the active species, for instance metal salts, the solvent is completely evaporated, resulting in the formation of a metal catalyst immobilized on a solid support. The incipient wetness impregnation method, a type of impregnation, is also well-known; this approach exploits the phenomenon whereby a minimum amount of metal-containing solution flows into the pores of a support by capillarity. After stirring

and drying, a supported catalyst can thus be obtained. Although impregnation-based methods are easy to implement, some key characteristics of the catalysts they produce, for instance stability and dispersion, tend not to be satisfactory, because of the physical adsorption of the active species onto the supports and remaining unnecessary chemicals.

Deposition–Precipitation^[3a,9b–d]

The deposition–precipitation method consists in the dispersion of the active species on the support as a consequence of the active species' precipitation on the support surface triggered by a decrease in the species solubility brought about by chemical reactions. In most cases, the pH control to basic solution using, for example, urea, NH_4OH , NaOH , or Na_2CO_3 , affords a metal hydroxide catalyst immobilized on a solid support. In the group of Mizuno and Yamaguchi, the deposition–precipitation method has been frequently used, because it enables researchers to easily obtain metal hydroxides that are highly dispersed onto the support and possess contiguous sites characterized by Lewis acidity and Brønsted basicity, which render the system produced able to catalyze a variety of reactions (Figure 1-4). Additionally, this method is effective for generating precursors for small active nanoparticles on supports in the absence of stabilizers like ligands and polymers (refer to section 1.1.3.2.3.).

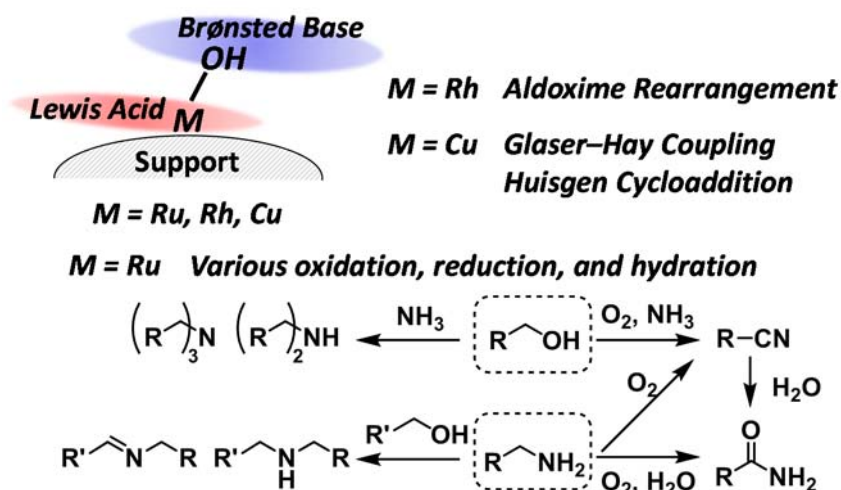


Figure 1-4. Catalysts composed of metal hydroxides dispersed on a support that are characterized by the contiguous presence of sites displaying Lewis acidity and Brønsted basicity that can be used to catalyze various molecular transformations.^[9c,d]

Ion exchange^[9e,3a]

The ion-exchange method consists in the immobilization of ionic active species in ion-exchange sites prepared on the surface of a support in advance by stirring the solution of active species and the prepared support. When this method is implemented, a homogeneous dispersion of the active species onto the surface of the support can be expected; after ion exchange, furthermore, the active species can be assumed to retain the structural features it displayed before method implementation, although the amount of metal centers ultimately present in the support is limited.

Equilibrium Deposition^[9f]

The equilibrium deposition method resembles impregnation up until the step whereby a solution of the active species and the support are mixed together; in equilibrium deposition, however, the final procedure for the removal of the solvent is not evaporation but filtration. Naturally, the amount of active species present on the support after performing equilibrium deposition is smaller than the amount obtained after impregnation. By the same token, the active species present on the support are comparatively stable, because the ones interacting only weakly with the support are removed alongside the solvent.

Selective Deposition^[9g]

In general, balancing the goal of producing a high level of dispersion of metal species on the support with having a large amount of these species on the said support is quite difficult. The selective deposition method has the potential to address this difficulty; in fact, a Pt-based species to a final proportion of ~20wt% was loaded on a support, while keeping the nanoparticle size below 2 nm. Achieving the following three goals is important for the successful implementation of this approach: i) precise control of the formula of the metal precursor in the solution before the deposition of the active species onto the support, generally using bases like NaOH; ii) keeping the suspension until reaching the equilibrium composition; and iii) aging the suspension at constant temperature before proceeding with the dehydration step and with the condensation of the active species on the support surface (Figure 1-5). The first goal mentioned above is similar to its counterpart in SHC and SOMC, although in the latter cases it is achieved

without the use of bases, as explained below. The main shortcomings of this method are that it is time-consuming and basically only applicable to noble metals.

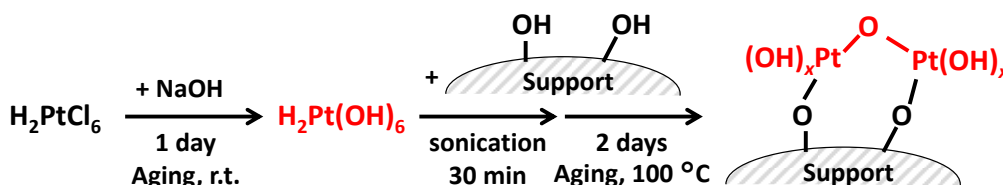


Figure 1-5. Selective deposition of a Pt-based species on a support. r.t.: room temperature.

Supported Homogeneous Catalysis (SHC)^[9h,18]

SHC consists in the deposition of metal species on a support *via* the use of ligand-grafted supports that coordinate homogeneous metal catalysts (Figure 1-6). This method is basically used for immobilizing well-established homogeneous catalysts onto a support in order to perform heterogeneously catalyzed reactions like epoxidations, cross-couplings, cyclopropanations, and hydroformylations. (for the details, see section 1.1.5.); however, the weak interaction between grafted ligands and metal complexes sometimes causes the active species to be leached from the support, which leads to homogeneous catalysis taking place alongside its heterogeneous counterpart and difficulty in the reuse of the catalyst.

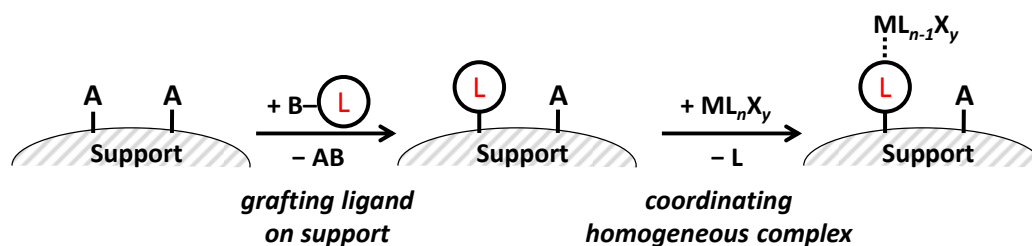


Figure 1-6. General procedure of the supported homogeneous catalysis.

Surface Organometallic Chemistry (SOMC)^[9h,i]

SOMC can be viewed as the combination of selective deposition and SHC (Figure 1-7). Instead of grafting ligands on the surface of the support, hydroxyl groups on the surface of an oxide support work as the ligand that coordinate the metal

complexes. The number of hydroxyl groups on the surface of the support can be controlled by performing a dehydration reaction under reduced pressure. The OH groups afford a comparatively strong bond with metal centers, which keeps the active species stably bound to the surface of the support during liquid-phase reactions. Moreover, heating of the oxide-supported catalyst under vacuum can result in the generation of a well-defined isolated metal catalyst on the surface. As mentioned above, SHC and SOMC are suitable approaches to stabilizing a molecular catalyst on the surface of a support without sintering; in other words, they are useful methods to prepare single-atom catalysts.

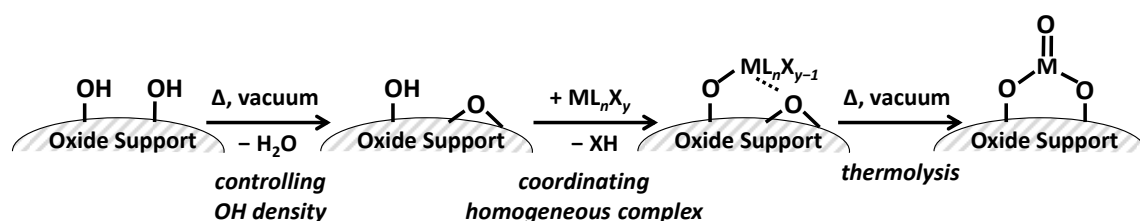


Figure 1-7. General procedure for surface organometallic chemistry.

Photo-assisted Deposition^[9j-m]

The photo-assisted deposition method consists in preparing and depositing onto a support nanoparticles from metal salt sources present in solution in a single step. Notably, this method can only be applied to photocatalytically active supports. In this case, UV light irradiation excites electrons in the support, which are used to reduce dissolved metal species that find themselves in contact with the support's surface to produce supported nanoparticles. For instance, in the case of a mesoporous silica support that comprises titanium centers in its structure, the titanium sites (and only them) exhibited a photocatalytic activity that, following UV irradiation, afforded the generation of localized O^- holes and Ti^{3+} reduction sites, which in turn assisted the formation of small nanoparticles and narrow distribution on the support (Figure 1-8).^[9m]

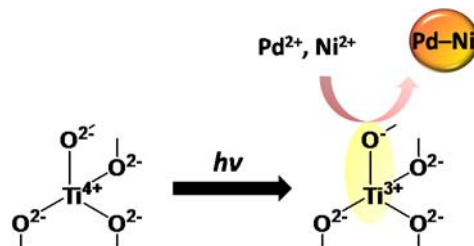


Figure 1-8. Preparation of Pd-Ni alloy nanoparticles by photo-assisted deposition.^[9m]

Sol-immobilization^[9n-p]

Sol-immobilization is a method to deposit nanoparticles protected by ligands or polymers, as sol being present, on an inorganic support (for the preparation of the sol, see section 1.1.3.2.3.). As with the other methods for immobilizing nanoparticles on a support, the types of sol stabilizers and supports utilized affect substantially the characteristics of the resulting catalysts. The simplified description of this method is as follows: a support is added into the solution of the sol nanoparticle prepared in advance, and the pH of the resulting mixture is adjusted to a value below the isoelectric point of the support, usually ~ 1 , so as to cause the formation of ionic bonds between the anionic sol and the protonated support. Notably, the stabilizers left in the heterogeneous catalyst thus prepared have an influence on the catalytic reactions; however, the removal of stabilizers present on the supports has been recently reported to be achievable not only calcination but also by washing the catalysts with hot water, through a method that was proven to provoke little change in either the nanoparticles' morphology or size.^[9p]

1.1.3.2.3. Nanoparticles

Metal nanoparticles have been the subject of much active research, with particular attention being dedicated to the unique characteristics they display with respect to the bulk metal as a consequence of the quantum size effect.^[10a] A large number of reports exist on catalysis by support-immobilized nanoparticles, and they will be discussed in section 1.1.4.3. In this section, I will focus on the main preparation methods for nanoparticles in solution or on supports.

Nanoparticle Preparation in Solution

When nanoparticles are prepared in solution, the use of stabilizers like ligands and polymers is necessary to block nanoparticle sintering. The first example of nanoparticle preparation in solution is said to be Michael Faraday's successful preparation of gold nanoparticles using citric acid as both reductant and ligand.^[10b,c] Now, based on organometallic chemistry, many studies have been published on nanoparticle stabilization by metallophilic ligands, such as phosphines and thiols, in the presence of reductants like citric acid and borohydrides.^[10d-h]

Nanoparticle stabilization with polymers is said to have been introduced by Nord and coworkers through the preparation of palladium and platinum nanoparticles using poly(vinyl alcohol) (PVA).^[10i] PVA and poly(*N*-vinyl-2-pyrrolidone) (PVP) are normally used as nanoparticle stabilizers thanks to their high water-solubility. In the presence of polymers, nanoparticles are assumed to be generated as follows (Figure 1-9):^[10a] after polymers coordinate metal cations to produce polymer–metal ion complexes, the addition of reductants affords the production of polymer–metal atom complexes. These complexes then accumulate toward the desired polymer–metal cluster complexes. Crucially, if the described reduction reaction were to precede the metal cation coordination by polymers, the size of the nanoparticles could not be controlled. Moreover, if alcohols are used as solvents instead of water, they can also be employed as the reductant. As a consequence of the simplicity of the preparation procedures, many kinds of relatively uniform and small nanoparticles have been successfully prepared.
[10j,k]

Although the nanoparticles thus prepared in solution can be used to catalyze reactions as they are, their stability is generally not high, so it is often better to deposit them on stable supports by sol-immobilization (refer to section 1.1.3.2.2.).

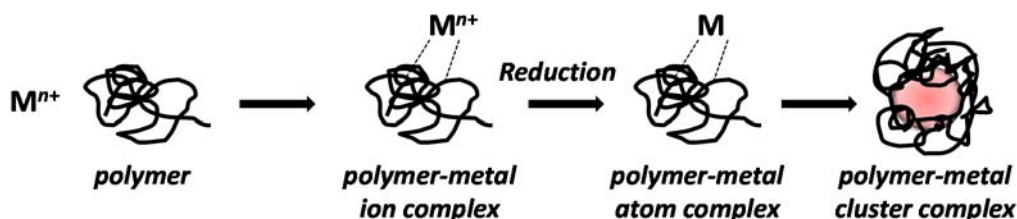


Figure 1-9. Preparation of nanoparticles *via* polymer stabilization.^[10a]

Nanoparticle Preparation on Supports

Supports on whose surfaces are dispersed metal centers can have the same role that stabilizers have in solution with respect to nanoparticles; in fact, metals immobilized on the surface of supports can be reduced to nanoparticles. The size of the nanoparticles thus obtained depends on the immobilization technique utilized, as described in section 1.1.3.2.2., and on the reduction approach implemented, such as borohydride reduction, H_2 reduction, and calcination. For example, in the case of Au nanoparticles, implementation of the deposition–precipitation method affords narrowly distributed

nanoparticles whose sizes are in the 2–3 nm range. On the other hand, impregnation of Au sources, typically hydrated HAuCl_4 , produces large nanoparticles (>10 nm).^[10l,m] One reason for the increase in the size of nanoparticles associated with the implementation of the impregnation method is the residue of Cl causing Au–Cl–Au linkages.^[10n-p] When impregnated Au species are washed with NH_3 , nanoparticles with sizes comparable with those obtained employing the deposition–precipitation method can be formed through the removal of Cl^- .^[10m-p] The support-immobilized high-valent Au species, mainly Au(III), can be easily reduced to produce Au nanoparticles by calcination even in the air. In general, the higher the temperature at which the calcination is performed, the larger the nanoparticles formed as a result. Notably, as the size of the nanoparticles increases, their catalytic activity decreases. As an example., in one report, Au/TiO₂ nanoparticles obtained following calcination performed at 200 °C displayed higher catalytic activity in CO oxidation than nanoparticles obtained following calcination at higher temperatures.^[10q]

1.1.3.2.4. Bimetallic Nanoparticles

Bimetallic systems have been investigated as a means to control catalytic activity, selectivity, and durability.^[4c] In particular, bimetallic nanoparticles have acquired much importance in recent years as tools to tune and develop novel unique nanoparticle-based catalytic reactions.^[10a] Bimetallic nanoparticles have diverse structures, including alloy, core-shell, and cluster-in-cluster (Figure 1-10).^[10a] Notably, alloys are further subdivided into solid-solution alloys, which can be either substitutional or interstitial, or intermetallic compounds (Figure 1-11).^[11a] The various bimetallic nanoparticle structures described above and drawn in Figures 1-10 and 1-11 can be accessed by implementing different preparation methods (see below).

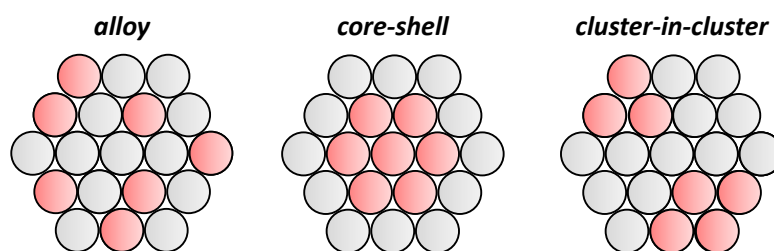


Figure 1-10. Different structures of bimetallic nanoparticles.

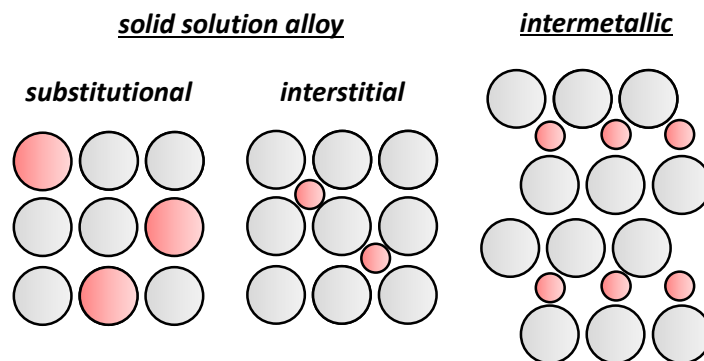


Figure 1-11. Possible structures of alloys.

Solid-solution Alloys

Solid-solution alloys are characterized by random atomic arrangements of the two metals they are composed of.^[10a,11a] In general, when the atomic sizes of the two metals are similar, substitutional solid-solution alloys can be obtained. When one metal is small enough to fit in the voids of the other metal's lattice, interstitial solid-solution alloys can be prepared.^[10a,11a] Basically, the contemporary reduction of two metals results in the formation of solid-solution alloys. For example, using ethylene glycol as both the solvent and the reductant, Cu–Pd and Ni–Pd alloy nanoparticles were obtained using PVP stabilizers.^[11b–e] Additionally, two metallic species supported on the same solid surface can be reduced to produce solid-solution alloys supported on the mentioned solid surface. For instance, Au- and Pd-based species were initially immobilized onto the same Al₂O₃ support, before undergoing H₂ reduction to afford Al₂O₃-supported Au–Pd alloy nanoparticles.^[11f]

Intermetallic Compounds^[11a, 11g]

Intermetallic compounds are characterized by highly ordered atomic arrangements of two metallic species possessing different characters. Not only does the ordered structure of these compounds help us elucidate the mechanism of the catalytic reaction taking place on their surfaces, but also presents unprecedented steric effects of bimetallic nanoparticles (refer to section 1.1.4.4.). Generally, in these compounds, one metal is the catalytically-active species, and it is a late-transition metal, like Fe, Co, Ni, Rh, Pd, or Pt. The other metal is a typical metal or half metal, such as Al, Zn, Ga, Ge, In, Sn, Sb, Pb, or Bi. When these metal combinations are desired, most

support-immobilized intermetallic compounds can be easily obtained *via* impregnation of two metallic species followed by reduction by H₂ gas.

Core-shell

In order to produce core-shell structures, two noble metals in combination, like Au and Pd, Pt and Pd, Au and Pt, or Pt and Rh, are simultaneously treated with an alcohol acting as both the solvent and the reductant in the presence of PVP used as a stabilizer. The result of this approach is the formation of core-shell structures like Au@Pd, Pt@Pd, Au@Pt, or Pt@Rh, instead of alloys. Remarkably, these same conditions can be applied to another type of metal combination to lead to the formation of Cu–Pd and Ni–Pd alloy nanoparticles.^[10a] This difference in behavior is due to preferential reduction of one metal by the other working as the electron mediator between the alcohol and the first metal, in a mechanism called, “geared step-cycled reduction”, (see as an example the Au–Pd case reported in Figure 1-12).^[10a]

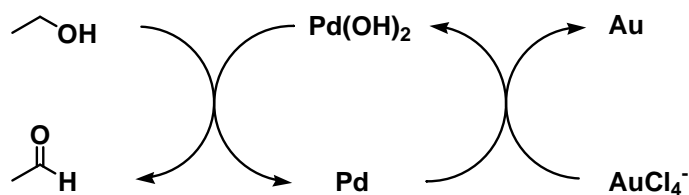


Figure 1-12. Geared step-cycled reduction of the Au–Pd noble metal combination.^[10a]

The two-step reduction of metal sources is another effective approach to forming core-shell structures using strong reductants like NaBH₄ and metal hydrides generated *in situ* from molecular hydrogen and noble metal nanoparticles.^[11h,i] An example, the Pd@Au core-shell nanoparticle formation *via* the two-step reduction is depicted in Figure 1-13.^[11h] In this case, Pd nanoparticles were prepared in advance using ethylene glycol as reductant and PVP as stabilizer; subsequently, the Pd nanoparticles were placed in a H₂ atmosphere, causing the formation of nanoparticles with Pd–H moieties present on their surfaces; to these modified Pd nanoparticles was then added an Au source, giving rise to Pd@Au core-shell nanoparticles protected by PVP. If the solvent, an alcohol, is used as the sole reductant, cluster-in-cluster structures tend to be prepared, as discussed below.

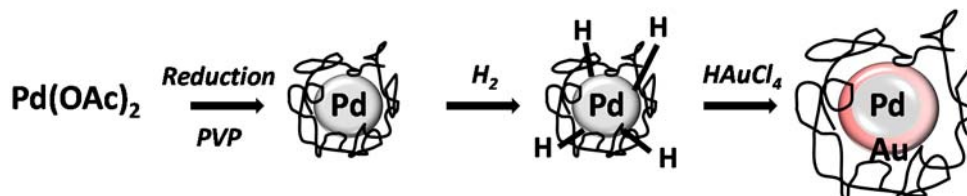


Figure 1-13. Pd@Au core-shell structure formation by two-step reduction.^[11h]

The redox-transmetalation system, which is a galvanic replacement reaction and can be viewed as a combination of the aforementioned two methods (geared step-cycled reduction and two-step reduction), is also an important approach to preparing core-shell nanoparticles.^[11j,k] As an example of this system, the formation of the Ni@Au core-shell structure is depicted in Figure 1-14.^[11k] As with the two-step reduction, one-metal nanoparticles need to be prepared beforehand in solution. For this purpose, the metals to be chosen must be easily oxidizable, like for example Ni. Subsequently, a source of the other metal, for example Au, is added into the solution containing the previously prepared nanoparticles, so that the redox reaction between the two metals can proceed and lead to an exchange of metals on the original nanoparticle surface. After repeating the redox reaction, core-shell-structured nanoparticles can be given. The step needed to produce the core-shell structures does not require any additional reductants, and self-nucleation of the latter metals can be inhibited.

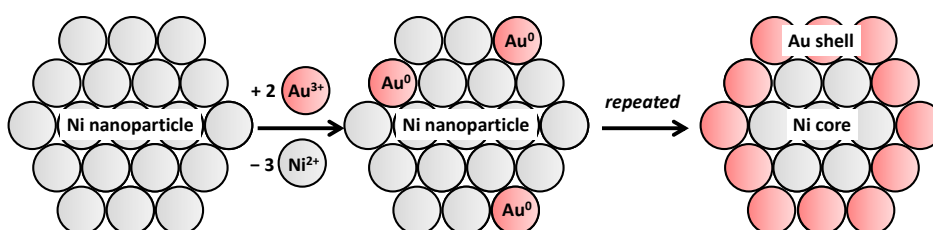


Figure 1-14. Ni@Au core-shell structure formation by the redox-transmetalation system.^[11k]

Although constructing core-shell nanoparticles is difficult to do after metal species have been immobilized on a solid support, Au@Pd core-shell nanoparticle structures can also be generated by calcinating at 200–400 °C Au–Pd precursors supported on

metal oxides like Al_2O_3 .^[11] In this approach, the reduction of Au species by calcination is assumed to involve Pd species reduction together to temporarily form Au–Pd alloys, followed by oxidation of the Pd species to Pd oxides that end up covering the nanoparticle. Notably, Au@Ni core-shell nanoparticle catalysts, which are utilized for industrial methyl methacrylate production *via* aerobic oxidative esterification, can also be prepared by the aforementioned calcination method.^[11m] As another approach to producing core-shell-like structures on solid supports, the surface modification of the galvanic replacement reaction of supported intermetallic nanoparticles with a third metal has been recently reported, although the surface of intermetallic compounds was not completely covered by the third metal.^[11n]

Cluster-in-cluster

As mentioned above, cluster-in-cluster structures can be formed using an alcohol as solvent and the sole reductant.^[10a] For instance, in the presence of PVP and an alcoholic solvent, the two-step reduction of Pd and Au was carried out in the mentioned order to produce Au–Pd cluster-in-cluster nanoparticles.^[11o] If the order of the reductions was reversed, a mixture of the relevant one-metal nanoparticles was obtained. This difference in behavior descends from the fact that the oxidative potential of the Au cation is higher than that of the Pd cation. Au(III) oxidizes a proportion of the Pd(0) nanoparticles formed in advance to generate Pd(II)-leaching species; these Pd(II) species get again deposited on the nanoparticles *via* alcohol-driven reduction, resulting in the formation of Au–Pd cluster-in-cluster structures.^[11o]

1.1.4. Systems Specific to Solid Catalysts

As mentioned in section 1.1.3., the design and preparation of solid catalysts is completely different from that of homogeneous catalysts. Accordingly, unique catalytic properties that are difficult or impossible for homogeneous catalysts to possess are assumed to be conferrable upon solid catalysts through their specific catalytic systems. In this section, I will describe four unique systems that are specific to solid catalysts: i) bulk/surface chemical and physical properties, ii) function-integrated catalysts, iii) nanoparticles/nanoclusters, and iv) bimetallic catalysts.

1.1.4.1. Chemical and Physical Properties of Bulk and Surface

Solid catalysts have a variety of chemical and physical properties that are specific to their bulk and surface elements and structures, such as acid-base properties, redox potential, metal valence, structure, surface area, porosity, and size.^[6b] Importantly, bulk properties have a tendency to affect surface properties and catalysis. As one of the most famous family of materials whose chemical and physical properties can be readily yet diversely tuned, LDHs will be described in detail in the following.

An LDH is composed of a cation layer, comprising a mixed metal hydroxide, and a hydrated anion layer, as can be evinced from Figure 1-15.^[12a-1] Hydrotalcite (HT, $[\text{Mg}_3\text{Al}(\text{OH})_8][(\text{CO}_3)_{1/2} \cdot 2\text{H}_2\text{O}]$) is known as the most common LDH, and LDHs are also referred to as hydrotalcite-like compounds. The mixed metal hydroxide layer of LDHs is positively charged because part of the Mg^{2+} ions in the brucite structure of $\text{Mg}(\text{OH})_2$ are replaced by Al^{3+} ions. Consequently, hydrated carbonate ions form an anion layer that compensates the overall positive charge of the metal hydroxide layer. The Mg^{2+} , Al^{3+} , and CO_3^{2-} ions can be replaced by various divalent and trivalent metal species and by anions of varying valence, respectively, and the divalent-to-trivalent metal ratio can be tuned; the general formula of LDHs is $[\text{M}^{\text{II}}_{1-x}\text{M}^{\text{III}}_x(\text{OH})_2]^{x+}(\text{Anion}^{n-})_{x/n} \cdot m\text{H}_2\text{O}$ ($x = 0.2\text{--}0.4$). The ionic radii of metallic species that can replace Mg^{2+} and Al^{3+} centers in the metal hydroxide layer are not significantly different from those of the hexacoordinate octahedral Mg^{2+} (0.72 Å) and Al^{3+} (0.54 Å) ions, and the typical metal species forming LDHs are summarized in Table 1-2. For instance, since Be^{2+} is too small and Ca^{2+} and Ba^{2+} are too large, they do not form LDHs, although the partial substitutions of Mg^{2+} and Al^{3+} centers by metal ions that are not listed in Table 1-2 have

been reported.^[12a,m,n] Moreover, various anionic species can be immobilized into the anionic layers, including Cl⁻, F⁻, NO₃⁻, organic anions, anionic metal complexes, and polyoxometalates.^[12h]

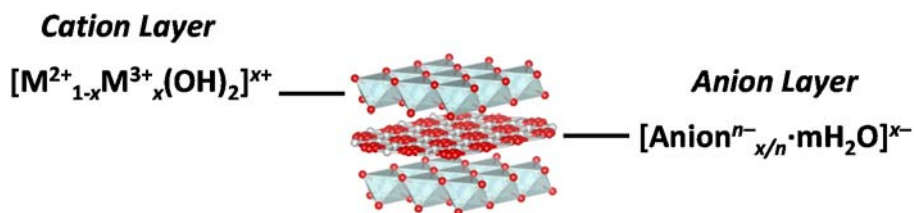


Figure 1-15. Structure of a layered double hydroxide.

Table 1-2. Typical metallic species forming layered double hydroxides and their ionic radii (Å).^[12a]

M ²⁺	Mg (0.65), Ni (0.72), Co (0.74), Zn (0.74), Fe (0.76), Mn (0.80)
M ³⁺	Al (0.50), Ni (0.62), Co (0.63), Fe (0.64), Mn (0.66), Cr (0.69)

The structural changes that LDHs undergo as a consequence of calcination are also widely known.^[12a,h] In HT, interlayered water is released at 100–250 °C, and hydroxyl groups of mixed metal hydroxides are released at 350–400 °C. Since carbonate ions are also desorbed at 420–470 °C, rock salt-type MgO is formed at around 450 °C. At temperatures higher than 700 °C, Mg–Al mixed metal oxides (MMO) of the rock salt and spinel types are formed, a phenomenon that can be exploited as a simple approach to MMO formation. Furthermore, in LDHs containing the easily oxidizable Co(II), Fe(II), Ni(II), Mn(II), *etc.*, an oxidation reaction simultaneously proceeds during heating, and the desorption temperature of hydroxyl groups decreases to 250–300 °C. In this case, a pure spinel mixed metal oxide can be obtained at about 300 °C.^[12o–q]

In addition, after calcinating LDHs at typically less than 600 °C to change the original LDH structure, if the material thus obtained is exposed to the anion and/or to OH⁻ ions present in the aqueous solution, the LDH structure is regenerated, in a process called “memory effect” (Figure 1-16).^[12f,j] Through this approach, anions that are difficult to introduce in LDHs by mere anion exchange can be immobilized into the anionic layer. Please note that LDHs obtained exploiting the memory effect display different morphologies from the original species if the structure of the LDH has changed significantly following calcination, and that LDHs can be also synthesized

even when the mixture of oxides not derived from LDH calcination is stirred in water. In fact, a report exists according to which LDH reconstruction after substantial structural changes should be called direct synthesis, not memory effect.^[12r]

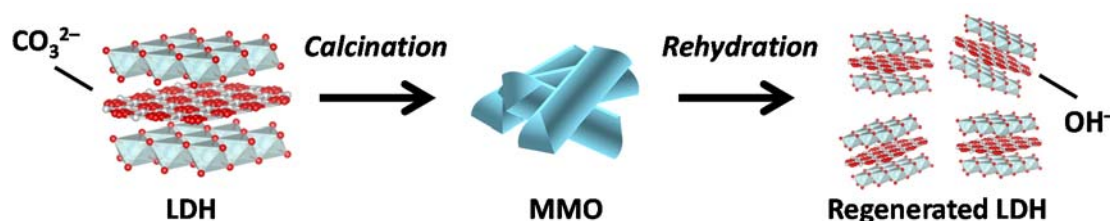


Figure 1-16. Memory effect (direct synthesis) of a layered double hydroxide (LDH).

The aforementioned diverse structural control of LDHs affords the fine tunings of LDHs' chemical properties, like for instance acidity and basicity. The following three parameters affect the basicity of LDHs: i) the identities of the metal ions (M^{2+} and M^{3+}), ii) the atomic ratio of M^{2+} to M^{3+} , and iii) the nature of the anions.^[12k] The catalytic activities of LDHs in the cyanoethylation of methanol have been reported to decrease when the Mg^{2+} centers in $\text{Mg}_3\text{Al-LDH}$ were partially replaced by metals like Mn, Fe, Co, Ni, Cu, and Zn.^[12s] Subsequently, evidence indicated that in the case of Mg–Al LDH, when the Mg/Al ratio increases, so does the total number of basic sites, whereas the system's basicity decreases.^[12k,t] Finally, as can be evinced from the structures depicted in Figure 1-16, the layered anion can be replaced by OH^- ions *via* memory effect, leading to an increase in LDH basicity.^[12j,k,u]

Based on the aforementioned approaches to controlling LDH properties, LDHs have been utilized to catalyze various acid-base reactions, including the Knoevenagel condensation, the Claisen–Schmidt condensation, and the Michael addition. Moreover, the substituent metals in LDHs and/or interlayered anions themselves can function as the catalysts for various oxidations, including for instance olefin epoxidation, alcohol oxidation, and Baeyer–Villiger oxidation.^[12d–f,h] MMOs generated by LDH calcination are also utilized in a number of catalytic reactions, such as CO_2 stabilization to epoxides^[12v] and 2'-hydroxychalcone and flavanone synthesis *via* Claisen–Schmidt condensation and Michael addition.^[12w]

Notably, many reports also exist of the use of LDHs and MMOs as supports:^[12x] cross-coupling reactions like the Mizoroki–Heck reaction, the Stille coupling, the Suzuki–Miyaura coupling, and the Sonogashira coupling have been performed using Pd/Mg–Al LDH and Rh/Mg–Al LDH as catalysts;^[12y–aa] the synthesis of methyl isobutyl ketone from acetone has been achieved using as catalysts Pd/Mg–Al MMO and Ni/Mg–Al MMO;^[12ab] the synthesis of quinoline from 2-aminobenzylalcohols and carbonyl compounds has been performed using Ru/Mg–Al LDH;^[12ac] and the alkylation of nitriles using alcohols has been performed with Ru/Mg–Al LDH as catalyst.^[12ad]

1.1.4.2. Function-integrated Catalysts

Various active sites can be integrated in the surface of a solid catalyst, without any observed loss of the inherent activities of these sites. As can be evinced from the depictions in Figure 1-17, the catalytic activities of function-integrated catalysts can be classified into two groups: i) multiple catalysis, whereby different reactions are promoted by a single system; and ii) concerted catalysis, whereby one reaction is promoted *via* the simultaneous activation of substrates and/or intermediates.^[13a,b]

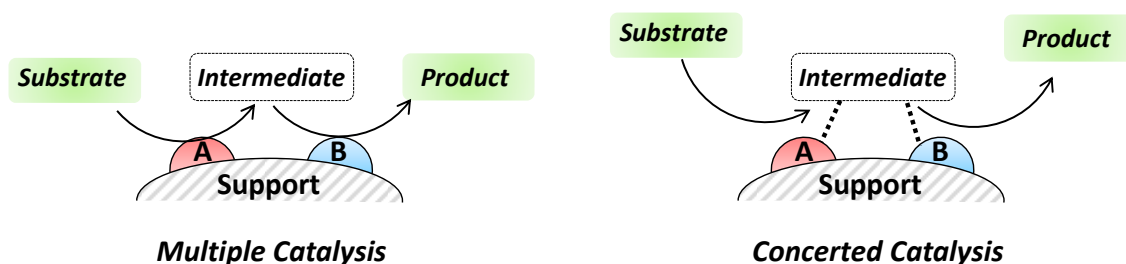


Figure 1-17. Typical catalytic activities of function-integrated catalysts.^[13a,b]

Multiple Catalysis

Multiple catalysis has enabled different reactions to proceed in the presence of one function-integrated solid catalyst by utilizing the support-immobilized active sites and/or the intrinsic properties of the supports, leading to the catalysis of a large number of heterogeneous one-pot syntheses and tandem reactions.^[13] For example, Kobayashi *et al.* have succeeded in catalyzing a tandem reaction consisting of aerobic alcohol oxidation followed by Michael addition to produce carbonyl compounds using Au–Pd alloy nanoparticles and tetravalent boron catalysts immobilized on polymer-incarcerated carbon black (PICB–Au/Pd/B) (Figure 1-18).^[13d,e] In particular, after the aerobic alcohol oxidation to produce α,β -unsaturated carbonyl compounds has been realized *via* catalysis by Au–Pd alloy nanoparticles immobilized on PICB, the Michael addition of 1,3-dicarbonyl compounds to form the corresponding enones occurs *via* Lewis acid-based catalysis of tetravalent boron-based compounds generated by the NaBH_4 used as reductant in the preparation of the catalyst.

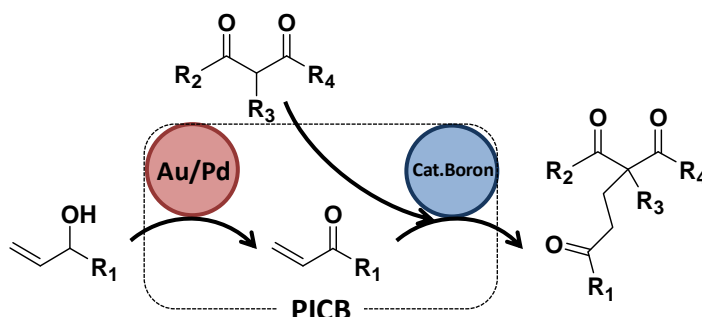


Figure 1-18. Heterogeneous one-pot synthesis of carbonyl compounds catalyzed by Au–Pd alloy nanoparticles and tetraivalent boron catalysts immobilized on polymer-incarcerated carbon black (PICB).^[13d,e]

Concerted Catalysis

Concerted catalysis whereby accumulated active sites simultaneously activate substrates and/or intermediates is an important phenomenon in imparting a uniquely high activity to solid catalysts. Many examples of this type of reactivity have been reported that rely on organic anchors and the combination of supports and metal nanoparticles (for examples of the latter category of catalysts, see section 1.1.4.3.).^[14] For instance, when an amine-modified $\text{SiO}_2\text{--Al}_2\text{O}_3$ ($\text{SiO}_2\text{--Al}_2\text{O}_3/\text{NEt}_2$ — NEt_2 = diethyl amine) was used as an acid-base catalyst, both a nucleophile and an electrophile were contiguously activated on its surface to promote a nucleophilic addition to the electrophile (Figure 1-19).^[13a,14a,b] This concerted effect had a great impact on a Michael addition. Notably, this reaction hardly progressed in the presence of $\text{SiO}_2\text{--Al}_2\text{O}_3$ and triethylamine, whereas the Michael adduct was obtained in 94% yield in the presence of the $\text{SiO}_2\text{--Al}_2\text{O}_3/\text{NEt}_2$ acting as catalyst.

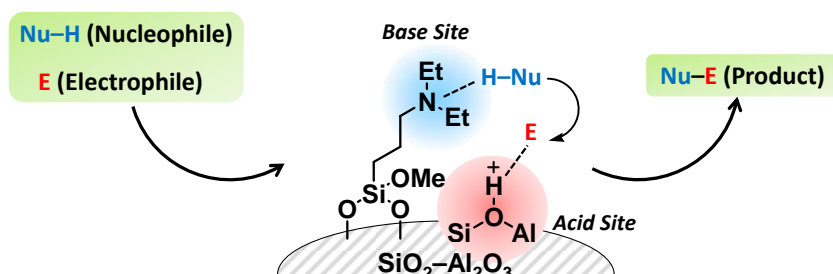


Figure 1-19. Concerted catalysis of $\text{SiO}_2\text{--Al}_2\text{O}_3/\text{NEt}_2$. NEt_2 : diethylamine.^[13a,14a,b]

Furthermore, the transfer of electrons to a support driven by the redox property or the defect sites of the support itself often contributes to an enhancement of the catalytic activities.^[15] For example, when copper hydroxide-based catalysts supported on manganese oxide octahedral molecular sieves (Cu/OMS-2) were used to catalyze the aerobic Glaser–Hay coupling, OMS-2 acted as the electron mediator between the copper centers and molecular oxygen to efficiently promote the desired overall reaction (Figure 1-20).^[15a,b] Also, spillover, hydrogen transfer of noble metal-dissociated molecular hydrogen to supports, can be useful to promote various reactions.^[15c-e]

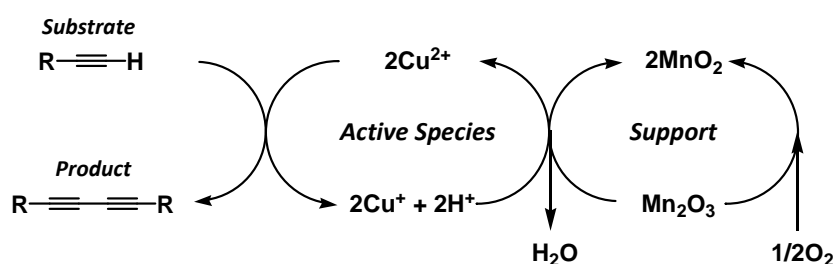


Figure 1-20. The Glaser–Hay coupling catalyzed by a copper hydroxide-based catalysts supported on manganese oxide octahedral molecular sieves proceeding *via* a rapid electron transfer.^[15a,b]

1.1.4.3. Nanoparticles/Nanoclusters

In recent years, metal nanocatalysts, that is metal nanoparticles and nanoclusters, have been the focus of significant research efforts due to their unique properties, like the quantum size effect.^[16] Nanoclusters, characterized by particles typically less than 2 nm in size, have different properties from nanoparticles. For instance, they display no plasmon resonance effect, molecular discrete electronic structures and energy levels, and more unsaturated active sites.^[16a] In addition, the fact that the nanoclusters are mono-dispersed and their structures are well established renders the analysis and elucidation of the catalysts' structure–activity relationship relatively easy to perform.^[16a] Nevertheless, the number of reports on the catalytic applications of nanoparticles is much higher than the number of reports focusing on the catalytic application of nanoclusters;^[16b–d] this observation is likely the result of the fact that the preparation of nanoparticles and the methods to immobilize them on a support are well established and easy to implement (refer to section 1.1.3.2.3.), whereas the synthesis of nanoclusters generally requires unnecessary ligands. In this section will be introduced an Au nanoparticle catalyst, one of the most important members of the nanoparticle-based catalyst family, due to its unique catalytic properties.

Gold used to be regarded as a stable and non-catalytic noble metal, but since Haruta *et al.* reported that supported Au nanoparticles (Au/ α -Fe₂O₃, Au/Co₃O₄, Au/NiO) prepared *via* a co-precipitation method displayed high catalytic activity in the aerobic oxidation of CO and H₂ even at low temperatures,^[16e,f] the catalytic use of Au nanoparticles has become a very active field of research.^[16b–d] At the present time, Au nanoparticles are known to activate various molecules and catalyze different reactions: isomerization to allyl alcohol^[16g] and stabilization of CO₂ *via* epoxide activation and/or CO₂,^[16h] homocoupling *via* activation of boronic acids,^[16i] synthesis of silanols,^[16j] reduction of amide/sulfoxide/pyridine *N*-oxides,^[16k] hydrosilylation of alkynes,^[16l] and dehydrogenative coupling of silanes and alkynes *via* silane and/or alkyne activation,^[16m] *etc.*

Among the various organic reactions catalyzed by Au nanoparticles, alcohol oxidation, one of the key reactions in synthetic chemistry, driven by molecular oxygen as the sole oxidant, has been the focus of particular attention.^[16b] Transition-metal oxides, such as Fe₃O₄, TiO₂, and CeO₂, have been used widely as the supports of

heterogeneous catalysts in order to utilize the supports' redox properties. In recent years, the highly efficient alcohol oxidation catalyzed by Au nanoparticles supported on LDH (Au/LDH) has also been reported.^[16n-p] The putative mechanism of alcohol oxidation catalyzed by Au/LDH is depicted in Figure 1-21.^[16q,r] Although several mechanisms for alcohol oxidation have been proposed in the case of catalysts comprising other metal oxides as supports, in general the reaction course is thought to proceed *via* deprotonation/hydride elimination, a hypothesis supported also by the results of theoretical calculations.^[16s] Considering the reaction course just alluded to, it can be said that the alcohol oxidation proceeds efficiently thanks to the basicity of LDH, which promotes the deprotonation step.

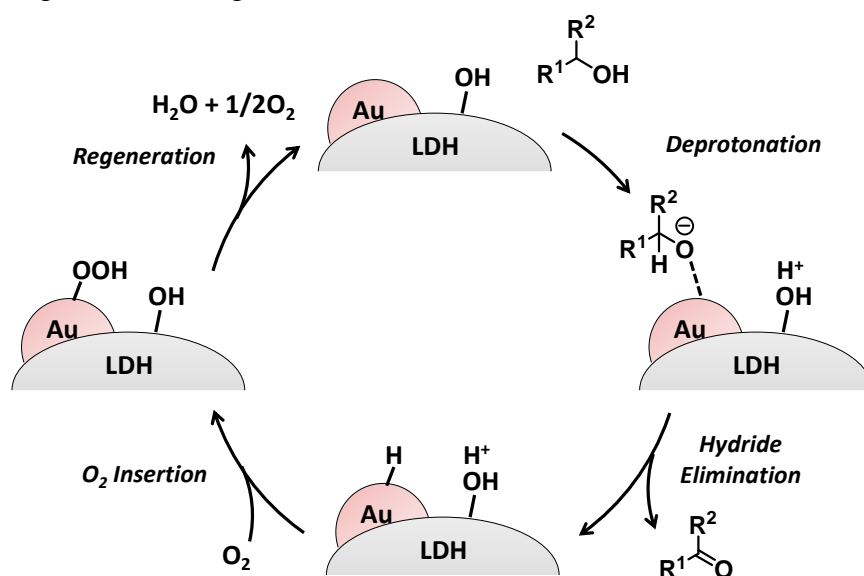


Figure 1-21. Putative mechanism of aerobic alcohol oxidation catalyzed by gold nanoparticles supported on a layered double hydroxide (LDH).^[16q-s]

In a similar way to the aforementioned alcohol oxidation, many cases exist whereby a reaction proceeds efficiently as a consequence of the concerted catalysis by Au nanoparticles and their support (refer to section 1.1.4.2.). For example, catalysts consisting of supported Au nanoparticles also catalyze reduction reactions that rely on molecular hydrogen as the sole reductant,^[16t] including the reduction of α,β -unsaturated ketones to produce allyl alcohols or saturated ketones,^[16u,v] the reduction of quinolines,^[16w] and the reduction of epoxides to alkene.^[16x] In these types of reactions, the heterolytic cleavage of molecular hydrogen is believed to occur concertedly at both

the gold nanoparticle sites and the basic sites of the supports to generate Au–H species, which drive substrate reduction (Figure 1-22). As an example of a reaction system that effectively exploits the concerted heterolytic cleavage of molecular hydrogen, Mitsudome *et al.* designed Au@CeO₂ core-shell nanoparticle catalysts possessing maximized interfacial sites between Au and CeO₂ that afforded the highly selective semihydrogenation of alkynes to alkenes (Figure 1-23).^[16y] Notably, when normal (non-core-shell) Au nanoparticles supported on CeO₂ (Au/CeO₂) were used to catalyze phenylacetylene reduction, the semihydrogenated product, styrene, was not produced selectively; in other words, substrate over-reduction took place in this case to produce mostly ethylbenzene. On the other hand, in the presence of Au@CeO₂, the highly selective semihydrogenation of the substrate was successfully achieved to afford only styrene. The high selectivity of this semihydrogenation reaction is assumed to be the result of the fact that at the interfacial sites of Au@CeO₂ the dominant reaction is the heterolytic dissociation of molecular hydrogen; the interfacial Au–H species have no potential to reduce alkenes whereas Au–H species produced as a consequence of the homolytic cleavage of H₂ on Au nanoparticles are able to reduce alkenes. A similar system was also declared using Ag@CeO₂ core-shell nanoparticles to catalyze chemoselective reduction reactions.^[16z]

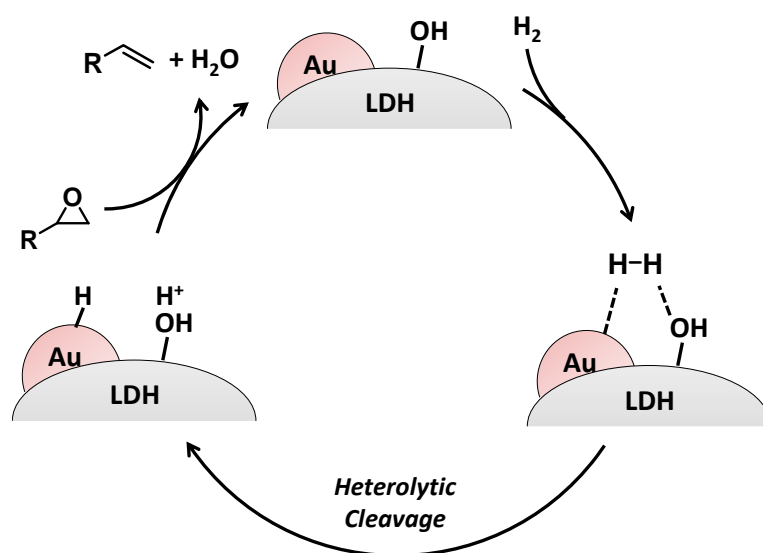


Figure 1-22. Putative mechanism of epoxide reduction catalyzed by gold nanoparticles supported on a layered double hydroxide (LDH).^[16x]

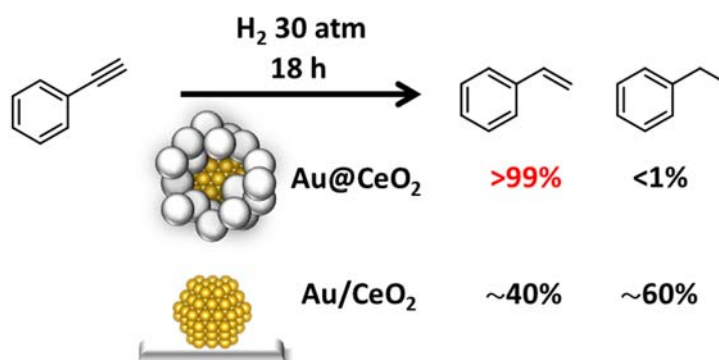


Figure 1-23. Selectivities of the Au@CeO_2 -catalyzed semihydrogenation of phenylacetylene, top, and of the same reaction catalyzed by normal Au nanoparticles supported on CeO_2 (Au/CeO_2), bottom.^[16y]

In addition, the described redox properties of Au nanoparticles can be applied to the catalysis of various tandem reactions, including the synthesis of lactones from diols,^[16aa] the reductive amination of alcohols through a hydrogen-borrowing system (Figure 1-24),^[16ab] and the oxidative acylation of amines to amides (refer to section 1.1.5.).

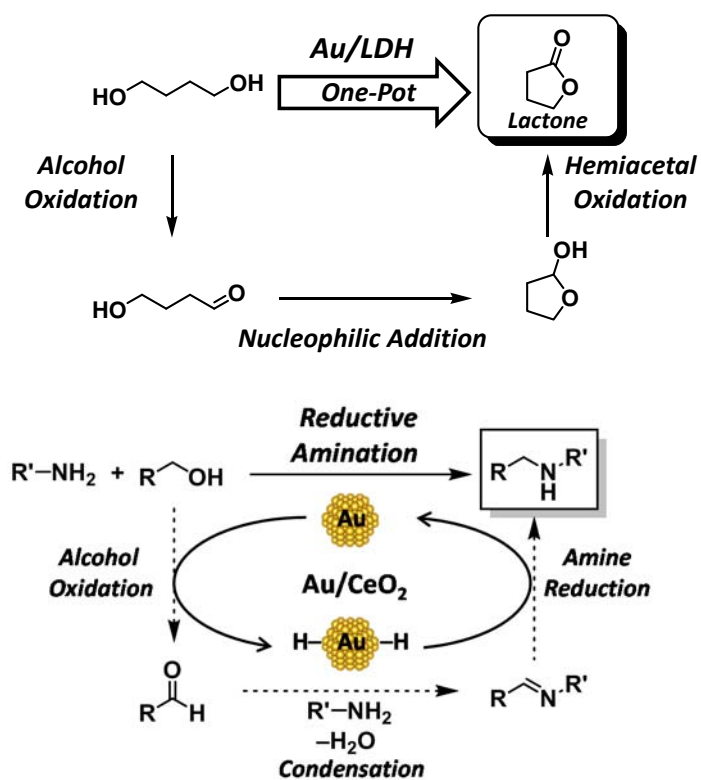


Figure 1-24. Tandem reactions that occur as a consequence of the redox properties of gold nanoparticle catalysts.^[16aa,ab]

1.1.4.4. Bimetallic Catalysts

As discussed in section 1.1.3.2.4., bimetallic nanoparticles can be designed to acquire various structures, such as solid-solution alloy, intermetallic compounds, core-shell, and cluster-in-cluster. A variety of effects influence the catalytic properties of bimetallic systems, including ligand effects, ensemble effects, steric effects, resistance to oxidation, stabilization of active sites, and concerted catalysis.^[11a,17a,b]

The change of catalytic properties in alloyed metals is mainly explained by the ligand effect attributable to the change in the electronic state with the alloyed metal and by the ensemble effect attributable to the change in the number and arrangement of alloyed metals.^[17c] In the case of the Au–Pd alloy, electrons are transferred from the palladium to the gold centers, as a consequence of the high electronegativity of Au. Subsequently, the s and p electrons of Au become abundant, whereas charge compensation is performed with d electrons to increase d electrons of Pd because of the overlap between the 5d orbital of Au and the 4d orbital of Pd. As a result, Au becomes slightly electron-rich *via* the ligand effect.^[17c,d] Also, given that the Au–Pd alloy is a complete solid solution, when the amount of Au centers in the random alloy structure increases, so does the number of monoatomic Pd sites; in other words, as the number of Au centers in the random alloy structure increases, the number of continuous ensemble sites of Pd decreases. For example, according to evidence from a study conducted by Miura *et al.*, when the Au/Pd molar ratio increased, the alloy's catalytic activity in the hydrosilylation of enones increased, even though the reaction hardly proceeded when either Au or Pd were used as catalysts (Figure 1-25).^[17e] Indeed, in this alloyed system, the aforementioned electron transfer from Pd to Au and the increase in isolated Pd sites as a consequence of the increase in the number of Au centers in the alloy structure were observed by X-ray photoelectron spectroscopy (XPS) and X-ray absorption fine structure. Moreover, in the syntheses of vinyl acetate and hydrogen peroxide, other researchers have proposed an ensemble effect to decrease the number of sites active for decomposition reactions and improve the desired selectivity.^[17c] However, since the ligand and ensemble effects occur at the same time, it is generally difficult to determine whether either or both influence the supported alloy's catalytic properties.^[17f]

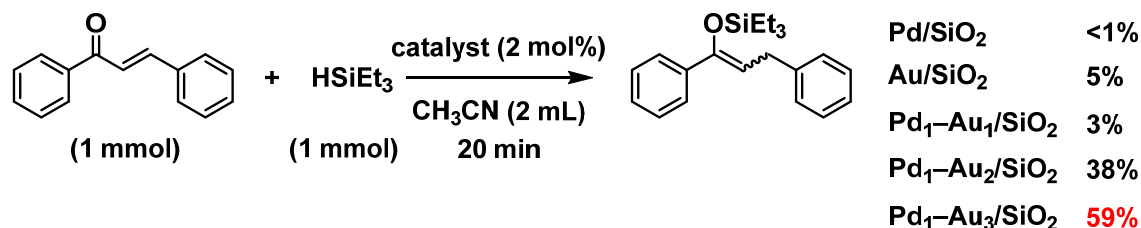


Figure 1-25. Effect of Pd/Au ratio on the yield of the hydrosilylation of enones using a Pd–Au alloy immobilized on an SiO₂ support (Pd–Au/SiO₂).^[17e]

Recently, as the novel alloying effect besides the ligand effect and the ensemble effect, the steric effect on the alloy surface has been declared in the case of intermetallic nanoparticles. Furukawa *et al.* pioneered the heterogeneous metal-catalyzed selective semihydrogenation of diphenylacetylene to produce *trans*-stilbene but not *cis*-stilbene, using as catalysts Rh-based intermetallic compounds like SiO₂-supported Rh₂Sb nanoparticles (Rh₂Sb/SiO₂) (Figure 1-26).^[17g,h] The observed specific stereochemistry was realized by the intermetallic ordered alloy-derived geometric restriction of hydrogen access to the half-hydrogenated intermediate on the surface.

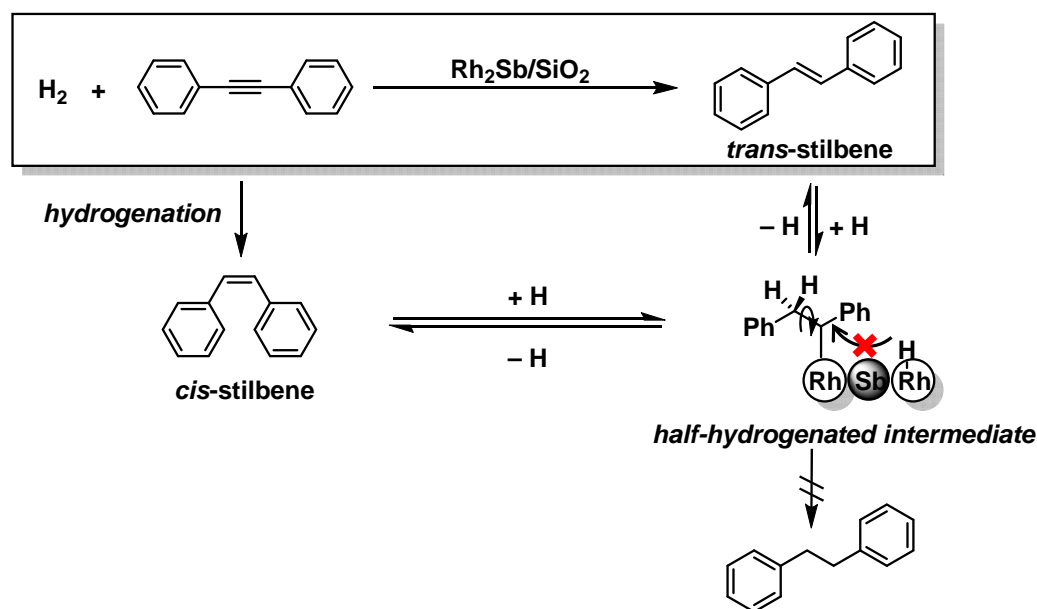


Figure 1-26. Unusual semihydrogenation of diphenylacetylene to produce *trans*-stilbene that exploits the unique steric effect of intermetallic, Rh- and Sb-containing, nanoparticles immobilized on an SiO₂ support (Rh₂Sb/SiO₂).^[17g,h]

Au-based bimetallic systems have also been reported to stabilize zero-valent Rh and Pd and thus improve the systems' resistance to oxidation by molecular oxygen^[17i,j]. Thanks to the stability of Pd(0) in Au–Pd nanoparticles to O₂-driven oxidation, catalytic reactions whereby Pd(0) nanoparticles function as the active species can be carried out even under an air or O₂ atmosphere using molecular oxygen as the sole oxidant; in fact, the research group led by Mizuno and Yamaguchi found that catalysts consisting of supported Au–Pd nanoparticles efficiently catalyzed dehydrogenative aromatization reactions under atmospheric air, whereas the same reactions hardly proceeded in the presence of supported Pd- or Au-based catalysts, although it was difficult to determine that only the stabilization of Pd(0) species affected the activity of Au–Pd alloy nanoparticles for the aerobic aromatization reactions (Figure 1-27).^[17k,l]

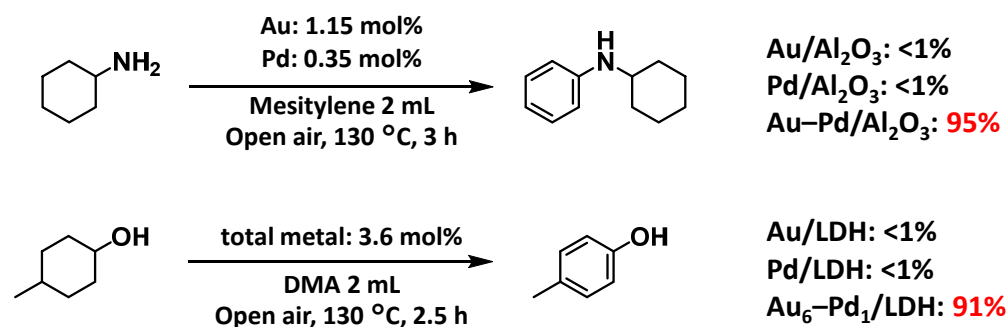


Figure 1-27. Aerobic dehydrogenative aromatization reactions catalyzed by supported Au–Pd alloy nanoparticles.^[17k,l] DMA: *N,N*-dimethylacetamide; LDH: layered double hydroxide.

Moreover, many reports exist on the use of bimetallic systems to stabilize a catalyst's active sites and thus inhibit the catalyst deactivation resulting from the leaching or sintering of metallic species.^[17m–q] For instance, Sakurai *et al.* reported that, although the oxidative addition of aryl halides to Pd clusters led to leaching of the Pd species, Au–Pd clusters prevented the mentioned oxidative adduct from leaching by way of a quick spillover of halogen atoms from Pd sites to Au sites (Figure 1-28).^[17q] Furthermore, by utilizing the concerted catalysis for C–Cl dissociation,^[17r–t] the Ullmann coupling, which neither Au-based nor Pd-based monometallic catalysts promoted, was successfully achieved at low temperatures in the presence of Au–Pd clusters (Figure 1-29).^[17s]

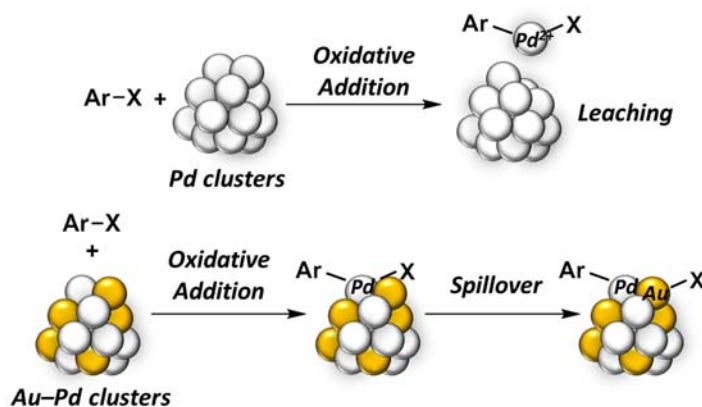


Figure 1-28. Oxidative addition of aryl halides to Pd nanoclusters or Au-Pd alloy nanoclusters.^[17q]

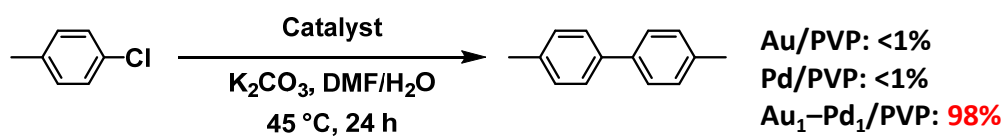


Figure 1-29. Ullmann coupling achieved via C-Cl bond dissociation catalyzed by Au-Pd alloy nanoclusters immobilized on a support.^[17s]

1.1.5. Liquid-phase Organic Synthesis via Heterogeneous Catalysis

As described in section 1.1.2., although heterogeneous catalysts occupy most of the industrial use in gas-phase reactions, their use in liquid-phase organic reactions has also been extensively studied. Although the catalysis of reactions in the liquid-phase using heterogeneous systems has the disadvantage that the reaction rate is usually slow compared to the same reactions catalyzed by homogeneous systems, heterogeneous catalysis has the key advantage that simple filtration can be employed to separate the reaction solution from the catalyst, which renders the purification of the product and the reuse of catalyst and solvent easier to achieve. Since in most cases, moreover, the catalyst does not leach into the solution, the reaction product is not contaminated by metallic species. Additionally, in general, handling heterogeneous catalysts is relatively easy, as a consequence of their high stability in air. On the other hand, the highly reactive homogeneous catalysts generally require careful handling procedures, and they may contaminate the reaction products. Notably, the presence of impurities is a particularly serious problem in the pharmaceutical field. Therefore, liquid-phase heterogeneous organic syntheses are attracting attention not only in bulk chemical synthesis but also in the pharmaceutical and fine chemical fields; additionally, the study of these types of syntheses is very important from the viewpoint of green, sustainable chemistry.^[18a-c]

As already mentioned in section 1.1.4.2., solid catalysts are capable of simultaneously possessing active sites with different characteristics, such as acid-base sites on the surface, exhibiting multiple catalysis advantageous for one-pot synthesis.^[13] One-pot syntheses are environmentally-friendly methods that do not involve the tedious separation and purification of intermediates, and their implementation can improve atomic efficiency, increase the E-factor (weight ratio of total amount of wastes to desired products), and decrease energy consumption. One-pot syntheses may involve changing the reaction conditions for each reaction in one vessel. However, an ideal one-pot synthesis consists of an orthogonal tandem reaction, which allows all reactions promoted by different catalysts to proceed under the same reaction conditions,^[18d] and it is also effective to apply heterogeneous catalysts to such systems. In short, one-pot syntheses, including orthogonal tandem reactions, are relatively easy to realize using

liquid-phase heterogeneous catalysis reaction systems, and such reaction systems possess a number of advantages from an environmental point of view.

In recent years, in addition to the conventional batch liquid-phase organic syntheses described above, the development of liquid-phase flow syntheses has attracted much research attention.^[18e-h] Liquid-phase flow syntheses present many advantages, in terms of, for instance, productivity, thermal efficiency, stirring efficiency, safety, and reproducibility, over batch-type syntheses. Furthermore, multi-step reactions can be achieved just by connecting columns used for flow syntheses. Although most bulk chemical syntheses performed under harsh conditions (*e.g.*, high temperature and high pressure) are flow syntheses, given that, in flow syntheses, reactions are difficult to control and the synthesis of fine chemicals requires precise transformations, batch-type syntheses have been the mainstay approach to the synthesis of fine chemicals. In 2015, Kobayashi *et al.* effected the eight-step synthesis of rolipram by liquid-phase flow organic reactions using only columns packed with heterogeneous catalysts, which can be regarded as a demonstration of precise transformations realized by way of heterogeneous catalysis (Figure 1-30).^[18e] Since in this approach only a solid catalyst was used, no leaching of metal species was observed and no procedure for the separation of the catalyst needed to be implemented, which makes this reaction a good example of how to take advantage of heterogeneous catalysts in flow syntheses. To date, the use of solid catalysts in liquid-phase batch systems has been deemed to be too difficult in the industrial setting, based on the low thermal efficiency of this approach, the deterioration of stirring efficiency accompanying scale-up, the damage to reaction vessels caused by the collision of solids, the difficulty in washing, *etc.* However, flow syntheses can solve these problems. Therefore, the emergence of flow synthesis is expected to cause a dramatic expansion of the application and utilization of solid catalysts.

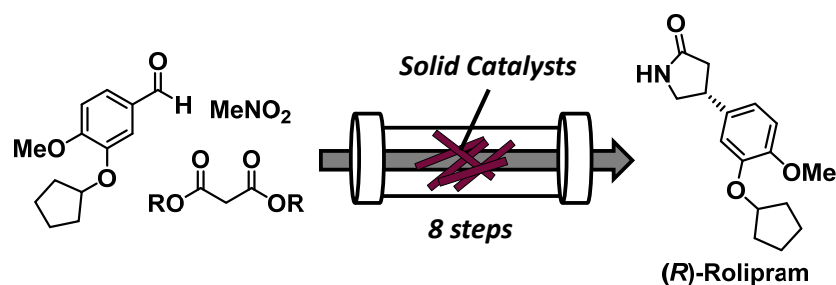


Figure 1-30. The heterogeneous catalysis-based flow synthesis of rolipram developed by Kobayashi and coworkers.^[18e]

As described above, liquid-phase organic synthesis *via* heterogeneous catalysis has drawn much attention in terms of the engineering advantages. In fact, numerous fundamental organic reactions have been successfully performed using inorganic heterogeneous catalysts; these reactions include Friedel–Crafts reactions, aromatic nitrations, Knoevenagel condensations, Claisen–Schmidt condensations, Michael additions, olefin isomerizations, olefin epoxidations, alcohol oxidations, Baeyer–Villiger oxidations, carbonyl reductions, alkyne/alkene hydrogenations, and Meerwein–Ponndorf–Verley reductions.^[18a,i,j] Additionally, various metal complex-based catalysts immobilized on solids and metal nanoparticle-based catalysts have been developed for useful and comparatively advanced organic reactions, in addition to the aforementioned ones, including hydroformylations, cross-coupling reactions like the Suzuki–Miyaura coupling (Figure 1-31), click reactions, hydrosilylations, aldehyde–alkyne–amine (A^3)-couplings, cyclopropanations, olefin metatheses, and asymmetric reactions,^[16, 18k–p] which are otherwise well-established homogeneously-catalyzed reactions. Notably, heterogeneously catalyzed one-pot syntheses and tandem reactions mainly consist of combinations of these reactions.^[13]

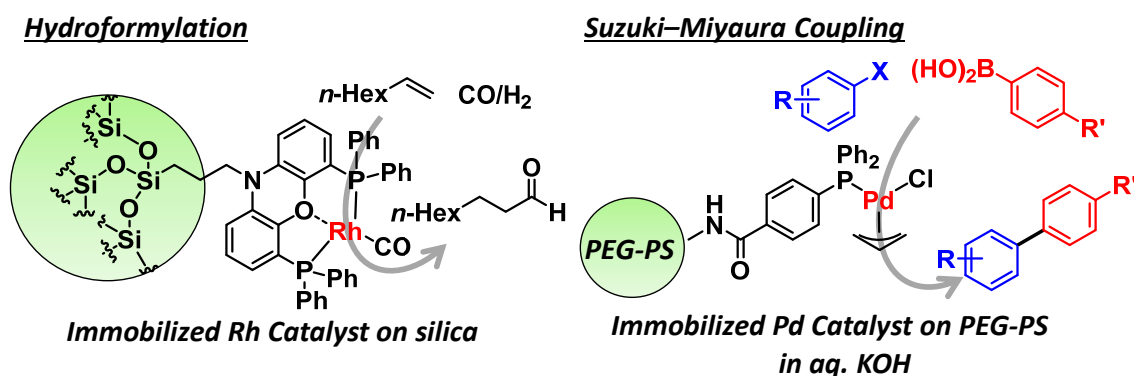


Figure 1-31. Examples of useful organic reactions catalyzed by immobilized metal complexes.^[18o,p] aq.: aqueous; PEG-PS: polyethylene glycol-polystyrene.

Furthermore, as a consequence of the future depletion of petroleum resources, the utilization of biomass, especially lignocellulose, which is cheap and non-edible, has been the focus of much attention recently. Since biomass-derived chemicals and fuels may have to replace the present oil-derived ones, it is indispensable to create large-scale bulk production systems dedicated to transforming biomass. Therefore, many

investigations are being actively pursued that are dedicated to the development of efficient and durable heterogeneous catalysts that can be used for various transformations of biomass components, mainly platform compounds like furans, glycerol, and sugars.^[18q-z]

Even though a large number of studies exist focusing on heterogeneous catalytic liquid-phase organic synthesis aimed at the practical and industrial use, the development of unprecedented reactions, which has played a pivotal role in the progress of organic and catalytic chemistry, has been hardly reported. Although biomass transformation seems to require several novel systems, most of the relevant transformation routes comprise simple acid-base and redox reactions, which typically do not lead to novel molecular transformations; moreover, the range of target molecules in biomass transformation is quite narrow compared to the compounds used in the pharmaceutical field.

Finally, I will discuss rare examples of unprecedented liquid-phase organic reactions that rely on the use of heterogeneous catalysts, basically support-immobilized nanoparticles, due to the unique characteristics, as described in section 1.1.4.3.^[19]

With no previous reports on the reduction of amides to amines under mild conditions (*e.g.*, low H₂ pressure and low temperature) to draw upon, Mitsudome *et al.* reported the first example of amide reduction to amines under surprisingly mild conditions: 70 °C and using molecular hydrogen at < 30 bar pressure as the sole reductant, in the presence of V-decorated Pt nanoparticles immobilized on a hydroxyapatite support (Pt/V/HAP) (Figure 1-32).^[19a] This amide reduction efficiently proceeded *via* Pt-catalyzed hydrogenation of amidic C=O bonds activated by *in situ*-generated V³⁺.

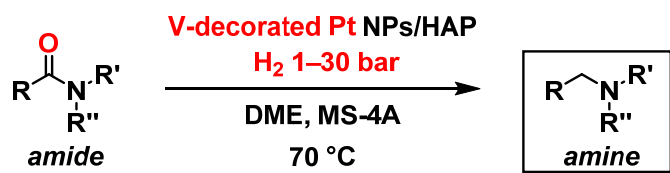


Figure 1-32. Amide reduction to amines catalyzed by V-decorated Pt nanoparticles immobilized on a hydroxyapatite support (Pt/V/HAP) under mild conditions using low-pressure H₂ as the sole reductant.^[19a] NPs: nanoparticles, DME: 1,2-dimethoxyethane, MS-4A: molecular sieves 4A.

Reactions affording the production of amides, an important class of compounds in fields like medicinal chemistry, are also invaluable. Wang and coworkers were the first to develop the aerobic synthesis of secondary and tertiary amides starting from alcohols and amines using catalysts comprising Au nanoparticles supported on DNA.^[19b] Almost simultaneously, Kobayashi and coworkers reported conducting the same reaction using immobilized Au or Au–3d metal (Fe, Ni, or, Co) nanoparticles as catalysts (Figure 1-33).^[19c] The present aerobic acylation of amines to amides was made possible by an Au nanoparticle-catalyzed tandem oxidation consisting in the following efficient sequential reactions: alcohol oxidation, nucleophilic addition, and hemiaminal oxidation. As for primary amide synthesis *via* the described aerobic acylation, in 2012, Mizuno *et al.* demonstrated the first direct amide synthesis from alcohols and aqueous NH₃ in the presence of OMS-2 catalysts that was achieved *via* alcohol oxidation/dehydration condensation/imine oxidation/nitrile hydration (see reference [46a] in Chapter IV).

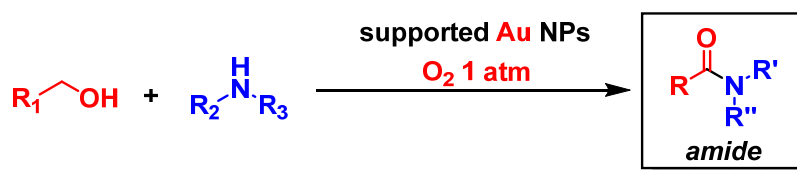


Figure 1-33. Aerobic acylation of amines to amides catalyzed by support-immobilized Au nanoparticles (NPs).^[19b,c]

Ammonia, an ideal nitrogen source, can also be utilized in other heterogeneously catalyzed reactions, thanks to the comparatively high resistance of solid catalysts to NH₃. Recently, Hara *et al.* reported an efficient reductive amination of carbonyl compounds to primary amines that is applicable to reduction-sensitive carbonyl compounds, including furfural, which involves the use of NH₃, H₂, and a catalyst consisting of Ru nanoparticles immobilized on an Nb₂O₅ support.^[19d] During the same year, Beller *et al.* developed an MOF-derived Co nanoparticle-catalyzed reductive amination that is applicable to a much wider range of carbonyl compounds and affords the corresponding primary amines, surprisingly 85 examples, under high pressures of H₂ and NH₃ (Figure 1-34).^[19e] This method was also successfully applied to substrates like primary amines, secondary amines, nitro compounds, and formaldehyde, resulting in a product scope consisting of more than 140 compounds.

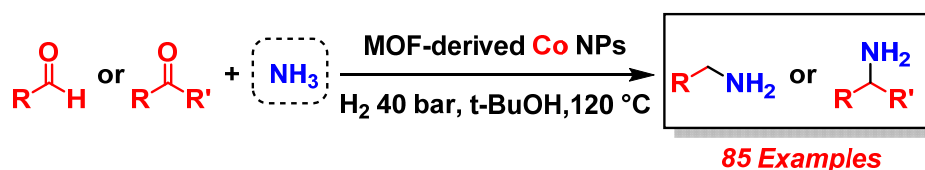


Figure 1-34. Reductive amination reaction applicable to a wide substrate scope and relying on NH_3 and H_2 as reactants developed by Beller *et al.*^[19e] MOF: metal-organic framework; NPs: nanoparticles.

Since in 2011 Stahl *et al.* reported the homogeneous Pd-catalyzed aerobic dehydrogenation of cyclohexanones to phenols, the Pd-catalyzed dehydrogenative aromatization strategy for the synthesis of phenol and aniline derivatives has emerged.^[19f] In a subsequent study, Stahl and coworkers also reported that Pd nanoparticles had the ability to catalyze dehydrogenative aromatization reactions and were more effective in the aromatization of cyclohexenone intermediates to phenols than homogeneous molecular Pd-based species.^[19g] Differently from molecular Pd complexes, Pd nanoparticles are deemed suitable for the catalysis of dehydrogenative aromatization under reductive conditions.^[19h,i] In fact, Li *et al.* developed an unprecedented direct cross-coupling of phenols and amines to anilines based on a Pd nanoparticle-catalyzed dehydrogenative aromatization strategy involving the reduction of phenols (Figure 1-35).^[19i] The research group led by Mizuno and Yamaguchi reported several novel acceptorless dehydrogenative aromatization reactions involving the utilization of NH_3 that rely on catalysis by Pd nanoparticles (see references [32] in Chapter IV).

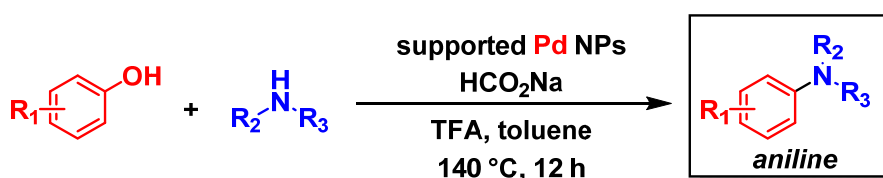


Figure 1-35. Direct cross-coupling of phenols and amines through a dehydrogenative aromatization catalyzed by Pd nanoparticles (NPs) developed by Li *et al.*^[19i] TFA: trifluoroacetic acid.

In terms of additional examples of unprecedented reactions realized *via* heterogeneous catalysts, Mizuno *et al.* also reported the use of supported Au nanoparticles to catalyze cross-dehydrogenative couplings aimed at the synthesis of silyl isocyanates and enaminals (Figure 1-36) (see references [9] in Chapter III and [48] in Chapter IV). The Shishido group developed the novel synthesis of multi-substituted phthalide derivatives and γ -hydroxybutenolides catalyzed by support-immobilized Ru complexes, although the same reactions did occur to produce moderate yields of γ -hydroxybutenolides also in the presence of homogeneous Ru catalysts, according to the literatures.^[19j,k] Quite recently, Zhang *et al.* reported the first selective sulfonylation of tetrahydroxyquinoxalines with sodium sulfinates using MOF-derived Co nanocluster-based catalysts.^[19l]

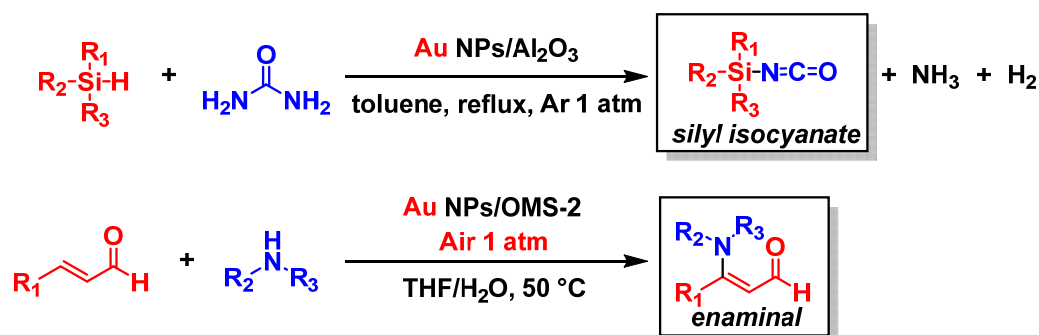


Figure 1-36. Novel cross-dehydrogenative coupling reactions catalyzed by support-immobilized Au nanoparticles (NPs) and developed by Mizuno *et al.* OMS-2: manganese oxide octahedral molecular sieves.

As can be evinced from the descriptions above, several excellent reports have been published on the development of novel organic reactions that rely on solid catalysts, but their number is quite small compared with the corresponding number of studies focusing on organic reactions catalyzed by homogeneous catalysts; moreover, the types of heterogeneously catalyzed reactions developed thus far are limited. In particular, almost all selective molecular transformations have been developed by homogeneous catalysts from historically important ones to quite recently reported ones.^[7c,d,20,21] Overall, guidelines and strategies for the design of heterogeneous catalysts that afford unprecedented selective organic reactions are still lacking.

1.2. Purpose and Concept of This Dissertation

In this chapter, I described the utility of catalysts, compared the characteristics of homogeneous *versus* heterogeneous catalysts, discussed practical preparation and design methods for solid catalysts based on their composition, systems specific to heterogeneous catalysts which are much different from those of homogeneous ones, and surroundings of heterogeneously catalyzed liquid-phase organic syntheses.

As mentioned in section 1.1.5., most conventional studies focusing on liquid-phase heterogeneous organic synthesis have concentrated on engineering aspects of the heterogeneous systems conceived to catalyze reactions well known to progress in the presence of homogeneous catalysts; by contrast very few studies have pioneered novel organic reactions, especially selective molecular transformations. As green chemistry's momentum grows, it is important to develop intrinsically environmentally-friendly solid catalysts; however, knowledge is lacking on how to develop new organic reactions, an essential goal to achieve for truly advancing and establishing liquid-phase heterogeneous organic synthesis.

On the other hand, as described in sections 1.1.3. and 1.1.4., solid catalysts have the potential to exhibit unique catalytic properties that are different from those of homogeneous catalysts. With proper catalyst design and full utilization of the catalytic potential specific to solid catalysts, the development of unexplored organic reactions becomes highly likely.

In this doctoral dissertation, I propose an original strategy for establishing liquid-phase heterogeneous organic synthesis and further elevate its value in organic and catalytic chemistry. In particular, I will focus on the rational construction of systems specific to solid catalysts for the development of unprecedented catalytic selective molecular transformations. The details of the strategy proposed herein are as follows: firstly, a target selective molecular transformation is divided into elementary reactions, and the possible relevant side reactions are identified in order to clarify what functions are necessary to achieve the desired synthesis (Figure 1-37). Subsequently, based on the composition of the heterogeneous catalysts as discussed in section 1.1.3.2., the stepwise design of function-integrated solid catalysts for achieving respective elementary reactions in the following order (Figure 1-38): I) a support possessing unique surface/bulk chemical properties, II) a support-immobilized nanoparticle as the main

catalyst engaging in multiple catalysis and/or concerted catalysis with its support, III) a support-immobilized bimetallic nanoparticle whose second metal is a promoter typically controlled by ligand and ensemble effects, and IV) a structure-controlled bimetallic nanoparticle immobilized on a support such as an alloy, a core-shell, or a cluster-in-cluster.

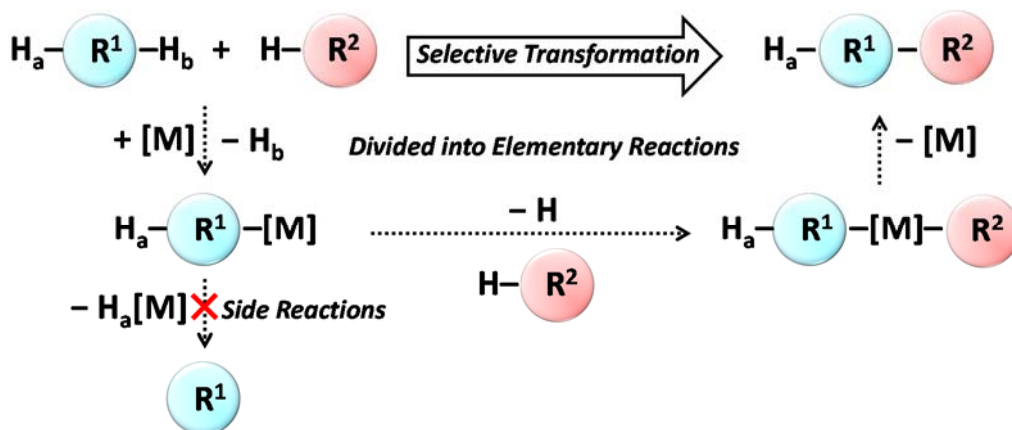


Figure 1-37. Overview of the research strategy consisting in the sub-division of a target reaction into elementary reactions, including putative side reactions.

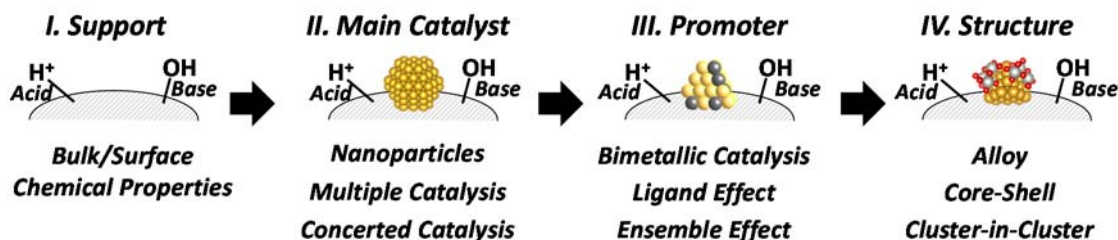
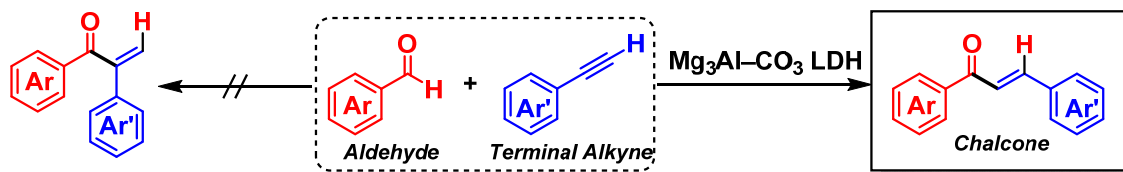


Figure 1-38. Rational construction of systems specific to solid catalysts.

Based on the strategy just detailed, as part of the research work described in this doctoral dissertation, I successfully developed various kinds of unprecedented catalytic selective molecular transformations (Figure 1-39): a) transition-metal-free, $\text{Mg}_3\text{Al}-\text{CO}_3$ LDH-catalyzed regioselective formal hydroacylation of terminal alkynes through nucleophilic addition/prototropy relying on the basicity and ionicity of LDH (Chapter II); b) one-pot selective flavone synthesis catalyzed by Au nanoparticles supported on $\text{Mg}_2\text{Al}-\text{CO}_3$ LDH (Au/LDH), starting from aldehydes and ketones, and proceeding *via* a sequence consisting of Claisen–Schmidt condensation (LDH catalysis), oxa-Michael addition (LDH catalysis), and aerobic oxidative dehydrogenation (concerted catalysis

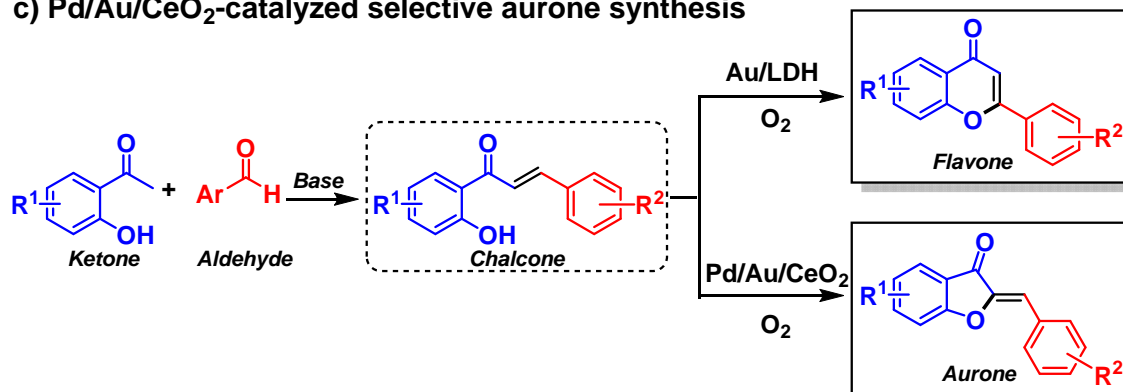
between Au and LDH) (Chapter III); c) selective aurone synthesis catalyzed by Pd-on-Au nanoparticles supported on CeO₂ and starting from simple chalcones through a process that included control of catalytic aurone synthesis, promotion of the catalysis, and inhibition of side reactions, fully in accordance with the aforementioned catalyst design approach (Chapter III); d) selective acceptorless dehydrogenative aromatization of cyclic secondary amines catalyzed by Pd nanoparticles supported on Mg₃Al–CO₃ LDH and achieved by exploiting the fast dehydrogenation of unstable imines (Chapter IV); e) selective formal α -oxygenation of secondary and tertiary amines catalyzed by Au nanoparticles supported on an Al₂O₃ support and proceeding through amine oxidation/hydration/hemiaminal oxidation (Chapter IV); and f) the unusual regioselective α -alkynylation of tertiary amines catalyzed by a system comprising Au nanoparticles supported on a hydroxyapatite and ZnBr₂ salts that relies on the unique catalytic characteristics of Au nanoparticles with respect to tertiary amine oxidation and Zn-promoted alkynyl addition (Chapter IV). I believe that the successful development of these selective molecular transformations that utilize systems specific to solid catalysts will contribute to further establishing organic synthesis based on heterogeneous catalysis.

a) $\text{Mg}_3\text{Al-CO}_3$ LDH-catalyzed selective formal hydroacylation



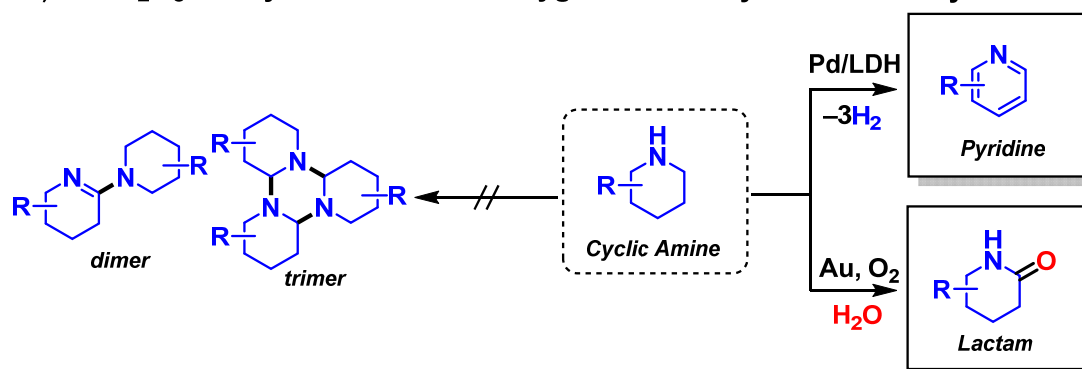
b) Au/LDH-catalyzed selective flavone synthesis

c) Pd/Au/CeO₂-catalyzed selective aurone synthesis



d) Pd/LDH-catalyzed selective dehydrogenative aromatization of cyclic amines

e) Au/Al₂O₃-catalyzed selective α -oxygenation of cyclic secondary amines



e) Au/Al₂O₃-catalyzed selective α -oxygenation of tertiary amines

f) Au/HAP and ZnBr₂-catalyzed selective α -alkynylation of tertiary amines

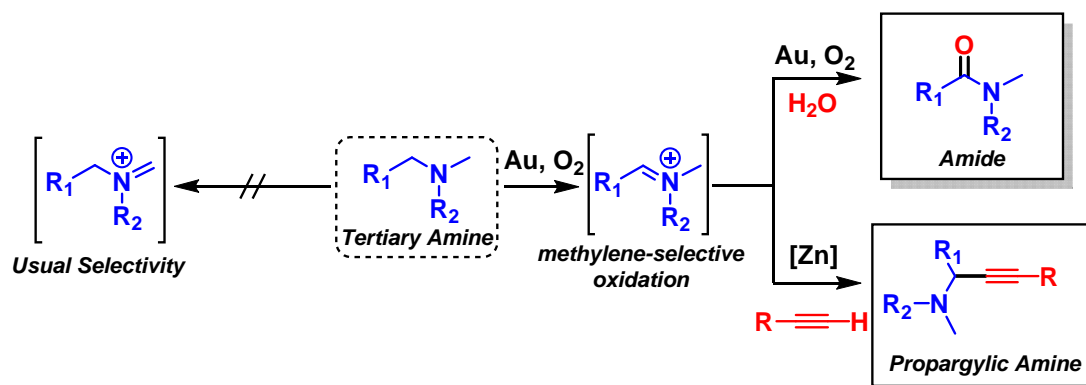


Figure 1-39. Unprecedented catalytic selective transformations developed in this study.

1.3. References

- [1] a) W. Ostwald, *Z. Phys. Chem.* **1894**, *15*, 706; b) G. Ertl, *Angew. Chem. Int. Ed.* **2009**, *48*, 6600; c) E. Roduner, *Chem. Soc. Rev.* **2014**, *43*, 8226.
- [2] a) P. G. Menon, *Chem. Rev.* **1994**, *94*, 1021; b) J.A. Moulijn, A.E. van Diepen, F. Kapteijn, *Appl. Catal. A* **2001**, *212*, 3; c) C. H. Bartholomew, *Appl. Catal. A* **2001**, *212*, 17; d) R. H. Crabtree, *Chem. Rev.* **2015**, *115*, 127.
- [3] a) *Handbook of Heterogeneous Catalysis*, G. Ertl, H. Knözinger, F. Schüth, J. Weitkamp, Eds.; Wiley-VCH Verlagsgesellschaft mbH, Weinheim, **1997**; Vol. 1; b) *Principles and Practice of Heterogeneous Catalysis*, J. M. Thomas, W. J. Thomas, Eds.; Wiley-VCH Verlagsgesellschaft mbH, Weinheim, and Wiley-VCH Publishers Inc., New York, NY, **1997**.
- [4] a) *Catalysis of Organic Reactions*, R. L. Augustine Ed.; Marcel Dekker, Inc. New York, NY, **1985**; b) J. M. Thomas, *Angew. Chem. Int. Ed. Engl.* **1994**, *33*, 913; c) *Handbook of Heterogeneous Catalysis*, G. Ertl, H. Knözinger, F. Schüth, J. Weitkamp, Eds.; Wiley-VCH Verlagsgesellschaft mbH, Weinheim, **1997**; Vol. 4 and Vol. 5; d) H. A. Wittcoff, B.G. Reuben, J. S. Plotkin, *Industrial Organic Chemicals*, John Wiley & Sons, Inc. Hoboken, New Jersey, **2004**; e) *Metal-catalysis in Industrial Organic Processes*, G. P. Chiusoli, P. M. Maitlis, Eds.; The Royal Society of Chemistry, Thomas Graham House, Science Park, Milton Road, Cambridge, CB4 0WF, UK, **2006**.
- [5] a) P. T. Anastas, J. C. Warner, *Green Chemistry: Theory and Practice*, Oxford Science Publications, Oxford, **1998**; b) B. M. Trost, *Angew. Chem. Int. Ed.* **1995**, *34*, 259; c) R. A. Sheldon, *J. Chem. Tech, Biotechnol.* **1997**, *68*, 381; d) R. A. Sheldon, *Green Chem.* **2007**, *9*, 1273; e) R. A. Sheldon, *Chem. Soc. Rev.* **2012**, *41*, 1437.
- [6] a) H. P. Dijkstra, G. P. M. Van Klink, G. Van Koten, *Acc. Chem. Res.* **2002**, *35*, 798; b) *Handbook of Heterogeneous Catalysis*, G. Ertl, H. Knözinger, F. Schüth, J. Weitkamp, Eds.; Wiley-VCH Verlagsgesellschaft mbH, Weinheim, **1997**; Vol. 2; c) A. J. Rossini, A. Zagdoun, M. Lelli, A. Lesage, C. Copéret, L. Emsley, *Acc. Chem. Res.* **2013**, *46*, 1942; d) F. Tao, P. A. Crozier, *Chem. Rev.* **2016**, *116*, 3487.
- [7] a) J. F. Hartwig, *Organotransition Metal Chemistry From Bonding to Catalysis*, University Science Books, Mill Valley, California, **2010**; b) R. H. Crabtree, *The Organometallic Chemistry of the Transition Metals*, 6th Edition, John Wiley & Sons, Inc. Hoboken, New Jersey, **2014**; c) S. Afewerki, A. Córdova, *Chem. Rev.* **2016**, *116*.

13512; d) D.-S. Kim, W.-J. Park, C.-H. Jun, *Chem. Rev.* **2017**, *117*, 8977; e) K. Ziegler, *Consequences and Development of an Invention. In Nobel Lectures, Chemistry 1963–1970*, Elsevier, Amsterdam, Netherlands, **1972**; f) G. Natta, *From the Stereospecific Polymerization to the Asymmetric Autocatalytic Synthesis of Macromolecules. In Nobel Lectures, Chemistry 1963–1970*, Elsevier, Amsterdam, Netherlands, **1972**; g) A. Miyashita, A. Yasuda, H. Takaya, K. Toriumi, T. Ito, T. Souchi, R. Noyori, *J. Am. Chem. Soc.* **1980**, *102*, 7932; h) W. S. Knowles, M. J. Sabacky, *Chem. Commun. (London)* **1968**, 1445; i) T. Katsuki, K. B. Sharpless, *J. Am. Chem. Soc.* **1980**, *102*, 5974; j) R. H. Grubbs, T. K. Brunck, *J. Am. Chem. Soc.* **1972**, *94*, 2538; k) R. R. Schrock, *J. Am. Chem. Soc.* **1974**, *96*, 6796; l) J.-L. Hérisson, Y. Chauvin, *Makromol. Chem.* **1971**, *141*, 161; m) N. Miyaura, K. Yamada, A. Suzuki, *Tetrahedron Lett.* **1979**, *20*, 3437; n) N. Miyaura, A. Suzuki, *J. Chem. Soc., Chem. Commun.* **1979**, 866; o) E.-I. Negishi, S. Baba, *J. Chem. Soc., Chem. Commun.* **1976**, 596b; p) S. Baba, E.-I. Negishi, *J. Am. Chem. Soc.* **1976**, *98*, 6729; q) R. F. Heck, *J. Am. Chem. Soc.* **1968**, *90*, 5518; r) C. M. Marson, *Chem. Soc. Rev.* **2012**, *41*, 7712; s) D. J. Durand, N. Fey, *Chem. Rev.* **2019**, *119*, 6561; t) G. Lelais, D. W. C. MacMillan, *Aldrichimica Acta* **2006**, *39*, 79; u) S. Shirakawa, K. Maruoka, *Angew. Chem. Int. Ed.* **2013**, *52*, 4312; v) T. Akiyama, K. Mori, *Chem. Rev.* **2015**, *115*, 9277; w) M. Hatano, K. Ishihara, *Asian J. Org. Chem.* **2014**, *3*, 352.

[8] a) C. T. Kresge, M. E. Leonowicz, W. J. Roth, J. C. Vartuli, J. S. Beck, *Nature* **1992**, *359*, 710; b) Y. Miyamoto, Y. Kuroda, T. Uematsu, H. Oshikawa, N. Shibata, Y. Ikuhara, K. Suzuki, M. Hibino, K. Yamaguchi, N. Mizuno, *Sci. Rep.* **2015**, *5*, 15011; c) D. R. Modeshia, R. I. Walton, *Chem. Soc. Rev.* **2010**, *39*, 4303; d) A. Rabenau, *Angew. Chem. Int. Ed. Engl.* **1985**, *24*, 1026.

[9] a) H. Gong, J. Zhu, K. Lv, P. Xiao, Y. Zhao, *New J. Chem.* **2015**, *39*, 9380; b) K. P. de Jong, *Deposition Precipitation in Synthesis of Solid Catalysts*, K. P. de Jong, Ed.; Wiley-VCH, Weinheim, **2009**; c) K. Yamaguchi, N. Mizuno, *Synlett* **2010**, *16*, 2365; d) K. Yamaguchi, N. Mizuno, *Top. Catal.* **2014**, *57*, 1196; e) S. Nojima, K. Kamata, K. Suzuki, K. Yamaguchi, N. Mizuno, *ChemCatChem* **2015**, *7*, 1097; f) J. Vakros, C. Kordulis, A. Lycourghiotis, *Langmuir* **2002**, *18*, 417; g) Y. Sunagawa, K. Yamamoto, H. Takahashi, A. Muramatsu, *Catal. Today* **2008**, *132*, 81; h) C. Copéret, F. Allouche, K. W. Chan, M. P. Conley, M. F. Delley, A. Fedorov, I. B. Moroz, V. Mougél, M. Pucino, K.

Searles, K. Yamamoto, P. A. Zhizhko, *Angew. Chem. Int. Ed.* **2018**, *57*, 6398; i) C. Copéret, A. Comas-Vives, M. P. Conley, D. P. Estes, A. Fedorov, V. Mougel, H. Nagae, F. Núñez-Zarur, P. A. Zhizhko, *Chem. Rev.* **2016**, *116*, 323; j) S. Shironita, K. Mori, T. Shimizu, T. Ohmichi, N. Mimura, H. Yamashita, *Appl. Surf. Sci.* **2008**, *254*, 7604; k) K. Mori, T. Araki, S. Shironita, J. Sonoda, H. Yamashita, *Catal. Lett.* **2009**, *131*, 337; l) R. M. Mohamed, *J. Mater. Proc. Technol.* **2009**, *209*, 577; m) K. Fuku, T. Sakano, T. Kamegawa, K. Mori, H. Yamashita, *J. Mater. Chem.* **2012**, *22*, 16243; n) F. Porta, L. Prati, M. Rossi, S. Coluccia, G. Martra, *Catal. Today* **2000**, *61*, 165; o) A. Villa, D. Wang, G. M. Veith, F. Vindigni, L. Prati, *Catal. Sci. Technol.* **2013**, *3*, 3036; p) J. A. Lopez-Sanchez, N. Dimitratos, C. Hammond, G. L. Brett, L. Kesavan, S. White, P. Miedziak, R. Tiruvalam, R. L. Jenkins, A. F. Carley, D. Knight, C. J. Kiely, G. J. Hutchings, *Nat. Chem.* **2011**, *3*, 551.

[10] a) N Toshima, T. Yonezawa, *New J. Chem.* **1998**, 1179; b) M. Faraday, *Philos. Trans. R. Soc. London.* **1857**, *147*, 145; c) M. Kerker, *J. Colloid Interface Sci.* **1986**, *112*, 302; d) G. Schmid, R. Pfeil, R. Boese, F. Bandermann, S. Meyer, G. H. M. Calis, J. W. A. van der Velden, *Chem. Ber.* **1981**, *114*, 3634; e) M. Brust, M. Walker, D. Bethell, D. J. Schiffrin, R. Whyman, *J. Chem. Soc., Chem. Commun.* **1994**, 801; f) M. Brust, J. Fink, D. Bethell, D. J. Schiffrin, C. Kiely, *J. Chem. Soc. Chem. Commun.* **1995**, 1655; g) T. Yonezawa, M. Sutoh, T. Kunitake, *Chem. Lett.* **1997**, *26*, 619; h) G. Schmid, A. Lehnert, *Angew. Chem. Int. Ed. Engl.* **1989**, *28*, 780; i) L. D. Rampino, F. F. Nord, *J. Am. Chem. Soc.* **1941**, *63*, 2745; j) H. Hirai, Y. Nakao, N. Toshima, *Chem. Lett.* **1978**, *7*, 545; k) H. Hirai, Y. Nakao, N. Toshima, *J. Macromol. Sci. Chem.* **1979**, *A13*, 727; l) R. Zanella, L. Delannoy, C. Louis, *Appl. Catal. A Gen.* **2005**, *291*, 62; m) W.-C. Li, M. Comotti, F. Schüth, *J. Catal.* **2006**, *237*, 190; n) S. Ivanova, C. Petit, V. Pitchon, *Appl. Catal. A Gen.* **2004**, *267*, 191; o) S. Ivanova, V. Pitchon, Y. van Zimmermann, C. Petit, *Appl. Catal. A Gen.* **2006**, *298*, 57; p) E. del Río, D. Gaona, J. C. Hernández-Garrido, J. J. Calvino, M. G. Basallote, M. J. Fernández-Trujillo, J. A. Pérez-Omil, J. M. Gatica, *J. Catal.* **2014**, *318*, 119; q) A. Wolf, F. Schüth, *Appl. Catal. A Gen.* **2002**, *226*, 1.

[11] a) S. Furukawa, T. Komatsu, *ACS Catal.* **2017**, *7*, 735; b) N. Toshima, Y. Wang, *Chem. Lett.* **1993**, *22*, 1611; c) N. Toshima, Y. Wang, *Langmuir*, **1994**, *10*, 4574; d) N. Toshima, Y. Wang, *Adv. Mater.* **1994**, *6*, 245; e) N. Toshima, P. Lu, *Chem. Lett.* **1996**, *25*, 729; f) K. Taniguchi, X. Jin, K. Yamaguchi, N. Mizuno, *Catal. Sci. Technol.* **2016**, *6*,

3929; g) T. Komatsu, S. Furukawa, *Mater. Trans.* **2015**, *56*, 460; h) Y. Shiraishi, D. Ikenaga, N. Toshima, *Aust. J. Chem.* **2003**, *56*, 1025; i) J. Pritchard, M. Piccinini, R. Tiruvalam, Q. He, N. Dimitratos, J. A. Lopez-Sanchez, D. J. Morgan, A. F. Carley, J. K. Edwards, C. J. Kiely, G. J. Hutchings, *Catal. Sci. Technol.* **2013**, *3*, 308; j) W. Lee, M. G. Kim, J. Choi, J. Park, S. J. Ko, S. J. Oh, J. Cheon, *J. Am. Chem. Soc.* **2005**, *127*, 16090; k) D. Chen, S. Liu, J. Li, N. Zhao, C. Shi, X. Du, J. Sheng, *J. Alloy. Compd.* **2009**, *475*, 494; l) A. A. Herzing, M. Watanabe, J. K. Edwards, M. Conte, Z.-R. Tang, G. J. Hutchings, C. J. Kiely, *Faraday Discuss.* **2008**, *138*, 337; m) K. Suzuki, T. Yamaguchi, K. Matsushita, C. Iitsuka, J. Miura, T. Akaogi, H. Ishida, *ACS Catal.* **2013**, *3*, 1845; n) M. Miyazaki, S. Furukawa, T. Takayama, S. Yamazoe, T. Komatsu, *ACS Appl. Nano Mater.* **2019**, *2*, 3307; o) M. Harada, K. Asakura, N. Toshima, *J. Phys. Chem.* **1993**, *97*, 5103.

[12] a) F. Cavani, F. Trifirò, A. Vaccari, *Catal. Today* **1991**, *11*, 173; b) M. J. Climent, A. Corma, S. Iborra, J. Primo, *J. Catal.* **1995**, *151*, 60; c) B. M. Choudary, M. L. Kantam, C. R. V. Reddy, K. K. Rao, F. Figueras, *J. Mol. Catal. A* **1999**, *146*, 279; d) K. Kaneda, K. Yamaguchi, K. Mori, T. Mizugaki, K. Ebitani, *Catal. Surv. Jpn.* **2000**, *4*, 31; e) B. F. Sels, D. E. De Vos, P. A. Jacobs, *Catal. Rev.: Sci. Eng.* **2001**, *43*, 443; f) K. Takehira, T. Shishido, *Catal. Surv. Asia* **2007**, *11*, 1; g) D. P. Debecker, E. M. Gaigneaux, G. Busca, *Chem. Eur. J.* **2009**, *15*, 3920; h) Z. P. Xu, J. Zhang, M. O. Adebajo, H. Zhang, C. Zhou, *Appl. Clay Sci.* **2011**, *53*, 139; i) G. Fan, F. Li, D. G. Evans, X. Duan, *Chem. Soc. Rev.* **2014**, *43*, 7040; j) K. Takehira, *Appl. Clay Sci.* **2017**, *136*, 112; k) W. Y. Hernández, J. Lauwaert, P. V. D. Voort, A. Verberckmoes, *Green Chem.* **2017**, *19*, 5269; l) M. J. Wu, J. Z. Wu, J. Zhang, H. Chen, J. Z. Zhou, G. R. Qian, Z. P. Xu, Z. Du, Q. L. Rao, *Catal. Sci. Technol.* **2018**, *8*, 1207; m) K. Kaneda, T. Yamashita, T. Matsushita, K. Ebitani, *J. Org. Chem.* **1998**, *63*, 1750; n) T. Matsushita, K. Ebitani, K. Kaneda, *Chem. Commun.* **1999**, 265; o) Z. P. Xu, H. C. Zeng, *Chem. Mater.* **1999**, *11*, 67; p) Z. P. Xu, H. C. Zeng, *Chem. Mater.* **2000**, *12*, 3459; q) J. Zhang, Y. F. Xu, G. R. Qian, Z. P. Xu, C. Chen, Q. Liu, *J. Phys. Chem. C* **2010**, *114*, 10768; r) G. Mascolo, M. C. Mascolo, *Microporous Mesoporous Mater.* **2015**, *214*, 246; s) O. D. Pavel, D. Tichit, I.-C. Marcu, *Appl. Clay Sci.* **2012**, *61*, 52; t) J. S. Valente, H. Pfeiffer, E. Lima, J. Prince, J. Flores, *J. Catal.* **2011**, *279*, 196; u) S. Abelló, F. Medina, D. Tichit, J. Pérez-Ramírez, Y. Cesteros, P. Salagre, J. E. Sueiras, *Chem. Commun.* **2005**, 1453; v) K. Yamaguchi, K. Ebitani, T. Yoshida, H.

Yoshida, K. Kaneda, *J. Am. Chem. Soc.* **1999**, *121*, 4526; w) L. B. Kunde, S. M. Gade, V. S. Kalyani, S. P. Gupte, *Catal. Commun.* **2009**, *10*, 1881; x) J. Feng, Y. He, Y. Liu, Y. Du, D. Li, *Chem. Soc. Rev.* **2015**, *44*, 5291; y) B. M. Choudary, S. Madhi, N. S. Chowdari, M. L. Kantam, B. Sreedhar, *J. Am. Chem. Soc.* **2002**, *124*, 14127; z) T. H. Bennur, A. Ramani, R. Bal, B. M. Chanda, S. Sivasanker, *Catal. Commun.* **2002**, *3*, 493; aa) M. L. Kantam, S. Roy, M. Roy, B. Sreedhar, B. M. Choudary, R. L. De, *J. Mol. Catal. A Chem.* **2007**, *273*, 26; ab) N. Das, D. Tichit, R. Durand, P. Graffin, B. Coq, *Catal. Lett.* **2001**, *71*, 181; ac) K. Motokura, T. Mizugaki, K. Ebitani, K. Kaneda, *Tetrahedron Lett.* **2004**, *45*, 6029; ad) K. Motokura, D. Nishimura, K. Mori, T. Mizugaki, K. Ebitani, K. Kaneda, *J. Am. Chem. Soc.* **2004**, *126*, 5662.

[13] a) K. Motokura, *Bull. Chem. Soc. Jpn.* **2017**, *90*, 137; b) K. Motokura, *ChemCatChem* **2014**, *6*, 3067; c) K. Kaneda, K. Ebitani, T. Mizugaki, K. Mori, *Bull. Chem. Soc. Jpn.* **2006**, *79*, 981; d) W.-J. Yoo, H. Miyamura, S. Kobayashi, *J. Am. Chem. Soc.* **2011**, *133*, 3095; e) H. Miyamura, S. Kobayashi, *Acc. Chem. Res.* **2014**, *47*, 1054; f) B. M. Choudary, N. S. Chowdari, S. Madhi, M. L. Kantam, *J. Org. Chem.* **2003**, *68*, 1736; g) B. M. Choudary, N. S. Chowdari, K. Jyothi, N. S. Kumar, M. L. Kantam, *Chem. Commun.* **2002**, 586; h) B. M. Choudary, N. S. Chowdari, S. Madhi, M. L. Kantam, *Angew. Chem. Int. Ed.* **2001**, *40*, 4619; i) B. M. Choudary, S. Madhi, N. S. Chowdari, M. L. Kantam, *Top. Catal.* **2004**, *29*, 183; j) B. M. Choudary, K. Jyothi, M. L. Kantam, B. Steedhar, *Adv. Synth. Catal.* **2004**, *346*, 1471; k) K. Motokura, N. Fujita, K. Mori, T. Mizugaki, K. Ebitani, K. Kaneda, *Tetrahedron Lett.* **2005**, *46*, 5507; l) K. Motokura, N. Fujita, K. Mori, T. Mizugaki, K. Ebitani, K. Jitsukawa, K. Kaneda, *Chem. Eur. J.* **2006**, *12*, 8228; m) K. Motokura, T. Mizugaki, K. Ebitani, K. Kaneda, *Tetrahedron Lett.* **2004**, *45*, 6029; n) Y. Z. Chen, C. M. Hwang, C.W. Liaw, *Appl. Catal. A Gen.* **1998**, *169*, 207; o) N. R. Shiju, A. H. Alberts, S. Khalid, D. R. Brown, G. Rothenberg, *Angew. Chem. Int. Ed.* **2011**, *50*, 9615; p) M. J. Climent, A. Corma, S. Iborra, *Chem. Rev.* **2011**, *111*, 1072; q) Y.-B. Huang, J. Liang, X.-S. Wang, R. Cao, *Chem. Soc. Rev.* **2017**, *46*, 126; r) D. Y. Murzin, *Catal. Lett.* **2017**, *147*, 613; s) A. Corma, J. Navas, M. J. Sabater, *Chem. Rev.* **2018**, *118*, 1410.

[14] a) K. Motokura, M. Tada, Y. Iwasawa, *J. Am. Chem. Soc.* **2007**, *129*, 9540; b) K. Motokura, M. Tomita, M. Tada, Y. Iwasawa, *Chem. Eur. J.* **2008**, *14*, 4017; c) U. Díaz, D. Brunel, A. Corma, *Chem. Soc. Rev.* **2013**, *42*, 4083; d) R. Raja, M. E. Potter, S. H.

Newland, *Chem. Commun.* **2014**, 50, 5940; e) Q. Yang, Q. Xu, H.-L. Jiang, *Chem. Soc. Rev.* **2017**, 46, 4774.

[15] a) T. Oishi, K. Yamaguchi, N. Mizuno, *ACS Catal.* **2011**, 1, 1351; b) D. Yoshii, X. Jin, T. Yatabe, K. Yamaguchi, N. Mizuno, *Chem. Commun.* **2016**, 52, 14314; c) W. C. Conner, J. L. Falconer, *Chem. Rev.* **1995**, 95, 759; d) R. Prins, *Chem. Rev.* **2012**, 112, 2714; e) M. Choi, S. Yook, H. Kim, *ChemCatChem* **2015**, 7, 1048.

[16] a) Y. Du, H. Sheng, D. Astruc, M. Zhu, *Chem. Rev.* **2019**, 10.1021/acs.chemrev.8b00726; b) A. Corma, H. Garcia, *Supported Gold Nanoparticles as Oxidation Catalysts in Nanoparticles and Catalysis*, Didier Astruc, Ed.; Wiley-VCH, Weinheim, **2008**; c) C. D. Pina, E. Falletta, L. Prati, M. Rossi, *Chem. Soc. Rev.* **2008**, 37, 2077; d) M. Stratakis, H. Garcia, *Chem. Rev.* **2012**, 112, 4469; e) M. Haruta, T. Kobayashi, H. Sano, N. Yamada, *Chem. Lett.* **1987**, 16, 405; f) M. Haruta, N. Yamada, T. Kobayashi, S. Iijima, *J. Catal.* **1989**, 115, 301; g) C. Raptis, H. Garcia, M. Stratakis, *Angew. Chem. Int. Ed.* **2009**, 48, 3133; h) F. Shi, Q. Zhang, Y. Ma, Y. He, Y. Deng, *J. Am. Chem. Soc.* **2005**, 127, 4182; i) H. Tsunoyama, H. Sakurai, N. Ichikuni, Y. Negishi, T. Tsukuda, *Langmuir*, **2004**, 20, 11293; j) T. Mitsudome, A. Noudjima, T. Mizugaki, K. Jitsukawa, K. Kaneda, *Chem. Commun.* **2009**, 5302; k) Y. Mikami, A. Noudjima, T. Mitsudome, T. Mizugaki, K. Jitsukawa, K. Kaneda, *Chem. Eur. J.* **2011**, 17, 1768; l) A. Corma, C. Gonzalez-Arellano, M. Iglesias, F. Sanchez, *Angew. Chem. Int. Ed.* **2007**, 46, 7820; m) K. Yamaguchi, Y. Wang, T. Oishi, Y. Kuroda, N. Mizuno, *Angew. Chem. Int. Ed.* **2013**, 52, 5627; n) T. Mitsudome, A. Noudjima, T. Mizugaki, K. Jitsukawa, K. Kaneda, *Adv. Synth. Catal.* **2009**, 351, 1890; o) P. Liu, Y. Guan, R. A. van Santen, C. Li, E. J. M. Hensen, *Chem. Commun.* **2011**, 47, 11540; p) J. Wang, X. Lang, B. Zhaorigetu, M. Jia, J. Wang, X. Guo, J. Zhao, *ChemCatChem* **2014**, 6, 1737; q) T. Mitsudome, A. Noudjima, Y. Mikami, T. Mizugaki, K. Jitsukawa, K. Kaneda, *Angew. Chem. Int. Ed.* **2010**, 49, 5545; r) S. Nishimura, Y. Yakita, M. Katayama, K. Higashimine, K. Ebitani, *Catal. Sci. Technol.* **2013**, 3, 351; s) C. Shang, Z.-P. Liu, *J. Am. Chem. Soc.* **2011**, 133, 9938; t) T. Mitsudome, K. Kaneda, *Green Chem.* **2013**, 15, 2636; u) P. G. N. Merten, P. Vandezande, X. Ye, H. Poelman, I. F. J. Vankelecom, D. E. De Vos, *Appl. Catal. A* **2009**, 355, 176; v) X. Zhang, Y. C. Guo, Z. C. Zhang, J. S. Gao, C. M. Xu, *J. Catal.* **2012**, 292, 213; w) D. Ren, L. He, L. Yu, R.-S. Ding, Y.-M. Liu, Y. Cao, H.-Y. He, K.-N. Fan, *J. Am. Chem. Soc.* **2012**, 134, 17592; x) A. Noudjima, T. Mitsudome, T. Mizugaki, K. Jitsukawa,

K. Kaneda, *Angew. Chem. Int. Ed.* **2011**, *50*, 2986; y) T. Mitsudome, M. Yamamoto, Z. Maeno, T. Mizugaki, K. Jitsukawa, K. Kaneda, *J. Am. Chem. Soc.* **2015**, *137*, 13452; z) T. Mitsudome, Y. Mikami, M. Matoba, T. Mizugaki, K. Jitsukawa, K. Kaneda, *Angew. Chem. Int. Ed.* **2012**, *51*, 136; aa) T. Mitsudome, A. Noujima, T. Mizugaki, K. Jitsukawa, K. Kaneda, *Green Chem.* **2009**, *11*, 793; ab) A. Corma, J. Navas, M. J. Sabater, *Chem. Eur. J.* **2012**, *18*, 14150.

[17] a) I. N. Francesco, F. F.- Vive, S. Antoniotti, *ChemCatChem* **2014**, *6*, 2784; b) S. Furukawa, A. Suga, T. Komatsu, *ACS Catal.* **2015**, *5*, 1214; c) F. Gao, D. W. Goodman, *Chem. Soc. Rev.* **2012**, *41*, 8009; d) X. Zhu, Q. Guo, Y. Sun, S. Chen, J.-Q. Wang, M. Wu, W. Fu, Y. Tang, X. Duan, D. Chen, Y. Wan, *Nat. Commun.* **2019**, *10*, 1428; e) H. Miura, K. Endo, R. Ogawa, T. Shishido, *ACS Catal.* **2017**, *7*, 1543; f) P. Liu, J. K. Nørskov, *Phys. Chem. Chem. Phys.* **2001**, *3*, 3814; g) S. Furukawa, A. Yokoyama, T. Komatsu, *ACS Catal.* **2014**, *4*, 3581; h) S. Furukawa, K. Ochi, H. Luo, M. Miyazaki, T. Komatsu, *ChemCatChem* **2015**, *7*, 3472; i) A. Villa, D. Wang, D. S. Su, L. Prati, *Catal. Sci. Technol.* **2015**, *5*, 55; j) Z. Konuspayeva, P. Afanasiev, T.-S. Nguyen, L. D. Felice, F. Morfin, N.-T. Nguyen, J. Nelayah, C. Ricolleau, Z. Y. Li, J. Yuan, G. Berhault, L. Piccolo, *Phys. Chem. Chem. Phys.* **2015**, *17*, 28112; k) K. Taniguchi, X. Jin, K. Yamaguchi, N. Mizuno, *Chem. Commun.* **2015**, *51*, 14969; l) X. Jin, K. Taniguchi, K. Yamaguchi, N. Mizuno, *Chem. Sci.* **2016**, *7*, 5371; m) D. Wang, A. Villa, F. Porta, L. Prati, D. Su, *J. Phys. Chem. C* **2008**, *112*, 8617; n) T. Yasukawa, H. Miyamura, S. Kobayashi, *J. Am. Chem. Soc.* **2012**, *134*, 16963; o) C. Rossy, J. Majimel, E. Fouquet, C. Delacôte, M. Boujtita, C. Labrugère, M. Tréguer-Delapierre, F.-X. Felpin, *Chem. Eur. J.* **2013**, *19*, 14024; p) X. Wu, L. Tan, D. Chen, X. Meng, F. Tang, *Chem. Commun.* **2014**, *50*, 539; q) S. Karanjit, A. Jinasan, E. Samsook, R. N. Dhital, K. Motomiya, Y. Sato, K. Tohji, H. Sakurai, *Chem. Commun.* **2015**, *51*, 12724; r) R. N. Dhital, H. Sakurai, *Chem. Lett.* **2012**, *41*, 630; s) R. N. Dhital, C. Kamonsatikul, E. Somsook, K. Bobuatong, M. Ehara, S. Karanjit, H. Sakurai, *J. Am. Chem. Soc.* **2012**, *134*, 20250; t) B. Boekfa, E. Pahl, N. Gaston, H. Sakurai, J. Limtrakul, M. Ehara, *J. Phys. Chem. C* **2014**, *118*, 22188.

[18] a) R. A. Sheldon, R. S. Downing, *Appl. Catal. A Gen.* **1999**, *189*, 163; b) F.-X. Felpin, E. Fouquet, *ChemSusChem* **2008**, *1*, 718; c) C. Yu, J. He, *Chem. Commun.* **2012**, *48*, 4933; d) T. L. Lohr, T. J. Marks, *Nat. Chem.* **2015**, *7*, 477; e) T. Tsubogo, H.

Oyamada, S. Kobayashi, *Nature* **2015**, 520, 329; f) T. Tsubogo, T. Ishiwata, S. Kobayashi, *Angew. Chem. Int. Ed.* **2013**, 52, 6590; g) J. C. Pastre, D. L. Browne, S. V. Ley, *Chem. Soc. Rev.* **2013**, 42, 8849; h) C. G. Frost, L. Mutton, *Green Chem.* **2010**, 12, 1687; i) *Catalysts for Fine Chemical Synthesis*, E. G. Derouane, Ed.; John Wiley & Sons Ltd, The Atrium, Southern Gate, Chichester, West Sussex, PO19 8SQ, England, **2006**; Vol. 4; j) T. Mallat, A. Baiker, *Chem. Rev.* **2004**, 104, 3037; k) *Chiral Catalyst Immobilization and Recycling*, D. E. De Vos, I. F. J. Vankelecom, P. A. Jacobs, Eds.; Wiley-VCH Verlagsgesellschaft GmbH, D-69469 Weinheim, **2000**; l) D. E. De Vos, M. Dams, B. F. Sels, P. A. Jacobs, *Chem. Rev.* **2002**, 102, 3615; m) T. Kitanosono, K. Masuda, P. Xu, S. Kobayashi, *Chem. Rev.* **2018**, 118, 679; n) W. Wang, L. Cui, P. Sun, L. Shi, C. Yue, F. Li, *Chem. Rev.* **2018**, 118, 9843; o) A. J. Sandee, L. A. van der Veen, J. N. H. Reek, P. C. J. Kamer, M. Lutz, A. L. Spek, P. W. N. M. van Leeuwen, *Angew. Chem. Int. Ed.* **1999**, 38, 3231; p) Y. Uozumi, H. Danjo, T. Hayashi, *J. Org. Chem.* **1999**, 64, 3384; q) J. C. Serrano-Ruiz, R. Luque, A. Sepúlveda-Escribano, *Chem. Soc. Rev.* **2011**, 40, 5266; r) C.-H. Zhou, X. Xia, C.-X. Lin, D.-S. Tong, J. Beltramini, *Chem. Soc. Rev.* **2011**, 40, 5588; s) D. M. Alonso, S. G. Wettstein, J. A. Dumesic, *Chem. Soc. Rev.* **2012**, 41, 8075; t) P. Lanzafame, G. Centi, S. Perathoner, *Chem. Soc. Rev.* **2014**, 43, 7562; u) D. Esposito, M. Antonietti, *Chem. Soc. Rev.* **2015**, 44, 5821; v) S. Chen, R. Wojcieszak, F. Dumeignil, E. Marceau, S. Royer, *Chem. Rev.* **2018**, 118, 11023; w) K. Gupta, R. K. Rai, S. K. Singh, *ChemCatChem* **2018**, 10, 2326; x) Z. Zhang, G. W. Huber, *Chem. Soc. Rev.* **2018**, 47, 1351; y) P. Sudarsanam, R. Zhong, S. Van den Bosch, S. M. Coman, V. I. Parvulescu, B. F. Sels, *Chem. Soc. Rev.* **2018**, 47, 8349; z) P. Sudarsanam, E. Peeters, E. V. Makshina, V. I. Parvulescu, B. F. Sels, *Chem. Soc. Rev.* **2019**, 48, 2366.

[19] a) T. Mitsudome, K. Miyagawa, Z. Maeno, T. Mizugaki, K. Jitsukawa, J. Yamasaki, Y. Kitagawa, K. Kaneda, *Angew. Chem. Int. Ed.* **2017**, 56, 9381; b) Y. Wang, D. Zhu, L. Tang, S. Wang, Z. Wang, *Angew. Chem. Int. Ed.* **2011**, 50, 8917; c) J.-F. Soulé, H. Miyamura, S. Kobayashi, *J. Am. Chem. Soc.* **2011**, 133, 18550; d) T. Komanoya, T. Kinemura, Y. Kita, K. Kamata, M. Hara, *J. Am. Chem. Soc.* **2017**, 139, 11493; e) R. V. Jagadeesh, K. Murugesan, A. S. Alshammari, H. Neumann, M.-M. Pohl, J. Radnik, M. Beller, *Science* **2017**, 358, 326; f) Y. Izawa, D. Pun, S. S. Stahl, *Science* **2011**, 333, 209; g) D. Pun, T. Diao, S. S. Stahl, *J. Am. Chem. Soc.* **2013**, 135, 8213; h) J. Zhang, Q. Jiang, D. Yang, X. Zhao, Y. Dong, R. Liu, *Chem. Sci.* **2015**, 6, 4674; i) Z. Chen, H. Zeng, S. A.

Girard, F. Wang, N. Chen, C.-J. Li, *Angew. Chem. Int. Ed.* **2015**, *54*, 14487; j) H. Miura, K. Tsutsui, K. Wada, T. Shishido, *Chem. Commun.* **2015**, *51*, 1654; k) H. Miura, K. Takeuchi, T. Shishido, *Angew. Chem. Int. Ed.* **2016**, *55*, 278; l) F. Xie, G.-P. Lu, R. Xie, Q.-H. Chen, H.-F. Jiang, M. Zhang, *ACS Catal.* **2019**, *9*, 2718.

[20] For reviews on catalytic selective transformations, see: a) H.-U. Blaser, C. Malan, B. Pugin, F. Spindler, H. Steiner, M. Studer, *Adv. Synth. Catal.* **2003**, *345*, 103; b) X. Cui, K. Burgess, *Chem. Rev.* **2005**, *105*, 3272; c) J. Mahatthananchai, A. M. Dumas, J. W. Bode, *Angew. Chem. Int. Ed.* **2012**, *51*, 10954; d) S. R. Neufeldt, M. S. Sanford, *Acc. Chem. Res.* **2012**, *45*, 936; e) L. Souillart, N. Cramer, *Chem. Rev.* **2015**, *115*, 9410; f) X.-P. Zeng, Z.-Y. Cao, Y.-H. Wang, F. Zhou, J. Zhou, *Chem. Rev.* **2016**, *116*, 7330; g) J. A. Leitch, C. G. Frost, *Chem. Soc. Rev.* **2017**, *46*, 7145; h) C. G. Newton, S.-G. Wang, C. C. Oliveira, N. Cramer, *Chem. Rev.* **2017**, *117*, 8908; i) Y. Park, Y. Kim, S. Chang, *Chem. Rev.* **2017**, *117*, 9247; j) K. P. Bryliakov, *Chem. Rev.* **2017**, *117*, 11406; k) C. Sambigiagio, D. Schönbauer, R. Blieck, T. Dao-Huy, G. Pototschnig, P. Schaaf, T. Wiesinger, M. F. Zia, J. Wencel-Delord, T. Besset, B. U. W. Maes, M. Schnürch, *Chem. Soc. Rev.* **2018**, *47*, 6603; l) P. Sivaguru, Z. Wang, G. Zanoni, X. Bi, *Chem. Soc. Rev.* **2019**, *48*, 2615.

[21] For recent examples of catalytic selective transformations, see: a) J. Zhao, T. Nanjo, E. C. de Lucca Jr, M. C. White, *Nat. Chem.* **2019**, *11*, 213; b) P. Hu, M. Tan, L. Cheng, H. Zhao, R. Feng, W.-J. Gu, W. Han, *Nat. Commun.* **2019**, *10*, 2425; c) A. M. Matínez-Gualda, R. Cano, L. Marzo, R. Pérez-Ruiz, J. Luis-Barrera, R. Mas-Bellesté, A. Fraile, V. A. de la Peña O'Shea, J. Alemán, *Nat. Commun.* **2019**, *10*, 2634; d) A. J. Boyington, C. P. Seath, A. M. Zearfoss, Z. Xu, N. T. Jui, *J. Am. Chem. Soc.* **2019**, *141*, 4147; e) B. S. Schreib, E. M. Carreira, *J. Am. Chem. Soc.* **2019**, *141*, 8758; f) S. A. Blaszczyk, G. Xiao, P. Wen, H. Hao, J. Wu, B. Wang, F. Carattino, Z. Li, D. A. Glazier, B. J. McCarty, P. Liu, W. Tang, *Angew. Chem. Int. Ed.* **2019**, *58*, 9542; g) P. Zheng, C. Wang, Y.-C. Chen, G. Dong, *ACS Catal.* **2019**, *9*, 5515; h) D.-W. Ji, Y.-C. Hu, H. Zheng, C.-Y. Zhao, Q.-A. Chen, V. M. Dong, *Chem. Sci.* **2019**, *10*, 6311; i) S. Wei, L. Yin, S. R. Wang, Y. Tang, *Org. Lett.* **2019**, *21*, 1458; j) M.-Q. Tian, C. Wang, X.-H. Hu, T.-P. Loh, *Org. Lett.* **2019**, *21*, 1607; k) J. Sun, D. Bai, P. Wang, K. Wang, G. Zheng, X. Li, *Org. Lett.* **2019**, *21*, 1789; l) M. Mei, D. Anand, L. Zhou, *Org. Lett.* **2019**, *21*, 3548; m) Ryan J. Scamp, Bradley Scheffer, Jennifer M. Schomaker, *Chem. Commun.* **2019**, *55*, 7362.

Chapter II

Transition-Metal-Free Selective Formal Hydroacylation of Terminal Alkynes Catalyzed by Layered Double Hydroxide

Adapted with permission from *ACS Catal.* **2018**, 8(12), 11564–11569.

Copyright 2018 American Chemical Society.

2.1. Introduction

Hydroacylation, which is the transformation of aldehydes into ketones without any byproducts, is an important, efficient, and environmentally friendly method of C–C bond formation from C–H bonds.^[1] In particular, many examples of alkynes/alkenes hydroacylation using transition metals, mainly Rh, as catalysts have been reported (Figure 2-1).^[1–3] However, this system still presents several problems, especially for intermolecular hydroacylation, owing to the intrinsic mechanism of Rh-catalyzed hydroacylation; (a) the use of precious metals, (b) competing decarbonylation of acylrhodium intermediates, and (c) difficulty in controlling the regioselectivity of insertion into alkynes/alkenes. Accordingly, the development of alternative catalytic hydroacylation systems is required to avoid these problems.^[1d]

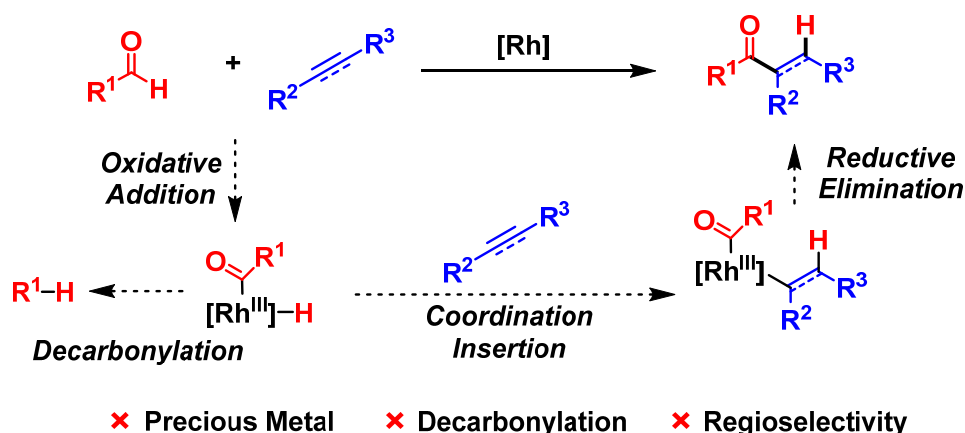


Figure 2-1. Classical Rh-catalyzed hydroacylation.

Alkenes/alkynes can be classified into four kinds, *i.e.*, internal alkenes, terminal alkenes, internal alkynes, and terminal alkynes. Among them, only terminal alkynes can be utilized as nucleophilic reagents after deprotonation. Recently, Hashmi *et al.* pioneered Au-catalyzed formal hydroacylation of terminal alkynes (defined as the hydroacylation affording the same product as the classical one catalyzed by Rh) using glyoxals as the aldehydes through aldehyde–alkyne–amine coupling (A³-coupling) and hydration (workup), which is completely different from classical Rh-catalyzed hydroacylation (Figure 2-2).^[4] Before Hashmi's report, the literature contains one report for Cu nanoparticles-catalyzed formal hydroacylation; however, the substrate scope was only limited to 2-formyl pyridine (or quinoline) and the reaction mechanism was unknown.^[5] Since this formal hydroacylation does not involve an oxidative addition

step or an insertion step, no decarbonylation or regioselectivity problems are observed. Since then, precious metal-free formal hydroacylation reactions using Cu catalysts have been developed.^[6] However, these A³-coupling systems require the use of transition-metal catalysts and (super)-stoichiometric amounts of amines.

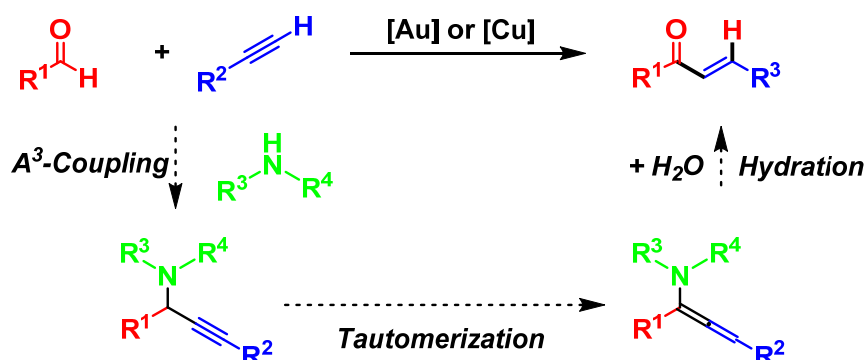


Figure 2-2. Formal hydroacylation of terminal alkynes *via* A³-coupling.^[5–8]

Interestingly, when the Favorskii reaction,^[7] *i.e.*, the addition of terminal alkynes to carbonyl compounds to afford propargylic alcohols using strong bases, *e.g.*, KOH,^[7a,b] *t*-BuOK,^[7c,e] and Bu₄NOH,^[7f] is performed using an aromatic aldehyde as the substrate, the side reaction to produce an α,β-unsaturated carbonyl compound occurs.^[8] This side reaction can be regarded as a transitionmetal-free formal hydroacylation; however, these systems require strong basic conditions, and the substrate scopes are quite limited (Figure 2-3).

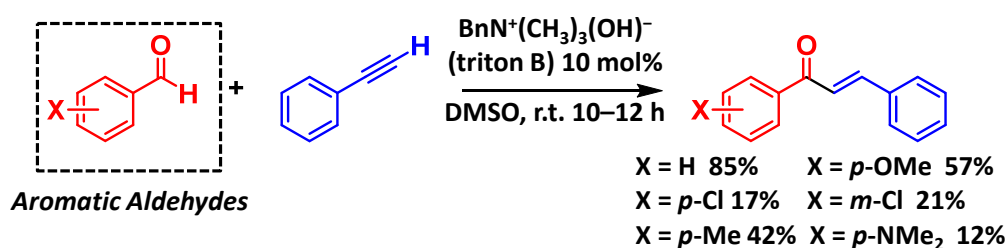
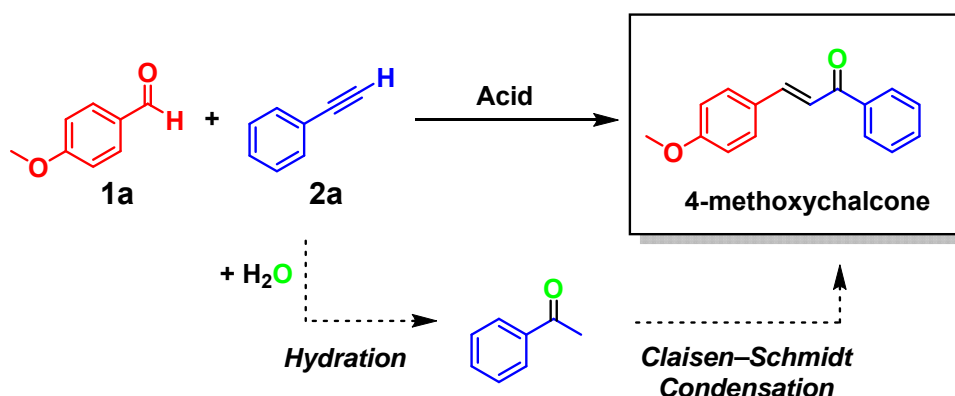


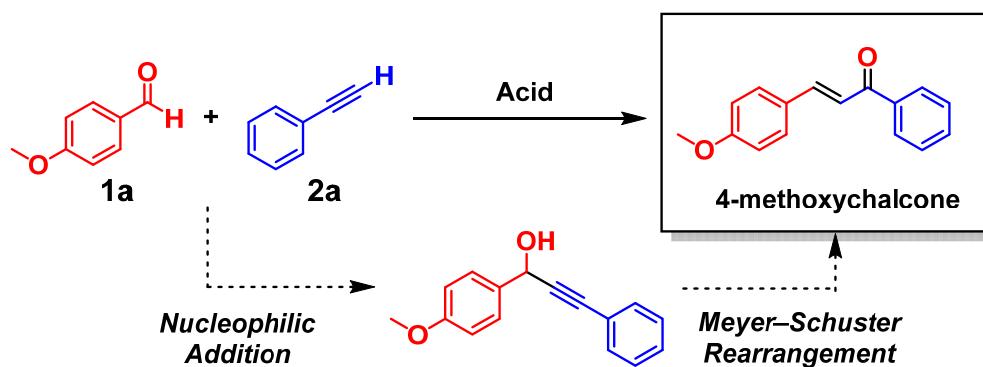
Figure 2-3. Formal hydroacylation *via* Favorskii reaction reported by Ishikawa *et al.*^[8b]

In addition, there are different procedures of aldehyde–alkyne couplings to produce enones such as hydration/aldol condensation,^[9a–c] nucleophilic addition/Meyer–Schuster rearrangement,^[9d,e] and aldehyde–alkyne metathesis^[9f–i]; however, the products possess substituent patterns opposite to those obtained by formal hydroacylation (Figure 2-4).

(a) Hydration/Aldol Condensation: NOT "Formal Hydroacylation"



(b) Addition/Meyer–Schuster Rearrangement: NOT "Formal Hydroacylation"



(c) Aldehyde–Alkyne Metathesis: NOT "Formal Hydroacylation"

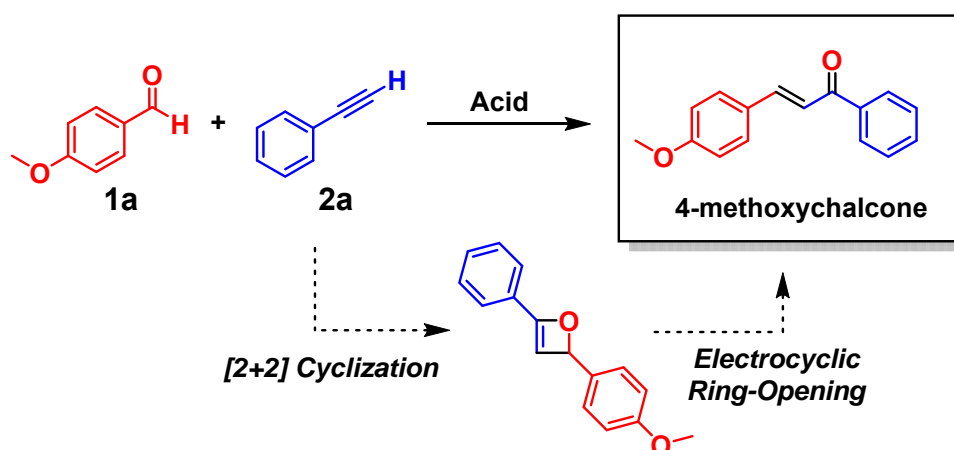


Figure 2-4. Different aldehyde–alkyne couplings using *p*-anisaldehyde (1a) and phenylacetylene (2a); (a) enone synthesis through hydration/aldol condensation, (b) enone synthesis through nucleophilic addition/Meyer–Schuster rearrangement, and (c) enone synthesis through aldehyde–alkyne metathesis.

In this chapter, I successfully achieved, for the first time, transition-metal-free formal hydroacylation of terminal alkynes catalyzed by a commercially available $\text{Mg}_3\text{Al-CO}_3$ -layered double hydroxide ($\text{Mg}_6\text{Al}_2(\text{OH})_{16}(\text{CO}_3)\cdot 4\text{H}_2\text{O}$, hereafter termed $\text{Mg}_3\text{Al-CO}_3$ LDH) through nucleophilic addition/prototropy utilizing the unique basic sites and ionicity of $\text{Mg}_3\text{Al-CO}_3$ LDH (Figure 2-5). As shown in Chapter I, $\text{Mg}_3\text{Al-CO}_3$ LDH is well-known as a solid base catalyst and is composed of cationic metal hydroxide layers ($[\text{Mg}_6\text{Al}_2(\text{OH})_{16}]^{2+}$) and hydrated anion layers ($[(\text{CO}_3)\cdot 4\text{H}_2\text{O}]^{2-}$) (see section 1.1.4.1. and the references of [12] in Chapter I). However, to the best of my knowledge, nucleophilic addition of alkynes or prototropy in propargylic alcohols promoted by $\text{Mg}_3\text{Al-CO}_3$ LDH has not been reported. $\text{Mg}_3\text{Al-CO}_3$ LDH shows moderate basicity compared to the strong bases typically used for the Favorskii reaction. This indicates a broad substrate scope in this system, which I have demonstrated using 22 examples including ester or cyano groups. In addition, the present catalysis is truly heterogeneous and the LDH catalyst can be reused without severe loss of its catalytic activity; thus, the system is also environmentally friendly.

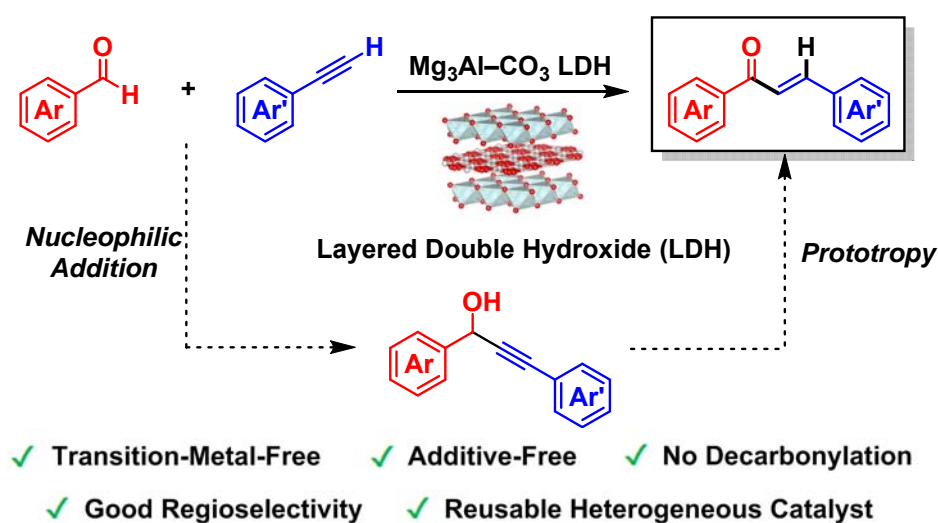


Figure 2-5. This work: $\text{Mg}_3\text{Al-CO}_3$ LDH-catalyzed formal hydroacylation.

2.2. Experimental

2.2.1. Instruments and Reagents

GC analyses were performed on Shimadzu GC-2014 with a FID detector equipped with a TC-5 capillary column. GC-MS spectra were recorded on Shimadzu GCMS-QP2010 equipped with an InertCap5 capillary column at an ionization voltage of 70 eV. Liquid-state ^1H , ^{13}C , and ^{19}F NMR spectra were recorded on JEOL JNM-ECA 500. ^1H and ^{13}C NMR were measured at 500 and 125 MHz, respectively, with TMS as an internal standard ($\delta = 0$ ppm). ^{19}F NMR was measured at 470 MHz with benzotrifluoride as an external standard ($\delta = -63.72$ ppm). ICP-AES analyses were performed on Shimadzu ICPS-8100. DR UV-Vis spectra were recorded on a JASCO V-570DS. XRD patterns were recorded using a Rigaku SmartLab instrument under Cu K α radiation (45 kV, 200 mA). BET surface areas were measured on micromeritics ASAP 2010 and calculated from the N $_2$ adsorption isotherm with the BET equation. IR spectra were measured on JASCO FT/IR-4100 using KBr disks. Raman spectra were recorded on a JASCO NRS-5100 spectrometer using a 633 nm laser. Elemental analyses for C, H, and N were performed on Elementar vario MICRO cube. Elemental analysis for Cl was performed on Thermo Fisher Scientific ICS-1600. $\text{Mg}_6\text{Al}_2(\text{OH})_{16}(\text{CO}_3) \cdot 4\text{H}_2\text{O}$ (47 m 2 g $^{-1}$, Cat. No. Tomita-AD 500, Tomita Pharmaceutical), hydroxyapatite (11 m 2 g $^{-1}$, Cat. No. 011-14882, FUJIFILM Wako), MgO (38 m 2 g $^{-1}$ after calcination at 600 °C for 2 h, Cat. No. 137-10831, FUJIFILM Wako), CaO (15 m 2 g $^{-1}$ after calcination at 600 °C for 2 h, Cat. No. 036-19655, FUJIFILM Wako), ZnO (7 m 2 g $^{-1}$ after calcination at 600 °C for 2 h, Cat. No. 265-00971, FUJIFILM Wako), CeO $_2$ (45 m 2 g $^{-1}$ after calcination at 600 °C for 2 h, Cat. No. 544841-25G, Aldrich), ZrO $_2$ (48 m 2 g $^{-1}$ after calcination at 600 °C for 2 h, Cat. No. JRC-ZRO-6, Catalysis Society of Japan), Al $_2$ O $_3$ (183 m 2 g $^{-1}$ after calcination at 600 °C for 2 h, Cat. No. KHS-24, Sumitomo Chemical), TiO $_2$ (66 m 2 g $^{-1}$ after calcination at 600 °C for 2 h, Cat. No. ST-01, Ishihara Sangyo Kaisha), and Ca(OH) $_2$ (Cat. No. 07069-00, Kanto Chemical) were commercially available. Solvents, substrates, and metal sources were obtained from Kanto Chemical, TCI, Wako, Nacalai Tesque, or Aldrich (reagent grade). Several substrates were purified by kugelrohr distillation just before the use for reactions.

2.2.2. Preparation of Catalysts

Preparation of $\text{Mg}_2\text{Al}-\text{CO}_3$ LDH: The $\text{Mg}_4\text{Al}_2(\text{OH})_{12}(\text{CO}_3) \cdot n\text{H}_2\text{O}$ ($\text{Mg}_2\text{Al}-\text{CO}_3$ LDH) was prepared as follows according to the previous report.^[10] An aqueous solution (60 mL) of $\text{MgCl}_2 \cdot 6\text{H}_2\text{O}$ (4.06 g) and $\text{AlCl}_3 \cdot 6\text{H}_2\text{O}$ (2.42 g) was gradually added into an aqueous solution of Na_2CO_3 (0.1 M, 100 mL) while the pH of the solution was retained ~ 10.0 using an aqueous solution of NaOH (2 M). After completing the addition, the mixture was stirred at 80°C for 14 h. The obtained slurry was filtrated, washed with deionized water (1 L), and dried at 80°C for 6 h, affording the desired $\text{Mg}_2\text{Al}-\text{CO}_3$ LDH ($100.6\text{ m}^2\text{ g}^{-1}$, 2.2 g, Mg/Al molar ratio determined by ICP-AES = 2.1). The $\text{Mg}_8\text{Al}_2(\text{OH})_{20}(\text{CO}_3) \cdot n\text{H}_2\text{O}$ ($\text{Mg}_4\text{Al}-\text{CO}_3$ LDH) was prepared in the same method (1.6 g, Mg/Al molar ratio = 4.0) using an aqueous solution (30 mL) of $\text{MgCl}_2 \cdot 6\text{H}_2\text{O}$ (4.06 g) and $\text{AlCl}_3 \cdot 6\text{H}_2\text{O}$ (1.21 g), and an aqueous solution of Na_2CO_3 (0.1 M, 50 mL).

Preparation of $\text{Mg}_3\text{Al}-\text{Cl}$ LDH: The $\text{Mg}_6\text{Al}_2(\text{OH})_{16}\text{Cl}_{1.6}(\text{CO}_3)_{0.2} \cdot n\text{H}_2\text{O}$ ($\text{Mg}_3\text{Al}-\text{Cl}$ LDH) was prepared as follows according to the previous report.^[11] $\text{MgCl}_2 \cdot 6\text{H}_2\text{O}$ (15.2 g) and $\text{AlCl}_3 \cdot 6\text{H}_2\text{O}$ (6.04 g) were dissolved into decarbonated water (100 mL). Into the solution was gradually added an aqueous solution of NaOH (2 M, 100 mL) under an Ar flow while the pH of the solution was retained ~ 10.0 using an aqueous solution of HCl . After adding all of the NaOH solution, the mixture was stirred at 70°C for 18 h with an Ar balloon (1 atm). The slurry was filtrated, washed with decarbonated water (500 mL), and dried at overnight, affording the desired $\text{Mg}_3\text{Al}-\text{Cl}$ LDH (6.2 g, Mg/Al molar ratio determined by ICP-AES = 2.9, Mg: 22.1wt%, Al: 8.36wt%, Cl: 8.90wt%). When NaCl remained in the obtained LDH, the LDH was dispersed into decarbonated water (200 mL) and stirred for 15 min, and then the white powder was retrieved in the above-mentioned manner, giving the pure $\text{Mg}_3\text{Al}-\text{Cl}$ LDH.

Preparation of $\text{Mg}(\text{OH})_2$: The $\text{Mg}(\text{OH})_2$ was prepared as follows. An aqueous solution (60 mL) of $\text{MgCl}_2 \cdot 6\text{H}_2\text{O}$ (3.1 g) was gradually added into an aqueous solution of NaOH (50 mL, pH = ~ 10) while the pH of the solution was retained ~ 11 using an aqueous solution of NaOH (2 M). After completing the addition, the mixture was stirred at 80°C for 24 h. The obtained slurry was filtrated, washed with deionized water (1 L), and dried at 80°C overnight, affording the desired $\text{Mg}(\text{OH})_2$ (0.62 g).

2.2.3. Reactions and Synthesis

Catalytic reaction: The catalytic reaction was typically carried out according to the following procedure. Into a glass schlenk tube (volume: ~20 mL) were successively added $\text{Mg}_3\text{Al-CO}_3$ LDH (130 mg), biphenyl (0.1 mmol, internal standard), *p*-anisaldehyde (**1a**, 0.5 mmol), phenylacetylene (**2a**, 0.5 mmol), toluene (2 mL), and a Teflon-coated magnetic stir bar. Through freeze-pump-thaw cycling, the dissolved gases were removed from the solution, and the atmosphere was replaced into an Ar atmosphere; the mixture was then stirred at 120 °C for 15 h under an Ar atmosphere with a balloon. The yields of products were determined by GC analysis using biphenyl as an internal standard. With respect to the isolation of products, after the reaction, the catalyst was removed by simple filtration and the filtrate was then concentrated by evaporation of toluene. The crude product was subjected to column chromatography on silica gel (typically using EtOAc/hexane = 2/8 as an eluent), giving the pure hydroacylated products.

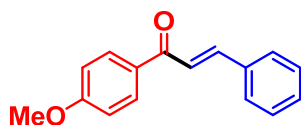
Leaching Test: To verify whether the catalytic reaction occurred on solid $\text{Mg}_3\text{Al-CO}_3$ LDH or not, the catalyst was removed by hot filtration 20 min after the reaction started under the optimized conditions and the reaction was again carried out with the filtrate under the same conditions. When the amount of leached metals was measured, the filtrate after the reaction for 15 h was evaporated *in vacuo*, treated with concentrated HNO_3 (1 mL), and sonicated. Then, Mg and Al species in the filtrate were analyzed by ICP-AES after the filtrate was moved into a 10 mL volumetric flask.

Reuse Test: Four runs under the optimized conditions were performed for three reuses not to change the amount of catalysts used for the respective reuses. After the reaction, $\text{Mg}_3\text{Al-CO}_3$ LDH was retrieved from the reaction mixture by simple filtration using a PTFE membrane filter. The retrieved $\text{Mg}_3\text{Al-CO}_3$ LDH catalyst after the reaction was washed with acetone (25 mL/run) and dried *in vacuo*. Then, 4–*N* runs were performed for the *N*th reuse, *i.e.*, three runs under the optimized conditions were performed for the first reuse using the retrieved catalyst. These reuse experiments were repeated until the third reuse.

Synthesis of benzaldehyde- α -d₁ (D-1d): Benzaldehyde- α -d₁ (D-1d) was synthesized in the following method. Benzylalcohol- α,α -d₂ (2.7 mmol) and Ru(OH)_x/Al₂O₃ (0.2 g, prepared referring to the previous report)^[12] were added to toluene (10 mL), and stirred for 4 h at 80 °C under an O₂ atmosphere with a balloon. After filtrating Ru(OH)_x/Al₂O₃, washing with toluene, and drying with Na₂SO₄, the solution was condensed till ~1 mL under reduced pressure. Benzaldehyde- α -d₁ was obtained as the mixture with toluene to inhibit the auto-oxidation (deuterated ratio: >99%, molar ratio: benzaldehyde- α -d₁/toluene = 1/0.32).

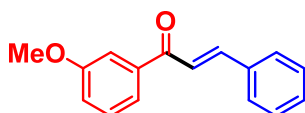
¹H NMR (500 MHz, CDCl₃, TMS): δ 7.51–7.56 (m, 2H), 7.63 (tdd, J = 7.0, 1.5 and 1.5 Hz, 1H), 7.87–7.91 (m, 2H).

2.2.4. Spectral Data of Products



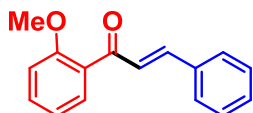
3aa (CAS No. 22966-19-4) (Eluent: EtOAc/hexane = 2/8)

(E)-4'-methoxychalcone (3aa): ^1H NMR (500 MHz, CDCl_3 , TMS): δ 3.88 (s, 3H), 6.97–7.00 (m, 2H), 7.38–7.43 (m, 3H), 7.55 (d, $J = 15.5$ Hz, 1H), 7.62–7.66 (m, 2H), 7.80 (d, $J = 15.5$ Hz, 1H), 8.03–8.06 (m, 2H). ^{13}C - $\{^1\text{H}\}$ NMR (125 MHz, CDCl_3 , TMS): δ 55.6, 114.0, 122.0, 128.5, 129.0, 130.4, 130.9, 131.2, 135.2, 144.1, 163.5, 188.8. MS (70 eV, EI): m/z (%): 239 (16), 238 (100) [M^+], 237 (80), 223 (18), 210 (13), 195 (15), 167 (13), 165 (12), 135 (67), 131 (16), 107 (16), 103 (29), 92 (24), 77 (62), 64 (13), 63 (11), 51 (14).



3ba (CAS No. 22966-24-1) (Eluent: EtOAc/hexane = 2/8)

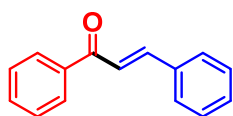
(E)-3'-methoxychalcone (3ba): ^1H NMR (500 MHz, CDCl_3 , TMS): δ 3.85 (s, 3H), 7.11 (ddd, $J = 8.5, 3.0$, and 1.0 Hz, 1H), 7.37–7.41 (m, 4H), 7.50 (d, $J = 15.5$ Hz, 1H), 7.54–7.55 (m, 1H), 7.59 (ddd, $J = 7.5, 1.0$, and 1.0 Hz, 1H), 7.61–7.64 (m, 2H), 7.80 (d, $J = 15.5$ Hz, 1H). ^{13}C - $\{^1\text{H}\}$ NMR (125 MHz, CDCl_3 , TMS): δ 55.5, 112.9, 119.3, 121.1, 122.1, 128.5, 129.0, 129.6, 130.6, 134.9, 139.6, 144.9, 159.9, 190.2. MS (70 eV, EI): m/z (%): 239 (16), 238 (96) [M^+], 237 (100), 223 (12), 135 (24), 131 (49), 107 (21), 103 (55), 102 (10), 92 (19), 77 (63), 64 (14), 63 (12), 51 (15).



3ca (CAS No. 40524-62-7) (Eluent: EtOAc/hexane = 2/8)

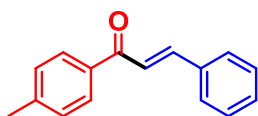
(E)-2'-methoxychalcone (3ca): ^1H NMR (500 MHz, CDCl_3 , TMS): δ 3.86 (s, 3H), 6.96–6.99 (m, 1H), 7.02 (td, $J = 7.5$ and 1.0 Hz, 1H), 7.35–7.39 (m, 4H), 7.43–7.47 (m, 1H), 7.55–7.59 (m, 2H), 7.62 (dd, $J = 7.5$ and 2.0 Hz, 1H), 7.62 (d, $J = 15.5$ Hz, 1H). ^{13}C - $\{^1\text{H}\}$ NMR (125 MHz, CDCl_3 , TMS): δ 55.8, 111.7, 120.8, 127.1, 128.4, 128.9, 129.2, 130.28, 130.35, 132.9, 135.1, 143.2, 158.1, 193.0. MS (70 eV, EI): m/z (%): 238

(50) [M^+], 237 (54), 223 (19), 221 (10), 219 (11), 179 (16), 178 (11), 167 (13), 165 (14), 160 (12), 152 (10), 147 (22), 135 (64), 131 (36), 121 (22), 120 (26), 119 (13), 105 (13), 104 (15), 103 (54), 102 (15), 92 (34), 91 (47), 78 (10), 77 (100), 76 (16), 64 (12), 63 (14), 51 (27).



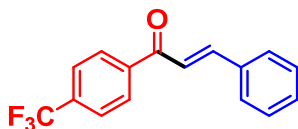
3da (CAS No. 614-47-1) (Eluent: EtOAc/hexane = 1/9)

(E)-chalcone (3da): ^1H NMR (500 MHz, CDCl_3 , TMS): δ 7.38–7.42 (m, 3H), 7.47–7.51 (m, 2H), 7.53 (d, J = 15.5 Hz, 1H), 7.57 (tdd, J = 7.5, 1.5 and 1.5 Hz, 1H), 7.61–7.65 (m, 2H), 7.81 (d, J = 15.5 Hz, 1H), 8.01–8.03 (m, 2H). ^{13}C – $\{^1\text{H}\}$ NMR (125 MHz, CDCl_3 , TMS): δ 122.1, 128.5, 128.6, 128.7, 129.0, 130.6, 132.9, 134.9, 138.2, 144.9, 190.6. MS (70 eV, EI): m/z (%): 209 (12), 208 (79) [M^+], 207 (100), 179 (23), 178 (12), 165 (12), 131 (43), 130 (16), 105 (35), 103 (46), 102 (16), 89 (11), 77 (97), 76 (13), 51 (36), 50 (10). This MS spectral data accords with that in the previous report.^[13]



3ea (CAS No. 14802-30-3) (Eluent: EtOAc/hexane = 1/9)

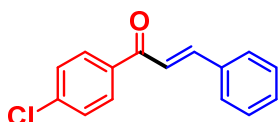
(E)-4'-methylchalcone (3ea): ^1H NMR (500 MHz, CDCl_3 , TMS): δ 2.41 (s, 3H), 7.27–7.29 (m, 2H), 7.36–7.42 (m, 3H), 7.52 (d, J = 15.5 Hz, 1H), 7.59–7.64 (m, 2H), 7.79 (d, J = 15.5 Hz, 1H), 7.92–7.94 (m, 2H). ^{13}C – $\{^1\text{H}\}$ NMR (125 MHz, CDCl_3 , TMS): δ 21.7, 122.1, 128.5, 128.7, 129.0, 129.4, 130.5, 135.0, 135.6, 143.7, 144.4, 190.0. MS (70 eV, EI): m/z (%): 223 (15), 222 (88) [M^+], 221 (100), 207 (26), 179 (28), 178 (19), 144 (10), 131 (28), 119 (49), 103 (35), 102 (10), 96 (11), 91 (55), 77 (35), 65 (30), 51 (16). This MS spectral data accords with that obtained from Wiley Subscription Services, Inc.



3fa (CAS No. 32120-33-5) (Eluent: CHCl_3 /hexane = 2/8)

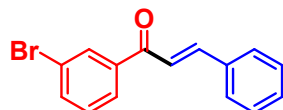
(E)-4'-(trifluoromethyl)chalcone (3fa): ^1H NMR (500 MHz, CDCl_3 , TMS): δ 7.41–7.45 (m, 3H), 7.49 (d, J = 15.5 Hz, 1H), 7.62–7.66 (m, 2H), 7.74–7.77 (m, 2H), 7.82 (d,

$J = 15.5$ Hz, 1H), 8.08–8.11 (m, 2H). $^{13}\text{C}-\{^1\text{H}\}$ NMR (125 MHz, CDCl_3 , TMS): δ 121.6, 123.8 (q, $J = 270.6$ Hz), 125.8, 128.7, 128.9, 129.2, 131.1, 134.1 (q, $J = 32.3$ Hz), 134.6, 141.1, 146.2, 189.7. ^{19}F NMR (470 MHz, CDCl_3 , benzotrifluoride): δ -64.2. MS (70 eV, EI): m/z (%): 277 (10), 276 (69) [M^+], 275 (100), 207 (14), 179 (12), 178 (11), 173 (13), 145 (39), 131 (37), 103 (44), 77 (35), 51 (14). This MS spectral data accords with that in the previous report.^[13]



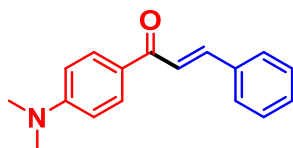
3ga (CAS No. 22966-22-9) (Eluent: EtOAc/hexane = 1/9)

(E)-4'-chlorochalcone (3ga): ^1H NMR (500 MHz, CDCl_3 , TMS): δ 7.38–7.41 (m, 3H), 7.43–7.45 (m, 2H), 7.47 (d, $J = 15.5$ Hz, 1H), 7.60–7.63 (m, 2H), 7.79 (d, $J = 15.5$ Hz, 1H), 7.92–7.96 (m, 2H). $^{13}\text{C}-\{^1\text{H}\}$ NMR (125 MHz, CDCl_3 , TMS): δ 121.4, 128.6, 128.96, 129.04, 130.0, 130.8, 134.7, 136.5, 139.2, 145.3, 189.1. MS (70 eV, EI): m/z (%): 244 (23), 243 (41) [M^+], 242 (67), 241 (100), 207 (46), 179 (19), 178 (24), 141 (11), 139 (32), 131 (36), 113 (13), 111 (41), 103 (48), 102 (13), 89 (21), 77 (45), 76 (21), 75 (28), 51 (22), 50 (12). This MS spectral data accords with that obtained from Wiley Subscription Services, Inc.



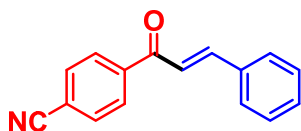
3ha (CAS No. 22966-26-3) (Eluent: CHCl_3 /hexane = 4/6)

(E)-3'-bromochalcone (3ha): ^1H NMR (500 MHz, CDCl_3 , TMS): δ 7.35 (t, $J = 8.0$ Hz, 1H), 7.38–7.42 (m, 3H), 7.44 (d, $J = 16.0$ Hz, 1H), 7.60–7.64 (m, 2H), 7.67 (ddd, $J = 8.0$, 2.0, and 1.0 Hz, 1H), 7.80 (d, $J = 16.0$ Hz, 1H), 7.91 (ddd, $J = 8.0$, 1.5, and 1.0 Hz, 1H), 8.12 (t, $J = 1.5$ Hz, 1H). $^{13}\text{C}-\{^1\text{H}\}$ NMR (125 MHz, CDCl_3 , TMS): δ 121.3, 123.0, 127.0, 128.6, 129.0, 130.2, 130.9, 131.5, 134.6, 135.6, 140.0, 145.7, 188.9. MS (70 eV, EI): m/z (%): 289 (10), 288 (64), 287 (100) [M^+], 286 (65), 285 (92), 207 (44), 185 (13), 183 (13), 179 (25), 178 (38), 157 (22), 155 (23), 131 (85), 104 (11), 103 (97), 102 (25), 89 (29), 77 (79), 76 (54), 75 (30), 74 (12), 51 (32), 50 (26).



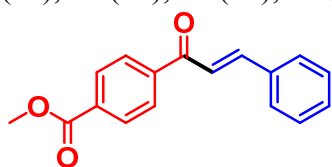
3ia (CAS No. 38239-50-8) (Eluent: EtOAc/hexane = 2/8)

(E)-4'-(dimethylamino)chalcone (3ia): ^1H NMR (500 MHz, CDCl_3 , TMS): δ 3.02 (s, 6H), 6.64–6.67 (m, 2H), 7.33–7.40 (m, 2H), 7.58 (d, J = 15.5 Hz, 1H), 7.60–7.63 (m, 2H), 7.78 (d, J = 15.5 Hz, 1H), 7.98–8.01 (m, 2H). ^{13}C – $\{^1\text{H}\}$ NMR (125 MHz, CDCl_3 , TMS): δ 40.0, 110.8, 122.2, 125.9, 128.3, 128.9, 129.9, 130.8, 135.5, 142.4, 153.4, 187.7. MS (70 eV, EI): m/z (%): 252 (18), 251 (100) [M^+], 250 (28), 223 (49), 222 (24), 207 (16), 148 (61), 125 (15), 105 (12), 104 (15), 103 (21), 78 (10), 77 (34), 51 (11). This MS spectral data accords with that in the previous report.^[13]



3ja (CAS No. 93628-96-7) (Eluent: EtOAc/hexane = 2/8)

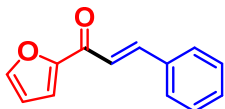
(E)-4'-cyanochalcone (3ja): ^1H NMR (500 MHz, CDCl_3 , TMS): δ 7.41–7.47 (m, 3H), 7.47 (d, J = 15.5 Hz, 1H), 7.63–7.67 (m, 2H), 7.79–7.82 (m, 2H), 7.83 (d, J = 15.5 Hz, 1H), 8.07–8.10 (m, 2H). ^{13}C – $\{^1\text{H}\}$ NMR (125 MHz, CDCl_3 , TMS): δ 116.0, 118.2, 121.2, 128.8, 129.0, 129.2, 131.3, 132.6, 134.4, 141.5, 146.7, 189.3. MS (70 eV, EI): m/z (%): 233 (60) [M^+], 232 (100), 204 (12), 131 (33), 130 (15), 103 (44), 102 (44), 78 (11), 77 (40), 76 (12), 75 (12), 51 (22).



3ka (CAS No. 1252617-32-5) (Eluent: CHCl_3 /hexane = 4/6, isolated concomitant with methyl 4-formylbenzoate (**1k**))

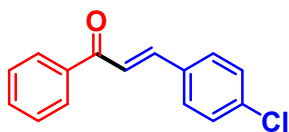
(E)-4'-(methoxycarbonyl)chalcone (3ka): ^1H NMR (500 MHz, CDCl_3 , TMS): δ 3.97 (s, 3H), 7.42–7.45 (m, 3H), 7.52 (d, J = 15.5 Hz, 1H), 7.64–7.67 (m, 2H), 7.83 (d, J = 15.5 Hz, 1H), 8.05–8.07 (m, 2H), 8.16–8.18 (m, 2H). ^{13}C – $\{^1\text{H}\}$ NMR (125 MHz, CDCl_3 , TMS): δ 52.7, 121.9, 128.5, 128.7, 129.2, 130.0, 131.0, 133.7, 134.7, 141.8, 145.9, 166.4, 190.2. MS (70 eV, EI): m/z (%): 267 (12), 266 (71) [M^+], 265 (100), 235

(10), 207 (33), 179 (13), 178 (18), 163 (15), 135 (11), 131 (38), 117 (16), 103 (58), 77 (36), 76 (18), 51 (11). This MS spectral data accords with that in the previous report.^[13]



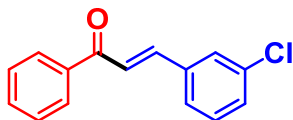
3la (CAS No. 42811-81-4) (Eluent: EtOAc/hexane = 1/9)

(E)-1-(furan-2-yl)-3-phenylprop-2-en-1-one (3la): ¹H NMR (500 MHz, CDCl₃, TMS): δ 6.58 (dd, J = 4.0 and 2.0 Hz, 1H), 7.34 (dd, J = 3.5 and 1.0 Hz, 1H), 7.38–7.42 (m, 3H), 7.45 (d, J = 15.5 Hz, 1H), 7.62–7.66 (m, 3H), 7.87 (d, J = 15.5 Hz, 1H). ¹³C–{¹H} NMR (125 MHz, CDCl₃, TMS): δ 112.6, 117.6, 121.2, 128.6, 129.0, 130.7, 134.7, 144.0, 146.6, 153.7, 178.0. MS (70 eV, EI): m/z (%): 199 (9), 198 (67) [M^+], 197 (100), 170 (6), 169 (17), 142 (10), 141 (52), 131 (12), 115 (18), 103 (36), 102 (15), 95 (24), 77 (39), 76 (7), 63 (6), 51 (19), 50 (7). This MS spectral data accords with that obtained from Wiley Subscription Services, Inc.



3db (CAS No. 22252-16-0) (Eluent: EtOAc/hexane = 1/9)

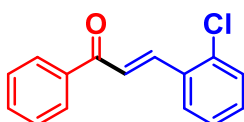
(E)-4-chlorochalcone (3db): ¹H NMR (500 MHz, CDCl₃, TMS): δ 7.36–7.39 (m, 2H), 7.48–7.61 (m, 6H), 7.75 (d, J = 16.0 Hz, 1H), 8.00–8.03 (m, 2H). ¹³C–{¹H} NMR (125 MHz, CDCl₃, TMS): δ 122.5, 128.6, 128.8, 129.3, 129.7, 133.0, 133.4, 136.5, 138.1, 143.4, 190.3. MS (70 eV, EI): m/z (%): 244 (31), 243 (33) [M^+], 242 (93), 241 (60), 208 (12), 207 (72), 179 (51), 178 (32), 167 (14), 165 (46), 139 (11), 137 (31), 130 (27), 105 (62), 102 (54), 101 (44), 89 (25), 77 (100), 76 (25), 75 (32), 74 (10), 51 (47), 50 (18). This MS spectral data accords with that obtained from Wiley Subscription Services, Inc.



3dc (CAS No. 22966-13-8) (Eluent: EtOAc/hexane = 1/9)

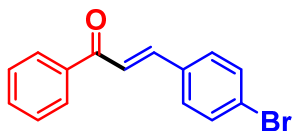
(E)-3-chlorochalcone (3dc): ¹H NMR (500 MHz, CDCl₃, TMS): δ 7.31–7.37 (m, 2H), 7.46–7.51 (m, 3H), 7.51 (d, J = 16.0 Hz, 1H), 7.56–7.61 (m, 2H), 7.71 (d, J = 16.0 Hz, 1H), 8.00–8.03 (m, 2H). ¹³C–{¹H} NMR (125 MHz, CDCl₃, TMS): δ 123.2, 126.9,

128.0, 128.6, 128.8, 130.3, 130.4, 133.1, 135.0, 136.8, 137.9, 143.1, 190.1. MS (70 eV, EI): m/z (%): 244 (26), 243 (29) [M^+], 242 (76), 241 (55), 208 (14), 207 (87), 179 (47), 178 (30), 167 (11), 165 (37), 137 (25), 130 (10), 105 (71), 102 (50), 101 (36), 89 (20), 77 (100), 76 (23), 75 (30), 51 (46), 50 (16).



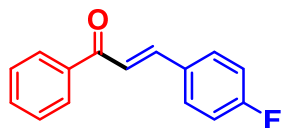
3dd (CAS No. 22966-11-6) (Eluent: EtOAc/hexane = 1/9)

(E)-2-chlorochalcone (3dd): ^1H NMR (500 MHz, CDCl_3 , TMS): δ 7.27–7.32 (m, 2H), 7.39–7.42 (m, 1H), 7.46–7.51 (m, 3H), 7.57 (tdd, $J = 7.5$, 1.5 and 1.5 Hz, 1H), 7.71–7.75 (m, 1H), 8.00–8.02 (m, 2H), 8.17 (d, $J = 16.0$ Hz, 1H). ^{13}C – $\{^1\text{H}\}$ NMR (125 MHz, CDCl_3 , TMS): δ 124.7, 127.2, 127.8, 128.6, 128.7, 130.3, 131.3, 133.0, 133.2, 135.5, 137.9, 140.6, 190.4. MS (70 eV, EI): m/z (%): 243 (3) [M^+], 242 (13), 208 (16), 207 (100), 179 (9), 178 (11), 165 (6), 137 (8), 105 (17), 102 (12), 101 (17), 89 (7), 77 (35), 76 (8), 75 (13), 51 (17), 50 (6). This MS spectral data accords with that in the previous report.^[14]



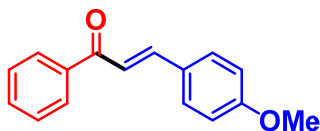
3de (CAS No. 22966-09-2) (Eluent: EtOAc/hexane = 1/9)

(E)-4-bromochalcone (3de): ^1H NMR (500 MHz, CDCl_3 , TMS): δ 7.46–7.53 (m, 7H), 7.57 (tdd, $J = 7.5$, 1.5 and 1.5 Hz, 1H), 7.72 (d, $J = 15.5$ Hz, 1H), 7.99–8.02 (m, 2H). ^{13}C – $\{^1\text{H}\}$ NMR (125 MHz, CDCl_3 , TMS): δ 122.5, 124.8, 128.6, 128.7, 129.9, 132.2, 133.0, 133.8, 138.0, 143.4, 190.2. MS (70 eV, EI): m/z (%): 288 (56), 287 (42) [M^+], 286 (57), 285 (36), 211 (21), 209 (23), 208 (16), 207 (94), 183 (11), 181 (12), 179 (52), 178 (42), 130 (31), 105 (62), 103 (12), 102 (100), 101 (20), 89 (27), 77 (96), 76 (38), 75 (28), 74 (12), 51 (45). This MS spectral data accords with that obtained from Wiley Subscription Services, Inc.



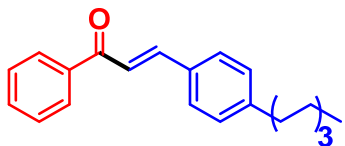
3df (CAS No. 22966-07-0) (Eluent: EtOAc/hexane = 1/9)

(E)-4-fluorochalcone (3df): ^1H NMR (500 MHz, CDCl_3 , TMS): δ 7.06–7.10 (m, 2H), 7.47–7.50 (m, 3H), 7.56 (tdd, J = 7.5, 1.5 and 1.5 Hz, 1H), 7.58–7.62 (m, 2H), 7.76 (d, J = 15.5 Hz, 1H), 8.00–8.02 (m, 2H). ^{13}C – $\{^1\text{H}\}$ NMR (125 MHz, CDCl_3 , TMS): δ 116.0, 116.2, 121.7, 128.5, 128.7, 130.37, 130.43, 131.1, 131.2, 132.9, 138.1, 143.5, 163.1, 165.1, 190.2. ^{19}F NMR (470 MHz, CDCl_3 , benzotrifluoride): δ –110.2. MS (70 eV, EI): m/z (%): 226 (100) [M^+], 225 (61), 197 (24), 183 (11), 149 (54), 130 (30), 121 (39), 120 (12), 105 (47), 102 (12), 101 (47), 95 (10), 77 (70), 75 (21), 51 (30), 50 (10). This MS spectral data accords with that obtained from Wiley Subscription Services, Inc.



3dg (CAS No. 22252-15-9) (Eluent: EtOAc/hexane = 1/9)

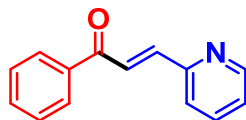
(E)-4-methoxychalcone (3dg): ^1H NMR (500 MHz, CDCl_3 , TMS): δ 3.81 (s, 3H), 6.90–6.92 (m, 2H), 7.40 (d, J = 15.5 Hz, 1H), 7.46–7.49 (m, 2H), 7.53–7.59 (m, 3H), 7.78 (d, J = 15.5 Hz, 1H), 7.99–8.02 (m, 2H). ^{13}C – $\{^1\text{H}\}$ NMR (125 MHz, CDCl_3 , TMS): δ 55.4, 114.4, 119.7, 127.6, 128.4, 128.6, 130.3, 132.6, 138.5, 144.7, 161.7, 190.5. MS (70 eV, EI): m/z (%): 239 (17), 238 (100) [M^+], 237 (50), 223 (24), 207 (21), 195 (15), 167 (12), 165 (13), 161 (49), 133 (32), 118 (14), 108 (51), 105 (29), 90 (16), 89 (19), 77 (67), 63 (11), 51 (21). This MS spectral data accords with that obtained from Wiley Subscription Services, Inc.



3dh (CAS No. 2249991-18-0) (Eluent: toluene)

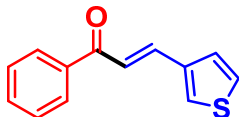
(E)-4-pentylchalcone (3dh): ^1H NMR (500 MHz, CDCl_3 , TMS): δ 0.89 (t, J = 7.0 Hz, 3H), 1.28–1.37 (m, 4H), 1.62 (quin, J = 7.5 Hz, 2H), 2.62 (t, J = 7.5 Hz, 2H), 7.20–7.22 (m, 2H), 7.46–7.50 (m, 2H), 7.49 (d, J = 15.5 Hz, 1H), 7.54–7.56 (m, 3H), 7.80 (d, J = 15.5 Hz, 1H), 8.00–8.02 (m, 2H). ^{13}C – $\{^1\text{H}\}$ NMR (125 MHz, CDCl_3 , TMS): δ 14.1,

22.6, 31.0, 31.5, 36.0, 121.1, 128.59, 128.65, 128.7, 129.1, 132.4, 132.7, 138.4, 145.1, 146.2, 190.7. MS (70 eV, EI): m/z (%): 278 (14) [M^+], 277 (17), 222 (5), 221 (24), 208 (17), 207 (100), 193 (10), 179 (5), 178 (15), 131 (7), 116 (5), 115 (17), 105 (13), 91 (6), 77 (21).



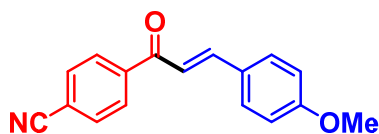
3di (CAS No. 20890-12-4) (Eluent: EtOAc/hexane = 2/8)

(E)-1-phenyl-3-(pyridin-2-yl)prop-2-en-1-one (3di): ^1H NMR (500 MHz, CDCl_3 , TMS): δ 7.28 (ddd, $J = 7.5$, 4.5 and 1.0 Hz, 1H), 7.46–7.52 (m, 3H), 7.58 (tdd, $J = 7.5$, 1.5 and 1.5 Hz, 1H), 7.72 (td, $J = 7.5$ and 2.0 Hz, 1H), 7.78 (d, $J = 15.5$ Hz, 1H), 8.09–8.11 (m, 2H), 8.12 (d, $J = 15.5$ Hz, 1H), 8.67–8.69 (m, 1H). ^{13}C – $\{^1\text{H}\}$ NMR (125 MHz, CDCl_3 , TMS): δ 124.5, 125.5, 128.7, 128.8, 133.2, 137.0, 137.8, 142.8, 150.1, 153.2, 190.5. MS (70 eV, EI): m/z (%): 210 (5), 209 (34) [M^+], 208 (5), 182 (5), 181 (41), 180 (100), 132 (39), 105 (25), 104 (34), 78 (33), 77 (55), 76 (7), 52 (7), 51 (35), 50 (10). This MS spectral data accords with that in the previous report.^[15]



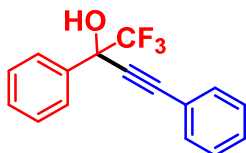
3dj (CAS No. 123293-65-2) (Eluent: EtOAc/hexane = 2/8)

(E)-1-phenyl-3-(thiophen-3-yl)prop-2-en-1-one (3dj): ^1H NMR (500 MHz, CDCl_3 , TMS): δ 7.34 (d, $J = 15.5$ Hz, 1H), 7.34–7.36 (m, 1H), 7.41 (dd, $J = 5.0$ and 1.5 Hz, 1H), 7.47–7.50 (m, 2H), 7.54–7.59 (m, 2H), 7.79 (d, $J = 15.5$ Hz, 1H), 7.98–8.01 (m, 2H). ^{13}C – $\{^1\text{H}\}$ NMR (125 MHz, CDCl_3 , TMS): δ 121.8, 125.3, 127.1, 128.5, 128.7, 129.3, 132.8, 138.2, 138.26, 138.32, 190.8. MS (70 eV, EI): m/z (%): 215 (16), 214 (100) [M^+], 213 (27), 186 (22), 185 (77), 184 (11), 141 (11), 137 (74), 130 (22), 109 (55), 105 (45), 77 (86), 65 (35), 51 (41), 50 (12).



3jg (CAS No. 1420765-33-8) (Eluent: toluene, Gradient eluent: CHCl₃, EtOAc)

4'-cyano-4-methoxychalcone (3jg): ¹H NMR (500 MHz, CDCl₃, TMS): δ 3.86 (s, 3H), 6.93–6.96 (m, 2H), 7.34 (d, *J* = 15.5 Hz, 1H), 7.59–7.62 (m, 2H), 7.77–7.80 (m, 2H), 7.80 (d, *J* = 15.5 Hz, 1H), 8.05–8.08 (m, 2H). ¹³C-{¹H} NMR (125 MHz, CDCl₃, TMS): δ 55.5, 114.6, 115.7, 118.2, 118.8, 127.1, 128.8, 130.6, 132.5, 141.9, 146.5, 162.2, 189.1. MS (70 eV, EI): *m/z* (%): 264 (18), 263 (100) [*M*⁺], 262 (69), 248 (26), 233 (10), 232 (53), 220 (15), 190 (10), 165 (10), 161 (56), 133 (39), 130 (15), 118 (20), 108 (52), 103 (13), 102 (50), 90 (21), 89 (23), 77 (19), 76 (10), 75 (14), 63 (14), 51 (13).



4na (CAS No. 117710-90-4)

1,1,1-trifluoro-2,4-diphenylbut-3-yn-2-ol (4na): ¹H NMR (500 MHz, CDCl₃, TMS, the crude product referring to the previous report)^[16]: δ 3.21 (s, 1H), 7.35–7.46 (m, 6H), 7.49–7.53 (m, 2H), 7.79–7.84 (m, 2H). MS (70 eV, EI): *m/z* (%): 276 (5) [*M*⁺], 209 (5), 208 (17), 207 (100), 179 (8), 178 (10), 130 (8), 129 (80), 105 (28), 101 (6), 78 (6), 77 (29), 76 (6), 75 (8), 51 (11).

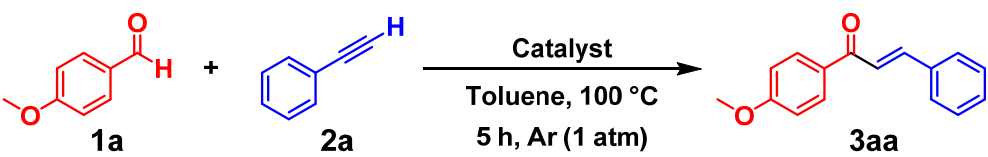
2.3. Results and Discussion

2.3.1. Effect of Catalysts and Optimization of Reaction Conditions

Initially, the synthesis of (*E*)-4'-methoxychalcone (**3aa**) from *p*-anisaldehyde (**1a**) and phenylacetylene (**2a**), *i.e.*, the formal hydroacylation of **2a** using **1a**, was carried out in the presence of various solid catalysts in toluene at 100 °C under an Ar atmosphere (Table 2-1). Surprisingly, of the catalysts examined, namely Mg₃Al–CO₃ LDH (Mg/Al = 3), hydroxyapatite (HAP), Mg(OH)₂, Ca(OH)₂, MgO, CaO, ZnO, Al₂O₃, CeO₂, ZrO₂, and TiO₂, **3aa** was afforded only when Mg₃Al–CO₃ LDH was used (Table 2-1, entries 1 and 3–12).

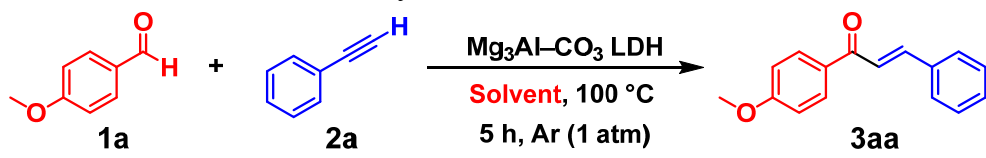
An LDH with an Mg/Al ratio of 2 also showed the catalytic activity whereas the use of an LDH with an Mg/Al ratio of 4 or Mg₃Al–CO₃ LDH calcined at 200, 300, or 400 °C hardly afforded **3aa**, indicating that the ionic layered structure of the LDH is important for the present formal hydroacylation (Table 2-1, entries 13–17, XRD patterns presented in Figure 2-6). The partial exchange of interlayer anions from CO₃²⁻ to Cl⁻ decreased the yield of **3aa**, indicating that the basicity of the interlayer anion also affected the catalytic activity (Table 2-1, entry 18). Moreover, in the presence of K₂CO₃, Na₂CO₃, NaHCO₃, *i*Pr₂EtN, the formal hydroacylation did not proceed at all (Table 2-1, entries 19–22). The effect of solvents on the formal hydroacylation was found to be remarkable, with low-polarity solvents such as methoxycyclopentane, PhCF₃, and toluene being effective (Table 2-2, entries 1–15). Once the temperature, the amount of the catalyst, and the reaction time had been optimized, the yield of **3aa** reached 87% (Table 2-1, entry 2 and Table 2-2, entries 16–18).

Table 2-1. Effect of base catalysts on the synthesis of 4'-methoxychalcone (**3aa**).^[a]

				
Entry	Catalyst	Conv. [%]		Yield [%]
		1a	2a	3aa
1	Mg ₃ Al–CO ₃ LDH	55	52	42
2 ^[b]	Mg ₃ Al–CO ₃ LDH	99	96	87
3	HAP	<1	1	<1
4	Mg(OH) ₂	<1	3	<1
5	Ca(OH) ₂	4	8	<1
6	MgO	1	5	<1
7	CaO	<1	2	<1
8	ZnO	<1	<1	<1
9	Al ₂ O ₃	10	6	<1
10	CeO ₂	6	1	<1
11	ZrO ₂	5	<1	<1
12	TiO ₂	<1	3	<1
13	Mg ₂ Al–CO ₃ LDH	52	48	39
14	Mg ₄ Al–CO ₃ LDH	<1	<1	<1
15	Mg ₃ Al–CO ₃ LDH_200_cal	5	10	3
16	Mg ₃ Al–CO ₃ LDH_300_cal	2	2	<1
17	Mg ₃ Al–CO ₃ LDH_400_cal	6	6	<1
18	Mg ₃ Al–Cl LDH	28	30	19
19	K ₂ CO ₃	2	3	<1
20	Na ₂ CO ₃	2	16	<1
21	NaHCO ₃	2	7	<1
22 ^[c]	<i>i</i> Pr ₂ EtN	2	7	<1

[a] Reaction conditions: **1a** (0.5 mmol), **2a** (0.5 mmol), catalyst (100 mg), toluene (2 mL), 100 °C, 5 h, Ar balloon (1 atm). Conversions and yields were determined by GC analysis using biphenyl as an internal standard. Mg₃Al–CO₃ LDH_xx_cal: Mg₃Al–CO₃ LDH calcined at xx °C for 3 h. [b] Catalyst (130 mg), 120 °C, 15 h. [c] **1a** (1 mmol), *i*Pr₂EtN (10 mol%).

Table 2-2. Effect of solvents on the synthesis of **3aa**.^[a]

				
Entry	Solvent	Conv. [%]		Yield [%]
		1a	2a	3aa
1	CPME	67	65	51
2	PhCF ₃	59	57	46
3	toluene	55	52	42
4	<i>n</i> -octane	29	29	13
5	<i>p</i> -xylene	23	—	13
6	<i>m</i> -xylene	21	—	13
7	mesitylene	21	22	10
8	DMSO	10	12	8
9	<i>o</i> -xylene	13	13	7
10	DMA	22	7	2
11	NMP	<1	11	<1
12	BuOAc	<1	<1	<1
13	1,4-dioxane	9	<1	<1
14	diglyme	7	24	<1
15	1-BuOH	11	4	<1
16 ^[b]	CPME	77	75	62
17 ^[b]	PhCF ₃	79	77	59
18 ^[b]	toluene	92	87	69

[a] Reaction conditions: **1a** (0.5 mmol), **2a** (0.5 mmol), Mg₃Al–CO₃ LDH (100 mg), solvent (2 mL), 100 °C, 5 h, Ar balloon (1 atm). Conversions and yields were determined by GC analysis using biphenyl as an internal standard. —: **2a** peak was not detected because of the solvent peak whose retention time is almost the same as that of **2a**. [b] 120 °C. CPME = methoxycyclopentane. DMSO = dimethyl sulfoxide. DMA = *N,N*-dimethylacetamide. NMP = *N*-methylpyrrolidone.

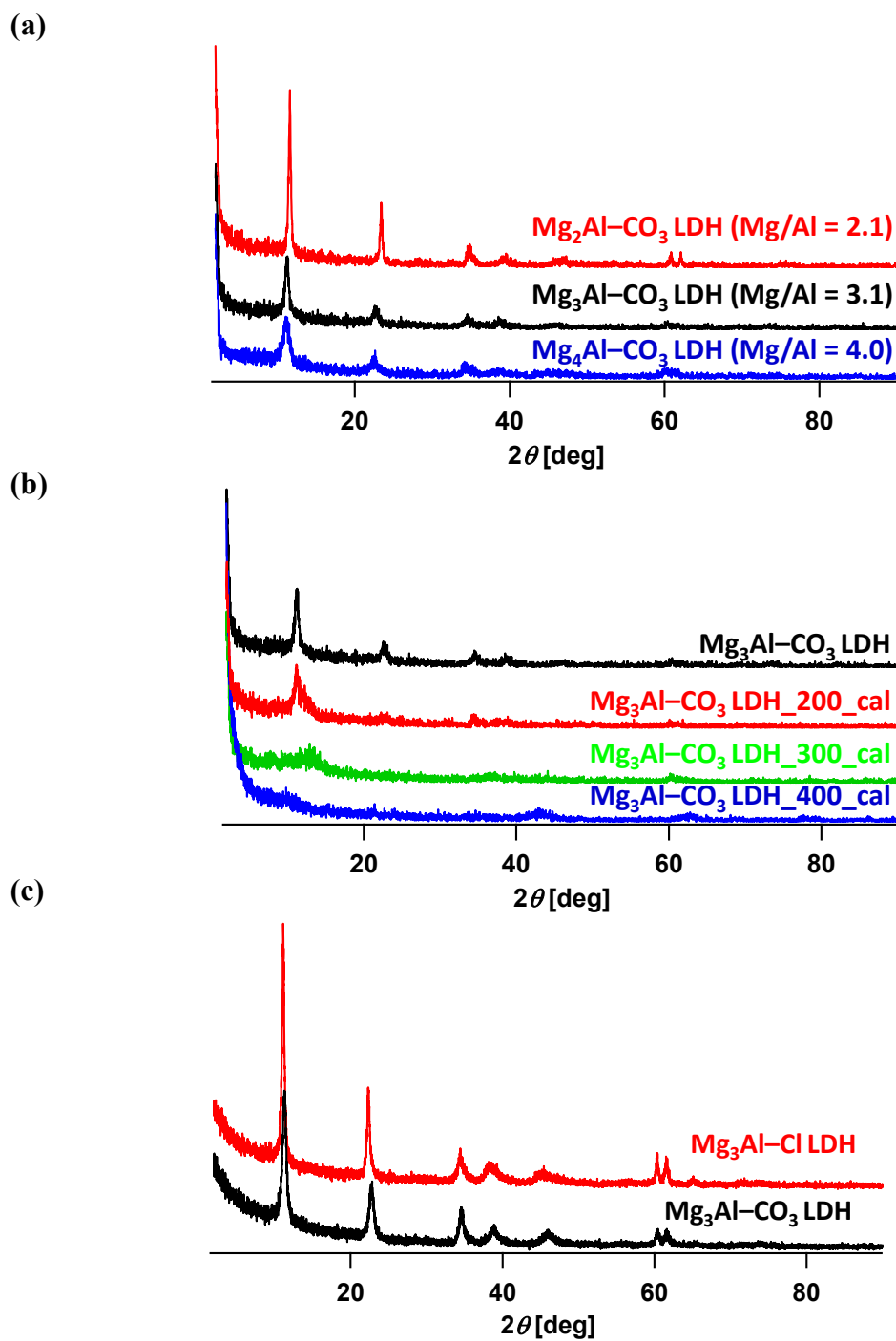


Figure 2-6. XRD patterns of LDH (a) when changing the ratio of Mg/Al ratio, (b) when calcined at various temperatures, and (c) when changing the interlayer anion. $\text{Mg}_3\text{Al-CO}_3$ LDH_xx_cal: $\text{Mg}_3\text{Al-CO}_3$ LDH calcined at xx °C for 3 h.

2.3.2. Interaction between Alkynes and Layered Double Hydroxide

To investigate the notable effect of catalysts on **3aa** synthesis, the interaction between the solid bases and **2a** was examined (Figure 2-7). When the solid bases were stirred with **2a** under the optimal reaction conditions for 2 h, those that exhibited the catalytic activity became colored, whereas the others exhibited no apparent change (except for CeO₂). Conversely, when diphenylacetylene, an internal alkyne, was stirred with Mg₃Al–CO₃ LDH or CeO₂, the color of Mg₃Al–CO₃ LDH did not change, whereas that of CeO₂ became almost the same as when CeO₂ interacted with **2a**, demonstrating the interaction between CeO₂ and the C≡C bond of alkynes (Figure 2-8). It is known that CeO₂ is colored by the adsorption of nitriles or phenols in addition to alkynes (see Chapter III).^[17] Therefore, the coloring interaction of Mg₃Al–CO₃ LDH with **2a** likely occurred through alkynyl species generated by deprotonation of terminal alkynes. When Mg₃Al–CO₃ LDH (100 mg) was stirred with **2a** (0.5 mmol) for 16 h (termed LDH–**2a**, colored reddish), the amount of **2a** incorporated into the LDH was ~3 μmol (determined by GC analysis after dissolution of LDH–**2a** with 1 M HCl followed by extraction of **2a** with CHCl₃). When the reaction of **1a** and LDH–**2a** was conducted under the optimized conditions, **3aa** was formed in 67% yield based on the amount of **2a** contained in LDH–**2a** (Figure 2-9). In addition, ¹H NMR analysis indicated that H/D exchange between **2a** and D₂O occurred using either Mg₃Al–CO₃ LDH or Al₂O₃, regardless of their catalytic activities for **3aa** synthesis (Figures 2-10 and 2-11). Considering these results, catalytic amounts of alkynyl nucleophilic species are probably formed by the basicity and stabilized by the ionicity of Mg₃Al–CO₃ LDH, which promotes the nucleophilic addition of alkynes to aldehydes unlike other solid catalysts.

XRD patterns, DR UV-Vis spectra, FT-IR spectra, and Raman spectra of LDH–**2a** (stirred for 15 h) and Mg₃Al–CO₃ LDH were shown in Figures 2-12, 2-13, 2-14, and 2-15, respectively. The XRD patterns indicated that the crystalline of LDH–**2a** decreased due to the adsorption of **2a**. In DR UV-Vis spectra broad peaks appeared in the visible light region after stirring with **2a**. However, it is difficult to determine how interaction between LDH and **2a** occurs because of the tiny amount of **2a** on LDH. Indeed, FT-IR spectra did not show any change after stirring with **2a**. I also attempted higher sensitive equipment such as Raman spectroscopy, affording no information on alkynes. In the future, the ongoing investigation with dynamic nuclear polarization

surface enhanced NMR spectroscopy (DNP SENS) would afford the detailed information on the interaction.

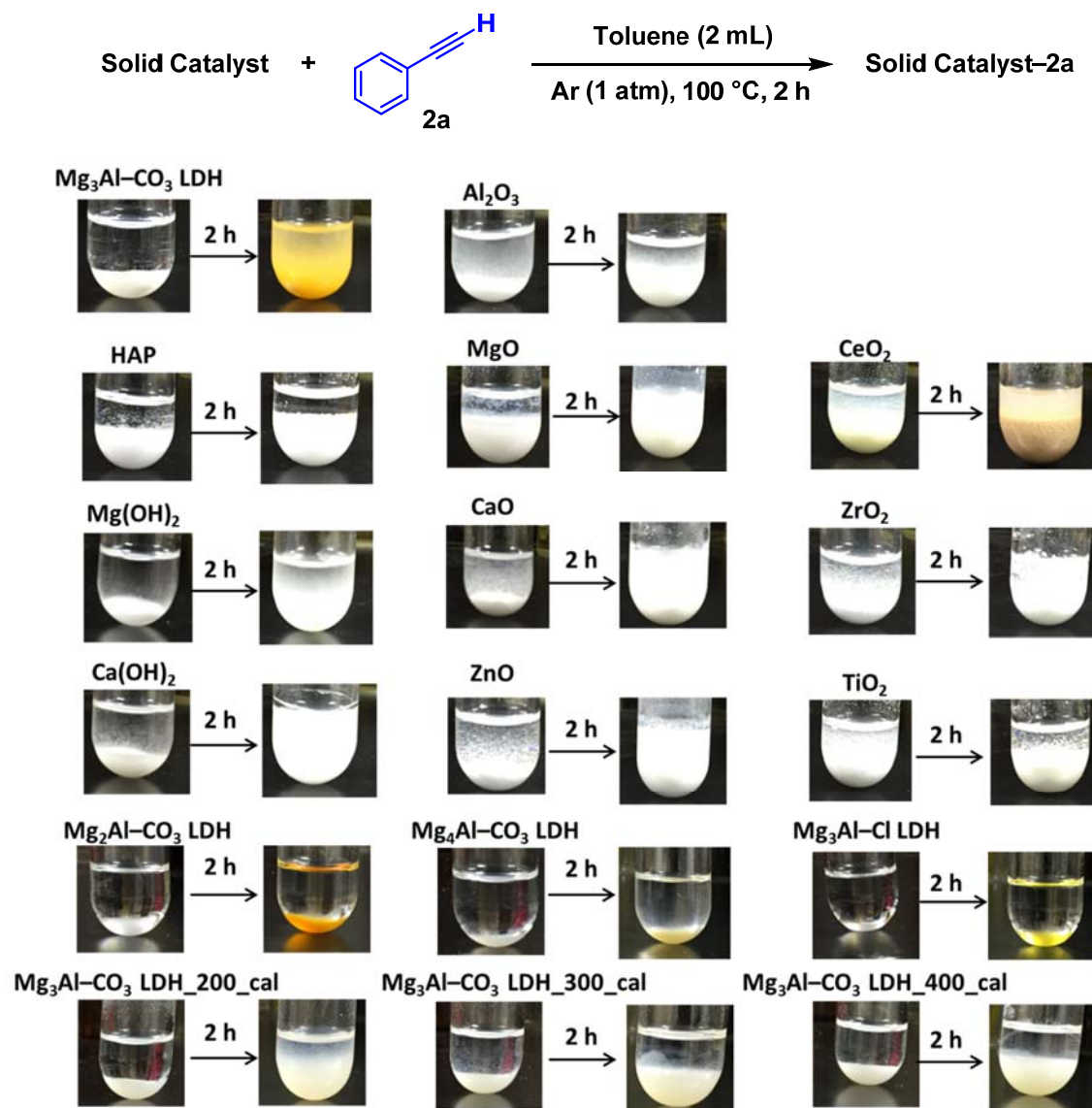


Figure 2-7. Photo images of solid catalysts before/after stirring with **2a**. Reaction conditions: **2a** (0.5 mmol), catalyst (100 mg), toluene (2 mL), Ar (1 atm), 100 °C, 2 h.

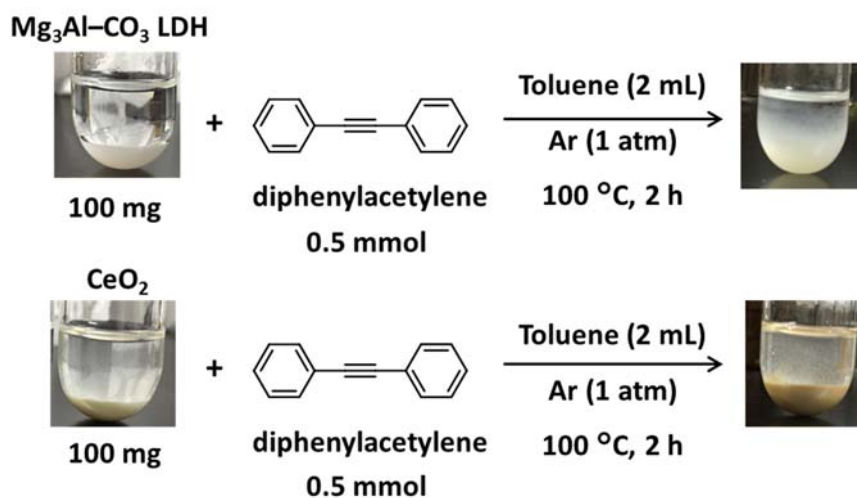


Figure 2-8. Photo images of solid catalysts before/after stirring with diphenylacetylene. Reaction conditions: diphenylacetylene (0.5 mmol), catalyst (100 mg), toluene (2 mL), Ar (1 atm), 100 °C, 2 h.

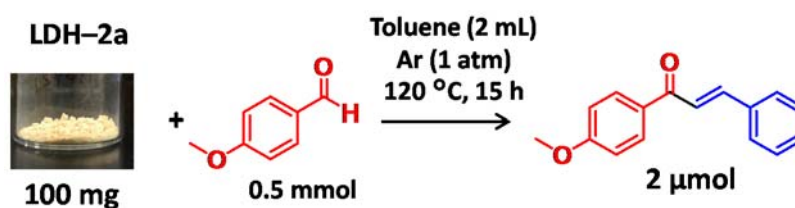


Figure 2-9. Synthesis of 4'-methoxychalcone (**3aa**) using LDH-2a. Reaction conditions: **1a** (0.5 mmol), LDH-2a (100 mg), toluene (2 mL), 120 °C, Ar balloon (1 atm), 15 h. Yields were determined by GC analysis using biphenyl as an internal standard.

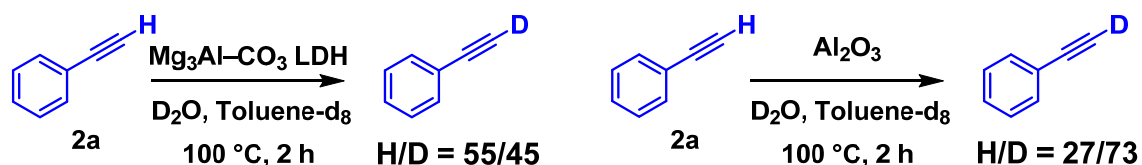


Figure 2-10. H/D exchange of **2a** with D₂O using Mg₃Al–CO₃ LDH or Al₂O₃ and their images before/after stirring with **2a**. Reaction conditions: **2a** (0.5 mmol), catalyst (100 mg), toluene-d₈ (2 mL), D₂O (50 μL), Ar (1 atm), 100 °C, 2 h.

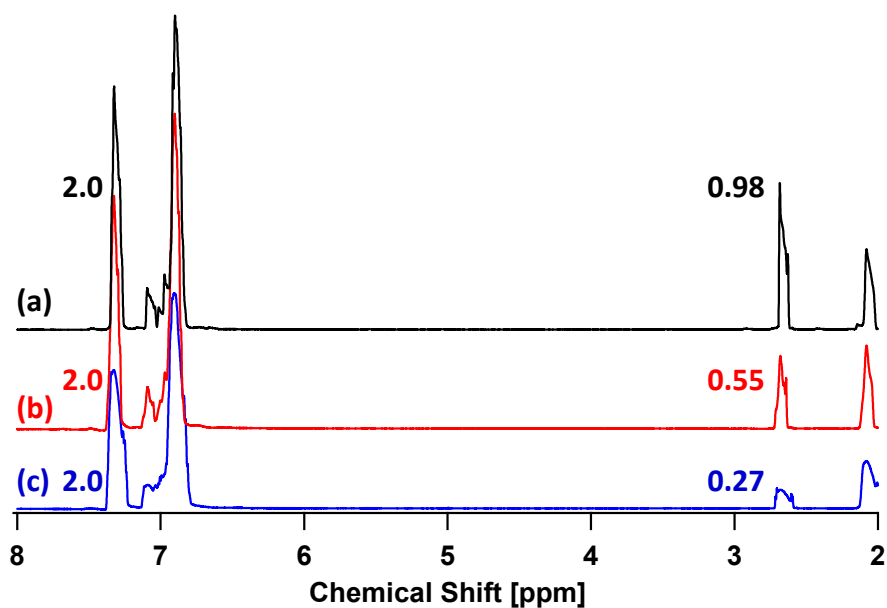


Figure 2-11. ^1H NMR (in toluene- d_8) spectra after the reaction of phenylacetylene (**2a**) with D_2O (50 μL) under the conditions shown in Figure 2-10 using (a) no catalysts, (b) $\text{Mg}_3\text{Al}-\text{CO}_3$ LDH, and (c) Al_2O_3 . The numbers next to peaks represent area ratios of the peaks.

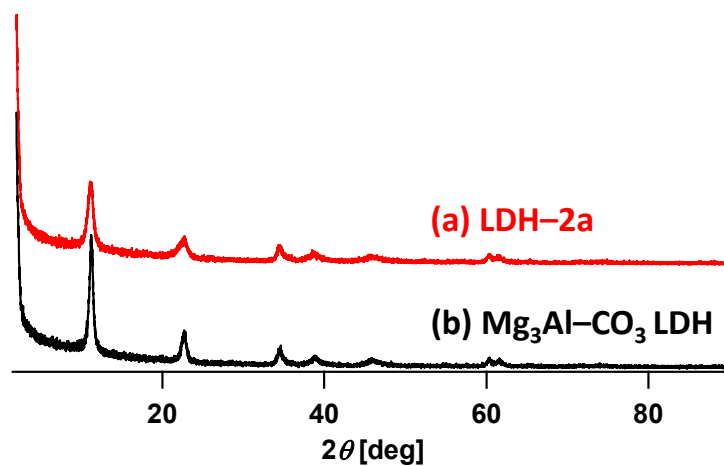


Figure 2-12. XRD patterns of (a) retrieved $\text{Mg}_3\text{Al}-\text{CO}_3$ LDH after stirring with **2a** and (b) fresh $\text{Mg}_3\text{Al}-\text{CO}_3$ LDH.

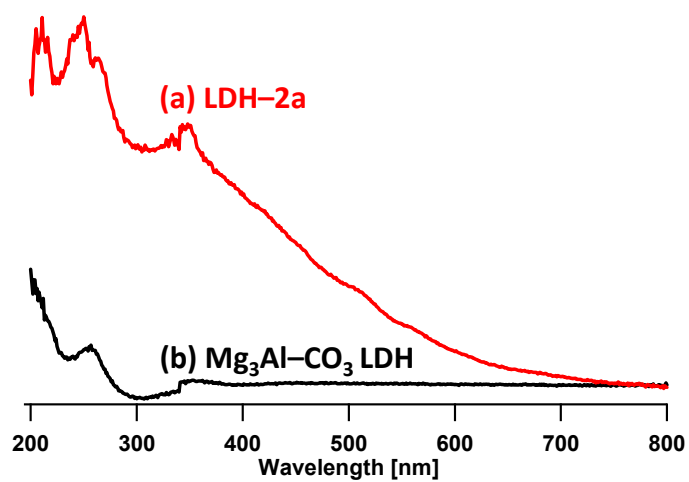


Figure 2-13. DR UV-Vis spectra of (a) retrieved Mg₃Al-CO₃ LDH after stirring with **2a** and (b) fresh Mg₃Al-CO₃ LDH.

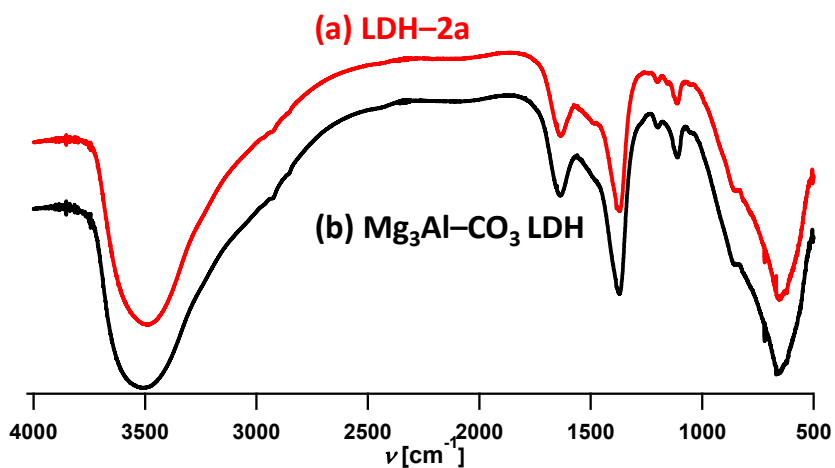


Figure 2-14. FT-IR spectra of (a) retrieved Mg₃Al-CO₃ LDH after stirring with **2a** and (b) fresh Mg₃Al-CO₃ LDH.

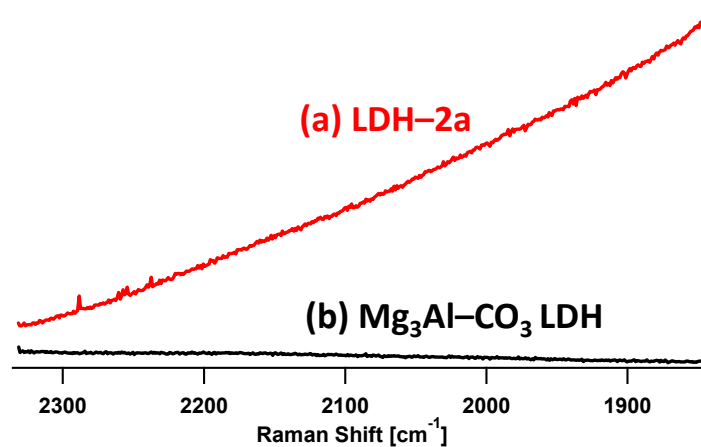


Figure 2-15. Raman spectra (633 nm laser) of (a) retrieved Mg₃Al-CO₃ LDH after stirring with **2a** and (b) fresh Mg₃Al-CO₃ LDH. For (a), exposure: 900 s, scan: 2, slit: 100×1000 μm, dimmer: OD4. For (b), exposure: 300 s, scan: 2, slit: 100×1000 μm, dimmer: OD1.

2.3.3. Heterogeneous Catalysis and Catalyst Reuse

To verify that this system is catalytic, several amounts of benzoic acid as specific inhibitors of basic sites were added to the optimized reaction (Figure 2-16). When the reaction from **1a** and **2a** with benzoic acid was conducted under the conditions where **3aa** yield reached 87% as of 24 h without benzoic acid, an induction period was observed, which was likely derived from the consumption of benzoic acid by dehydration condensation with basic sites of LDH and the formation of alkynyl nucleophilic species on Mg₃Al–CO₃ LDH (Figure 2-16a). Also, when the amount of benzoic acid was increased from 20 mol% to 40 mol%, the initial rate after the induction period decreased linearly (Figure 2-16b,c). With 50 mol% of benzoic acid, the initial rate became close to zero, and the yield of **3aa** was only 5% after 50 h, which was the same as that as of 24 h (Table 2-3), indicating that this system is catalytic.

Next, to establish whether the observed catalysis occurred heterogeneously on Mg₃Al–CO₃ LDH or arose from leached species in the solution, the catalyst was removed by hot filtration during the reaction, and the reaction was restarted with the filtrate under the same conditions. As expected, the production of **3aa** immediately ceased upon removing the catalyst (Figure 2-17). Additionally, after the reaction, the filtrate was analyzed using inductively coupled plasma-atomic emission spectroscopy (ICP-AES), and Mg and Al species were hardly detected (Mg < 4 × 10⁻⁶%, Al < 4 × 10⁻³%). Thus, the observed catalysis for the present formal hydroacylation is truly heterogeneous. Furthermore, the Mg₃Al–CO₃ LDH can be easily retrieved from the reaction mixture by simple filtration. The retrieved Mg₃Al–CO₃ LDH can be reused after washing the catalyst with acetone for the reaction of **1a** and **2a** at least three times without significant loss of catalytic activity (Table 2-4). The change of XRD patterns and appearances through the repeating use of Mg₃Al–CO₃ LDH indicated that the slight decrease of the catalytic performance was possibly caused by the adsorption of organic compounds (Figure 2-18).

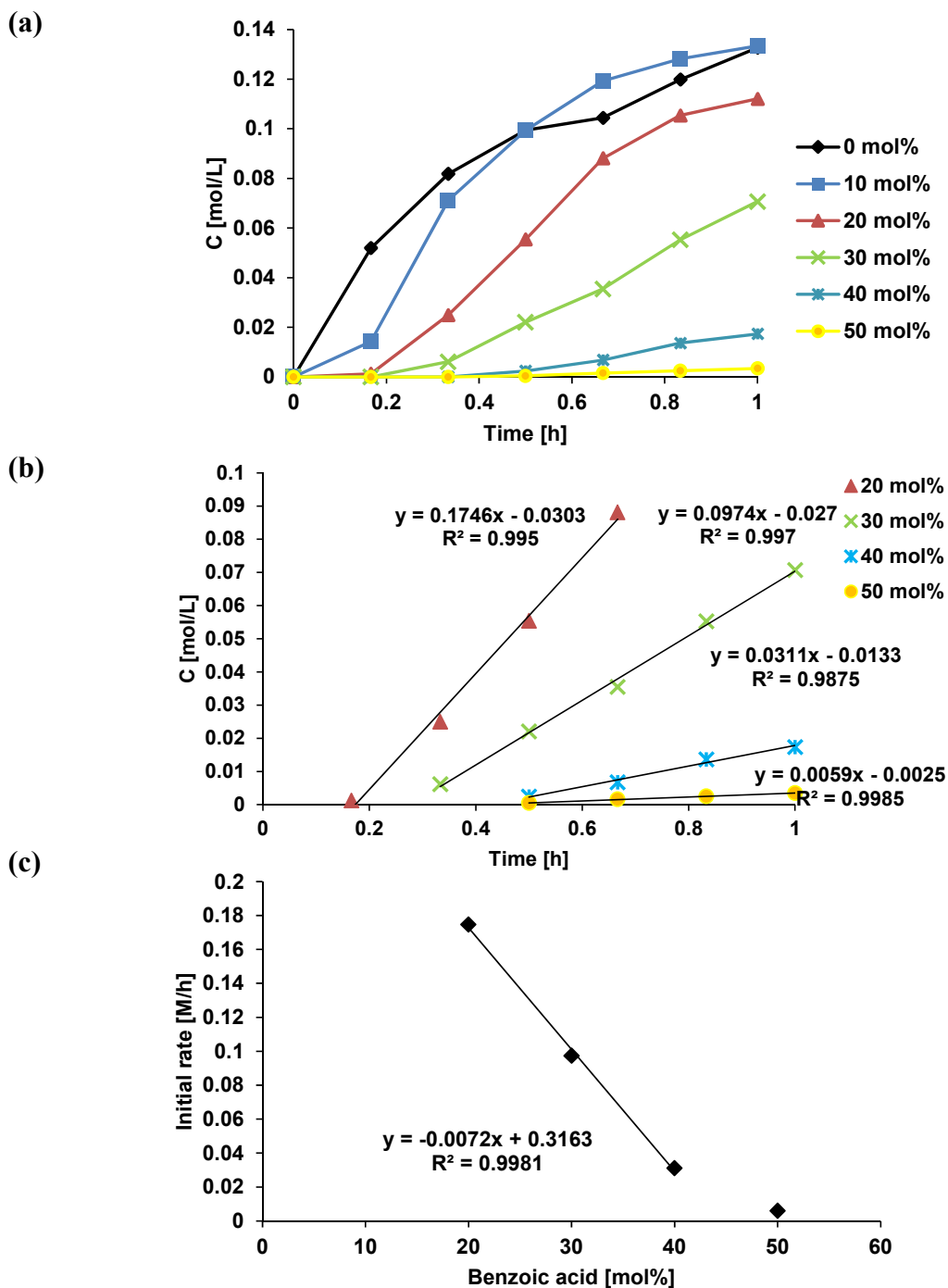
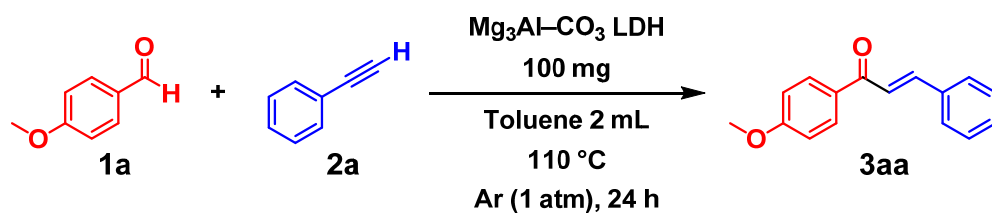


Figure 2-16. Reactions in the presence of benzoic acid. (a) The reaction profiles affected by changing the amount of benzoic acid from 0 mol% to 50 mol% by 10 mol%. (b) Calculation of initial rates after induction periods. (c) Relation between initial rate and the amount of benzoic acid. Reaction conditions: **1a** (0.5 mmol), **2a** (0.5 mmol), Mg₃Al–CO₃ LDH (100 mg), toluene (2 mL), 110 °C, Ar balloon (1 atm). Yields were determined by GC analysis using biphenyl as an internal standard.

Table 2-3. Effect of benzoic acid on the yield of **3aa**.^[a]



Entry	Amount of benzoic acid [mol%]	Conv. [%]		Yield [%]
		1a	2a	3aa
1	0	94	94	87
2	10	98	98	91
3	20	>99	98	76
4	30	94	93	81
5	40	39	46	25
6	50	10	11	5

[a] Reaction conditions: **1a** (0.5 mmol), **2a** (0.5 mmol), $\text{Mg}_3\text{Al-CO}_3$ LDH (100 mg), toluene (2 mL), 110 °C, 24 h, Ar balloon (1 atm). Conversions and yields were determined by GC analysis using biphenyl as an internal standard.

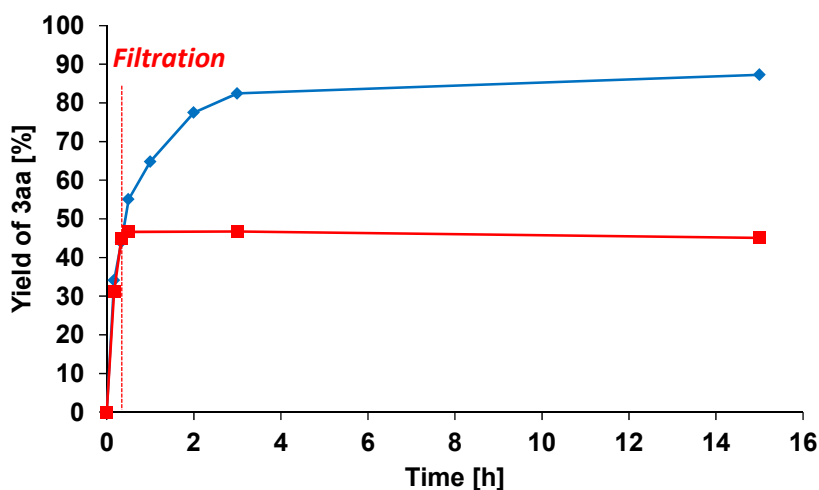


Figure 2-17. The reaction profile affected by removing $\text{Mg}_3\text{Al-CO}_3$ LDH in the middle of the reaction starting from **1a** and **2a** (verification of heterogeneous catalysis). Reaction conditions: **1a** (0.5 mmol), **2a** (0.5 mmol), $\text{Mg}_3\text{Al-CO}_3$ LDH (130 mg), toluene (2 mL), 120 °C, Ar balloon (1 atm). Yields were determined by GC analysis using biphenyl as an internal standard.

Table 2-4. Reuse of Mg₃Al–CO₃ LDH for the synthesis of **3aa**.^[a]

Entry	Mg ₃ Al–CO ₃ LDH	Conv. [%]		Yield [%]
		1a	2a	3aa
1 ^[b]	fresh	>99	87	91
2 ^[c]	1st reuse	92	77	80
3	2nd reuse	83	71	79
4	3rd reuse	84	71	73

[a] Reaction conditions: **1a** (0.5 mmol), **2a** (0.6 mmol), Mg₃Al–CO₃ LDH (130 mg), toluene (2 mL), 120 °C, 15 h, Ar balloon (1 atm). Conversions and yields were determined by GC analysis using biphenyl as an internal standard. LDH was washed with acetone (25 mL/run) after respective reactions. [b] Average values of three runs. [c] Average values of two runs.

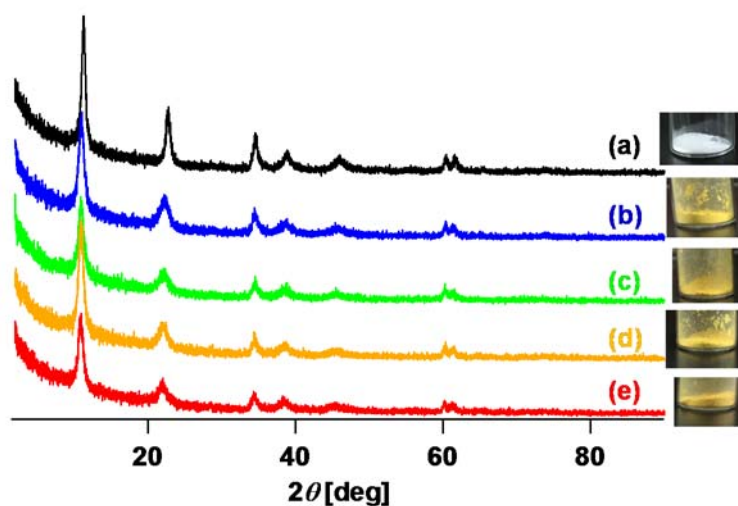
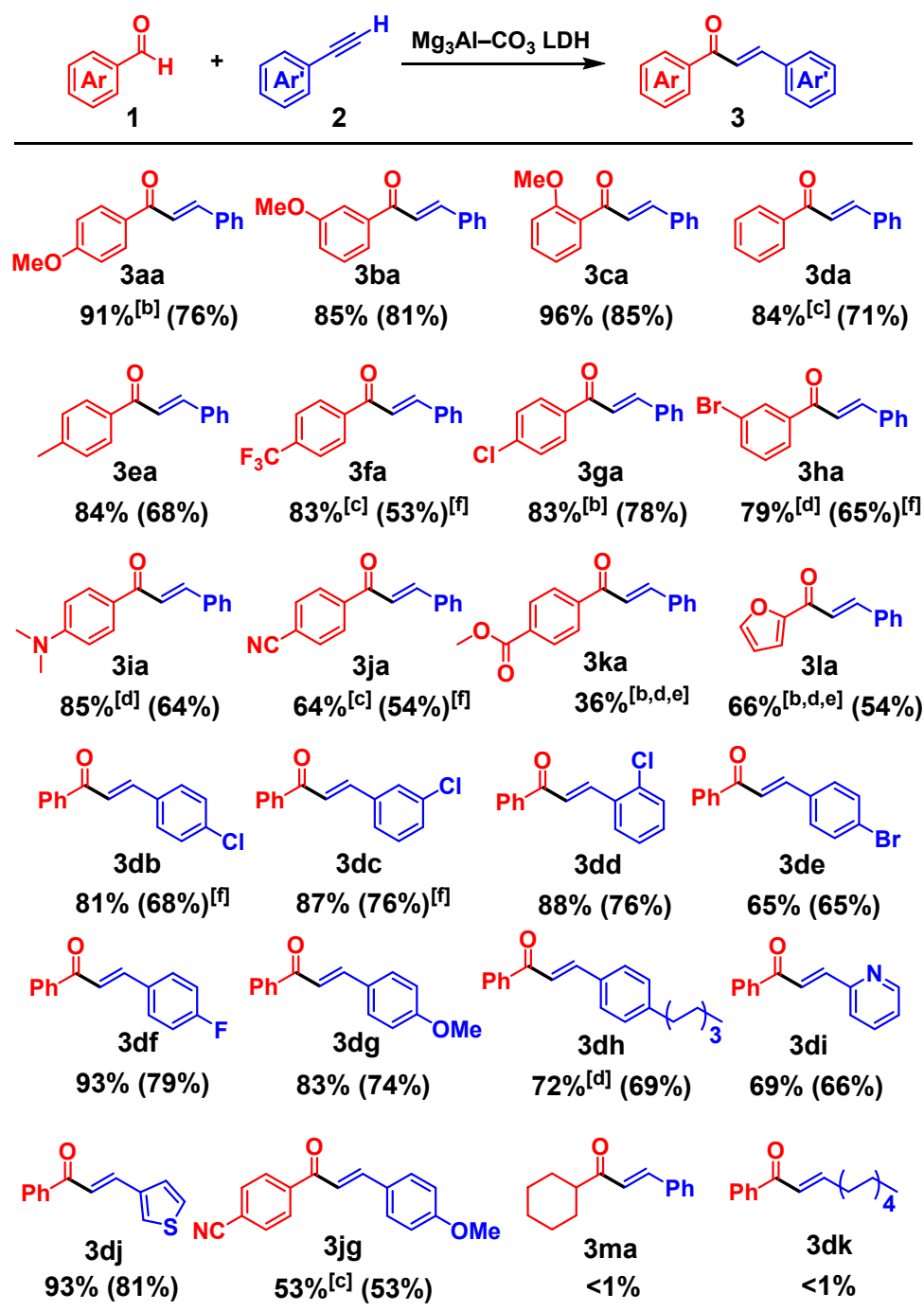


Figure 2-18. XRD patterns and images of (a) Mg₃Al–CO₃ LDH before use, (b) Mg₃Al–CO₃ LDH after the first use, (c) Mg₃Al–CO₃ LDH after the second use, (d) Mg₃Al–CO₃ LDH after the third use, and (e) Mg₃Al–CO₃ LDH after the fourth use.

2.3.4. Substrate Scope

Next, the substrate scope of the present system was investigated. Under the optimized reaction conditions, the formal hydroacylation using various aromatic aldehydes (**1**) and aromatic alkynes (**2**) proceeded efficiently to produce α,β -unsaturated ketones (**3**) in an (*E*)-selective fashion (Table 2-5). The desired products were isolated by simple column chromatography on silica gel (The isolation of (*E*)-4'-(methoxycarbonyl)chalcone (**3ka**) as the sole compound was unsuccessful because the separation of **3ka** and methyl 4-formylbenzoate (**1k**) was quite difficult). When benzaldehydes substituted with a methoxy group at the *o*-, *m*-, or *p*-position were used as the substrates, the formal hydroacylation proceeded efficiently to give the corresponding chalcones in high yields (**3aa–3ca**). Naturally, benzaldehyde can also be used as the substrate (**3da**). The use of benzaldehydes with different substituents, including methyl, trifluoromethyl, chloro, bromo, and amino groups, was also possible with this system (**3ea–3ia**). Moreover, owing to the mild basicity of $\text{Mg}_3\text{Al-CO}_3$ LDH, benzaldehydes possessing cyano or ester groups, for which it is difficult to react efficiently in strongly basic media, can be utilized (**3ja** and **3ka**). When furfural was used as the substrate, the corresponding enone was obtained (**3la**). As well as **2a**, a range of aromatic terminal alkynes can also be used for the present formal hydroacylation. Phenylacetylenes with a chloro group at the *o*-, *m*-, or *p*-position and benzaldehyde were successfully converted into the corresponding chalcones (**3db–3dd**). The formal hydroacylation proceeded efficiently even when using phenylacetylenes bearing a bromo, fluoro, methoxy, or pentyl group as the substrates (**3de–3dh**). Furthermore, 2-ethynylpyridine or 3-ethynylthiophene can be formally hydroacylated by benzaldehyde (**3di** and **3dj**). Using 4-formylbenzonitrile and 1-ethynyl-4-methoxybenzene, the corresponding multi-substituted chalcone can be synthesized (**3jg**). A larger-scale (5 mmol) α,β -unsaturated ketone synthesis was also effective to produce **3aa** in 67% yield from **1a** and **2a** under the conditions described in Figure 2-19. However, this system cannot be applied to aliphatic aldehydes or aliphatic alkynes (**3ma** and **3dk**). For example, when using cyclohexanecarboxaldehyde (**1m**) as the substrate, a byproduct that seemed to be the corresponding propargylic alcohol was obtained in 38% GC yield. When using 1-octyne (**2k**) as the substrate, **2k** was hardly converted and no byproducts were also detected.

Table 2-5. Substrate scope.^[a]



[a] Reaction conditions: **1** (0.5 mmol), **2** (0.6 mmol), $\text{Mg}_3\text{Al-CO}_3$ LDH (130 mg), toluene (2 mL), Ar balloon (1 atm), 120 °C, 15 h. GC Yields of the (*E*) isomers are displayed below chemical structures without parentheses. The values in parentheses are isolated yields. [b] The average value of two or three runs is displayed. [c] 16 h. [d] 24 h. [e] $\text{Mg}_3\text{Al-CO}_3$ LDH (200 mg). [f] The isolated yield includes the (*Z*) isomer (2–6%).

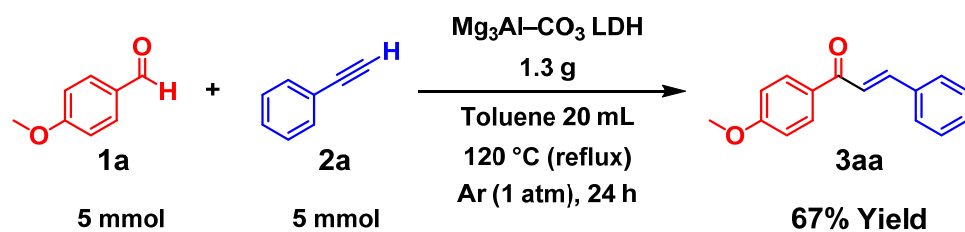


Figure 2-19. Larger-scale synthesis of **3aa** from **1a** and **2a**. Reaction conditions: **1a** (5 mmol), **2a** (5 mmol), $\text{Mg}_3\text{Al-CO}_3$ LDH (1.3 g), toluene (20 mL), 120 °C (reflux), Ar (1 atm), 24 h. The yield was determined by gas chromatography analysis using biphenyl as an internal standard.

2.3.5. Mechanistic Studies

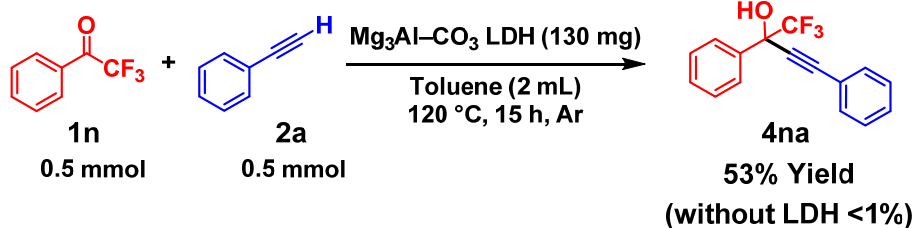
The most likely reaction mechanism of the present formal hydroacylation is the nucleophilic addition of an alkyne toward an aldehyde to produce a propargylic alcohol followed by the alcohol's rearrangement into an α,β -unsaturated carbonyl compound. However, no propargylic alcohol was detected during any of these formal hydroacylations in this system. Thus, to investigate the reaction path, the reaction of 2,2,2-trifluoroacetophenone (**1n**) and **2a** was carried out under the optimized conditions (Figure 2-20a). Consequently, the corresponding propargylic alcohol (**4na**) was produced in a moderate yield because the final rearrangement did not occur as it was a tertiary propargylic alcohol. In addition, using 1,3-diphenylprop-2-yn-1-ol (**4da**) as the substrate, the corresponding α,β -unsaturated carbonyl compound (**3da**) was obtained in 59% yield less than 10 min after the reaction started (Figure 2-20b). At the same time, **4da** was quantitatively converted (*i.e.*, it was undetectable by GC), and the $\text{Mg}_3\text{Al-CO}_3$ LDH became colored, suggesting that **4da** was rapidly deprotonated and adsorbed onto the $\text{Mg}_3\text{Al-CO}_3$ LDH. These results are consistent with the fact that propargylic alcohols cannot be observed when the present formal hydroacylation is conducted. After 3 h, the yield of **3da** increased from 59% to 77%, and the *E/Z* ratio became $>99/<1$ as with the present formal hydroacylation from aldehydes and alkynes though the *E/Z* ratio of **3da** was 86/14 as of 10 min. Naturally, without any catalysts, neither the nucleophilic addition of **2a** to **1n** nor the rearrangement of **4da** proceeded at all. From the above, the nucleophilic addition/rearrangement mechanism was strongly supported.

Next, to determine whether the rearrangement occurs *via* prototropy or hydride transfer (Figure 2-21), deuterated substrates were utilized in this reaction. When the reaction of **1a** and phenylacetylene- d_1 (**D-2a**) was carried out under the optimized conditions, no deuterated **3aa** was produced (Figure 2-20c and ^1H NMR spectra in Figure 2-22); when the reaction of benzaldehyde- $\alpha\text{-d}_1$ (**D-1d**) and **2b** was carried out under the optimized conditions, β -deuterated **3db** was produced, for which the H/D ratio determined by ^1H NMR was 60:40 (Figure 2-20d and Figure 2-23). Thus, the rearrangement of propargylic alcohols catalyzed by $\text{Mg}_3\text{Al-CO}_3$ LDH most likely occurred through prototropy^[8b,c,18] rather than hydride transfer.^[8a]

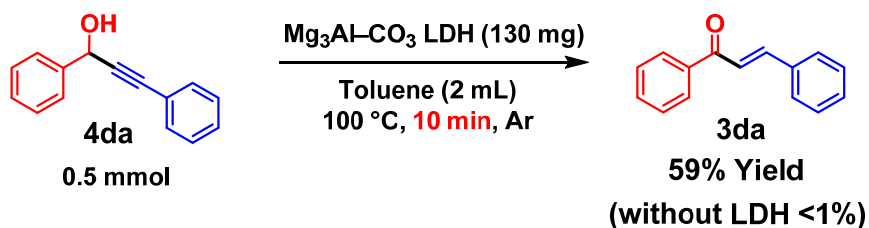
Given previous reports^[8b,c,18] and the results above, I propose a plausible reaction mechanism of the present $\text{Mg}_3\text{Al-CO}_3$ LDH-catalyzed formal hydroacylation as follows

(Figure 2-24). Nucleophilic addition of an alkynyl species catalytically produced owing to the basicity and ionicity of $\text{Mg}_3\text{Al}-\text{CO}_3$ LDH to an aldehyde affords a propargylic alcohol. The basicity necessary for the deprotonation of alkynes is possibly derived from the anionic hydrated layer ($[(\text{CO}_3)\cdot 4\text{H}_2\text{O}]^{2-}$) while the possibility of the metal hydroxide cationic layer ($[\text{Mg}_6\text{Al}_2(\text{OH})_{16}]^{2+}$) cannot be denied. The ionicity necessary for the stabilization of nucleophilic alkynyl anionic species is also derived from the metal hydroxide cationic layer ($[\text{Mg}_6\text{Al}_2(\text{OH})_{16}]^{2+}$) and/or the anionic hydrated layer protonated from alkynes ($[(\text{HCO}_3)\cdot 4\text{H}_2\text{O}]^-$). Then, a delocalized carbanion species is produced through deprotonation of the propargylic alcohol by $\text{Mg}_3\text{Al}-\text{CO}_3$ LDH. Subsequently, this species is protonated to produce an allenol, which immediately tautomerizes to give the formally hydroacylated product.

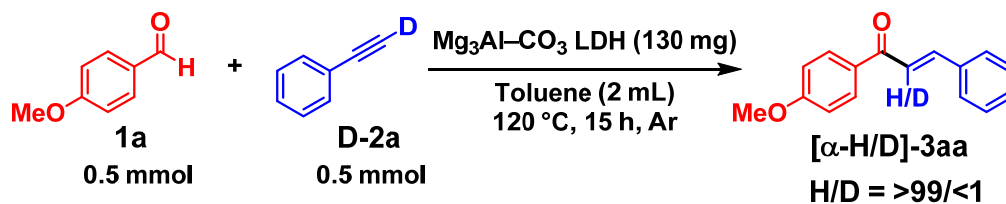
(a)



(b)



(c)



(d)

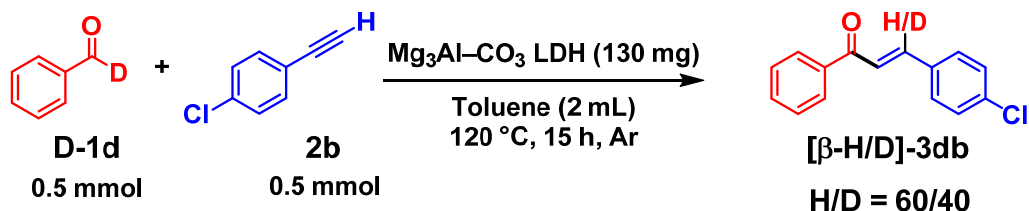
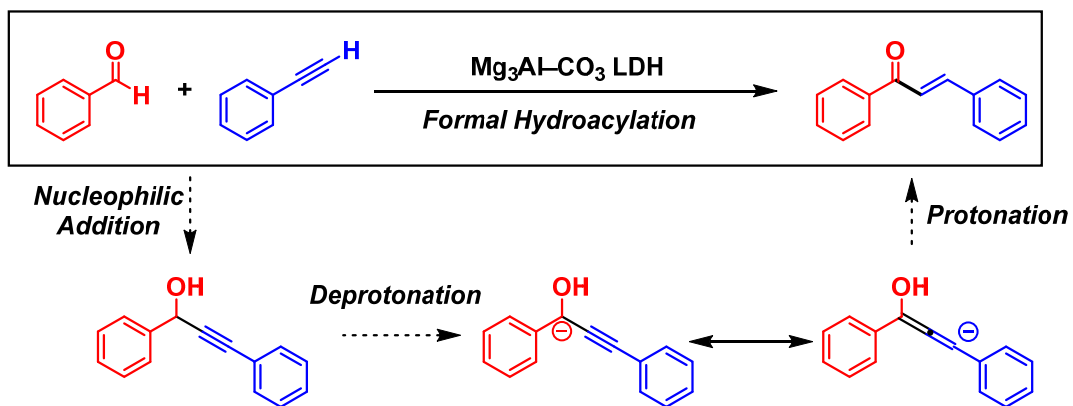


Figure 2-20. Mechanistic studies on the present formal hydroacylation. Reaction conditions are indicated above, and yields were determined by GC. (a) Nucleophilic addition of **2a** to **1n**. (b) Rearrangement from **4da**. (c) LDH-catalyzed formal hydroacylation using **D-2a**. (d) LDH-catalyzed formal hydroacylation using **D-1d**.

(a)



(b)

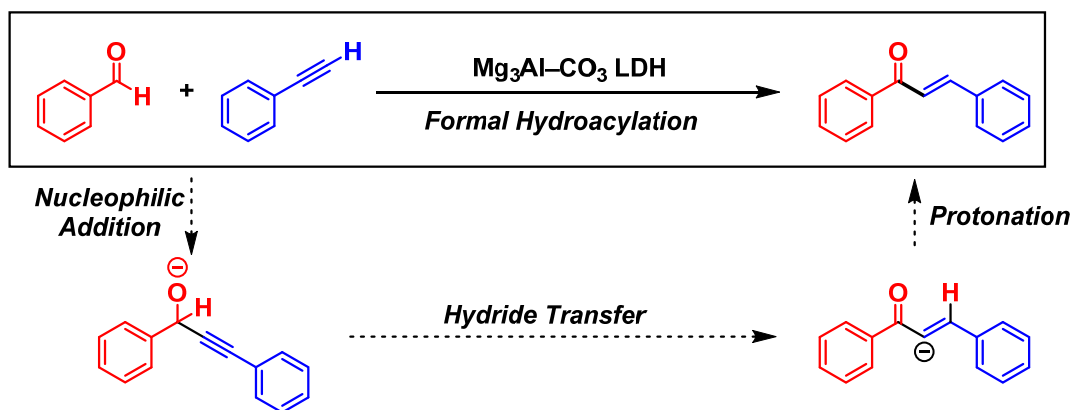


Figure 2-21. Proposed mechanisms of propargylic alcohol rearrangement; (a) prototropy and (b) hydride transfer.

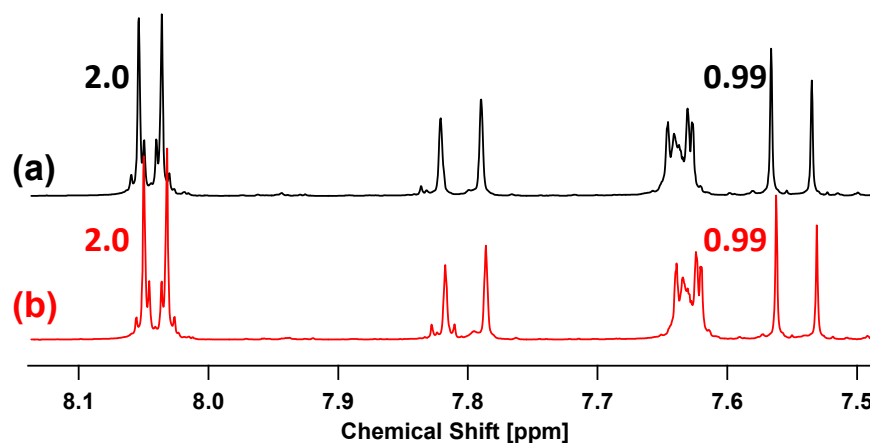


Figure 2-22. ^1H NMR (in CDCl_3) spectra of crude solution after the reaction under the optimized conditions using (a) *p*-anisaldehyde (**1a**) and phenylacetylene (**2a**), and (b) *p*-anisaldehyde (**1a**) and phenylacetylene- d_1 (**D-2a**) as substrates respectively. The numbers next to peaks represent areas of the peaks.

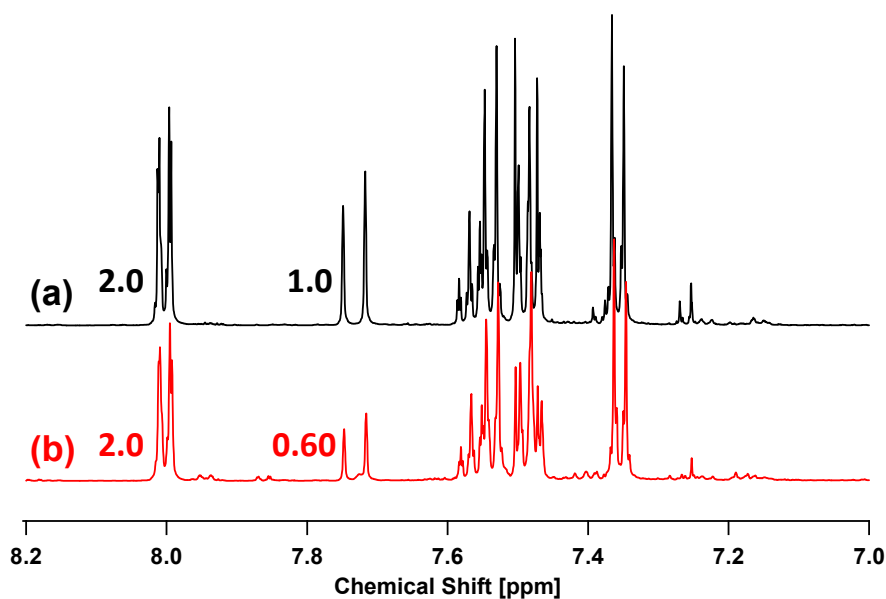


Figure 2-23. ^1H NMR (in CDCl_3) spectra of crude solution after the reaction under the optimized conditions using (a) benzaldehyde (**1d**) and 4-chlorophenylacetylene (**2b**), and (b) benzaldehyde- α - d_1 (**D-1d**) and 4-chlorophenylacetylene (**2b**) as substrates respectively. The numbers next to peaks represent areas of the peaks.

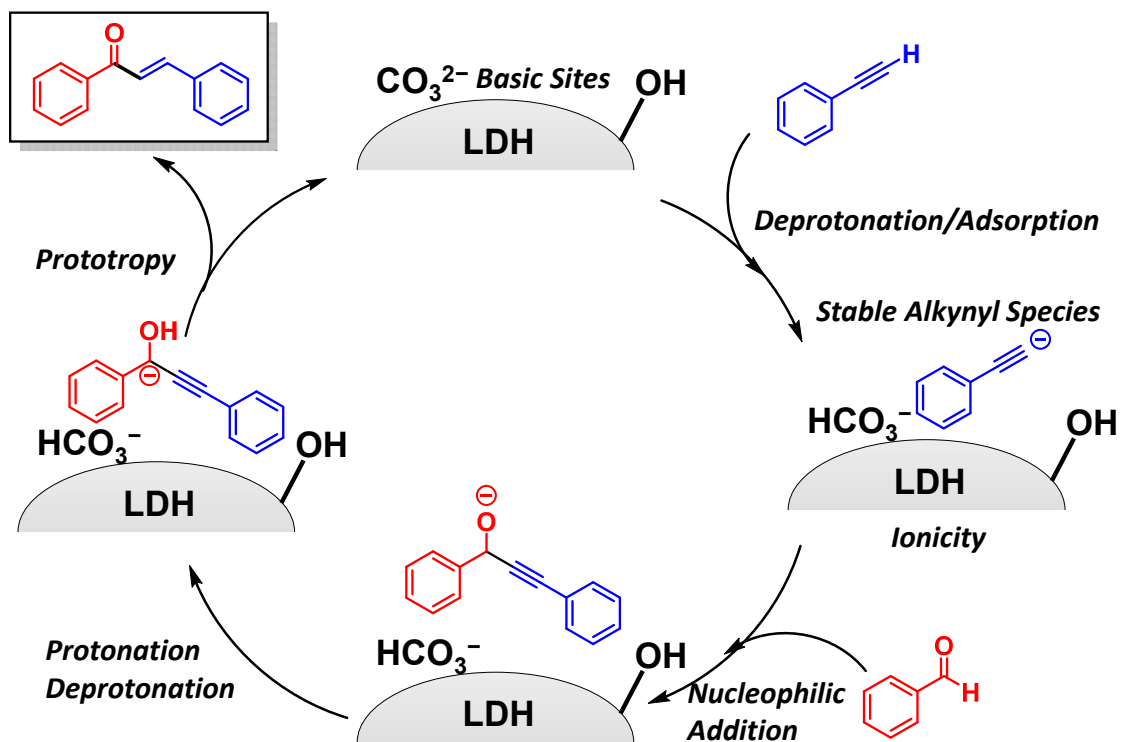


Figure 2-24. Proposed mechanism of $\text{Mg}_3\text{Al-CO}_3$ LDH-catalyzed formal hydroacylation.

2.4. Summary

In summary, I have developed the first transition-metal-free/additive-free regioselective formal hydroacylation of terminal alkynes catalyzed by a commercially available $\text{Mg}_3\text{Al-CO}_3$ LDH. This efficient transformation is enabled by the unique ionicity and basicity of $\text{Mg}_3\text{Al-CO}_3$ LDH, which promotes both the nucleophilic addition of terminal alkynes and prototropy of propargylic alcohols effectively. This system is applicable to various combinations of substrates, even including those with cyano or ester groups, to produce a range of substituted α,β -unsaturated ketones. The present catalysis was confirmed to be truly heterogeneous, and the catalyst can be reused several times without severe loss of its catalytic activity. Considering the fact that hydroacylation is highly atomically economical, the present formal hydroacylation is clearly environmentally friendly. I believe this novel catalysis that exploits the unique properties of $\text{Mg}_3\text{Al-CO}_3$ LDH will allow the future development of novel organic reactions utilizing the specific properties of solid catalysts.

2.5. References

- [1] For reviews on hydroacylation, see: a) C.-H. Jun, E.-A. Jo, J.-W. Park, *Eur. J. Org. Chem.* **2007**, 1869; b) Y. J. Park, J.-W. Park, C.-H. Jun, *Acc. Chem. Res.* **2008**, *41*, 222; c) M. C. Willis, *Chem. Rev.* **2010**, *110*, 725; d) J. C. Leung, M. J. Krische, *Chem. Sci.* **2012**, *3*, 2202; e) S. K. Murphy, V. M. Dong, *Chem. Commun.* **2014**, *50*, 13645; f) A. Ghosh, K. F. Johnson, K. L. Vickerman, J. A. Walker, L. M. Stanley, *Org. Chem. Front.* **2016**, *3*, 639; g) J. D. Neuhaus, M. C. Willis, *Org. Biomol. Chem.* **2016**, *14*, 4986; h) R. Guo, G. Zhang, *Synlett* **2018**, *29*, 1801.
- [2] For examples of hydroacylation with compounds except for alkenes/alkynes, see: a) K. Fuji, T. Morimoto, K. Tsutsumi, K. Kakiuchi, *Chem. Commun.* **2005**, 3295; b) Z. Chen, H. A. Khan, V. M. Dong, *J. Am. Chem. Soc.* **2008**, *130*, 2916; c) K. G. M. Kou, D. N. Le, V. M. Dong, *J. Am. Chem. Soc.* **2014**, *136*, 9471; d) X. Wu, Z. Chen, Y.-B. Bai, V. M. Dong, *J. Am. Chem. Soc.* **2016**, *138*, 12013.
- [3] For examples of hydroacylation catalyzed by transition metal except for Rh, such as Ru, Ni, Ir, Pd, and Co, see: a) S. Omura, T. Fukuyama, J. Horiguchi, Y. Murakami, I. Ryu, *J. Am. Chem. Soc.* **2008**, *130*, 14094; b) Y. Nakao, H. Idei, K. S. Kanyiva, T. Hiyama, *J. Am. Chem. Soc.* **2009**, *131*, 5070; c) S. Hatanaka, Y. Obora, Y. Ishii, *Chem. Eur. J.* **2010**, *16*, 1883; d) T. Fujihara, Y. Katafuchi, T. Iwai, J. Terao, Y. Tsuji, *J. Am. Chem. Soc.* **2010**, *132*, 2094; e) J. Yang, N. Yoshikai, *J. Am. Chem. Soc.* **2014**, *136*, 16748.
- [4] S. Shi, T. Wang, V. Weingand, M. Rudolph, A. S. K. Hashmi, *Angew. Chem. Int. Ed.* **2014**, *53*, 1148.
- [5] M. J. Albaladejo, F. Alonso, M. Yus, M. Chem. *Eur. J.* **2013**, *19*, 5242.
- [6] a) S. Chen, X. Li, H. Zhao, B. Li, *J. Org. Chem.* **2014**, *79*, 4137; b) M. J. Albaladejo, F. Alonso, M. J. González-Soria, *ACS Catal.* **2015**, *5*, 3446; c) U. C. Rajesh, G. Purohit, D. S. Rawat, *ACS Sustainable Chem. Eng.* **2015**, *3*, 2397; d) N. B. Nguyen, G. H. Dand, D. T. Le, T. Truong, N. T. S. Phan, *ChemPlusChem* **2016**, *81*, 361; e) Y. Zhao, Q. Song, *Org. Chem. Front.* **2016**, *3*, 294.
- [7] a) A. E. Favorskii, *J. Russ. Phys. Chem. Soc.* **1905**, *37*, 643; b) R. J. Tedeschi, *J. Org. Chem.* **1965**, *30*, 3045; c) J. H. Babler, V. P. Liptak, N. Phan, *J. Org. Chem.* **1996**, *61*, 416; d) D. Tzalis, P. Knochel, *Angew. Chem. Int. Ed.* **1999**, *38*, 1463; e) H. Miyamoto, S. Yasaka, K. Tanaka, *Bull. Chem. Soc. Jpn.* **2001**, *74*, 185; f) E. Y. Schmidt, N. A.

- Cherimichkina, I. A. Bidusenko, N. I. Protzuk, B. A. Trofimov, *Eur. J. Org. Chem.* **2014**, 4663; g) B. A. Trofimov, E. Y. Schmidt, *Russ. Chem. Rev.* **2014**, 83, 600.
- [8] a) T. Baba, H. Kizuka, H. Handa, Y. Ono, *Appl. Catal. A Gen.* **2000**, 194, 203; b) T. Ishikawa, T. Mizuta, K. Hagiwara, T. Aikawa, T. Kudo, S. Saito, *J. Org. Chem.* **2003**, 68, 3702; c) M. Sun, Q. Shi, G. Huang, Y. Liang, Y. Ma, *Synthesis* **2005**, 15, 2482; d) E. Y. Schmidt, I. A. Bidusenko, N. I. Protsuk, I. A. Ushakov, A. V. Ivanov, A. I. Mikhaleva, B. A. Trofimov, *Chem. Heterocycl. Compd.* **2012**, 48, 822.
- [9] For examples on hydration of alkynes/aldol condensation, see: a) H.-P. Jia, D. R. Dreyer, C. W. Bielawski, *Adv. Synth. Catal.* **2011**, 353, 528; b) N. Mameda, S. Peraka, S. Kodumuri, D. Chevella, R. Banothu, V. Amrutham, N. Nama, *RSC Adv.* **2016**, 6, 58137; c) Y. Zhou, Z. Li, X. Yang, X. Chen, M. Li, T. Chen, S.-F. Yin, *Synthesis* **2016**, 48, 231. For examples on nucleophilic addition/Meyer–Schuster rearrangement, see: d) D. A. Engel, G. B. Dudley, *Org. Lett.* **2006**, 8, 4027; e) E. Mattia, A. Porta, V. Merlini, G. Zanoni, G. Vidari, *Chem. Eur. J.* **2012**, 18, 11894. For examples on aldehyde–alkyne metathesis, see: f) A. Hayashi, M. Yamaguchi, M. Hiram, *Synlett* **1995**, 195; g) K. Miura, K. Yamamoto, A. Yamanobe, K. Ito, H. Kinoshita, J. Ichikawa, A. Hosomi, *Chem. Lett.* **2010**, 39, 766; h) Y. Masuyama, W. Takamura, N. Suzuki, *Eur. J. Org. Chem.* **2013**, 8033; i) K. Murai, K. Tateishi, A. Saito, *Org. Biomol. Chem.* **2016**, 14, 10352.
- [10] Y. Kuroda, Y. Miyamoto, M. Hibino, K. Yamaguchi, N. Mizuno, *Chem. Mater.* **2013**, 25, 2291.
- [11] B. M. Choudary, N. S. Chowdari, M. L. Kantam, K. V. Raghavan *J. Am. Chem. Soc.* **2001**, 123, 9220.
- [12] K. Yamaguchi, N. Mizuno, *Angew. Chem. Int. Ed.* **2002**, 41, 4538.
- [13] X.-F. Wu, H. Neumann, A. Spannenberg, T. Schulz, H. Jiao, M. Beller, *J. Am. Chem. Soc.* **2010**, 132, 14596.
- [14] D. Huang, J.-X. Wang, Y. Hu, Y. Zhang, J. Tang, *Synth. Commun.* **2002**, 32, 971.
- [15] O. G. Schramm (née Dediu), T. J. J. Müller, *Adv. Synth. Catal.* **2006**, 348, 2565.
- [16] V. R. Chintareddy, K. Wadhwa, J. G. Verkade, *J. Org. Chem.* **2011**, 76, 4482.
- [17] M. Tamura, R. Kishi, A. Nakayama, Y. Nakagawa, J. Hasegawa, K. Tomishige, *J. Am. Chem. Soc.* **2017**, 139, 11857.

[18] For the reports on base-catalyzed isomerization of propargylic alcohols with electron withdrawing groups to enones, see: a) A. W. Nineham, R. A. Raphael, *J. Chem. Soc.* **1949**, 0, 118; b) J. P. Sonye, K. Koide, *Synth. Commun.* **2006**, 36, 599; c) P. Sonye, K. Koide, *J. Org. Chem.* **2006**, 71, 6254; d) P. Sonye, K. Koide, *J. Org. Chem.* **2007**, 72, 1846.

Chapter III

Selective Flavonoid Synthesis Enabled by Function-Integrated Solid Catalysts

3.1. Introduction of Flavonoids

Flavonoids—ubiquitous plant secondary metabolites possessing a C₆–C₃–C₆ skeleton whose rings are denoted as A-, C-, and B-rings, respectively, which originates from chalcones (2-benzylidene-2'-hydroxyacetophenone and its derivatives)—exhibit various biological activities such as anti-oxidant, anti-oncogenic, anti-inflammatory, cardiovascular action, and so on.^[1] Almost all of the flavonoids possess 6-membered C-ring that was derived from flavanones through 6-*endo-trig* cyclization of the chalcones that were easily catalyzed by chalcone isomerase (CHI) (Figure 3-1).^[1] In particular, flavonoids possessing flavan skeleton (Figure 3-2), such as flavones, flavanones, flavonols, *etc.* are classified into major flavonoids.^[1a] On the other hand, there are a few kinds of flavonoids that do not have a flavane backbone including chalcones and aurones, which are classified into minor flavonoids.^[1a] Aurones possess a unique 5-membered C-ring formed *via* exceptional biosynthetic routes (the details will be explained in section 3-2.1.)

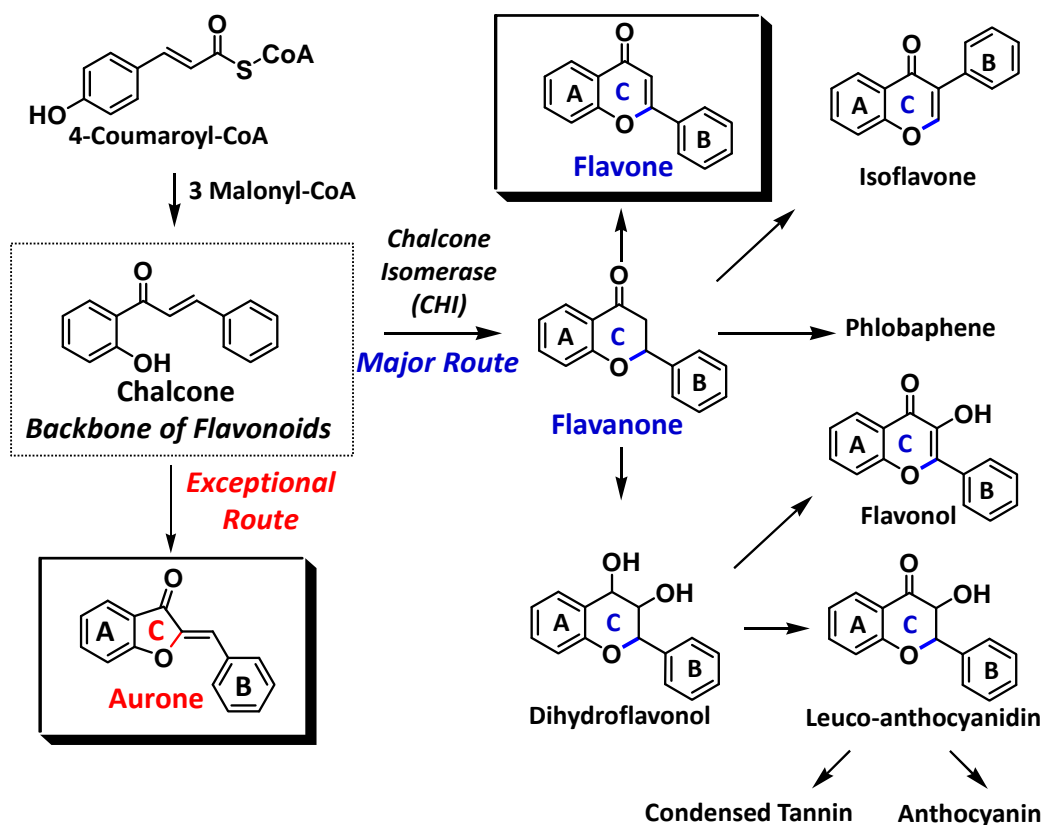


Figure 3-1. Biosynthetic routes of various flavonoids.

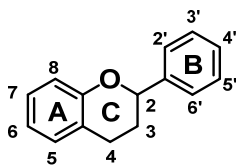


Figure 3-2. Flavan backbone.

Flavonoids have drawn much attention on a variety of biological activities derived from their skeletons, and the structure-activity relationships (SAR) have been investigated by medicinal researchers.^[1] Among various biological activities, anti-oxidants, which scavenge reactive oxygen species (ROS) like single oxygen, super oxide, hydrogen peroxide, and hydroxyl radical, have been widely studied.^[1,2b] Oxidative stress, defined as “a state where oxidative forces exceed the antioxidant systems due to loss of the balance between them”^[2a], is associated with several lifestyle-related diseases such as atherosclerosis, hypertension, diabetes mellitus, *etc.*^[2,3a], and the development of effective anti-oxidants is important. The anti-oxidant activity of major flavonoids depends on the following conditions about their structures; I) the catechol moiety at B-ring (hydroxylated at C-3' and C-4' positions) II) 4-oxo group with C=C bond, typically, α,β -unsaturated carbonyl structure at C-ring, III) 3- and 5-OH or other functional groups at these positions.^[1a,2b,3a] For examples, as to flavones, an ideal structure which has high potential of anti-oxidant abilities is shown in Figure 3-3 (left). In fact, quercetin, which satisfies all of the aforementioned requirements, shows substantially high anti-oxidant activity (Figure 3-3, right).^[2b] The first requirement is related to scavenging activities of ROS; the catechol group reacts with ROS to produce the corresponding quinone (Figure 3-4). The second one is necessary to delocalize electrons from a B-ring. The third one enables the flavones to chelate oxidative metal cations (Figure 3-5).^[1a,2b,3a]

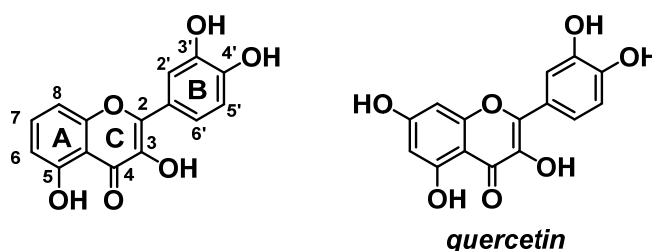


Figure 3-3. Flavone structure which demands all requirements for anti-oxidants.

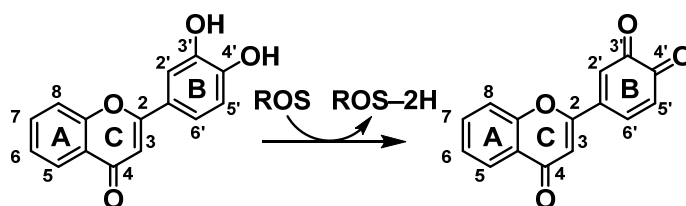


Figure 3-4. Reaction path of the catechol moiety at a B-ring with ROS.

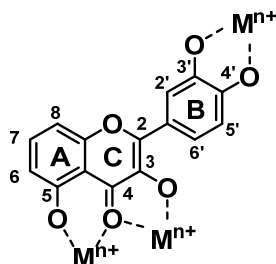


Figure 3-5. Possible chelation systems of flavones which meet the all requirements.

Another major and important biological activity which many flavonoids show is anti-cancer.^[1,3] Flavonoid structures affect the docking and interaction mode between medicinal criteria of flavonoids and target kinases such as cyclin-dependent kinases (CDKs), glycogen synthase kinase-3 (GSK3), dual specificity tyrosine-phosphorylation-regulated kinase 1A (DYRK1A), and cdc2-like kinase (CLK1), resulting in the change of their anti-cancer activities.^[1,3] For example, 8-substituted flavones were much more active toward CDKs, GSK3, and CLK1 than 6-substituted ones (Figure 3-6, IC₅₀: half maximal inhibitory concentration).^[3b] The IC₅₀ difference between the (*R*)- and (*S*)-isomer can be explained using docking molecular models, *i.e.*, the (*R*)-isomer establishes better interaction with the active site residues of CDK1 than the counterpart.^[3b]

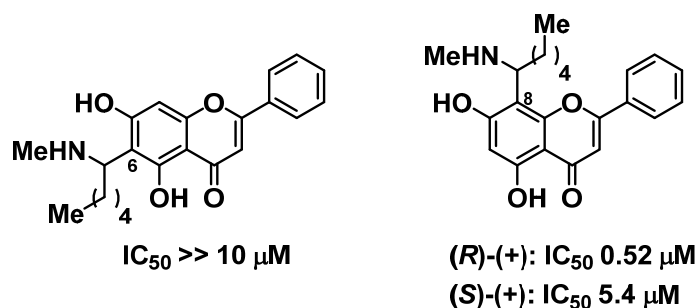


Figure 3-6. SAR of flavones toward CDK1.^[3b]

Besides flavones, aurones show various biological activities although the reported number is small compared with those of flavones.^[4] In terms of theoretical bond dissociation energy (BDE) and ionization potential (IP), 4'-O-H bond at the C-ring of aurones is generally weaker than those of their flavonoid analogues, revealing the high potential of aurones' antioxidant activities.^[4a] SAR of aurones toward several kinases have been also investigated.^[4] For instance, the activities of acetylcholinesterases (AChE) and/or butyrylcholinesterases (BChE), that is, human cholinesterases (ChEs), considered to be related to Alzheimer's disease, were inhibited by 4'-substituted aurones (Figure 3-7) *via* various interactions including hydrogen bonding, π - π stacking interaction, π -anion interaction, and π -alkyl interaction.^[4b] Considering the difference between two aurones' activities in Figure 3-7, the presence of π -alkyl interaction may be important for the aurones to inhibit BChE.

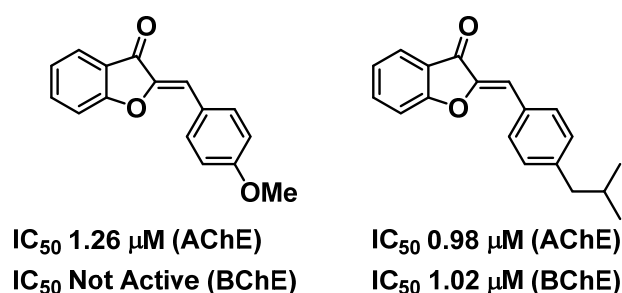


Figure 3-7. SAR of aurones toward ChEs.^[4b]

To broaden the pharmaceutical applications of flavonoids, efficient selective synthesis of respective flavonoids should be developed. Chalcones are easily synthesized through Claisen-Schmidt condensation from aldehydes and ketones, and plant-derived ones are also obtained as mentioned above. Thus, practical selective synthetic procedures from chalcones are desirable to promote researches on novel biological activities and SAR of flavonoids.

In this chapter, environmentally-friendly simple selective synthesis of flavones, one of the most major flavonoids, and aurones, a minor flavonoid possessing a unique structure, *via* chalcones have been established by utilizing function-integrated catalysts. Firstly, in the next section, one-pot selective flavone synthesis starting from aldehydes (or alcohols) and ketones will be developed in the presence of gold nanoparticle catalysts supported on a layered double hydroxide.

3-1 One-Pot Selective Flavone Synthesis Catalyzed by Gold Nanoparticles Supported on Layered Double Hydroxide

Adapted with permission from *Angew. Chem. Int. Ed.* **2015**, 54, 13302–13306.

Copyright 2015 John Wiley and Sons and Copyright Clearance Center.

3-1.1. Introduction

Flavones are a class of flavonoids based on the skeleton of 2-phenylchromen-4-one (shown as a green skeleton in Figure 3-8) and present in many fruits and vegetables.^[3] As mentioned in section 3.1., they possess a variety of biological activities due to the basic skeleton and have especially been found to be effective for several diseases related to oxidative stress, such as arteriosclerosis, diabetes, cancer, Alzheimer's disease, and Parkinson's disease.^[3] In addition, their activities and targets are largely dependent on their substitution patterns.^[3] Therefore, in order to discover flavone-based prominent lead compounds for varied diseases, not only the detailed investigations on their structure-activity dependences but also the development of new efficient procedures for their synthesis and structural modification is very important.

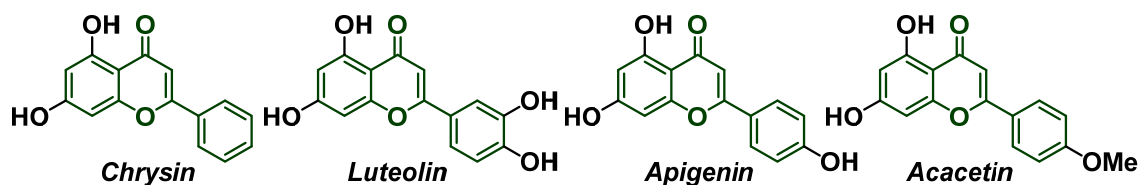


Figure 3-8. Representative flavones.

Until now, various kinds of flavones have been synthesized by utilizing two major routes (Routes A and B).^[3,5–7] Route A (β -diketone route) is traditional and the most frequently utilized choice (Figure 3-9). The second step of the procedure is known as Baker–Venkataraman rearrangement (Figure 3-10).^[5a,b] The flavone synthesis typically proceeds *via* the condensation of 2'-hydroxyacetophenones with acid chlorides followed by rearrangement to produce the β -diketone intermediates in the presence of strong bases. The reaction using anhydrides instead of acid chlorides is called Allan–Robinson reaction.^[5c] Then, the acid-catalyzed cyclodehydration of the β -diketones gives the corresponding flavones. Route A is intrinsically the step-by-step procedure, and the use

of strong acids, strong bases (typically in super-stoichiometric amounts), and pre-activated substrates ought to be required.^[5]

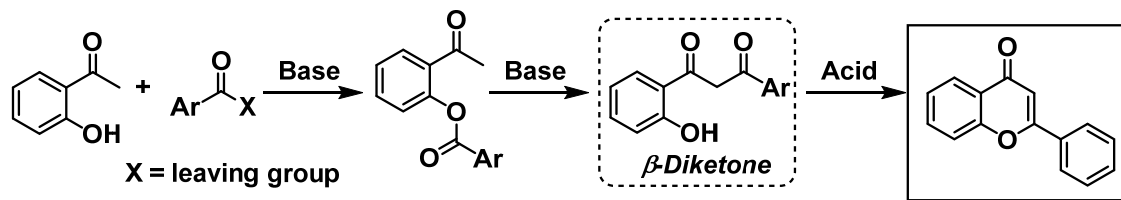


Figure 3-9. Flavone synthetic route A (β -diketone route).

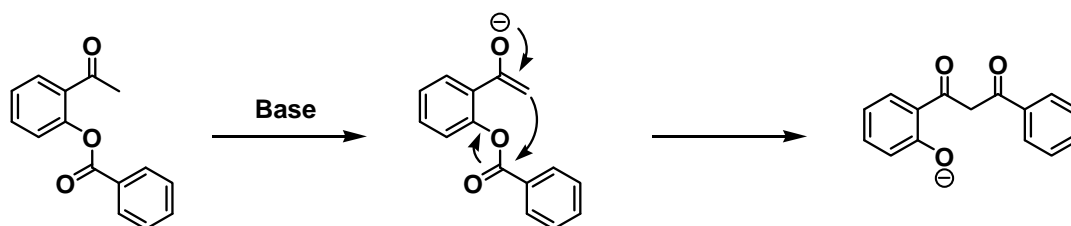


Figure 3-10. Baker–Venkataraman rearrangement.

Route B (chalcone route) is an attractive procedure because the 2'-hydroxychalcone intermediates can readily be synthesized by the base-catalyzed Claisen–Schmidt condensation of readily available 2'-hydroxyacetophenones and benzaldehydes (Figure 3-11).^[6] However, the oxidative dehydrogenation step in Route B is still problematic, and halogen-, organic-, or metal-based oxidants, *e.g.*, Br₂, I₂, DDQ (DDQ = 2,3-dichloro-5,6-dicyano-*p*-benzoquinone), I₂-DMSO (DMSO = dimethyl sulfoxide), and SeO₂, have generally been utilized.^[6] Although the ionic liquid-promoted homogeneously Cu-catalyzed aerobic oxidative cyclization of 2'-hydroxychalcones to flavones^[6k] and homogeneously Pd-catalyzed aerobic oxidative dehydrogenation of saturated ketones to α,β -unsaturated ketones including flavones^[8] have recently been reported, the direct synthesis from 2'-hydroxyacetophenones and benzaldehydes using molecular oxygen as the sole oxidant has not been demonstrated, and thus 2'-hydroxychalcones or flavanones should separately be prepared.

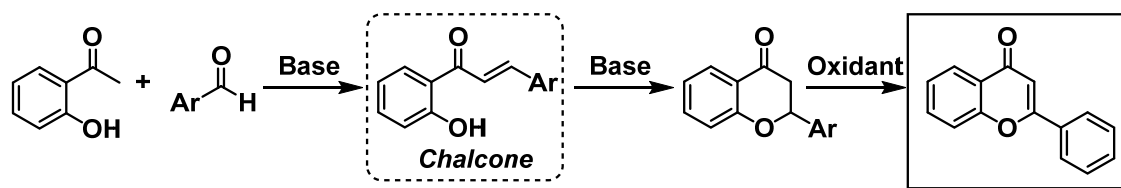


Figure 3-11. Flavone synthetic route B (chalcone route).

As written in Chapter I, the use of heterogeneous catalysts for liquid-phase fine chemical synthesis including one-pot synthesis has emerged, and numerous powerful catalysts and catalytic systems have been developed to date. Despite the advantages of heterogeneous catalysts, most of the previously reported systems for flavone synthesis are homogeneous ones.^[3,5-7] Thus, if the above-mentioned Route B can be realized as a heterogeneously catalyzed one-pot procedure using molecular oxygen (in air) as the terminal oxidant, it will be one of the greenest and powerful procedures for the synthesis of flavones.

In this section, I have successfully developed for the first time an efficient heterogeneously catalyzed one-pot synthesis of flavones and its derivatives starting directly from 2'-hydroxyacetophenones and benzaldehydes (or benzyl alcohols) in the presence of gold nanoparticles supported on $\text{Mg}_4\text{Al}_2(\text{OH})_{12}(\text{CO}_3) \cdot n\text{H}_2\text{O}$, *i.e.*, $\text{Mg}_2\text{Al}-\text{CO}_3$ layered double hydroxide (Au/LDH). The present one-pot procedure is composed of the sequence of Claisen–Schmidt condensation (base catalysis), intramolecular oxa-Michael addition (base catalysis), and aerobic oxidative dehydrogenation of chromanones (gold catalysis) (Figure 3-12). When using benzyl alcohols as the starting materials, the sequence begins with aerobic oxidation of alcohols (gold catalysis) (see the references of [16n–p] in Chapter I). Au/LDH plays the multiple roles to catalyze all the different types of reactions included in the sequence. In particular, supported gold-catalyzed oxidative dehydrogenation of chromanones is hitherto unknown although gold catalysts have emerged and been utilized for various oxidative functional group transformations (see section 1.1.4.3.). In Mizuno and co-workers' work on enaminal synthesis using Au nanoparticles supported on manganese oxide octahedral molecular sieves (Au/OMS-2), the oxidative dehydrogenation of saturated ketones by gold catalysis was reported, which was applied only to β -nitrogen substituted ones.^[9] The catalysis of Au/LDH is truly heterogeneous, and Au/LDH can be reused without a severe loss of its catalytic performance. The present procedure possesses several noteworthy features; for example, (i) use of the reusable heterogeneous catalyst, (ii) simple one-pot operation and avoidance of tedious isolation steps of the intermediates, (iii) use of the greenest oxidant of molecular oxygen (in air) as the terminal oxidant, (iv) use of readily available starting materials, (v) disuse of additives, and (vi) formation of water as the theoretical by-product.

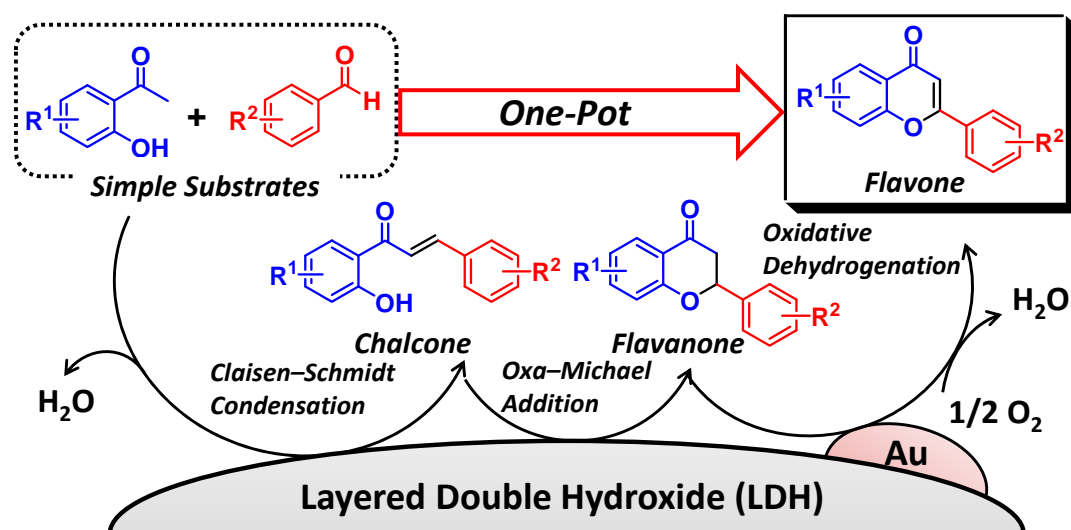


Figure 3-12. Overview of one-pot selective flavone synthesis catalyzed by Au/LDH.

3-1.2. Experimental

3-1.2.1. Instruments and Reagents

GC analyses were performed on Shimadzu GC-2014 with a FID detector equipped with a TC-5 capillary column. GC-MS spectra were recorded on Shimadzu GCMS-QP2010 equipped with an InertCap5 capillary column at an ionization voltage of 70 eV. Liquid-state ^1H and ^{13}C NMR spectra were recorded on JEOL JNM-ECA 500. ^1H and ^{13}C NMR were measured at 500 and 125 MHz, respectively, with TMS as an internal standard ($\delta = 0$ ppm). ICP-AES analyses were performed on Shimadzu ICPS-8100. TEM measurements were performed on JEOL JEM-2000EX II. TEM samples were prepared by placing a drop of the suspension on carbon-coated Cu grids and dried in air. BET surface areas were measured on micromeritics ASAP 2010 and calculated from the N_2 adsorption isotherm with the BET equation. XRD patterns were recorded using a Rigaku SmartLab instrument under $\text{Cu K}\alpha$ radiation (45 kV, 200 mA). The XPS measurements were carried out on JEOL JPS-9000 using $\text{Mg K}\alpha$ radiation ($h\nu = 1253.6$ eV, 8 kV, 10 mA). IR spectra were measured on Jasco FT/IR-4100 using KBr disks. Elemental analyses for C, H, and N were performed on Yanaco MT-6. Al_2O_3 ($160\text{ m}^2\text{ g}^{-1}$, Cat. No. KHS-24, Sumitomo Chemical), TiO_2 ($316\text{ m}^2\text{ g}^{-1}$, Cat. No. ST-01, Ishihara Sangyo Kaisya), and CeO_2 ($111\text{ m}^2\text{ g}^{-1}$, Cat. No. 544841-25G, Aldrich), were commercially available. Solvents and substrates were obtained from Kanto Chemical, TCI, Wako, or Aldrich (reagent grade). Substrates were purified by kugelrohr distillation just before the use for reactions.

3-1.2.2. Preparation of Catalysts

$\text{Mg}_4\text{Al}_2(\text{OH})_{12}(\text{CO}_3) \cdot n\text{H}_2\text{O}$ ($\text{Mg}_2\text{Al}-\text{CO}_3$ LDH) was prepared by the previously reported coprecipitation method (refer to section 2.2.2. in Chapter II). The supported gold nanoparticle catalyst on LDH (Au/LDH) was prepared as follows. $\text{Mg}_2\text{Al}-\text{CO}_3$ LDH (1.0 g) was added to an aqueous solution of HAuCl_4 (3 mM, 50 mL). After vigorously stirring the mixture for 2 min, aqueous NH_3 (10 %, 90 μL) was added, and the resulting mixture was stirred at room temperature for 14 h. The resulting slurry was filtered, washed with deionized water, and dried at room temperature under vacuum, giving the supported gold precursor. Then, the precursor (1.0 g) was dispersed in deionized water (100 mL) and treated with NaBH_4 (20 mg) at room temperature for 1 h. After filtration, washing, and drying, Au/LDH catalyst was obtained as reddish purple powder (Au content determined by ICP-AES: 2.4wt%, mean diameter: 4.2 nm).

Au/ TiO_2 (Au content: 1.9wt%, mean diameter: 4.4 nm), Au/ CeO_2 (Au content: 2.6wt%, mean diameter: 3.0 nm), and Au/ Al_2O_3 (Au content: 2.2wt%, mean diameter: 14.3 nm) were prepared in the same way as mentioned above. Au/ Al_2O_3 (Au content: 3.1wt%, mean diameter: 3.2 nm) was prepared by the reported procedure (see the reference of [17k] in Chapter I). For the preparation of Ru/LDH, Rh/LDH, and Pd/LDH, the supported hydroxide precursors were prepared according to the reported procedures,^[10] followed by the reduction using NaBH_4 . By the equilibrium adsorption method using K_2PtCl_6 without adjusting pH, the platinum species was supported on $\text{Mg}_2\text{Al}-\text{CO}_3$ LDH, followed by the reduction using NaBH_4 , giving Pt/LDH.

3-1.2.3. Reactions and Synthesis

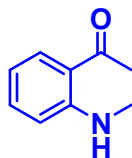
Catalytic Reaction: The catalytic reaction was typically carried out according to the following procedure. Into a Pyrex glass reactor (volume: ~20 mL) were successively placed Au/LDH (Au: 3 mol%), biphenyl (0.1 mmol, internal standard), 2'-hydroxyacetophenone (**1a**, 0.5 mmol), benzaldehyde (**2a**, 0.5 mmol), mesitylene (2 mL), and a Teflon-coated magnetic stir bar, and then the mixture was stirred at 130 °C under open air (1 atm). The yields of products were determined by GC analysis using biphenyl as an internal standard. As for isolation of products, an internal standard was not added. After the reaction, the catalyst was removed by simple filtration, and then the filtrate was concentrated by evaporation of mesitylene. The crude product was subjected to column chromatography on silica gel (typically using CHCl₃/EtOAc = 19/1 as an eluent), giving the pure flavone and its derivatives. The products were identified by GC-MS and NMR (¹H and ¹³C) analyses.

Leaching Test: To establish whether the catalytic reaction occurred on solid Au/LDH or not, the catalyst was removed by hot filtration 3 h after the reaction started under the optimized conditions and the reaction was again carried out with the filtrate under the same conditions. When the amount of leached metals was measured, the filtrate after the reaction for 24 h was evaporated *in vacuo*, treated with concentrated aqua regia (1 mL), and sonicated. Then, Au, Mg, and Al species in the filtrate were analyzed by ICP-AES after the filtrate was moved into a 100 mL volumetric flask.

Reuse Test: After the reaction, Au/LDH was retrieved from the reaction mixture by simple filtration using a PTFE membrane filter. The retrieved catalyst was washed with an aqueous solution of Na₂CO₃ (0.1 M), acetone and deionized water. Then, the catalyst was dried *in vacuo* for 1 h before being used for the reuse experiment.

Synthesis of 2'-(methylamino)acetophenone (1d**):** 2'-(methylamino)acetophenone (**1d**) was synthesized referring to the previous report.^[11] 2-Aminoacetophenone (17.5 mmol) and MeI (37.0 mmol) were added to dehydrated toluene (17.5 mL), and then stirred for 48 h under reflux conditions. After removing precipitation by filtration, the solution was evaporated under reduced pressure. The crude product was subjected to

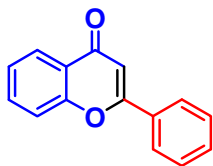
column chromatography on silica gel (hexane/EtOAc = 10/1 as an eluent), affording the desired **1d** as yellow liquid (0.88 g).



1d (CAS No. 1859-75-2)

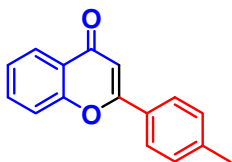
2'-(methylamino)acetophenone (1d): ^1H NMR (500 MHz, CDCl_3 , TMS): δ 2.58 (s, 3H), 2.92 (d, $J = 5.5$ Hz, 3H), 6.59 (ddd, $J = 8.0$, 7.0 and 1.0 Hz 1H), 6.69 (d, $J = 8.5$ Hz, 1H), 7.38 (ddd, 8.5, 7.0 and 1.5 Hz, 1H), 7.74 (dd, $J = 8.0$ and 1.5 Hz, 1H), 8.78 (s, 1H). MS (70 eV, EI): m/z (%): 149 (92) [M^+], 134 (100), 132 (37), 116 (22), 106 (33), 91 (21), 79 (25), 78 (12), 77 (39), 51 (13).

3-1.2.4. Spectral Data of Products



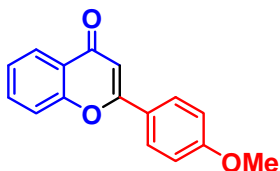
3aa (CAS No. 525-82-6)

2-phenylchromen-4-one (3aa): ^1H NMR (500 MHz, CDCl_3 , TMS): δ 6.82 (s, 1H), 7.42 (t, $J = 7.5$ Hz, 1H), 7.50–7.57 (m, 4H), 7.70 (ddd, $J = 8.5$, 7.0 and 1.5 Hz, 1H), 7.91–7.94 (m, 2H), 8.23 (dd, $J = 8.0$ and 1.5 Hz, 1H). ^{13}C – $\{^1\text{H}\}$ NMR (125 MHz, CDCl_3 , TMS): δ 107.71, 118.19, 124.09, 125.34, 125.82, 126.41, 129.15, 131.71, 131.90, 133.88, 156.38, 163.51, 178.54. MS (70 eV, EI): m/z (%): 223 (16), 222 (100) [M^+], 221 (33), 194 (46), 165 (12), 120 (61), 102 (10), 97 (14), 92 (42), 82 (12), 64 (14), 63 (12). Anal. Calcd. for $\text{C}_{15}\text{H}_{10}\text{O}_2$: C, 81.07; H, 4.54. Found: C, 81.49; H, 4.82.



3ab (CAS No. 41255-30-5)

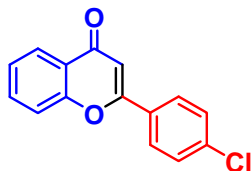
2-(4-methylphenyl)chromen-4-one (3ab): ^1H NMR (500 MHz, CDCl_3 , TMS): δ 2.43 (s, 3H), 6.79 (s, 1H), 7.32 (d, $J = 8.0$ Hz, 2H), 7.41 (t, $J = 7.5$ Hz, 1H), 7.55 (d, $J = 8.0$ Hz, 1H), 7.68 (ddd, $J = 9.0$, 7.5 and 2.0 Hz, 1H), 7.82 (d, $J = 8.5$ Hz, 2H), 8.23 (dd, $J = 8.0$ and 2.0 Hz, 1H). ^{13}C – $\{^1\text{H}\}$ NMR (125 MHz, CDCl_3 , TMS): δ 21.66, 107.11, 118.18, 124.13, 125.24, 125.81, 126.35, 129.10, 129.89, 133.76, 142.37, 156.38, 163.72, 178.57. MS (70 eV, EI): m/z (%): 237 (18), 236 (100) [M^+], 235 (22), 221 (31), 208 (33), 121 (10), 120 (50), 116 (23), 115 (38), 104 (10), 92 (37), 89 (15), 64 (13), 63 (15). Anal. Calcd. for $\text{C}_{16}\text{H}_{12}\text{O}_2$: C, 81.34; H, 5.12. Found: C, 81.84; H, 5.19.



3ac (CAS No. 4143-74-2)

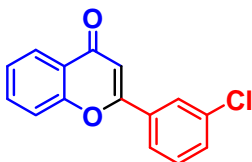
2-(4-methoxyphenyl)chromen-4-one (3ac): ^1H NMR (500 MHz, CDCl_3 , TMS): δ 3.89 (s, 3H), 6.74 (s, 1H), 7.00–7.03 (m, 2H), 7.40 (ddd, $J = 7.5$, 7.0 and 1.0 Hz, 1H), 7.54 (dd, $J = 8.5$ and 0.5 Hz, 1H), 7.68 (ddd, $J = 8.5$, 7.0 and 1.5 Hz, 1H), 7.86–7.89 (m, 2H), 8.22 (dd, $J = 8.0$ and 2.0 Hz, 1H). ^{13}C – $\{^1\text{H}\}$ NMR (125 MHz, CDCl_3 , TMS): δ 55.62,

106.30, 114.58, 118.08, 124.06, 124.14, 125.19, 125.78, 128.11, 133.68, 156.30, 162.53, 163.53, 178.50. MS (70 eV, EI): m/z (%): 253 (16), 252 (100) [M^+], 251 (29), 224 (11), 221 (15), 209 (14), 181 (10), 132 (80), 117 (23), 112 (10), 92 (20), 89 (28), 64 (12), 63 (19). Anal. Calcd. for $C_{16}H_{12}O_3$: C, 76.18; H, 4.79. Found: C, 76.50; H, 4.94.



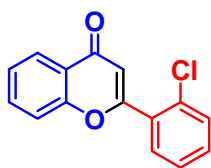
3ad (CAS No. 10420-75-4)

2-(4-chlorophenyl)chromen-4-one (3ad): 1H NMR (500 MHz, $CDCl_3$, TMS): δ 6.79 (s, 1H), 7.43 (t, $J = 7.5$ Hz, 1H), 7.49–7.51 (m, 2H), 7.56 (d, $J = 8.0$ Hz, 1H), 7.71 (ddd, $J = 8.5, 7.0$ and 1.5 Hz, 1H), 7.85–7.88 (m, 2H), 8.23 (dd, $J = 8.0$ and 1.5 Hz). ^{13}C – $\{^1H\}$ NMR (125 MHz, $CDCl_3$, TMS): δ 107.85, 118.17, 124.07, 125.50, 125.90, 127.68, 129.52, 130.41, 134.03, 138.02, 156.31, 162.34, 178.34. MS (70 eV, EI): m/z (%): 258 (34), 257 (24) [M^+], 256 (100), 255 (24), 230 (17), 228 (49), 221 (20), 165 (13), 136 (13), 120 (100), 114 (19), 101 (11), 92 (76), 82 (19), 75 (15), 64 (26), 63 (21). Anal. Calcd. for $C_{15}H_9O_2Cl$: C, 70.19; H, 3.53. Found: C, 70.72; H, 3.70.



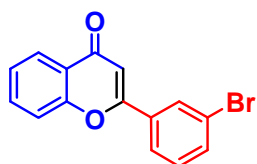
3ae (CAS No. 1849-61-2)

2-(3-chlorophenyl)chromen-4-one (3ae): 1H NMR (500 MHz, $CDCl_3$, TMS): δ 6.81 (s, 1H), 7.42–7.53 (m, 3H), 7.58 (d, $J = 8.0$ Hz, 1H), 7.72 (ddd, $J = 8.5, 7.0$ and 1.5 Hz, 1H), 7.79 (ddd, $J = 7.5, 1.5$ and 1.5 Hz, 1H), 7.93 (t, $J = 1.5$ Hz, 1H), 8.23 (dd, $J = 8.0$ and 2.0 Hz, 1H). ^{13}C – $\{^1H\}$ NMR (125 MHz, $CDCl_3$, TMS): δ 108.32, 118.23, 124.08, 124.52, 125.59, 125.91, 126.51, 130.47, 131.65, 133.76, 134.13, 135.43, 156.33, 161.94, 178.35. MS (70 eV, EI): m/z (%): 258 (28), 257 (25) [M^+], 256 (98), 255 (21), 230 (30), 228 (67), 221 (15), 165 (20), 120 (100), 114 (23), 92 (98), 82 (21), 75 (25), 74 (12), 64 (32), 63 (34), 50 (16). Anal. Calcd. for $C_{15}H_9O_2Cl$: C, 70.19; H, 3.53. Found: C, 70.37; H, 3.73.



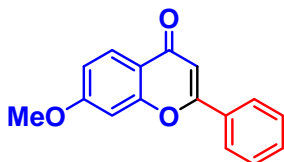
3af (CAS No. 116115-48-1)

2-(2-chlorophenyl)chromen-4-one (3af): ^1H NMR (500 MHz, CDCl_3 , TMS): δ 6.66 (s, 1H), 7.40–7.48 (m, 3H), 7.51–7.55 (m, 2H), 7.64 (dd, $J = 7.5$ and 2.0 Hz, 1H), 7.70 (ddd, $J = 9.0$, 7.0 and 2.0 Hz, 1H), 8.26 (dd, $J = 8.0$ and 1.5 Hz, 1H). ^{13}C – $\{^1\text{H}\}$ NMR (125 MHz, CDCl_3 , TMS): δ 113.12, 118.32, 123.96, 125.46, 125.86, 127.22, 130.76, 130.93, 131.90, 132.03, 133.04, 134.04, 156.71, 162.77, 178.24. MS (70 eV, EI): m/z (%): 258 (26), 257 (13) [M^+], 256 (79), 230 (12), 228 (36), 221 (40), 165 (13), 136 (10), 120 (100), 114 (13), 101 (13), 92 (85), 82 (17), 75 (18), 74 (11), 64 (32), 63 (27), 50 (10). Anal. Calcd. for $\text{C}_{15}\text{H}_9\text{O}_2\text{Cl}$: C, 70.19; H, 3.53. Found: C, 70.74; H, 3.66.



3ag (CAS No. 3754-53-8)

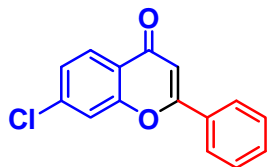
2-(3-bromophenyl)chromen-4-one (3ag): **3aa** is also formed as a by-product, and the mixture of **3ag** (63%) and **3aa** (8%) was isolated. ^1H NMR (500 MHz, CDCl_3 , TMS): δ 6.79 (s, 1H), 7.38–7.45 (m, 2H), 7.58 (d, $J = 8.0$ Hz, 1H), 7.65–7.73 (m, 2H), 7.83 (d, $J = 8.0$ Hz, 1H), 8.07 (t, $J = 2.0$ Hz, 1H), 8.22 (dd, $J = 8.0$ and 1.5 Hz, 1H). ^{13}C – $\{^1\text{H}\}$ NMR (125 MHz, CDCl_3 , TMS): δ 108.25, 118.19, 123.33, 124.00, 124.91, 125.53, 125.84, 129.33, 130.64, 133.88, 134.09, 134.52, 156.25, 161.75, 178.27. MS (70 eV, EI): m/z (%): 303 (10), 302 (62), 301 (15) [M^+], 300 (61), 274 (34), 272 (35), 221 (17), 165 (23), 137 (12), 136 (12), 120 (99), 101 (28), 92 (100), 83 (26), 76 (13), 75 (30), 74 (16), 64 (34), 63 (33), 51 (15), 50 (17).



3ba (CAS No. 22395-22-8)

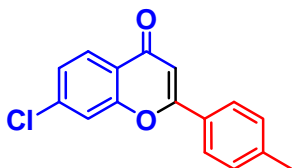
7-methoxy-2-phenylchromen-4-one: ^1H NMR (500 MHz, CDCl_3 , TMS): δ 3.93 (s, 3H), 6.76 (s, 1H), 6.96–6.99 (m, 2H), 7.49–7.55 (m, 3H), 7.89–7.91 (m, 2H), 8.5 (d, $J = 8.5$ Hz, 1H). ^{13}C – $\{^1\text{H}\}$ NMR (125 MHz, CDCl_3 , TMS): δ 55.96, 100.59, 107.69, 114.51,

118.01, 126.29, 127.21, 129.13, 131.52, 132.04, 158.15, 163.15, 164.34, 177.95. MS (70 eV, EI): m/z (%): 253 (17), 252 (100) [M^+], 251 (15), 224 (55), 209 (57), 152 (13), 122 (32), 107 (22), 79 (18), 77 (10), 63 (12), 51 (12). Anal. Calcd. for $C_{16}H_{12}O_3$: C, 76.18; H, 4.79. Found: C, 76.42; H, 4.89.



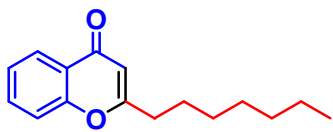
3ca (CAS No. 1148-48-7)

7-chloro-2-phenylchromen-4-one: 1H NMR (500 MHz, $CDCl_3$, TMS): δ 6.80 (s, 1H), 7.38 (dd, $J = 9.0$ and 2.0 Hz, 1H), 7.51–7.57 (m, 3H), 7.59 (d, $J = 2.0$ Hz, 1H), 7.89–7.91 (m, 2H), 8.16 (d, $J = 8.5$ Hz). ^{13}C – $\{^1H\}$ NMR (125 MHz, $CDCl_3$, TMS): δ 107.89, 118.30, 122.63, 126.20, 126.40, 127.21, 129.24, 131.48, 131.96, 139.89, 156.46, 163.67, 177.63. MS (70 eV, EI): m/z (%): 258 (32), 257 (27) [M^+], 256 (100), 255 (35), 230 (23), 229 (10), 228 (68), 165 (15), 156 (15), 154 (46), 128 (15), 126 (48), 114 (22), 102 (40), 98 (16), 82 (13), 76 (19), 75 (13), 74 (10), 63 (38), 51 (12), 50 (10). Anal. Calcd. for $C_{15}H_9O_2Cl$: C, 70.19; H, 3.53. Found: C, 70.53; H, 3.91.



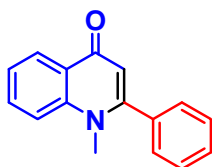
3cb (CAS No. 1809916-90-2)

7-chloro-2-(4-methylphenyl)chromen-4-one (3cb): 1H NMR (500 MHz, $CDCl_3$, TMS): δ 2.44 (s, 3H), 6.77 (s, 1H), 7.32 (d, $J = 8.0$ Hz, 2H), 7.37 (dd, $J = 8.5$ and 2.0 Hz, 1H), 7.58 (d, $J = 2.0$ Hz, 1H), 7.78–7.80 (m, 2H), 8.15 (d, $J = 8.5$ Hz, 1H). ^{13}C – $\{^1H\}$ NMR (125 MHz, $CDCl_3$, TMS): δ 21.68, 107.24, 118.27, 122.65, 126.09, 126.33, 127.18, 128.64, 129.96, 139.75, 142.69, 156.44, 163.87, 177.66. MS (70 eV, EI): m/z (%): 272 (31), 271 (23) [M^+], 270 (100), 269 (19), 257 (11), 255 (32), 244 (15), 242 (44), 154 (15), 126 (23), 121 (10), 116 (71), 115 (90), 103 (11), 98 (10), 91 (10), 89 (28), 76 (13), 63 (30). Anal. Calcd. for $C_{16}H_{11}O_2Cl$: C, 70.99; H, 4.10. Found: C, 71.39; H, 4.22.



3ah (CAS No. 158634-31-2)

2-heptylchromen-4-one (3ah): ^1H NMR (500 MHz, CDCl_3 , TMS): δ 0.89 (t, $J = 7.0$ Hz, 3H), 1.24–1.43 (m, 8H), 1.74 (quin, $J = 7.5$ Hz, 2H), 2.62 (t, $J = 7.5$ Hz, 2H), 6.18 (s, 1H), 7.38 (ddd, $J = 8.0, 7.0$ and 1.0 Hz, 1H), 7.43 (dd, $J = 8.0$ and 0.5 Hz, 1H), 7.64 (ddd, $J = 8.5, 7.0$ and 1.5 Hz, 1H), 8.19 (dd, $J = 8.0$ and 1.0 Hz, 1H). ^{13}C – $\{^1\text{H}\}$ NMR (125 MHz, CDCl_3 , TMS): δ 14.17, 22.72, 26.91, 29.05, 31.77, 34.44, 109.91, 117.97, 123.84, 125.00, 125.77, 133.52, 156.63, 170.00, 178.55. MS (70 eV, EI): m/z (%): 244 (23) [M^+], 173 (49), 161 (11), 160 (88), 131 (17), 121 (100), 120 (26), 93 (10), 92 (25), 77 (11), 55 (10).



3da (CAS No. 17182-60-4)

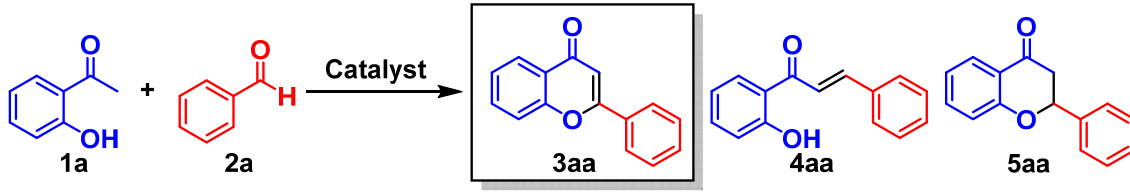
1-methyl-2-phenyl-4-quinolin-4-one (3da): The product was isolated as a monohydrate. ^1H NMR (500 MHz, CDCl_3 , TMS): δ 3.61 (s, 3H), 6.30 (s, 1H), 7.40–7.44 (m, 3H), 7.49–7.52 (m, 3H), 7.55 (d, $J = 8.5$ Hz, 1H), 7.71 (ddd, $J = 8.5, 7.0$ and 1.5 Hz, 1H), 8.50 (dd, $J = 8.0$ and 1.5 Hz, 1H). ^{13}C – $\{^1\text{H}\}$ NMR (125 MHz, CDCl_3 , TMS): δ 37.36, 112.79, 116.05, 123.76, 126.85, 126.97, 128.66, 128.91, 129.71, 132.44, 135.99, 142.03, 154.83, 177.68. MS (70 eV, EI): m/z (%): 236 (18), 235 (100) [M^+], 234 (10), 208 (13), 207 (84), 206 (40), 165 (11), 102 (11), 77 (16). Anal. Calcd. for $\text{C}_{16}\text{H}_{13}\text{NO} \cdot \text{H}_2\text{O}$: C, 75.87; H, 5.97; N, 5.53. Found: C, 76.36; H, 6.03; N, 5.58.

3-1.3. Results and Discussion

3-1.3.1. Effect of Catalysts

To begin with, I prepared various kinds of supported metal catalysts (given in the format: metal/support), and they were tested for the direct one-pot synthesis of flavone (**3aa**) starting from 2'-hydroxyacetophenone (**1a**) and benzaldehyde (**2a**). The reactions were carried out in mesitylene at 130 °C under open air (1 atm) using an equimolar mixture of **1a** and **2a**. Under the present reaction conditions, the reaction did not proceed at all in the absence of catalysts (Table 3-1, entry 11). Although the Claisen–Schmidt condensation product **4aa** and the oxa-Michael addition product **5aa** were formed when using just LDH, the oxidative dehydrogenation of **5aa** to **3aa** did not take place at all (Table 3-1, entry 10). In the presence of Ru/LDH, Rh/LDH, Pd/LDH, or Pt/LDH, **3aa** was barely produced though the Claisen–Schmidt condensation and the oxa-Michael addition proceeded (Table 3-1, entries 2–5), thus indicating that these supported metals are intrinsically inactive for the oxidative dehydrogenation under the present conditions. Fortunately, the desired **3aa** was obtained in 76 % yield when using Au/LDH (Table 3-1, entry 1). When the reaction was carried out with Au/LDH under an argon atmosphere, the yield of **3aa** decreased to 24 % (Table 3-1, entry 9). In this case, the hydrogenation of the carbon–carbon double bond of **4aa** also proceeded to some extent. Therefore, molecular oxygen (in air) acted as the terminal oxidant in the present system. The effect of the supports for gold was significant, and LDH showed the best performance among the supports examined (Table 3-1, entries 1 and 6–8) (Note: When using supported gold catalysts, aurone was formed as a by-product possibly *via* the dehydrogenation of the 5-*exo*-adduct in <5 % yield). The basic property of LDH possibly plays important roles for not only catalyzing the Claisen–Schmidt condensation and the oxa-Michael addition but also promoting the oxidative dehydrogenation of **5aa** (the details will be described later).

Table 3-1. Effect of catalysts on one-pot flavone (**3aa**) synthesis starting from **1a** and **2a**.^[a]

						
Entry	Catalyst	Conv. [%]		Yield [%]		
		1a	2a	3aa	4aa	5aa
1	Au/LDH	>99	97	76	<1	<1
2	Ru/LDH	70	78	<1	5	16
3	Rh/LDH	79	74	<1	20	39
4	Pd/LDH	84	>99	2	2	22
5	Pt/LDH	91	96	<1	20	44
6	Au/Al ₂ O ₃	79	83	58	2	3
7	Au/TiO ₂	46	56	34	<1	<1
8	Au/CeO ₂	40	78	3	<1	<1
9 ^[b]	Au/LDH	>99	>99	24	15	34
10	LDH	>99	90	<1	31	59
11	None	9	65	<1	<1	<1

[a] Reaction conditions: **1a** (0.5 mmol), **2a** (0.5 mmol), catalyst (130 mg), mesitylene (2 mL), 130 °C, open air (1 atm), 24 h. Conversions and yields were determined by gas chromatography analysis using biphenyl as an internal standard. [b] Ar atmosphere (1 atm).

3-1.3.2. Heterogeneous Catalysis and Catalyst Reuse

To verify whether the observed catalysis was derived from solid Au/LDH or leached metal species (gold, magnesium, and/or aluminum), Au/LDH was removed by hot filtration during the reaction at ~50 % yield of **3aa**, and then the reaction was again carried out with the filtrate under the same reaction conditions. As shown in Figure 3-13, the production of **3aa** was completely stopped by the removal of Au/LDH. In addition, I confirmed by the inductively coupled plasma atomic emission spectroscopy (ICP-AES) analysis that gold, magnesium, and aluminum species were hardly present in the filtrate (Au: <0.003 %, Mg: <0.02 %, Al: <0.4 %). The above experimental results can rule out any contribution to the observed catalysis from metal species that leached into the reaction solution, and the observed catalysis for the present one-pot flavone synthesis is truly heterogeneous.

After the reaction of **1a** and **2a** was completed, Au/LDH can readily be retrieved from the reaction mixture by simple filtration. The retrieved Au/LDH can be reused for the same reaction without a severe loss of its catalytic performance; however, the yield of **3aa** gradually decreased for each reuse experiment (Table 3-2). To elucidate the reason for the deactivation, several experiments were carried out. The average particle size of gold in the fresh Au/LDH was 4.2 nm ($\sigma = 1.2$ nm) and was unchanged after the second reuse experiment (4.3 nm, $\sigma = 1.2$ nm) (Figure 3-14). It was confirmed by the X-ray photoelectron spectroscopy (XPS) analysis that the oxidation state of gold was still zero after the reaction (Figure 3-15). The X-ray diffraction (XRD) analysis revealed that the structure of LDH was almost preserved after the reaction while the widths of peaks were broadened, suggesting the adsorption of something on LDH (Figure 3-16). The infrared (IR) spectrum of Au/LDH after the second reuse experiment showed the band around 1596 cm^{-1} assignable to carboxylate species, indicating the adsorption of carboxylic acids (formed *via* oxidation of aldehyde substrates and/or mesitylene) on the basic LDH surface (Figure 3-17). Therefore, the deactivation of Au/LDH is probably caused not by the change of gold nanoparticles but by the adsorption of acids on LDH although it is difficult to exclude the possibility of compounds adsorbed on gold nanoparticles.

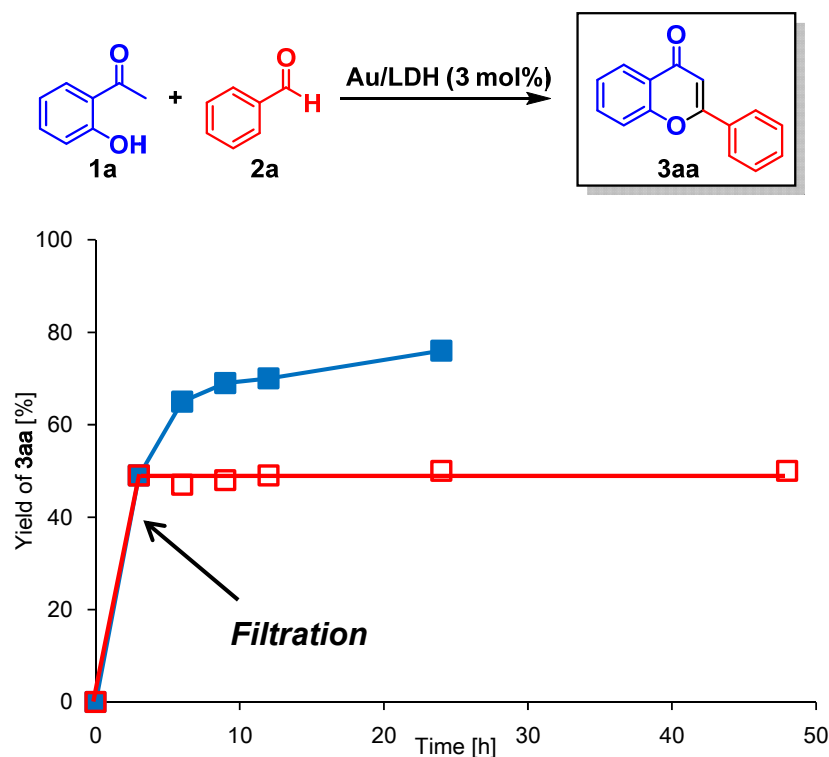


Figure 3-13. The effect of removal of Au/LDH for the one-pot synthesis of **3aa** from **1a** and **2a** (verification of heterogeneous catalysis). The reaction conditions were the same as those described in Table 3-1. GC yields are shown here.

Table 3-2: Reuse experiments.^[a]

		Yield [%]		
Entry	Catalyst	3aa	4aa	5aa
1	Fresh Au/LDH	96	<1	<1
2	1st reuse	84	<1	<1
3	2nd reuse	79	<1	<1

[a] Reaction conditions: **1a** (0.3 mmol), **2a** (0.6 mmol), catalyst (100 mg), mesitylene (2 mL), 130 °C, open air (1 atm), 24 h. Yields were determined by gas chromatography analysis using biphenyl as an internal standard.

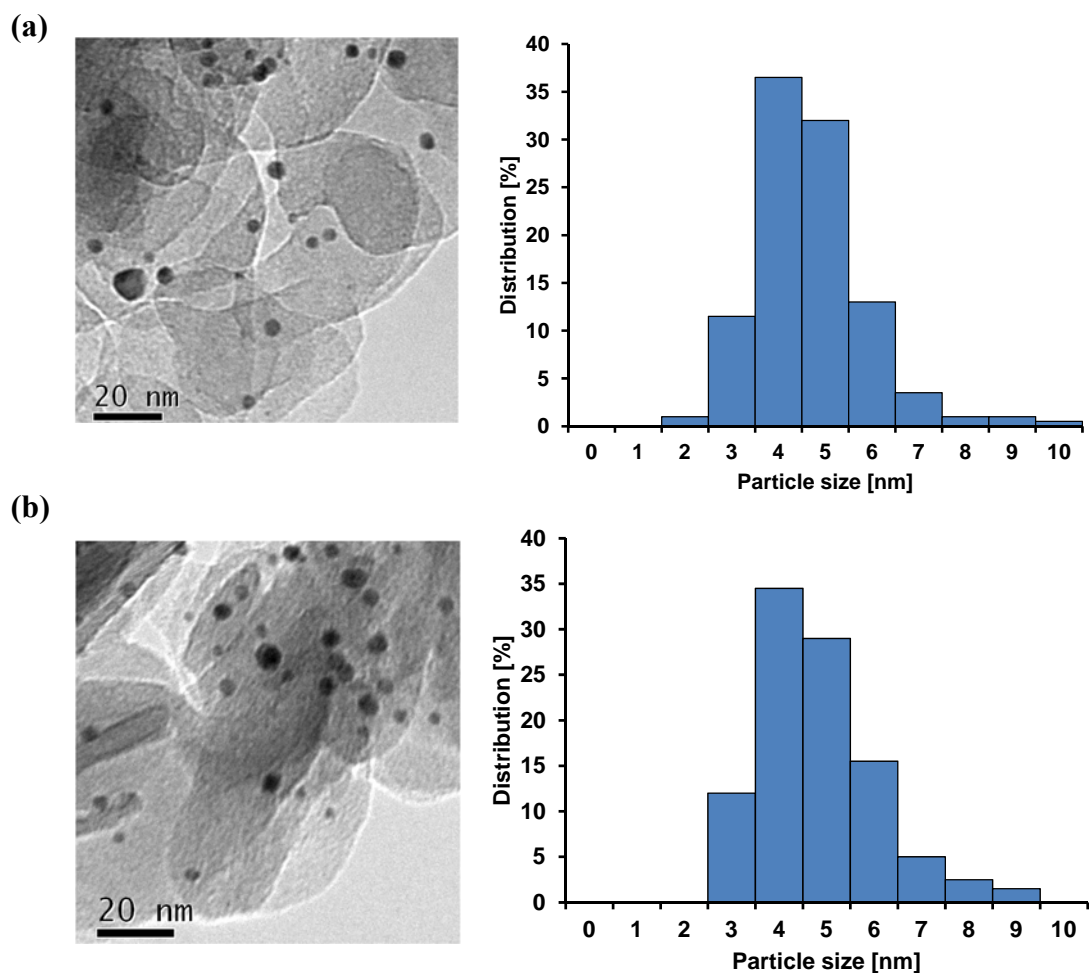


Figure 3-14. TEM images and Au particle size distributions of (a) fresh Au/LDH (mean diameter: 4.2 nm, $\sigma = 1.2$ nm) and (b) Au/LDH retrieved after the 2nd reuse experiment (mean diameter: 4.3 nm, $\sigma = 1.2$ nm). The size distributions were determined using 200 particles.

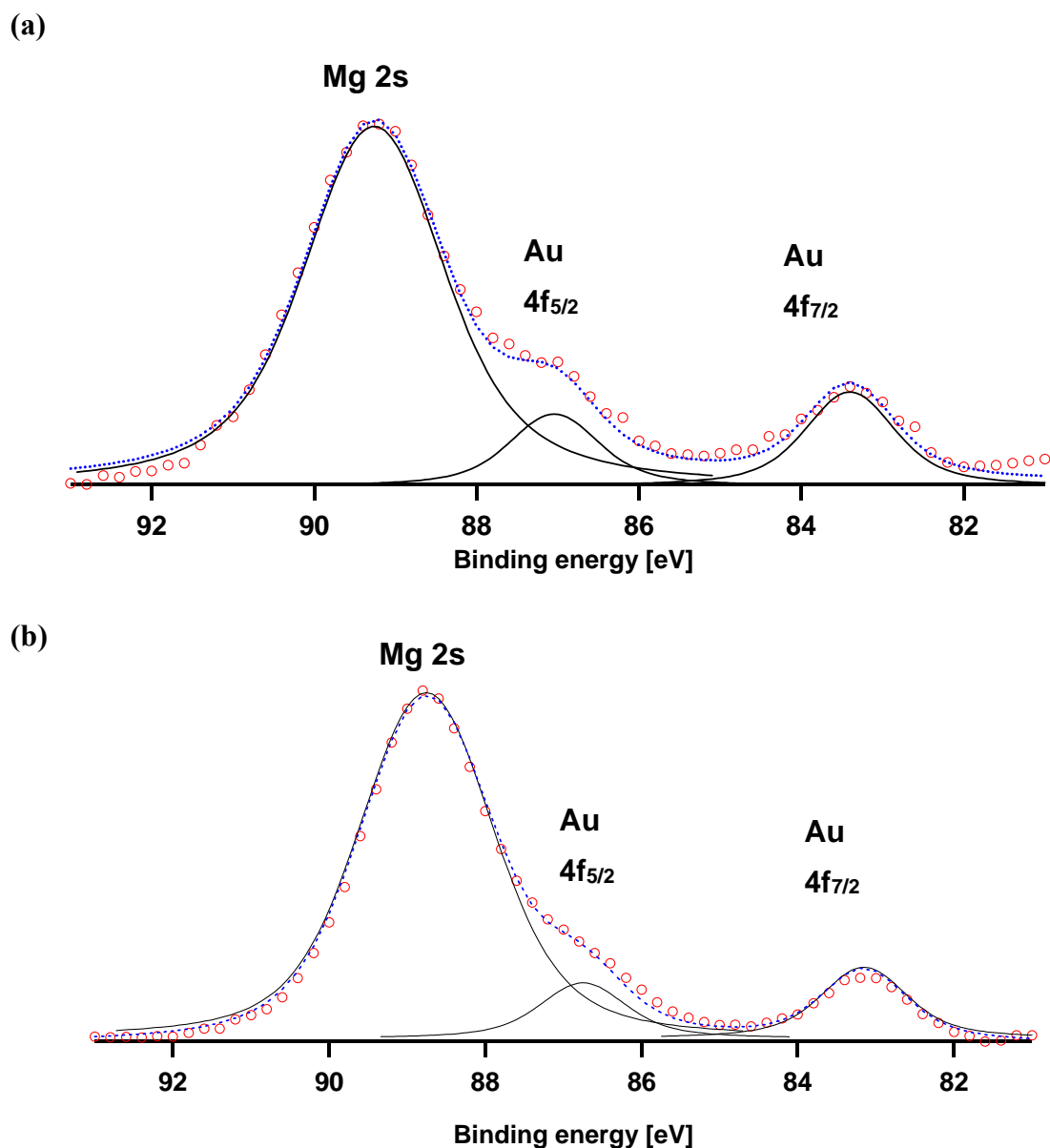


Figure 3-15. XPS spectra of (a) fresh Au/LDH and (b) Au/LDH retrieved after the 2nd reuse experiment. The red circles indicate the data points. The solid and broken lines indicate the deconvoluted signals and the sum of the deconvoluted signals using pseudo-Voigt function, respectively. The binding energy axis was calibrated by deposited gold (84.0 eV).

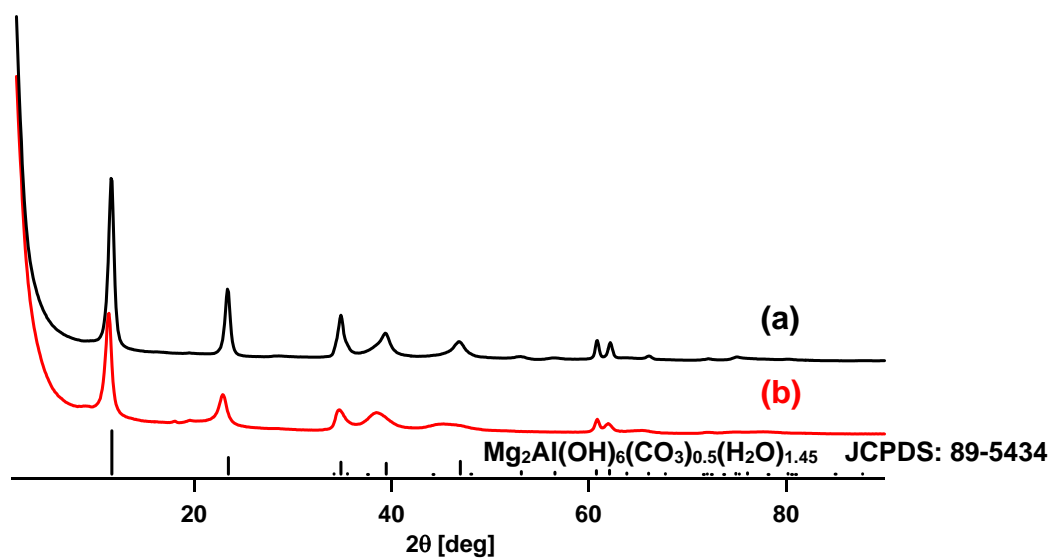


Figure 3-16. XRD patterns of (a) fresh Au/LDH and (b) Au/LDH retrieved after the 2nd reuse experiment.

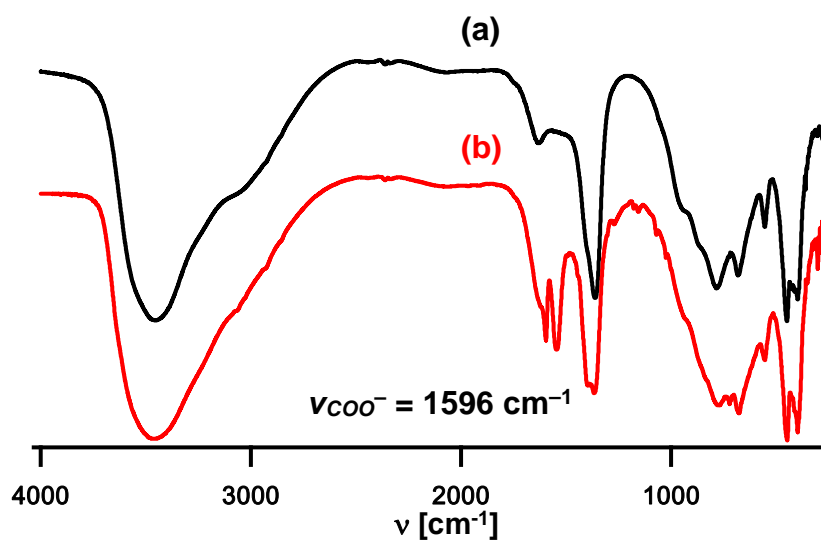
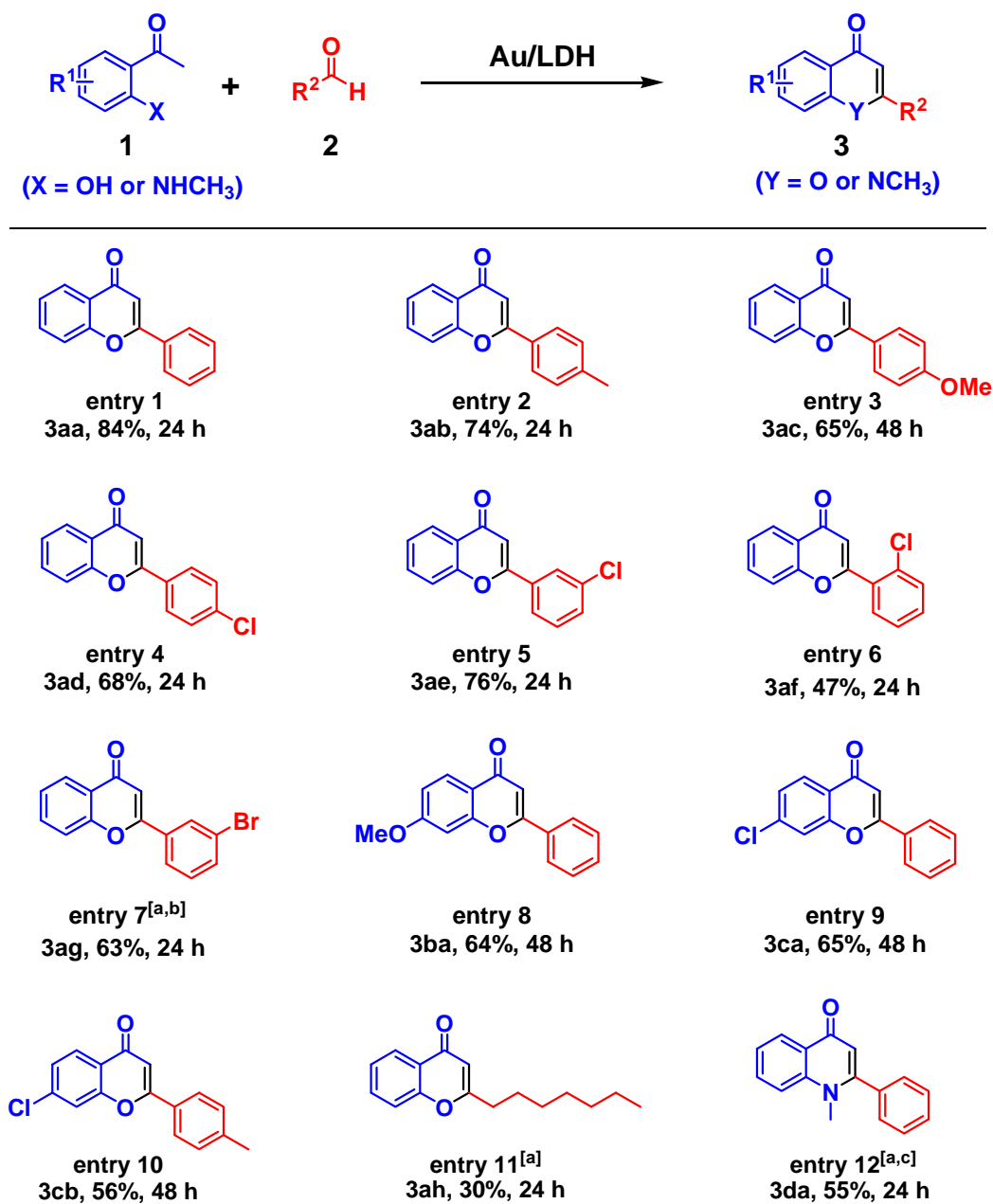


Figure 3-17. IR spectra of (a) fresh Au/LDH and (b) Au/LDH retrieved after the 2nd reuse experiment.

3-1.3.3. Substrate Scope

Next, I examined the scope of the present Au/LDH-catalyzed one-pot procedure. Under the optimized reaction conditions, various kinds of structurally diverse flavones can be synthesized starting directly from 2'-hydroxyacetophenones and benzaldehydes. The products can be readily isolated by simple column chromatography on silica gel, and the isolated yields are summarized in Table 3-3. The reaction of **1a** with benzaldehydes which possess electron-donating as well as electron-withdrawing substituents at each position of the benzene rings, can efficiently be converted into the corresponding flavones (Table 3-3, entries 1–7). In the case of *p*-tolualdehyde, the undesirable benzylic oxidation of the methyl group hardly proceeded (Table 3-3, entry 2). In addition, various substituted 2'-hydroxyacetophenones worked well as the reaction partners for benzaldehydes (Table 3-3, entries 8–10). By utilizing the present Au/LDH-catalyzed one-pot procedure, various halo-substituted flavones can efficiently be synthesized, and thus it would be possible to utilize these halo-functionalities for further derivatization of these flavone molecules. Besides benzaldehydes, aliphatic aldehydes can be utilized; for example, the reaction of **1a** with *n*-octanal afforded the corresponding chromone (Table 3-3, entry 11). Furthermore, by using 2'-(methylamino)acetophenone and **2a** as the starting materials, the present Au/LDH-catalyzed one-pot procedure successfully constructed the corresponding 4-quinolone skeleton (Table 3-3, entry 12). It is known that Au/LDH can act as an efficient heterogeneous catalyst for aerobic oxidation of alcohols (see the references of [16n–p] in Chapter I). Therefore, I expected that benzyl alcohols (instead of benzaldehydes) would be utilized as the starting materials for the present Au/LDH-catalyzed one-pot flavone synthesis. As shown in Figure 3-18, several substituted flavones were synthesized directly from **1a** and benzyl alcohols, as I had expected. To the best of my knowledge, such a heterogeneously catalyzed direct one-pot flavone synthesis from an alcohol is hitherto unknown. Furthermore, a larger-scale (5 mmol) synthesis was also effective and gave **3aa** in 64% yield under the conditions described in Figure 3-19.

Table 3-3. Substrate scope of Au/LDH-catalyzed one-pot flavone synthesis.



Reaction conditions: **1** (0.3 mmol), **2** (0.6 mmol), Au/LDH (100 mg), mesitylene (2 mL), 130 °C, open air (1 atm). Yields (based on **1**) of isolated products are shown. [a] Au/LDH (200 mg). [b] **3aa** was also formed (8 %). [c] The product was isolated as a monohydrate.

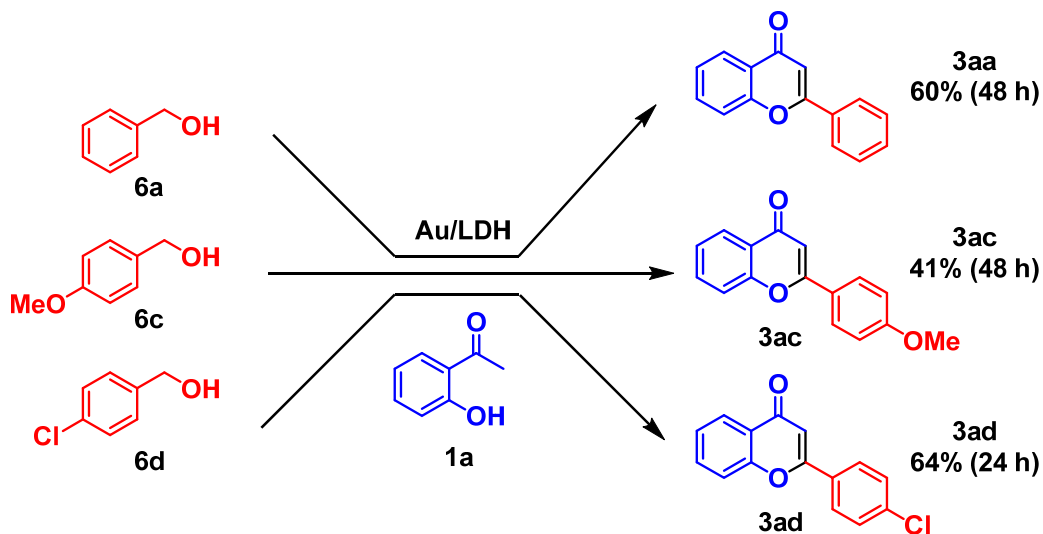


Figure 3-18. One-pot synthesis of flavones starting from **1a** and benzyl alcohols. Reaction conditions: **1** (0.5 mmol), **6** (0.5 mmol), Au/LDH (130 mg), mesitylene (2 mL), open air (1 atm), 130 °C. Yields were determined by GC analysis using biphenyl as an internal standard.

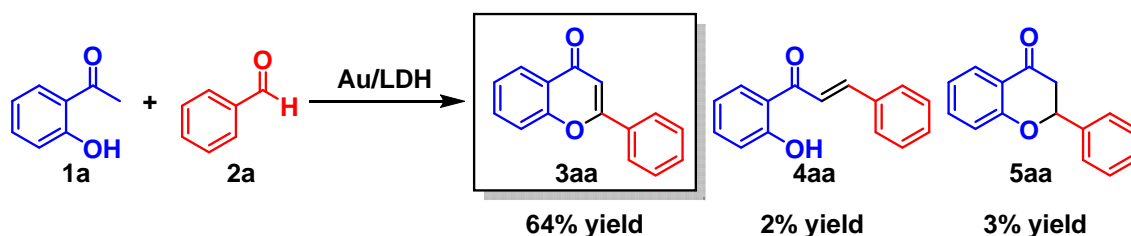


Figure 3-19. Larger-scale synthesis of **3aa**.

Reaction conditions: **1a** (5 mmol), **2a** (5 mmol), Au/LDH (1 g), mesitylene (20 mL), 130 °C, open air (1 atm), 48 h. Yields were determined by GC analysis using biphenyl as an internal standard.

3-1.3.4. Mechanistic Studies

The reaction profile for the Au/LDH-catalyzed transformation of **1a** and **2a** revealed that **4aa** and **5aa** are initially produced, followed by the formation of **3aa** (Figure 3-20). Furthermore, it was confirmed by the separate experiments that **3aa** can be synthesized starting from **4aa** (Figure 3-21) or **5aa** (Table 3-4) in the presence of Au/LDH. Therefore, the present one-pot procedure is composed of the sequence of the Claisen–Schmidt condensation of 2'-hydroxyacetophenones (**1**) and benzaldehydes (**2**) to 2'-hydroxychalcones (**4**), the intramolecular oxa-Michael addition of **4** to chromanones (**5**), and the oxidative dehydrogenation of **5**, affording the desired flavones (**3**). One can readily recognize that LDH can act as a solid base to catalyze the Claisen–Schmidt condensation and the oxa-Michael addition. When using benzyl alcohols as the starting materials, the sequence begins with aerobic alcohol oxidation *via* a typical alkoxide formation/hydride elimination mechanism (see section 1.1.4.3.).^[12]

To elucidate the roles of the catalysts in the oxidative dehydrogenation step in more detail, the following several experiments were carried out (Table 3-4). Firstly, the oxidative dehydrogenation of **5aa** to **3aa** was performed with various supported metal catalysts. Ru/LDH, Rh/LDH, Pd/LDH, and Pt/LDH were inactive for the dehydrogenation, and Au/LDH gave **3aa** in a significant yield (Table 3-4, entries 1 and 8–11). The results were consistent with those described in Table 3-1. The effect of the supports for gold was also significant (Table 3-4, entries 1, 3, 5 and 6); the catalytic performance was dependent on the kinds of supports and independent of either the specific surface areas or the electronic states of gold observed by XPS (Table 3-4 and Figure 3-22). Considering the gold particle mean sizes calculated from TEM images (Table 3-4 and Figure 3-23), it can be excluded that the difference of nanoparticle sizes on each support mainly affects the yields of **3aa**, though the slight effect of Au particle sizes was observed in the case of the same support (Table 3-4, entries 3 and 4) (In the previous study, the reaction for the gold-catalyzed oxidative dehydrogenation of β -nitrogen substituted ketones tends to become slower as the average particle size of gold increases).^[9] Thus, I concluded that the basic property of LDH can assist the gold-catalyzed oxidative dehydrogenation likely owing to the promotion of deprotonation from **5aa**. In addition, the physical mixture of Au/TiO₂ and LDH did not promote the dehydrogenation of **5aa** compared with only Au/TiO₂, indicating that it is

important to integrate basic sites and gold nanoparticles on the same support. Therefore, the concerted catalysis between basic sites and gold catalysts on the surface possibly occurs to promote this oxidative dehydrogenation of chromanones. Moreover, under an argon atmosphere Au/LDH-catalyzed oxidative dehydrogenation of **5aa** gave **3aa** in only 4 % yield while in an open air the yield of **3aa** was 66 % yield, revealing that the terminal oxidant is molecular oxygen in an air atmosphere (Table 3-4, entry 2).

The oxidative dehydrogenation of **5aa** was not influenced by the presence of an equimolar amount of a radical scavenger of 2,6-di-*tert*-butyl-4-methylphenol (BHT) with respect to **5aa** (Figure 3-24), indicating that radical species are not involved in the present transformation. Next, the oxidative dehydrogenation of **5aa** was carried out with 2,2,6,6-tetramethylpiperidine 1-oxyl (TEMPO). TEMPO is also a radical scavenger and known to be an effective hydrogen atom abstractor. In addition, it has been reported that TEMPO can abstract a hydrogen atom (one electron and one proton) from an Au–H species with the concomitant formation of 1-hydroxy-2,2,6,6-tetramethylpiperidine (TEMPOH).^[12] When the Au/LDH-catalyzed oxidative dehydrogenation of **5aa** was carried out with an equimolar amount of TEMPO with respect to **5aa**, the reaction was somewhat faster than that without TEMPO (Figure 3-24), and the formation of TEMPOH was observed (14% yield as of 1 h after the reaction started). Furthermore, under an Ar atmosphere, a little amount of 1-(2-hydroxyphenyl)-3-phenylpropan-1-one was produced by hydrogenation of **4aa** formed *via* the retro-Michael addition. These results indicate the formation of an Au–H species during the catalytic cycle.

Based on the above-mentioned experimental results, I here propose the possible mechanism for the gold-catalyzed oxidative dehydrogenation of **5** (Figure 3-25). The direct hydrogen atom abstraction pathway can be excluded because the reaction rates did not decrease even in the presence of radical scavengers such as BHT and TEMPO. Thus, I considered that the dehydrogenation possibly proceeds *via* a deprotonation/hydride elimination mechanism. At the 3-position of **5**, the abstraction of the relatively acidic hydrogen as a proton, which is promoted by LDH, and coordination toward an Au nanoparticle surface concertedly occur at the same time, and the proton is temporarily stored on the basic LDH surface. The hydrogen at the 2-position is eliminated as a hydride to form a transient Au–H species (Au–hydride or Au–hydrogen atom and delocalized electron). As above-mentioned, molecular oxygen (in air) acts as

the terminal oxidant in the present system. The role of molecular oxygen is to regenerate the active gold species by removing the hydrogen from the Au–H species *via* the hydroperoxide formation.^[12] The proton stored on LDH is consumed for the production of water.

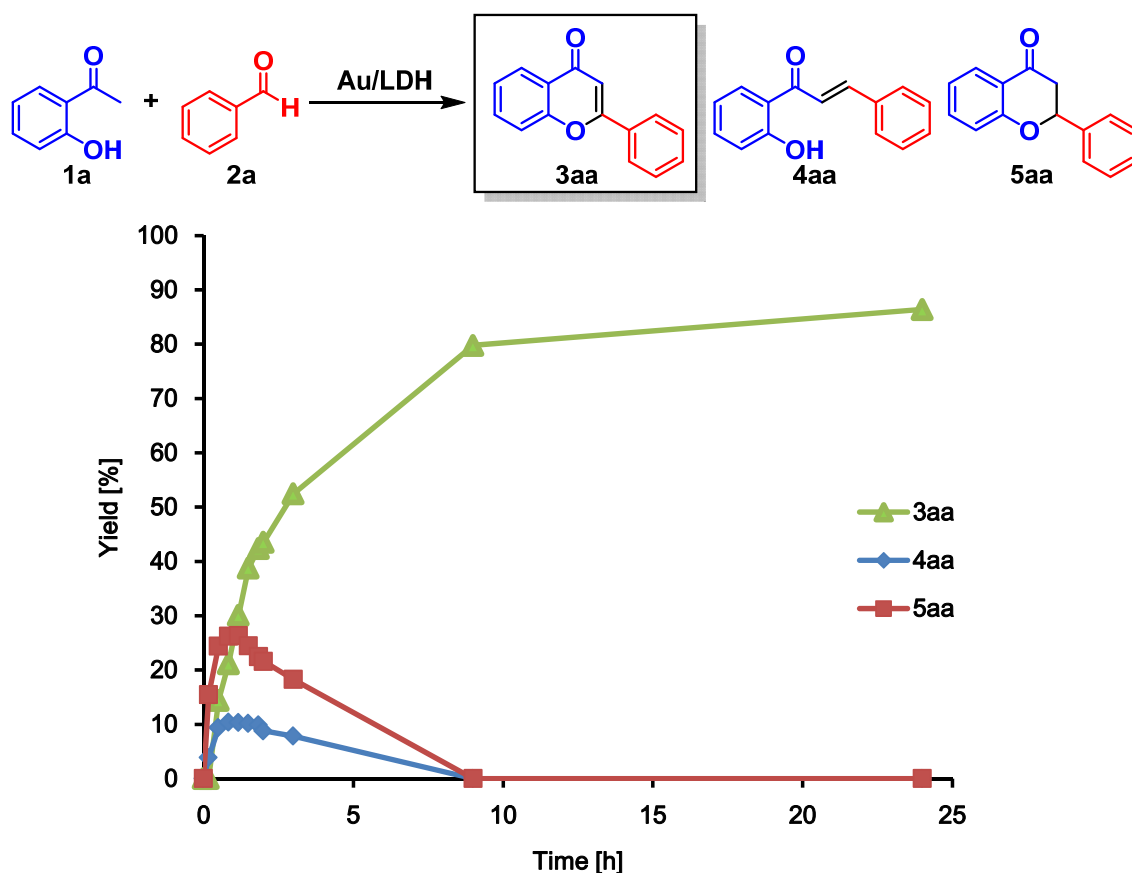


Figure 3-20. The reaction profile for the one-pot synthesis of **3aa** from **1a** and **2a**.

Reaction conditions: **1a** (0.3 mmol), **2a** (0.6 mmol), Au/LDH (100 mg), mesitylene (2 mL), 130 °C, open air (1 atm). Yields were determined by gas chromatography analysis using biphenyl as an internal standard.

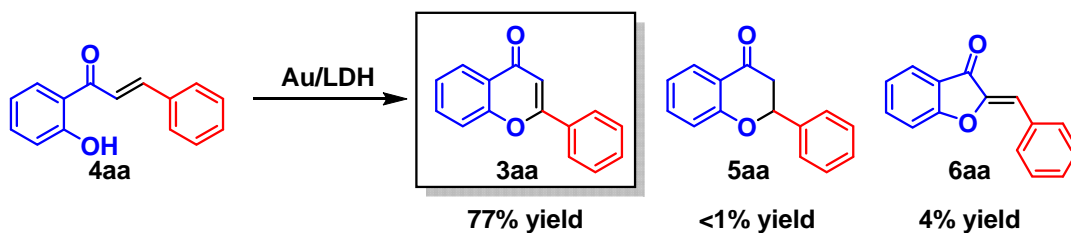
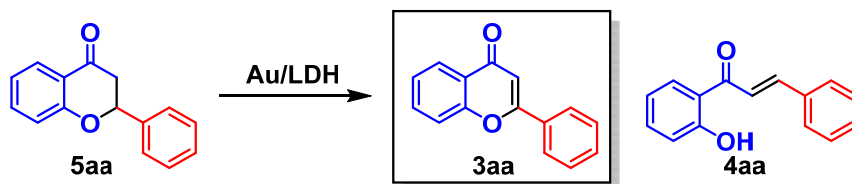


Figure 3-21. Synthesis of **3aa** from **4aa**.

Reaction conditions: **4aa** (0.5 mmol), Au/LDH (100 mg, Au: 2 mol%), mesitylene (2 mL), 130 °C, open air (1 atm), 24 h. Yields were determined by gas chromatography analysis using biphenyl as an internal standard.

Table 3-4. Synthesis of **3aa** starting from **5aa**.^[a]



Entry	Catalyst	Yield [%]		BET surface area [m ² g ⁻¹]	Au particle size [nm]	BE of Au 4f _{7/2} [eV]
		3aa	4aa			
1	Au/LDH	66	9	77	4.2 (σ = 1.2)	83.2
2 ^[b]	Au/LDH	4	30	77	4.2 (σ = 1.2)	83.2
3	Au/Al ₂ O ₃	24	25	160	3.2 (σ = 1.1)	83.1
4	Au/Al ₂ O ₃	13	27	155	14.3 (σ = 9.2)	—
5	Au/CeO ₂	30	6	61	3.0 (σ = 0.9)	83.3
6	Au/TiO ₂	23	18	92	4.4 (σ = 1.4)	83.7
7 ^[c]	Au/TiO ₂ + LDH	16	19	—	4.4 (σ = 1.4)	—
8	Ru/LDH	1	27	—	—	—
9	Rh/LDH	<1	28	—	—	—
10	Pd/LDH	<1	28	—	—	—
11	Pt/LDH	<1	29	—	—	—

[a] Reaction conditions: **5aa** (0.5 mmol), catalyst (metal: 1 mol%, 32–53 mg), mesitylene (2 mL), 130 °C, open air (1 atm), 3 h. Yields were determined by gas chromatography analysis using biphenyl as an internal standard. [b] Ar atmosphere (1 atm). [c] Au/TiO₂ (53 mg) was physically mixed with LDH (43 mg).

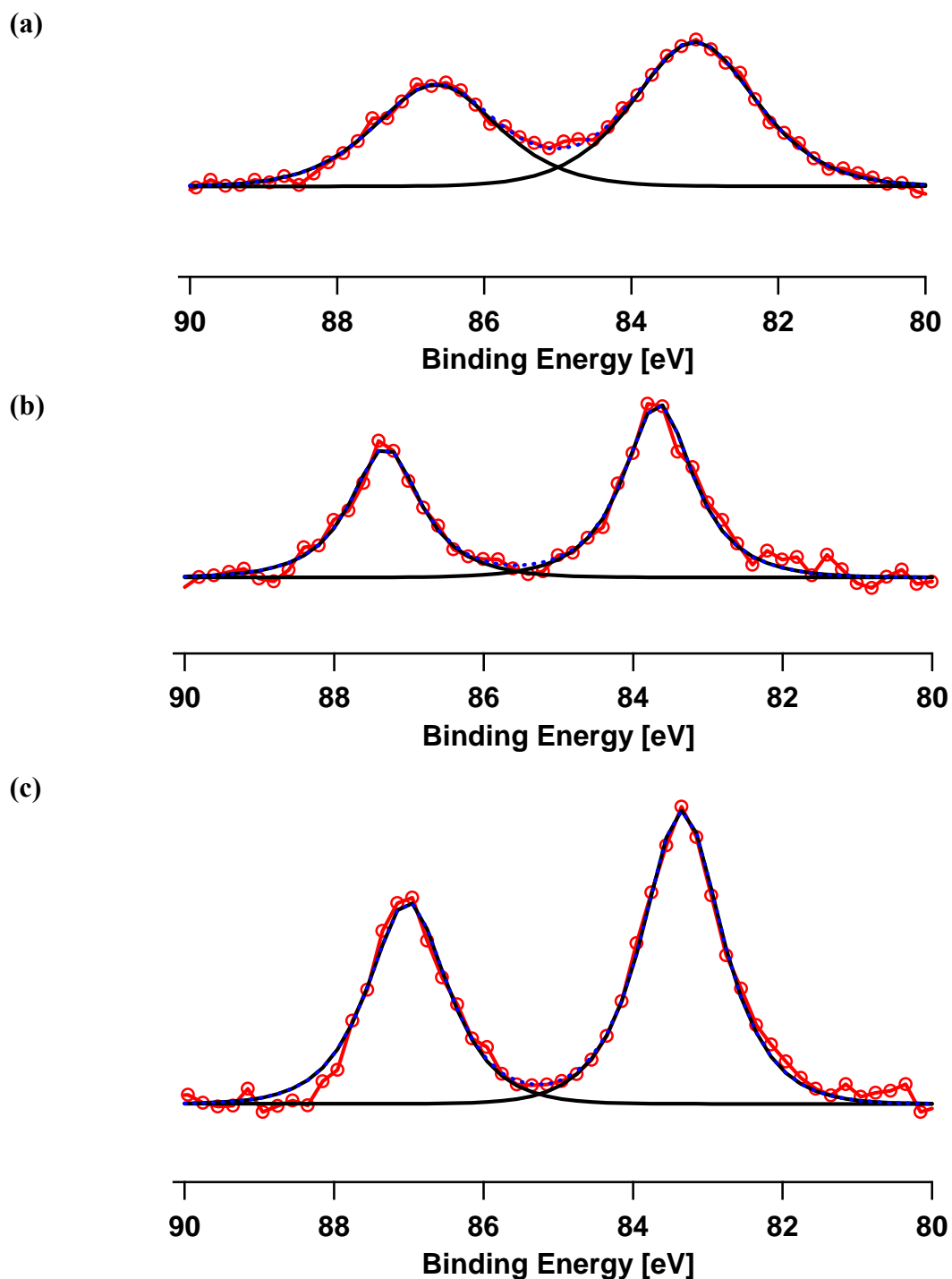


Figure 3-22. XPS spectra of (a) Au/Al₂O₃ prepared using an aqueous solution of NaOH, (b) Au/TiO₂, and (c) Au/CeO₂. The red circles and solid red lines indicate the data points. The black solid and blue broken lines indicate the deconvoluted signals and the sum of the deconvoluted signals using pseudo-Voigt function, respectively. The binding energy axis was calibrated by deposited gold (84.0 eV).

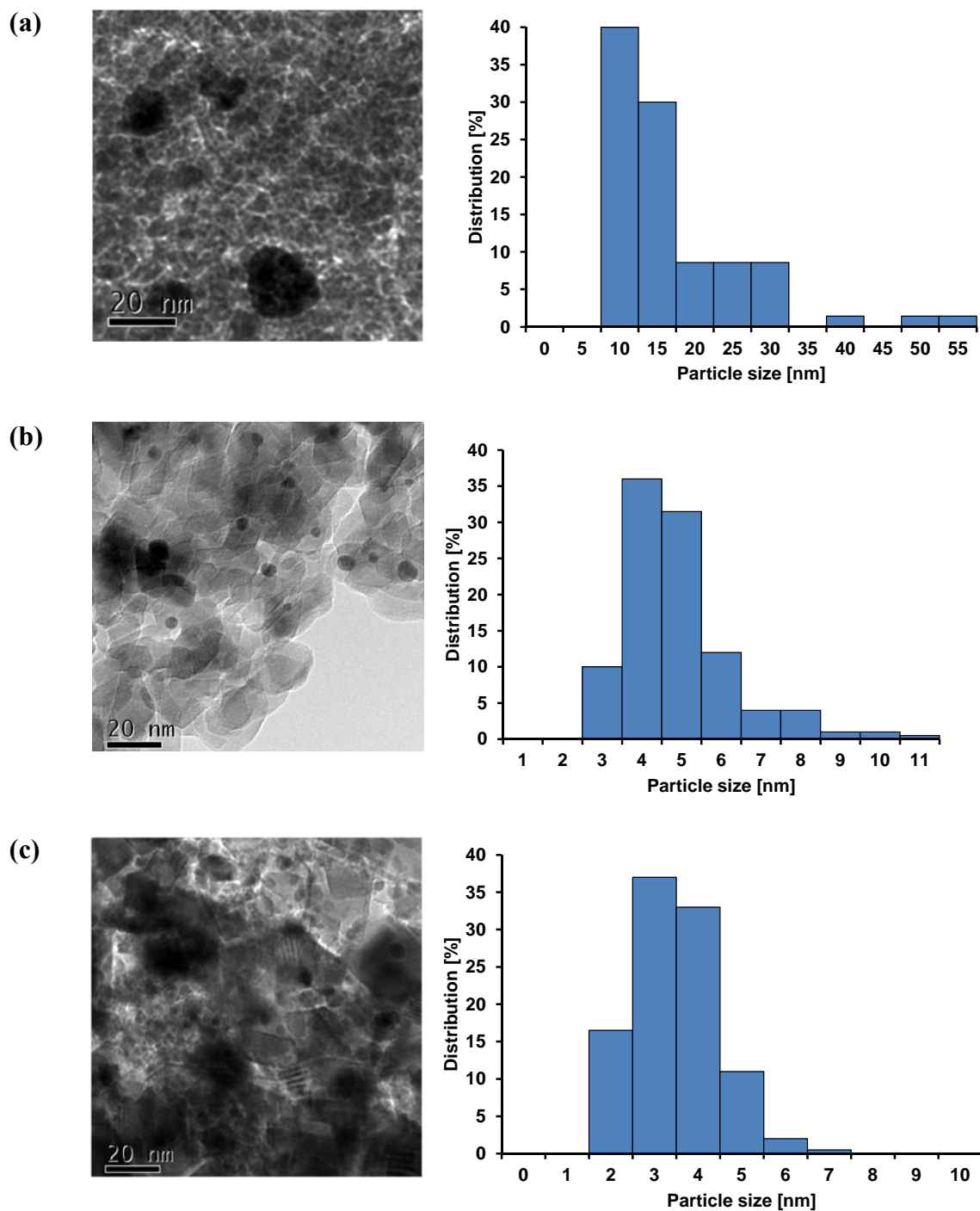


Figure 3-23. TEM images and Au particle size distributions of (a) Au/Al₂O₃ prepared using NH₄OH (mean diameter: 14.3 nm, σ = 1.2 nm, n = 70), (b) Au/TiO₂ (mean diameter: 4.4 nm, σ = 1.4 nm, n = 200), and (c) Au/CeO₂ (mean diameter: 3.0 nm, σ = 0.9 nm, n = 200).

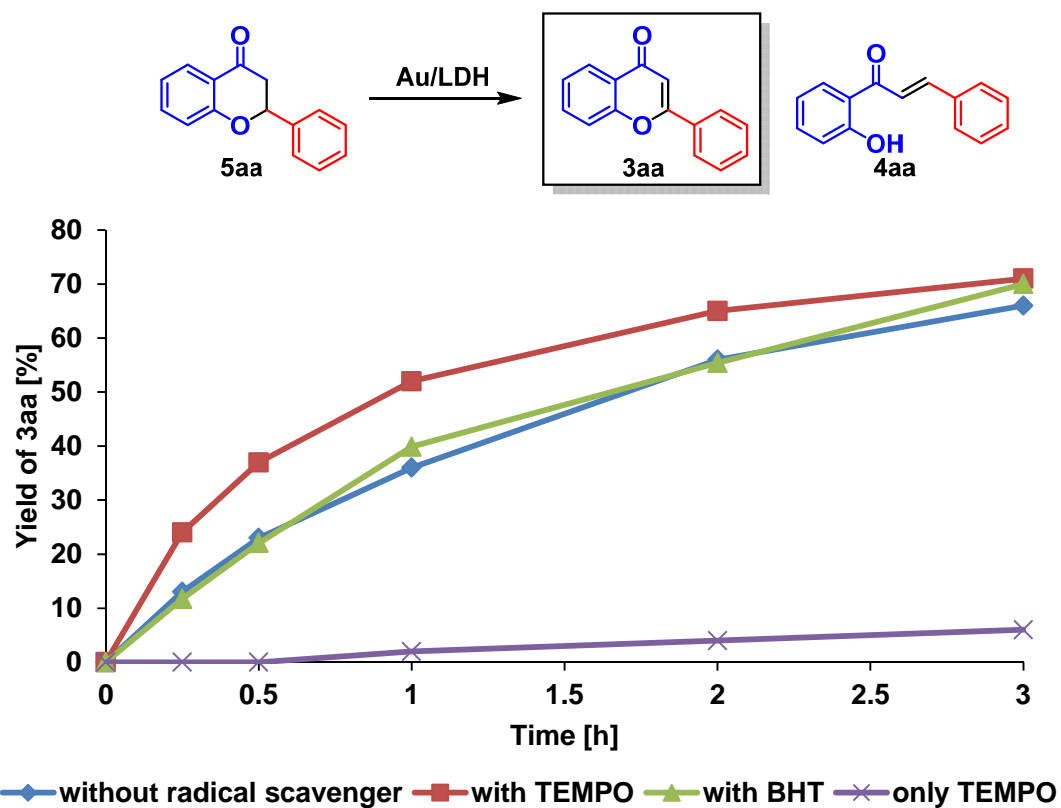


Figure 3-24. The effect of radical scavengers (BHT or TEMPO, 1 equivalent with respect to **5aa**) on the Au/LDH-catalyzed oxidative dehydrogenation of **5aa**.

Reaction conditions: **5aa** (0.5 mmol), Au/LDH (Au: 1 mol%, 43 mg), additive (0.5 mmol), mesitylene (2 mL), 130 °C, open air (1 atm), 3 h. Yields were determined by gas chromatography analysis using biphenyl as an internal standard.

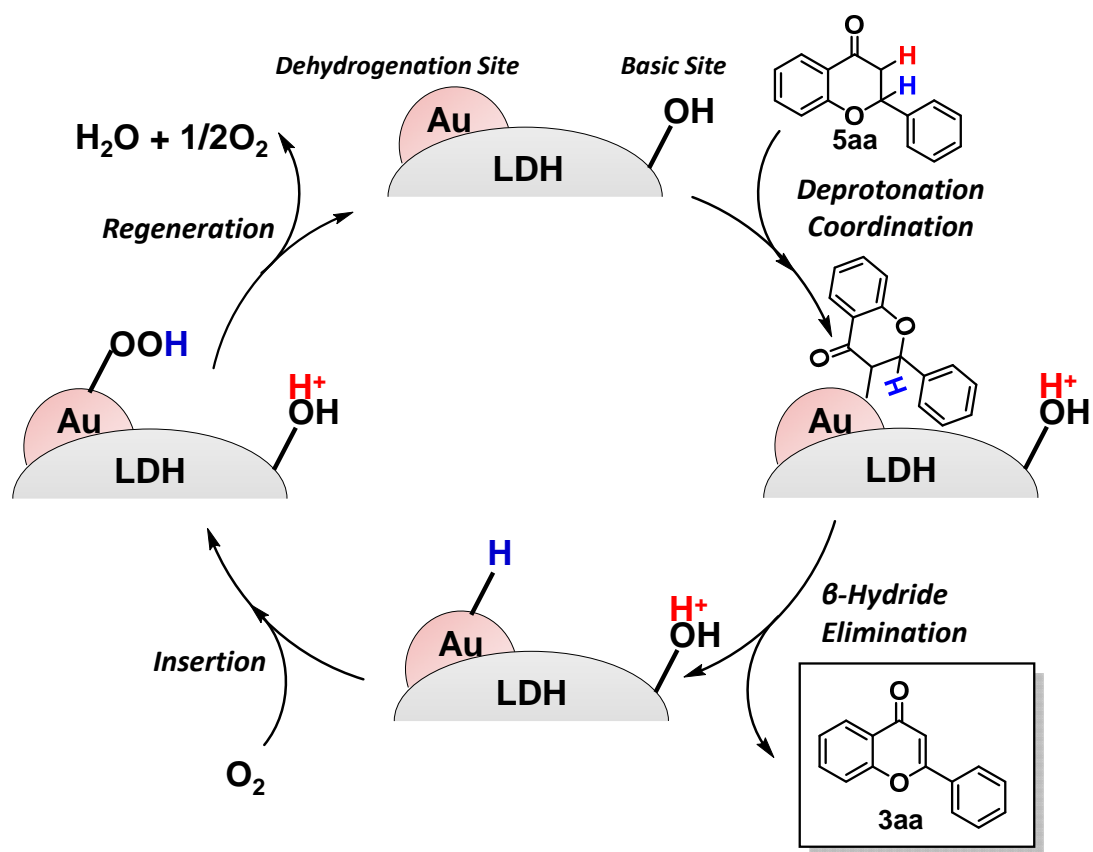


Figure 3-25. Possible reaction mechanism for the Au/LDH-catalyzed oxidative dehydrogenation of flavanones.

3-1.4. Summary

In summary, I have developed the first one-pot selective flavone synthesis starting from benzaldehydes (or benzyl alcohols) and 2'-hydroxyacetophenones using molecular oxygen in the air as the sole oxidant. This efficient flavone synthesis was enabled by gold nanoparticle catalysts supported on LDH, which show the multiple catalysis for (aerobic alcohol oxidation,) Claisen–Schmidt condensation, intramolecular oxa-Michael addition, and aerobic oxidative dehydrogenation. The key novel reaction is Au nanoparticles-catalyzed aerobic oxidative dehydrogenation concertedly promoted by basic sites on LDH. The catalysis of Au/LDH is truly heterogeneous, and Au/LDH can be reused without a severe loss of its catalytic performance. Besides, the present synthesis possesses several noteworthy features; simple one-pot operation and avoidance of tedious isolation steps of the intermediates, use of readily available starting materials, disuse of additives, and formation of water as the theoretical sole by-product. Therefore, this system will be one of the most environmentally friendly procedures for the synthesis of flavones and its derivatives.

In the next section, aurones, which were slightly observed using gold nanoparticle catalysts in this section, will be selectively synthesized *via* selectivity switch enabled by the design of a function-integrated heterogeneous catalyst.

3-2 Selective Aurone Synthesis Catalyzed by Palladium-on-Gold Bimetallic Nanoparticles Supported on Ceria

Adapted with permission from *ACS Catal.* **2018**, 8(12), 4969–4978. Copyright 2018 American Chemical Society.

3-2.1. Introduction

Aurones (2-benzylidene-coumaran-3-one and its derivatives), a class of minor flavonoids naturally that occur in limited plants such as *Antirrhinum majus* and *Cosmos*, possess an unusual 5-membered C-ring because of an exceptional mechanism (Figure 3-26).^[1,4a,13] Aurones are biosynthesized directly from chalcones *via* the oxidation of B-rings^[4a] mainly by polyphenol oxidases (PPO), such as aureusidin synthase (AmAS1)^[13a,b] and aurone synthase (AUS1)^[13c], or by peroxidases (PRX), such as MtPRXs.^[13d,e] Therefore, the chemical catalytic transformation from simple chalcones into aurones that do not occur naturally is attractive, which overcomes the drawback of known limited enzyme catalysis. Further, the above-mentioned transformation is one of the most useful synthetic methods to produce aurones as compared with that of the other synthetic methods^[14–17] because chalcones are easily available through synthesis from simple aldehydes and ketones *via* the Claisen–Schmidt condensation or by extraction from the plants. Recently, various biological activities of aurones have also been revealed along with those of other flavonoids,^[4] which have elevated the importance of the transformation into novel aurones in terms of their pharmaceutical application.

However, the literature contains no report about the catalytic transformation from simple chalcones into aurones.^[18] For one thing, the control of 5-*exo*/6-*endo*-*trig* cyclization of chalcones is quite difficult; only 6-*endo*-*trig* cyclization—*i.e.* intramolecular oxa-Michael addition—proceeds to produce flavanones^[19], which is similar to the biosynthesis of flavonoids in nature; to the best of my knowledge, the literature contains no reports about the 5-*exo*-*trig* cyclization. Thus, the direct oxidative cyclization of chalcones, 5-membered/6-membered oxidative cyclization, is also difficult to control; 6-membered oxidative cyclization dominantly proceeds to produce flavones *via* 6-*endo*-*trig* cyclization (Figure 3-27).^[6] Only when (super)stoichiometric amounts of metal oxidants, typically Hg(OAc)₂, are used, does the 5-membered

oxidative cyclization into aurones proceed because of the intermediate formed by the coordination of a chalcone to a metal species to inhibit the 6-membered cyclization (Figure 3-27).^[17]

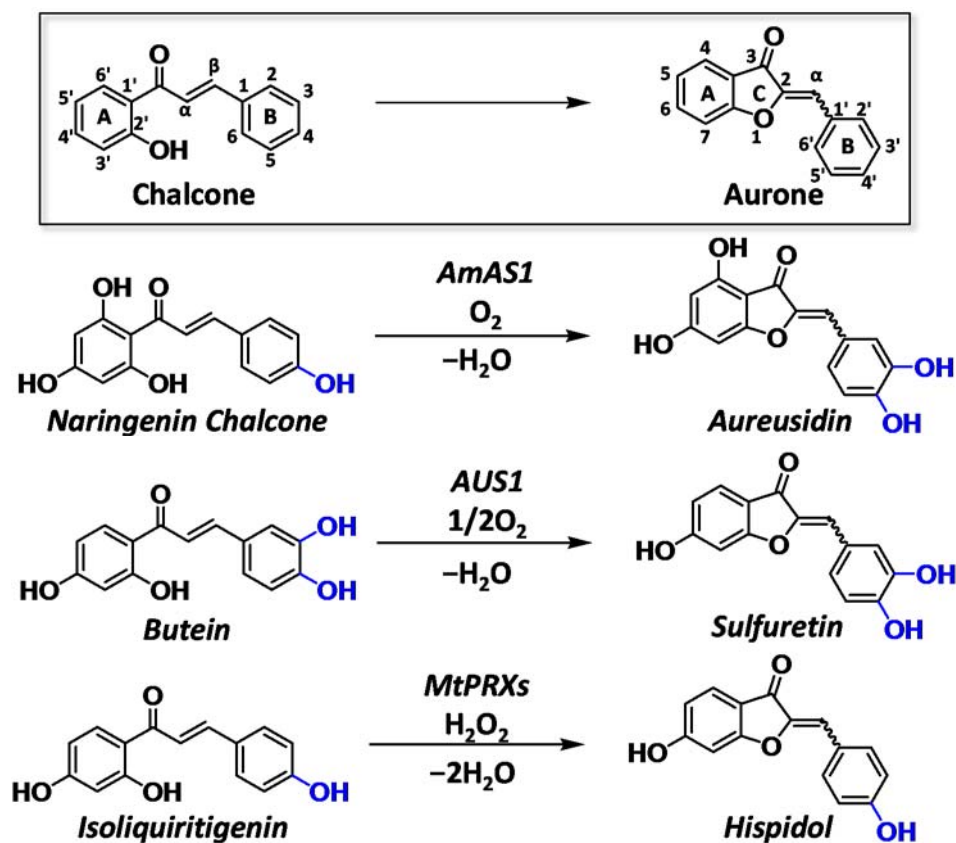


Figure 3-26. Biosynthetic routes of aurones from chalcones.

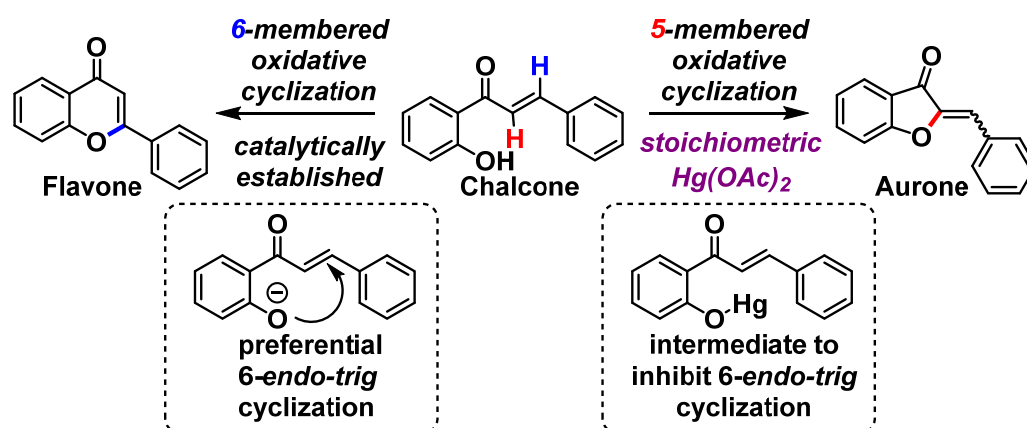


Figure 3-27. Difficulty with 5-membered ring formation from chalcones.

For another thing, the catalytic transformation from chalcones into aurones is regarded as “intramolecular α -olefinic C–H functionalization” (including formal C–H functionalization; in this chapter, an olefinic C–H bond closer to a directing group is defined as α -olefinic C–H), which has been rarely reported. To the best of my knowledge, a formal intramolecular α -olefinic C–H functionalization even *via* Pd-catalyzed Wacker-type cyclization has never been reported.^[20] Recently, a Rh-catalyzed pioneering formal intramolecular α -olefinic C–H functionalization of β -substituted-2'-hydroxyacrylophenone was reported by Glorius *et al.*; however, the system cannot be applied to the transformation of chalcones into aurones in the literature (Figure 3-28).^[21] As for intramolecular directed α -olefinic C–H functionalization, a recent report by Yu *et al.* to synthesize 4-imino- β -lactams was observed to be pioneering,^[22] while numerous examples of β -olefinic C–H functionalization have been reported.^[23] Therefore, the development of innovative multifunctional catalysts to control the difficult cyclization and the rare C–H functionalization is indispensable to achieve this challenging catalytic transformation into aurones.

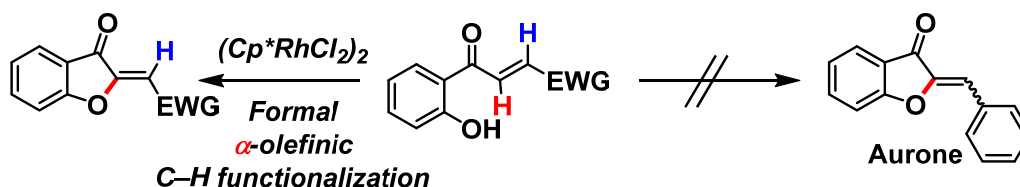


Figure 3-28. Rare “intramolecular α -olefinic C–H functionalization” pioneered by Glorius *et al.*

In this chapter, through the rational design of a function-integrated heterogeneous catalyst based on its components as mentioned in Chapter I, four requirements for the catalytic transformation of chalcones into aurones were achieved—a) a supported Pd catalyst: a catalyst for α -olefinic C–H functionalization of chalcones, b) an Au promoter: an improvement of the catalytic activity by the stabilization of Pd(0), c) a CeO₂ support: the inhibition of the 6-*endo-trig* cyclization utilizing the adsorption of chalcones, and d) a Pd-on-Au structure: the inhibition of Au-catalyzed flavone synthesis (Figure 3-29). That is, I have successfully developed an unusual catalytic transformation from simple chalcones into aurones over Pd-on-Au bimetallic nanoparticles supported

on CeO₂ (Pd/Au/CeO₂) using O₂ in air as the sole oxidant without any additives for the first time.

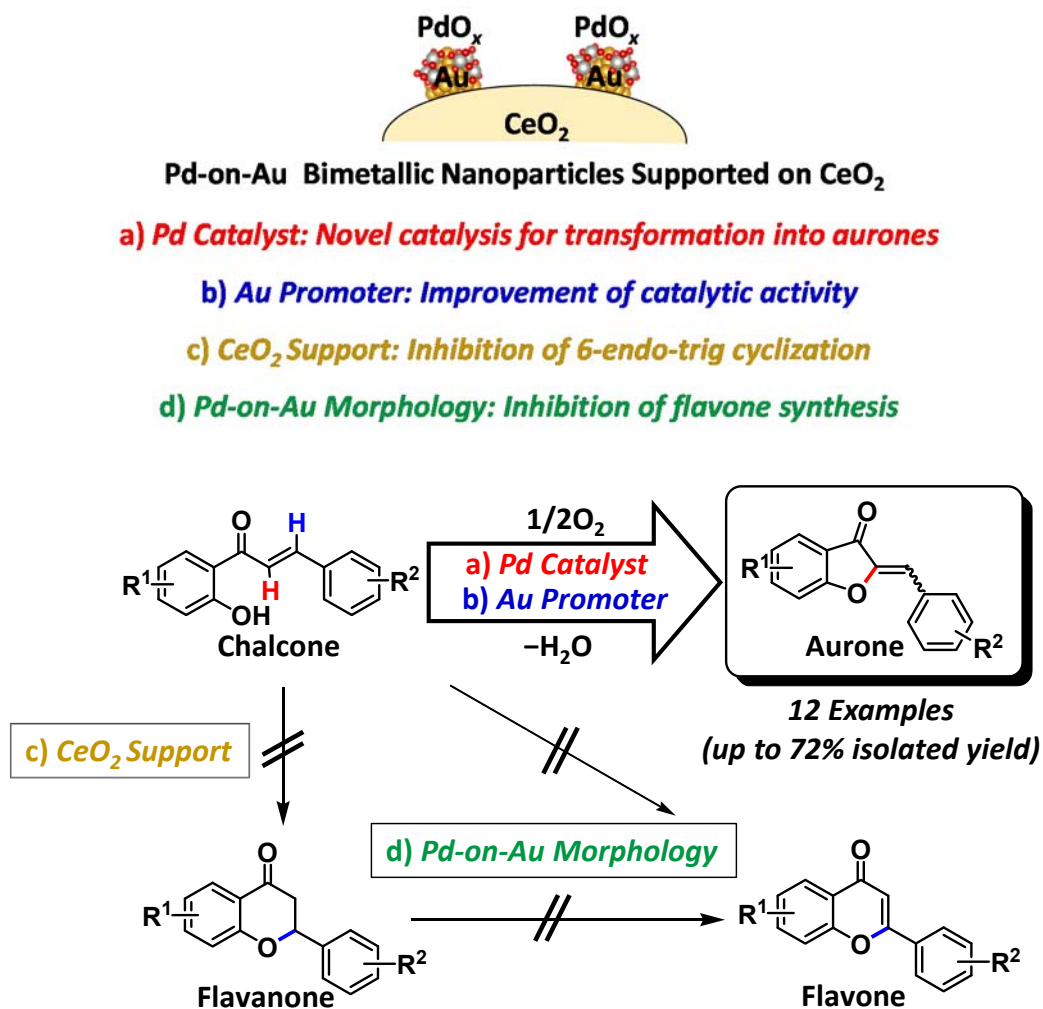


Figure 3-29. Strategy used in this work: Design of a function-integrated heterogeneous catalyst controlling each reaction to achieve the four requirements.

3-2.2. Experimental

3-2.2.1. Instruments and Reagents

GC analyses were performed on Shimadzu GC-2014 with a FID detector equipped with a TC-5 capillary column. GC-MS spectra were recorded on Shimadzu GCMS-QP2010 equipped with an InertCap5 capillary column at an ionization voltage of 70 eV. Liquid-state ^1H and ^{13}C NMR spectra were recorded on JEOL JNM-ECA 500. ^1H and ^{13}C NMR were measured at 500 and 125 MHz, respectively, with TMS as an internal standard ($\delta = 0$ ppm). ICP-AES analyses were performed on Shimadzu ICPS-8100. TEM measurements were performed on JEOL JEM-2000EX II. HAADF-STEM and STEM-EDS images were obtained using JEOL JEM-ARM 200F (200 kV). TEM and STEM samples were prepared by placing a drop of the suspension with EtOH on carbon-coated Cu grids and dried in air. DR UV-Vis spectra were recorded on a Jasco V-570DS. XRD patterns were recorded using a Rigaku SmartLab instrument under Cu K α radiation (45 kV, 200 mA). The XPS measurements were carried out on JEOL JPS-9000 using Mg K α radiation ($h\nu = 1253.6$ eV, 8 kV, 10 mA). XANES measurements were carried out at BL-9C of the Photon Factory in High Energy Accelerator Research Organization. IR spectra were measured on Jasco FT/IR-4100 using KBr disks. Al_2O_3 (160 $\text{m}^2 \text{g}^{-1}$, Cat. No. KHS-24, Sumitomo Chemical), TiO_2 (316 $\text{m}^2 \text{g}^{-1}$, Cat. No. ST-01, Ishihara Sangyo Kaisya), and CeO_2 (111 $\text{m}^2 \text{g}^{-1}$, Cat. No. 544841-25G, Aldrich), were commercially available. Solvents, substrates, and metal sources were obtained from Kanto Chemical, TCI, Wako, Kojima Chemicals, Nacalai Tesque, Strem Chemicals, or Aldrich (reagent grade). Some substrates were purified by kugelrohr distillation just before the use for reactions.

3-2.2.2. Preparation of Catalysts

Preparation of Pd/Au/CeO₂: The Pd-on-Au bimetallic nanoparticle catalyst supported on CeO₂ (Pd/Au/CeO₂) was prepared as follows. CeO₂ (2 g) was added to an aqueous solution of HAuCl₄ (3 mM, 100 mL), and the slurry was stirred for 2 min, followed by the addition of 10% aqueous NH₃ (360 μ L). After stirring for 14 h, the resulting mixture was filtered, washed with deionized water (1 L), and dried *in vacuo*, affording a supported Au precursor. This Au precursor was then dispersed in an aqueous solution of K₂PdCl₄ (3 mM), which was generated *in situ* from a mixture of PdCl₂ (0.3 mmol) and KCl (1.2 mmol) in 100 mL water, and stirred for 10 min. The pH of the solution was adjusted to 12.3 using an aqueous solution of NaOH (2 M). After the reaction mixture was stirred for 14 h, the precursor was filtered, washed, and dried in the aforementioned manner to give a supported Au–Pd precursor. After calcination of the Au–Pd precursor at 300 °C for 2 h, the desired Pd/Au/CeO₂ (Pd: 1.5wt%, Au: 2.7wt%) was obtained as a black powder. The catalysts for which the Pd/Au ratio is 1/3 (Pd: 0.7wt%, Au: 4.0wt%) or 3/1 (Pd: 2.2wt%, Au: 1.2wt%) were prepared using a similar procedure after adjusting the initial concentrations of metal sources to obtain the desired ratios. Similarly, Au/Pd/CeO₂ was prepared, by simply reversing the aforementioned order of the supporting metal species.

Preparation of Supported Catalysts: The Au–Pd bimetallic nanoparticle catalyst supported on CeO₂ (Au–Pd/CeO₂) was prepared as follows. CeO₂ (2 g) was added to an aqueous solution (100 mL) of HAuCl₄ (3 mM) and K₂PdCl₄ (3 mM), which was generated *in situ* from a mixture of PdCl₂ (0.3 mmol) and KCl (1.2 mmol), and the slurry was stirred for 10 min. The pH of the solution was adjusted to 10.0 using an aqueous solution of NaOH (2 M). After the reaction mixture was stirred for 14 h, the precursor was filtered, washed with deionized water (1 L), and dried *in vacuo* to give a supported Au–Pd precursor. Then, the precursor was dispersed in deionized water (100 mL) and treated with NaBH₄ (30 mg per 1 g precursor) at room temperature for 1 h. After filtration, washing, and drying, Au–Pd/CeO₂ was obtained (Pd: 1.4wt%, Au: 2.4wt%, mean nanoparticle diameter: 2.5 nm, standard deviation; 0.9 nm). The catalysts for which the Pd/Au ratio is 1/3 or 3/1 were prepared using a similar procedure after adjusting the initial concentrations of metal sources to obtain the desired ratios.

Cu–Pd/CeO₂ (Pd: 1.4wt%), Rh–Pd/CeO₂ (Pd: 1.3wt%), Ni–Pd/CeO₂ (Pd: 1.4wt%), Pb–Pd/CeO₂ (Pd: 1.5wt%), and Zn–Pd/CeO₂ (Pd: 1.5wt%) were prepared in the almost same way as mentioned above, adjusting the pH to 12.3 instead of 10.0 and using CuCl₂·2H₂O, RhCl₃·3H₂O, NiCl₂·6H₂O, PbCl₂, and ZnCl₂ as a respective metal source instead of HAuCl₄·4H₂O. Pd/CeO₂ (Pd: 0.7wt%, 1.5wt%, or 2.8wt%), Pd/TiO₂ (0.6wt%), Pd/Al₂O₃ (0.7wt%), Cu/CeO₂, Ru/CeO₂, Rh/CeO₂, and Ni/CeO₂ were also prepared in the almost same way, adjusting the pH to 12.3 and using the corresponding amounts of only one kind of metal source (Ru source: RuCl₃·*n*H₂O).

The Pt–Pd bimetallic nanoparticle catalyst supported on CeO₂ (Pt–Pd/CeO₂) was prepared as follows. CeO₂ (2 g) was added to an aqueous solution of H₂Pt(OH)₆ (3 mM, 100 mL) after adjusting the pH to 12.3, and the slurry was stirred for 10 min. The pH of the solution was adjusted to 7.0 using an aqueous solution of HCl (1 M). After stirring for 14 h, the resulting mixture was filtered, washed with deionized water (1 L), and dried *in vacuo*, affording a supported Pt precursor. This Pt precursor was then dispersed in an aqueous solution of K₂PdCl₄ (3 mM), which was generated *in situ* from a mixture of PdCl₂ (0.3 mmol) and KCl (1.2 mmol) in 100 mL water, and stirred for 10 min. The pH of the solution was adjusted to 12.3 using an aqueous solution of NaOH (2 M). After the reaction mixture was stirred for 14 h, the precursor was filtered, washed, and dried in the aforementioned manner to give a supported Pt–Pd precursor. The precursor (1 g) was dispersed in deionized water (100 mL) and treated with NaBH₄ (30 mg) at room temperature for 1 h. After filtration, washing, and drying, Pt–Pd/CeO₂ was obtained (Pd: 1.5wt%).

The gold nanoparticle catalyst supported on CeO₂ (Au/CeO₂) was prepared as follows. CeO₂ (2 g) was added to an aqueous solution of HAuCl₄ (3 mM or 6 mM, 100 mL). After stirring the mixture for 2 min, aqueous NH₃ (10 %, 360 or 720 µL) was added. Then, the resulting mixture was stirred at room temperature for 14 h. The resulting slurry was filtered, washed with deionized water (1 L), and dried *in vacuo*, giving the Au supported precursor. The precursor was dispersed in deionized water (100 mL) and treated with NaBH₄ (30 or 60 mg) at room temperature for 1 h. After filtration, washing, and drying, Au/CeO₂ was obtained (Au: 2.4 or 5.2wt%). In the case of Au/CeO₂ prepared through the reduction of Au by calcination, the aforementioned Au supported precursor was calcined at 300 °C for 2 h, affording the desired catalyst.

3-2.2.3. Reactions and Synthesis

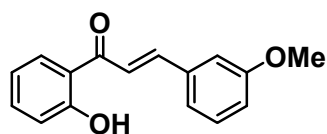
Catalytic reaction: The catalytic reaction was typically carried out according to the following procedure. Into a Pyrex glass reactor (volume: ~20 mL) were successively added Pd/Au/CeO₂ (100 mg, Au: 5 mol%, Pd: 5 mol%), biphenyl (0.1 mmol, internal standard), 2'-hydroxychalcone (**1a**, 0.3 mmol), BuOAc (2 mL), and a Teflon-coated magnetic stir bar; the mixture was then stirred at 100 °C under an open air atmosphere. The yields of products were determined by GC analysis using biphenyl as an internal standard. With respect to the isolation of products, after the reaction, the catalyst was removed by simple filtration and the filtrate was then concentrated by evaporation of BuOAc or DMA. The crude product was subjected to column chromatography on silica gel (typically using hexane/EtOAc = 8/2 as an eluent), giving the pure aurones.

Leaching Test: To verify whether the catalytic reaction occurred on solid Pd/Au/CeO₂ or not, the catalyst was removed by hot filtration 6 h after the reaction started under the optimized conditions and the reaction was again carried out with the filtrate under the same conditions. When the amount of leached metals was measured, the filtrate after the reaction for 24 h was evaporated *in vacuo*, treated with aqua regia (1 mL), and sonicated. Then, Au and Pd species in the filtrate were analyzed by ICP-AES.

Reuse Test: After the reaction under the optimized conditions, Pd/Au/CeO₂ was retrieved from the reaction mixture by simple filtration using a membrane filter. The retrieved Pd/Au/CeO₂ catalyst after the reaction was washed with acetone (100 mL) and dried *in vacuo*. Then, the catalyst was calcined at 300 °C for 2 h to reuse without a severe loss of its catalytic activity.

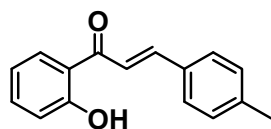
Synthesis of Substrates: 2'-Hydroxychalcones as substrates were synthesized as follows referring to the previous report.^[24] 2'-Hydroxyacetophenones (3 mmol) and benzaldehydes (3 mmol) were added to EtOH (9 mL). After the solution was stirred for 5 min, the pellets of sodium hydroxide (9 mmol) were added to the solution, and then the solution was stirred for 24–48 h until the substrates were almost completely converted. The pH of the solution was adjusted to 5 using an aqueous solution of 3 M HCl, giving yellow precipitation. The precipitation was retrieved by simple filtration.

After washing with EtOH and deionized water and drying *in vacuo*, the crude products were obtained. The crude products were added to Et₂O, removing insoluble matters by filtration. The solvent was evaporated under reduced pressure, affording the desired 2'-hydroxychalcones. As for some products, the crude product was subjected to column chromatography on silica gel using toluene as an eluent, giving the pure 2'-hydroxychalcones.



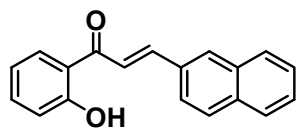
1c (CAS No. 7146-86-3)

(E)-2'-hydroxy-3-methoxychalcone (1c): ¹H NMR (500 MHz, CDCl₃, TMS): δ 3.82 (s, 3H), 6.91 (td, J = 7.0 and 1.0 Hz, 1H), 6.95 (dd, J = 8.0 and 2.0 Hz, 1H), 7.00 (dd, J = 8.0 and 1.0 Hz, 1H), 7.12 (t, J = 1.5 Hz, 1H), 7.22 (d, J = 8.0 Hz, 1H), 7.31 (t, J = 8.0 Hz, 1H), 7.46 (td, J = 7.0 and 1.5 Hz, 1H), 7.58 (d, J = 15.5 Hz, 1H), 7.83 (d, J = 15.5 Hz, 1H), 7.87 (dd, J = 8.0 and 1.5 Hz, 1H), 12.8 (s, 1H). MS (70 eV, EI): m/z (%): 255 (17), 254 (100) [M^+], 253 (77), 237 (13), 223 (22), 165 (12), 147 (85), 134 (54), 133 (10), 121 (46), 118 (17), 108 (16), 93 (19), 92 (13), 91 (11), 90 (16), 89 (14), 77 (18), 65 (33), 64 (10), 63 (13).



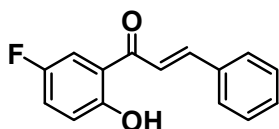
1e (CAS No. 16635-14-6)

(E)-2'-hydroxy-4-methylchalcone (1e): ¹H NMR (500 MHz, CDCl₃, TMS): δ 2.40 (s, 3H), 6.94 (ddd, J = 8.0, 7.0 and 1.0 Hz, 1H), 7.03 (dd, 8.0 and 1.0 Hz, 1H), 7.24 (d, J = 8.0 Hz, 2H), 7.49 (ddd, J = 8.5, 7.0 and 1.5 Hz, 1H), 7.90 (d, J = 15.5 Hz, 1H), 7.92 (dd, J = 8.5 and 2.0 Hz, 1H), 12.9 (s, 1H). MS (70 eV, EI): m/z (%): 239 (13), 238 (78) [M^+], 237 (87), 223 (30), 221 (15), 165 (11), 147 (69), 146 (13), 145 (13), 121 (45), 120 (20), 119 (13), 118 (100), 117 (46), 116 (13), 115 (56), 105 (21), 93 (21), 92 (22), 91 (37), 89 (13), 77 (10), 65 (59), 63 (16), 51 (11).



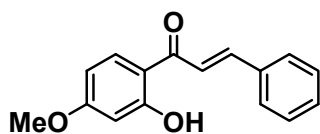
1f (CAS No. 83759-80-2)

(E)-2'-hydroxy-3-(2-naphthyl)-acrylophenone (1f): ^1H NMR (500 MHz, CDCl_3 , TMS): δ 6.95 (td, $J = 7.0$ and 1.0 Hz, 1H), 7.04 (dd, $J = 8.5$ and 1.0 Hz, 1H), 7.47–7.56 (m, 3H), 7.73 (d, $J = 15.5$ Hz, 1H), 7.78 (d, $J = 8.0$ and 1.5 Hz, 1H), 7.82–7.89 (m, 3H), 7.95 (dd, $J = 8.0$ and 1.5 Hz, 1H), 8.02 (s, 1H), 8.05 (d, $J = 15.5$ Hz, 1H), 12.9 (s, 1H). MS (70 eV, EI): m/z (%): 275 (20), 274 (100) [M^+], 273 (77), 257 (11), 155 (10), 154 (67), 153 (31), 152 (48), 151 (14), 147 (34), 141 (27), 128 (31), 127 (12), 121 (25), 93 (12), 65 (20).



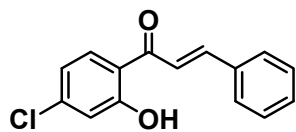
1g (CAS No. 1431-92-1)

(E)-5'-fluoro-2'-hydroxychalcone (1g): ^1H NMR (500 MHz, CDCl_3 , TMS): δ 6.99 (dd, $J = 9.0$ and 4.5 Hz, 1H), 7.21–7.26 (m, 1H), 7.43–7.47 (m, 3H), 7.53 (d, $J = 15.5$ Hz, 1H), 7.57 (d, $J = 9.0$ and 3.0 Hz, 1H), 7.65–7.68 (m, 2H), 7.94 (d, $J = 15.5$ Hz, 1H), 12.5 (s, 1H). MS (70 eV, EI): m/z (%): 243 (17), 242 (100) [M^+], 241 (98), 225 (15), 166 (10), 165 (94), 164 (12), 139 (34), 138 (69), 131 (15), 111 (19), 110 (23), 104 (47), 103 (51), 102 (13), 83 (31), 82 (11), 78 (10), 77 (49), 63 (10), 57 (19), 51 (19).



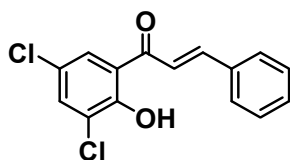
1h (CAS No. 39273-61-5)

(E)-2'-hydroxy-4'-methoxychalcone (1h): ^1H NMR (500 MHz, CDCl_3 , TMS): δ 3.85 (s, 3H), 6.40–6.50 (m, 3H), 7.40–7.44 (m, 3H), 7.55–7.66 (m, 3H), 7.82 (d, $J = 8.5$ Hz, 1H), 7.88 (d, $J = 15.5$ Hz, 1H), 13.5 (s, 1H). MS (70 eV, EI): m/z (%): 255 (17), 254 (100) [M^+], 253 (82), 178 (11), 177 (92), 151 (37), 150 (24), 103 (14), 77 (11).



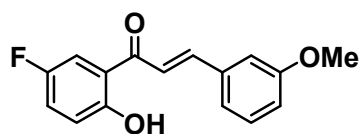
1i (CAS No. 1148-03-4)

(E)-4'-chloro-2'-hydroxychalcone (1i): ^1H NMR (500 MHz, CDCl_3 , TMS): δ 6.90 (dd, $J = 8.5$ and 2.0 Hz, 1H), 7.02 (d, $J = 2.0$ Hz, 1H), 7.41–7.45 (m, 3H), 7.55 (d, $J = 15.5$ Hz, 1H), 7.62–7.66 (m, 2H), 7.82 (d, $J = 8.5$ Hz, 1H), 7.91 (d, $J = 15.5$ Hz, 1H), 13.0 (s, 1H). MS (70 eV, EI): m/z (%): 260 (27), 259 (45) [M^+], 258 (82), 257 (100), 241 (13), 223 (12), 183 (21), 181 (66), 155 (25), 154 (11), 131 (12), 104 (34), 103 (25), 99 (10), 77 (18).



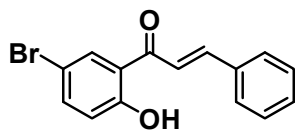
1j (CAS No. 70308-50-8)

(E)-3',5'-dichloro-2'-hydroxychalcone (1j): ^1H NMR (500 MHz, CDCl_3 , TMS): δ 7.44–7.50 (m, 3H), 7.54 (d, $J = 15.5$ Hz, 1H), 7.58 (d, $J = 2.5$ Hz, 1H), 7.67–7.70 (m, 2H), 7.80 (d, $J = 2.5$ Hz, 1H), 7.98 (d, $J = 15.5$ Hz, 1H), 13.4 (s, 1H). MS (70 eV, EI): m/z (%): 296 (12), 295 (18), 294 (67), 293 (61) [M^+], 292 (97), 291 (73), 275 (10), 217 (22), 215 (35), 192 (13), 191 (14), 190 (61), 189 (21), 188 (97), 165 (17), 135 (15), 133 (21), 131 (32), 105 (12), 104 (100), 103 (83), 102 (19), 97 (24), 96 (10), 91 (10), 82 (13), 78 (16), 77 (78), 76 (11), 75 (11), 63 (16), 62 (11), 51 (27).



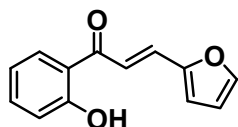
1k (CAS No. 1381931-08-3)

(E)-5'-fluoro-2'-hydroxy-3-methoxychalcone (1k): ^1H NMR (500 MHz, CDCl_3 , TMS): δ 3.88 (s, 3H), 6.98–7.02 (m, 2H), 7.17 (t, $J = 2.0$ Hz, 1H), 7.23–7.28 (m, 2H), 7.37 (t, $J = 8.0$ Hz, 1H), 7.52 (d, $J = 15.5$ Hz, 1H), 7.58 (dd, $J = 9.0$ and 3.0 Hz, 1H), 7.91 (d, $J = 15.5$ Hz, 1H), 12.5 (s, 1H). MS (70 eV, EI): m/z (%): 273 (17), 272 (100) [M^+], 271 (71), 255 (17), 254 (36), 241 (27), 239 (20), 165 (71), 139 (25), 135 (10), 134 (85), 133 (13), 118 (17), 111 (15), 108 (16), 104 (11), 91 (10), 90 (15), 89 (13), 83 (23), 77 (14), 63 (11), 57 (11).



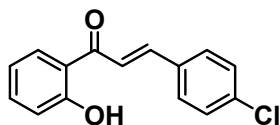
1m (CAS No. 1218-22-0)

(E)-5'-bromo-2'-hydroxychalcone (1m): ^1H NMR (500 MHz, CDCl_3 , TMS): δ 6.90 (d, $J = 9.0$ Hz, 1H), 7.40–7.45 (m, 3H), 7.51 (d, $J = 15.5$ Hz, 1H), 7.52 (dd, $J = 9.0$ and 2.5 Hz, 1H), 7.63–7.66 (m, 2H), 7.90 (d, $J = 15.5$ Hz, 1H), 7.96 (d, $J = 2.5$ Hz, 1H), 12.8 (s, 1H). MS (70 eV, EI): m/z (%): 305 (15), 304 (92), 303 (93) [M^+], 302 (92), 301 (80), 287 (12), 285 (15), 227 (70), 226 (15), 225 (70), 224 (11), 223 (15), 201 (23), 200 (80), 199 (24), 198 (80), 194 (10), 177 (10), 176 (12), 173 (11), 172 (18), 171 (11), 170 (17), 165 (23), 152 (11), 145 (15), 143 (19), 131 (33), 104 (74), 103 (100), 102 (30), 97 (10), 92 (10), 91 (16), 88 (18), 82 (13), 78 (18), 77 (92), 76 (17), 75 (14), 64 (16), 63 (47), 62 (11), 53 (17), 51 (36), 50 (13).



1n (CAS No. 2875-23-2)

(E)-3-(2-furanyl)-2'-hydroxyacrylophenone (1n): ^1H NMR (500 MHz, CDCl_3 , TMS): δ 6.50 (dd, $J = 3.5$ and 2.0 Hz, 1H), 6.73 (d, $J = 3.5$ Hz, 1H), 6.91 (td, $J = 6.5$ and 1.5 Hz, 1H), 7.00 (dd, $J = 8.5$ and 1.0 Hz, 1H), 7.46 (td, $J = 6.5$ and 1.5 Hz, 1H), 7.52 (d, $J = 15.0$ Hz, 1H), 7.53 (d, $J = 1.5$ Hz, 1H), 7.65 (d, $J = 15.0$ Hz, 1H), 7.88 (dd, $J = 8.0$ and 1.5 Hz, 1H), 12.9 (s, 1H). MS (70 eV, EI): m/z (%): 215 (14), 214 (100) [M^+], 213 (12), 160 (12), 157 (25), 131 (14), 128 (12), 121 (99), 120 (20), 94 (72), 93 (24), 92 (15), 81 (25), 66 (13), 65 (63), 64 (12), 63 (17).

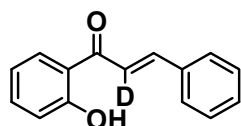


1o (CAS No. 3033-96-3)

(E)-4-chloro-2'-hydroxychalcone (1o): ^1H NMR (500 MHz, CDCl_3 , TMS): δ 6.95 (td, $J = 7.0$ and 1.5 Hz, 1H), 7.03 (dd, 8.5 and 1.0 Hz, 1H), 7.38–7.42 (m, 2H), 7.50 (td, $J = 7.0$ and 1.5 Hz, 1H), 7.57–7.60 (m, 2H), 7.62 (d, $J = 15.5$ Hz, 1H), 7.85 (d, $J = 15.5$ Hz, 1H), 7.90 (dd, $J = 8.0$ and 1.5 Hz, 1H), 12.8 (s, 1H). MS (70 eV, EI): m/z (%): 260 (21),

259 (35) [M^+], 258 (65), 257 (80), 241 (15), 223 (12), 165 (25), 148 (10), 147 (100), 146 (21), 140 (12), 139 (14), 138 (29), 137 (18), 125 (10), 121 (64), 120 (86), 111 (12), 103 (10), 102 (40), 101 (39), 97 (13), 93 (28), 92 (30), 82 (12), 77 (12), 76 (13), 75 (30), 65 (51), 64 (10), 63 (17), 51 (18), 50 (12).

Synthesis of [α -D]-2'-Hydroxychalcone: [α -D]-2'-Hydroxychalcone was synthesized as follows. Initially, [α,α,α -D₃]-2'-hydroxyacetophenone was synthesized referring to the previous report.^[25] 2'-Acetophenone (3 mmol) and NaOD/D₂O (40wt%, 188 μ L) were added to D₂O (30 mL) and stirred for 12 h at room temperature. The solution was extracted using Et₂O (3 \times 30 mL) and dried with Na₂SO₄. After evaporating the solvent under reduced pressure, the desired [α,α,α -D₃]-2'-hydroxyacetophenone was obtained (deuterated ratio: 95%). Next, using benzaldehyde (3 mmol) and the two runs of [α,α,α -D₃]-2'-hydroxyacetophenone as the substrates, NaOD/D₂O (40wt%, 600 μ L) as the base, and CD₃OD (9 mL) as the solvent, the crude [α -D]-2'-hydroxychalcone was synthesized in the same synthetic procedure of the other 2'-hydroxychalcones as mentioned above. The crude product was subjected to column chromatography on silica gel using toluene as an eluent, affording the pure [α -D]-2'-hydroxychalcone (deuterated ratio: 95%).

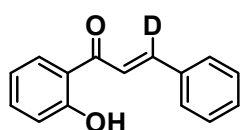


[α -D]-1a (CAS No. 55124-71-5)

(E)-[α -D]-2'-hydroxychalcone ([α -D]-1a): ¹H NMR (500 MHz, DMSO-*d*₆, TMS): δ 7.00–7.03 (m, 2H), 7.46–7.49 (m, 3H), 7.57 (ddd, J = 8.5, 7.0 and 1.5 Hz, 1H), 7.84 (s, 1H), 7.89–7.93 (m, 2H), 8.25 (dd, J = 8.5 and 1.5 Hz, 1H), 12.5 (s, 1H). MS (70 eV, EI): m/z (%): 226 (14), 225 (88) [M^+], 224 (92), 223 (18), 208 (14), 149 (10), 148 (100), 147 (16), 132 (12), 121 (41), 120 (50), 105 (22), 104 (36), 103 (14), 93 (18), 92 (21), 78 (24), 77 (26), 65 (29), 51 (14).

Synthesis of [β -D]-2'-Hydroxychalcone: [β -D]-2'-Hydroxychalcone was synthesized as follows. First, [α -D]-benzaldehyde was synthesized in the following method. [α,α -D₂]-Benzylalcohol (5 mmol) and α -MnO₂ (0.5 g, prepared referring to the

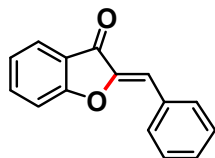
previous report)^[26] were added to toluene (15 mL), and stirred for 40 h at 80 °C. After filtrating α -MnO₂ and washing with toluene, the solution was condensed till ~1 mL under reduced pressure. Next, the solution and 2'-hydroxyacetophenone (0.45 mmol) were mixed in toluene (15 mL), and stirred for 5 min. After adding sodium hydroxide (0.6 g), the solution was stirred for 24 h. The pH of the solution was adjusted to 5 using 3 M HCl, extracted with toluene, and dried by Na₂SO₄. After evaporating toluene, the crude product was subjected to column chromatography on silica gel using toluene as an eluent, affording the pure [β -D]-2'-hydroxychalcone (deuterated ratio: 99%).



[β -D]-1a (CAS No. 55124-72-6)

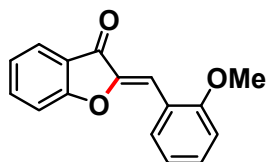
(*E*)-[β -D]-2'-hydroxychalcone ([β -D]-1a): ¹H NMR (500 MHz, DMSO-*d*₆, TMS): δ 7.02 (ddd, *J* = 8.5, 7.5 and 1.0 Hz, 2H), 7.47–7.50 (m, 3H), 7.57 (ddd, *J* = 8.0, 6.5 and 1.5 Hz, 2H), 7.90–7.94 (m, 2H), 8.04 (s, 1H), 8.26 (dd, *J* = 8.5 and 1.5 Hz, 1H), 12.5 (s, 1H). MS (70 eV, EI): *m/z* (%): 226 (13), 225 (79) [*M*⁺], 224 (52), 223 (25), 208 (12), 149 (11), 148 (100), 147 (11), 132 (13), 121 (39), 120 (50), 105 (23), 104 (38), 103 (11), 93 (18), 92 (25), 78 (26), 77 (25), 65 (31), 51 (15).

3-2.2.4. Spectral Data of Products



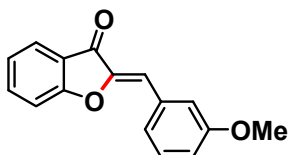
2a (CAS No. **582-04-7**) (Eluent: EtOAc/hexane = 2/8)

(Z)-aurone (2a): ^1H NMR (500 MHz, CDCl_3 , TMS): δ 6.90 (s, 1H), 7.22 (t, J = 8.0 Hz, 1H), 7.33 (d, J = 8.5 Hz, 1H), 7.39–7.42 (m, 1H), 7.46 (t, J = 7.0 Hz, 2H), 7.66 (td, J = 7.0 and 1.5 Hz, 1H), 7.81 (dd, J = 8.0 and 1.0 Hz, 1H), 7.93 (d, J = 7.5 Hz, 2H). ^{13}C – $\{^1\text{H}\}$ NMR (125 MHz, CDCl_3 , TMS): δ 113.08, 113.21, 121.75, 123.61, 124.81, 129.09, 130.04, 131.67, 132.42, 137.05, 147.00, 166.28, 184.96. MS (70 eV, EI): m/z (%): 223 (8), 222 (53) [M^+], 221 (100), 165 (8), 120 (6), 92 (12), 90 (6), 89 (7), 76 (13), 64 (5), 63 (7), 50 (6).



2b (CAS No. **61370-67-0**) (Eluent: EtOAc/hexane = 2/8)

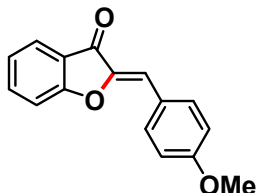
(Z)-2'-methoxyaurone (2b): ^1H NMR (500 MHz, CDCl_3 , TMS): δ 3.90 (s, 3H), 6.93 (d, J = 8.0 Hz, 1H), 7.06 (td, J = 7.5 and 0.5 Hz, 1H), 7.21 (t, J = 7.5 Hz, 1H), 7.32 (dd, J = 8.0 and 0.5 Hz, 1H), 7.37 (td, J = 8.5 and 1.0 Hz, 1H), 7.48 (s, 1H), 7.64 (ddd, J = 9.0, 7.5, and 1.5 Hz, 1H), 7.81 (ddd, J = 7.5, 1.0, and 1.0 Hz, 1H), 8.31 (dd, J = 7.5 and 1.5 Hz, 1H). ^{13}C – $\{^1\text{H}\}$ NMR (125 MHz, CDCl_3 , TMS): δ 55.72, 107.41, 110.86, 113.03, 120.95, 121.41, 121.99, 123.41, 124.74, 131.63, 132.13, 136.75, 147.04, 158.97, 166.07, 184.85. MS (70 eV, EI): m/z (%): 252 (22) [M^+], 222 (17), 221 (100), 165 (5), 152 (7), 131 (7), 121 (5), 89 (5), 77 (7), 76 (9), 63 (5).



2c (CAS No. **61370-63-6**) (Eluent: EtOAc/hexane = 2/8)

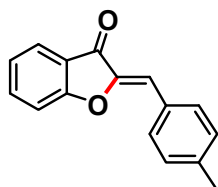
(Z)-3'-methoxyaurone (2c): ^1H NMR (500 MHz, CDCl_3 , TMS): δ 3.88 (s, 3H), 6.86 (s, 1H), 6.96 (ddd, J = 8.0, 2.5 and 1.0 Hz, 1H), 7.22 (td, J = 8.5 and 1.0 Hz, 1H), 7.32 (d, J = 8.5 Hz, 1H), 7.37 (t, J = 8.5 Hz, 1H), 7.48–7.50 (m, 2H), 7.65 (ddd, J = 8.5, 7.0, and 1.5 Hz, 1H), 7.81 (dd, J = 7.5 and 1.0 Hz, 1H). ^{13}C – $\{^1\text{H}\}$ NMR (125 MHz, CDCl_3 ,

TMS): δ 55.45, 113.08, 115.86, 116.63, 121.71, 123.63, 124.43, 124.80, 129.96, 133.61, 137.06, 147.08, 159.88, 166.26, 184.91. MS (70 eV, EI): m/z (%): 253 (17), 252 (100) [M^+], 251 (94), 237 (21), 222 (16), 221 (96), 209 (16), 208 (15), 152 (15), 132 (11), 102 (10), 92 (13), 89 (13), 77 (15), 76 (24), 63 (13), 51 (11), 50 (10).



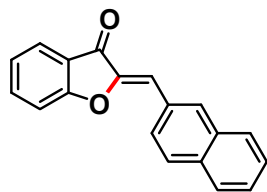
2d (CAS No. 4940-51-6) (Eluent: EtOAc/hexane = 2/8)

(Z)-4'-methoxyaurone (2d): ^1H NMR (500 MHz, CDCl_3 , TMS): δ 3.87 (s, 3H), 6.89 (s, 1H), 6.99 (d, $J = 9.0$ Hz, 1H), 6.99 (q, $J = 5.0$ Hz, 1H), 7.21 (td, $J = 7.5$ and 0.5 Hz, 1H), 7.32 (d, $J = 8.0$ Hz, 1H), 7.64 (ddd, $J = 8.5$, 7.0, and 1.5 Hz, 1H), 7.81 (dd, $J = 8.0$ and 1.0 Hz, 1H), 7.90 (d, $J = 9.0$ Hz, 1H), 7.90 (q, $J = 5.0$ Hz, 1H). ^{13}C - $\{^1\text{H}\}$ NMR (125 MHz, CDCl_3 , TMS): δ 55.53, 113.01, 113.58, 114.63, 122.06, 123.40, 124.69, 125.17, 133.58, 136.68, 146.01, 161.19, 165.96, 184.71. MS (70 eV, EI): m/z (%): 253 (17), 252 (100) [M^+], 251 (72), 237 (23), 221 (33), 209 (15), 152 (15), 132 (29), 89 (12), 77 (12), 76 (13).



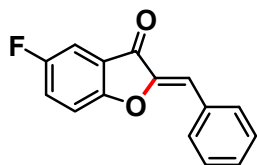
2e (CAS No. 61370-66-9) (Eluent: EtOAc/hexane = 2/8)

(Z)-4'-methylaurone (2e): ^1H NMR (500 MHz, CDCl_3 , TMS): δ 2.41 (s, 3H), 6.89 (s, 1H), 7.22 (td, $J = 7.5$ and 1.0 Hz, 1H), 7.27 (d, $J = 8.0$ Hz, 2H), 7.33 (d, $J = 8.5$ Hz, 1H), 7.65 (ddd, $J = 8.5$, 7.0, and 1.5 Hz, 1H), 7.79–7.84 (m, 3H). ^{13}C - $\{^1\text{H}\}$ NMR (125 MHz, CDCl_3 , TMS): δ 21.79, 113.06, 113.51, 121.90, 123.49, 124.75, 129.64, 129.85, 131.72, 136.87, 140.65, 146.65, 166.15, 184.90. MS (70 eV, EI): m/z (%): 237 (12), 236 (70) [M^+], 235 (69), 222 (17), 221 (100), 117 (15), 115 (15), 92 (11), 76 (14).



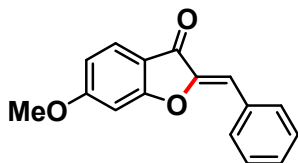
2f (CAS No. 70170-86-4) (Eluent: EtOAc/hexane = 2/8)

(Z)-2-(2-naphthylidene)coumaran-3-one (2f): ^1H NMR (500 MHz, CDCl_3 , TMS): δ 7.05 (s, 1H), 7.23 (td, J = 7.5 and 1.0 Hz, 1H), 7.38 (dd, J = 8.0 and 1.0 Hz, 1H), 7.50–7.55 (m, 2H), 7.67 (ddd, J = 9.0, 7.5, and 1.5 Hz, 1H), 7.82–7.93 (m, 4H), 8.08 (d, J = 8.5 and 2.0 Hz, 1H), 8.32 (brs, 1H). ^{13}C – $\{^1\text{H}\}$ NMR (125 MHz, CDCl_3 , TMS): δ 113.14, 113.43, 121.83, 123.64, 124.84, 126.76, 127.65, 127.82, 127.88, 128.72, 128.89, 132.50, 133.46, 133.86, 137.01, 147.21, 166.26, 184.88. MS (70 eV, EI): m/z (%): 273 (12), 272 (68) [M^+], 271 (100), 215 (8), 152 (24), 151 (7), 140 (5), 139 (12), 136 (7), 76 (9).



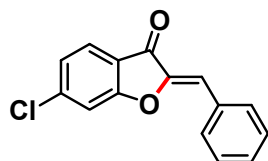
2g (CAS No. 1800-77-7) (Eluent: EtOAc/hexane = 2/8, then DCM)

(Z)-5-fluoroaurone (2g): ^1H NMR (500 MHz, CDCl_3 , TMS): δ 6.90 (s, 1H), 7.29–7.48 (m, 6H), 7.89–7.91 (m, 2H). ^{13}C – $\{^1\text{H}\}$ NMR (125 MHz, CDCl_3 , TMS): δ 110.22, 110.41, 114.10, 114.22, 114.27, 122.40, 122.46, 124.32, 124.52, 126.25, 129.08, 130.32, 131.79, 132.15, 147.53, 157.95, 159.90, 162.24, 184.24, 184.27. MS (70 eV, EI): m/z (%): 241 (8), 240 (54) [M^+], 239 (100), 183 (8), 138 (10), 110 (16), 106 (6), 102 (5), 94 (11), 90 (7), 89 (8), 82 (8), 63 (6).



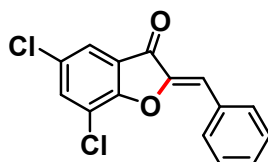
2h (CAS No. 4940-52-7) (Eluent: EtOAc/hexane = 2/8)

(Z)-6-methoxyaurone (2h): ^1H NMR (500 MHz, CDCl_3 , TMS): δ 3.93 (s, 3H), 6.75–6.78 (m, 2H), 6.82 (s, 1H), 7.37–7.41 (m, 1H), 7.43–7.47 (m, 2H), 7.71 (d, J = 8.5 Hz, 1H), 7.88–7.91 (m, 2H). ^{13}C – $\{^1\text{H}\}$ NMR (125 MHz, CDCl_3 , TMS): δ 56.18, 96.77, 112.04, 112.34, 114.96, 125.99, 128.98, 129.75, 131.45, 132.55, 147.96, 167.59, 168.73, 183.21. MS (70 eV, EI): m/z (%): 253 (9), 252 (60) [M^+], 251 (100), 236 (10), 209 (5), 208 (5), 152 (6), 122 (7), 107 (6), 106 (6), 90 (7), 89 (6), 63 (16).



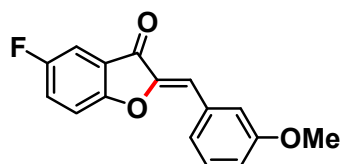
2i (CAS No. 3260-82-0) (Eluent: EtOAc/hexane = 2/8, then DCM)

(Z)-6-chloroaurone (2i): ^1H NMR (500 MHz, CDCl_3 , TMS): δ 6.92 (s, 1H), 7.22 (dd, J = 8.5 and 2.0 Hz, 1H), 7.38 (d, J = 1.5 Hz, 1H), 7.40–7.49 (m, 3H), 7.74 (d, J = 8.5 Hz, 1H), 7.89–7.92 (m, 2H). ^{13}C – $\{^1\text{H}\}$ NMR (125 MHz, CDCl_3 , TMS): δ 113.79, 114.05, 120.45, 124.56, 125.60, 129.13, 130.37, 131.78, 132.09, 143.07, 147.07, 166.36, 183.48. MS (70 eV, EI): m/z (%): 258 (17), 257 (39) [M^+], 256 (51), 255 (100), 165 (5), 128 (5), 126 (9), 110 (12), 102 (7), 90 (8), 89 (10), 75 (11), 74 (5), 63 (10).



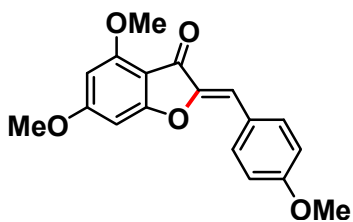
2j (CAS No. 460728-81-8) (Eluent: DCM/hexane = 8/2, then EtOAc/hexane = 2/8)

(Z)-5,7-dichloroaurone (2j): ^1H NMR (500 MHz, CDCl_3 , TMS): δ 6.98 (s, 1H), 7.43–7.51 (m, 3H), 7.65 (d, J = 2.0 Hz, 1H), 7.68 (d, J = 2.0 Hz, 1H), 7.94 (dd, J = 8.0 and 1.0 Hz, 2H). ^{13}C – $\{^1\text{H}\}$ NMR (125 MHz, CDCl_3 , TMS): δ 115.78, 119.62, 122.77, 124.16, 126.08, 129.09, 129.27, 129.54, 130.88, 131.69, 132.17, 136.09, 146.71, 160.31, 182.72. MS (70 eV, EI): m/z (%): 293 (15), 292 (33), 291 (68) [M^+], 290 (52), 289 (100), 188 (11), 132 (10), 90 (11), 89 (12).



2k (CAS No. 2222315-70-8) (Eluent: EtOAc/hexane = 2/8, then DCM)

(Z)-5-fluoro-3'-methoxyaurone (2k): ^1H NMR (500 MHz, CDCl_3 , TMS): δ 3.88 (s, 3H), 6.88 (s, 1H), 6.97–6.99 (m, 1H), 7.30 (dd, J = 9.0 and 4.0 Hz, 1H), 7.35–7.41 (m, 2H), 7.45–7.49 (m, 3H). ^{13}C – $\{^1\text{H}\}$ NMR (125 MHz, CDCl_3 , TMS): δ 55.49, 110.27, 110.46, 114.04, 114.26, 114.32, 116.11, 116.78, 122.38, 122.45, 124.38, 124.57, 130.04, 133.36, 147.64, 157.99, 159.92, 162.26, 184.28. MS (70 eV, EI): m/z (%): 273 (16), 272 (97), 271 (69), 255 (17), 254 (35), 241 (27), 239 (20), 183 (11), 165 (80), 161 (10), 139 (30), 135 (13), 134 (100), 133 (14), 121 (10), 118 (20), 111 (18), 108 (19), 104 (13), 103 (11), 91 (13), 90 (19), 89 (16), 83 (29), 78 (10), 77 (19), 63 (16), 57 (15).



2l (CAS No. 10493-04-6) (Eluent: EtOAc/CHCl₃ = 2/8)

(Z)-4,4',6-trimethoxyaurone (2l): ¹H NMR (500 MHz, CDCl₃, TMS): δ 3.84 (s, 3H), 3.88 (s, 3H), 3.92 (s, 3H), 6.08 (d, J = 1.5 Hz, 1H), 6.34 (d, J = 1.5 Hz, 1H), 6.72 (s, 1H), 6.93 (d, J = 8.5 Hz, 1H), 7.80 (d, J = 9.0 Hz, 1H). ¹³C-¹H NMR (125 MHz, CDCl₃, TMS): δ 55.37, 56.11, 56.20, 89.17, 93.92, 105.41, 110.96, 114.35, 125.31, 132.89, 146.80, 159.30, 160.57, 168.73, 168.79, 180.63. MS (70 eV, EI): m/z (%): 313 (20), 312 (100) [M^+], 311 (38), 283 (22), 282 (15), 281 (65), 156 (10), 137 (10), 121 (25), 108 (24), 106 (11), 91 (14), 77 (16), 69 (10), 63 (15), 51 (11).

3-2.3. Results and Discussion

3-2.3.1. Catalyst Characterization

Hutchings *et al.* reported Au@Pd core-shell structures formed from Au and Pd species impregnated on metal oxides by calcination at approximately 200–400 °C (see the reference of [111] in Chapter I). Referring to the report, in the present work, I prepared Pd/Au/CeO₂ through calcination at 300 °C for 2 h after Au and Pd species were supported on CeO₂ separately in this order *via* a deposition-precipitation method (see section 3-2.2.2. in this chapter). Transmission electron microscopy (TEM) images of the Pd/Au/CeO₂ revealed that the metal species were dispersedly supported on CeO₂ as nanoparticles with a mean diameter of 2.2 nm ($\sigma = 1.0$ nm) (Figure 3-30a,b). The high-angle annular dark-field scanning transmission electron microscopy (HAADF-STEM) image in Figure 2c and STEM energy-dispersive X-ray spectroscopy (STEM-EDS) mapping images (Figure 3-30d–f) indicate that the nanoparticles consisted of both Au and Pd. Each particle observed by HAADF-STEM possessed almost the same structure, though clear direct observation of the Pd-on-Au structure was quite difficult because of the small nanoparticle size (Figure 3-31). In addition, X-ray photoelectron spectroscopy (XPS) spectra of the freshly prepared Pd/Au/CeO₂ catalyst indicate a Pd valence of II and an Au valence of 0 (Figure 3-30g,h). Given the aforementioned results, the proposed structure of Pd oxides covering the surface of Au nanoparticles is valid. According to the X-ray diffraction (XRD) (Figure 3-32) and Ce L_{III}-edge X-ray absorption near edge structure (XANES) analyses (Figure 3-33), the structure of the CeO₂ support was not affected by the preparation. Thus, the Pd-on-Au bimetallic nanoparticle catalyst supported on CeO₂ was successfully prepared.

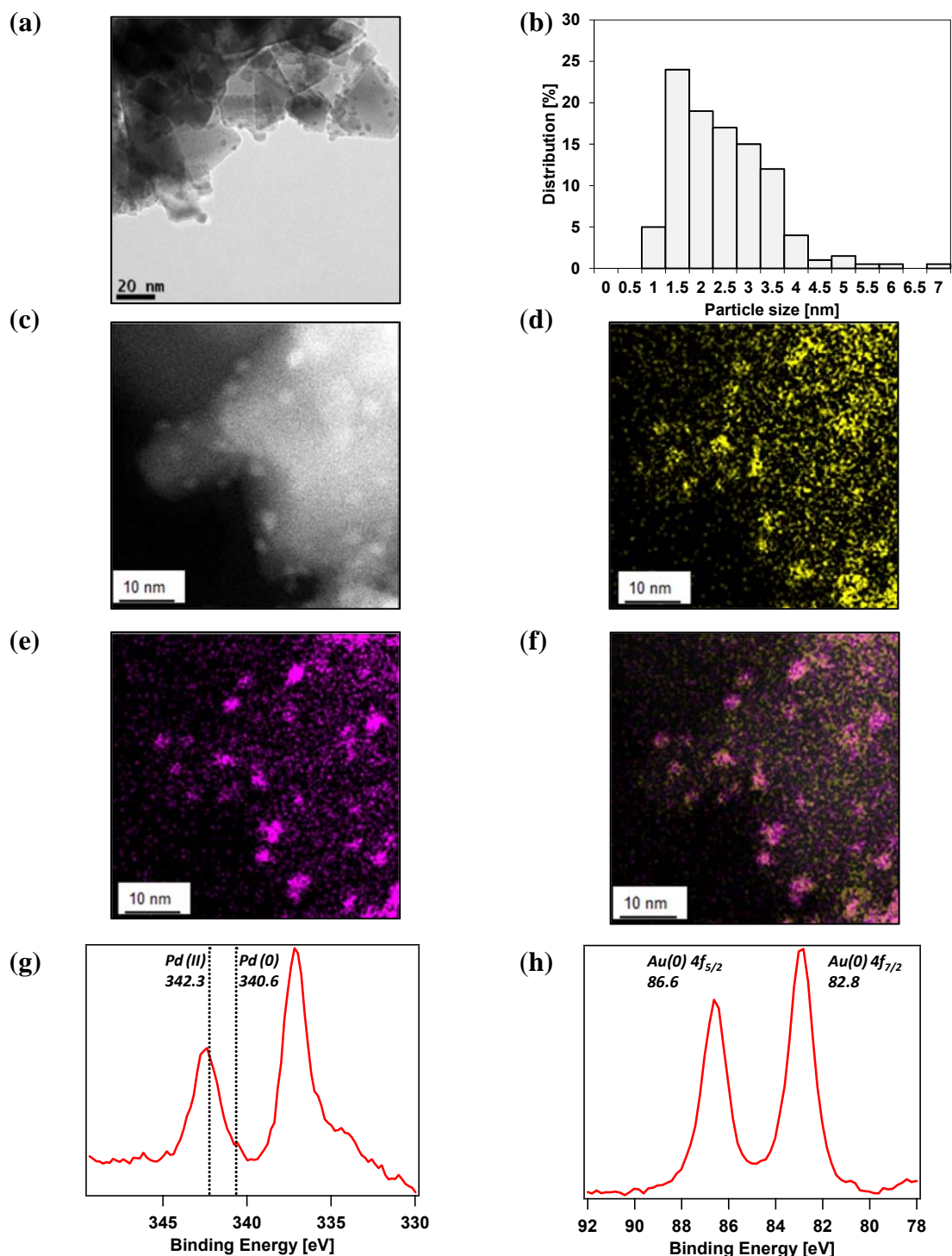


Figure 3-30. Characterization of Pd/Au/CeO₂: (a), (b) TEM images and nanoparticle size distributions of Pd/Au/CeO₂ (mean diameter: 2.2 nm, $\sigma = 1.0$ nm). The size distributions were determined using 200 particles; (c) HAADF-STEM image and STEM-EDS mapping images of Pd/Au/CeO₂, showing the distributions of (d) Pd (yellow), (e) Au (magenta) and (f) Au and Pd together; (g), (h) XPS spectra of Pd/Au/CeO₂ around the Pd 3d region and Au 4f region, respectively; peak positions were calibrated using the C 1s peak (284.2 eV).

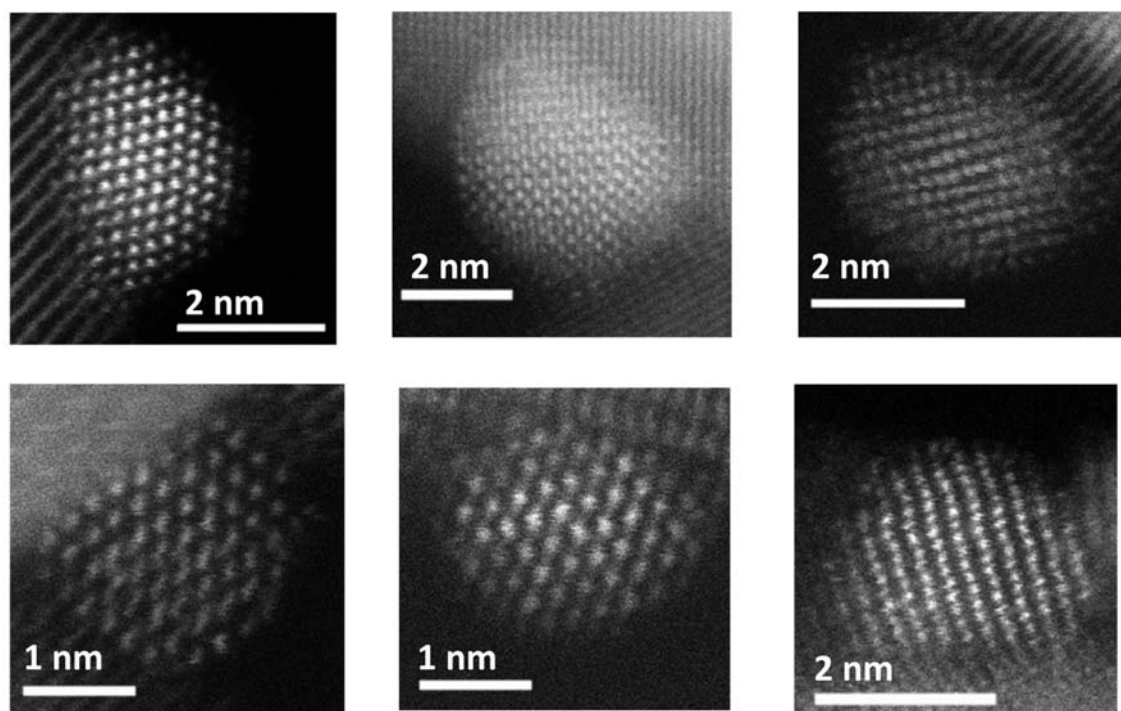


Figure 3-31. HAADF-STEM images of nanoparticles in Pd/Au/CeO₂.

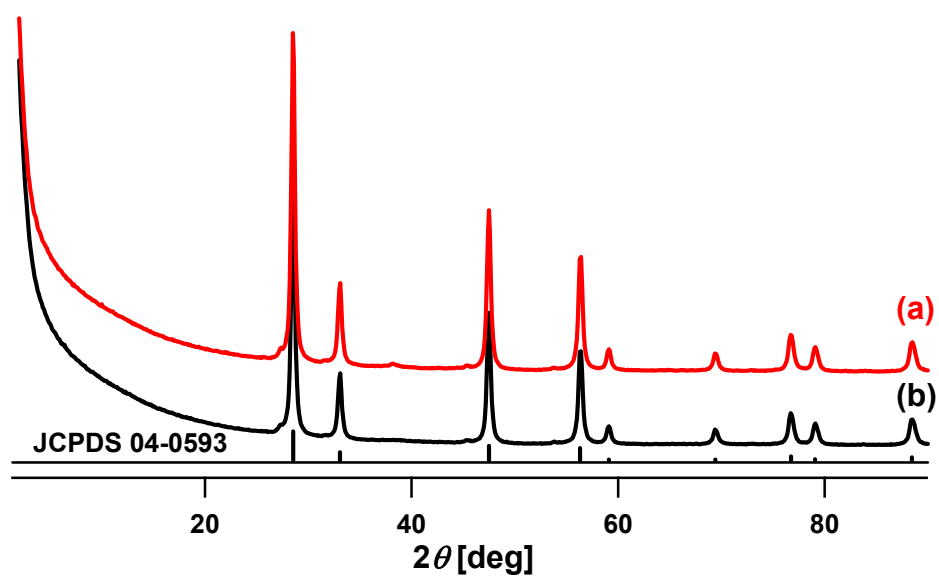


Figure 3-32. XRD patterns of (a) Pd/Au/CeO₂ and (b) Au-Pd/CeO₂.

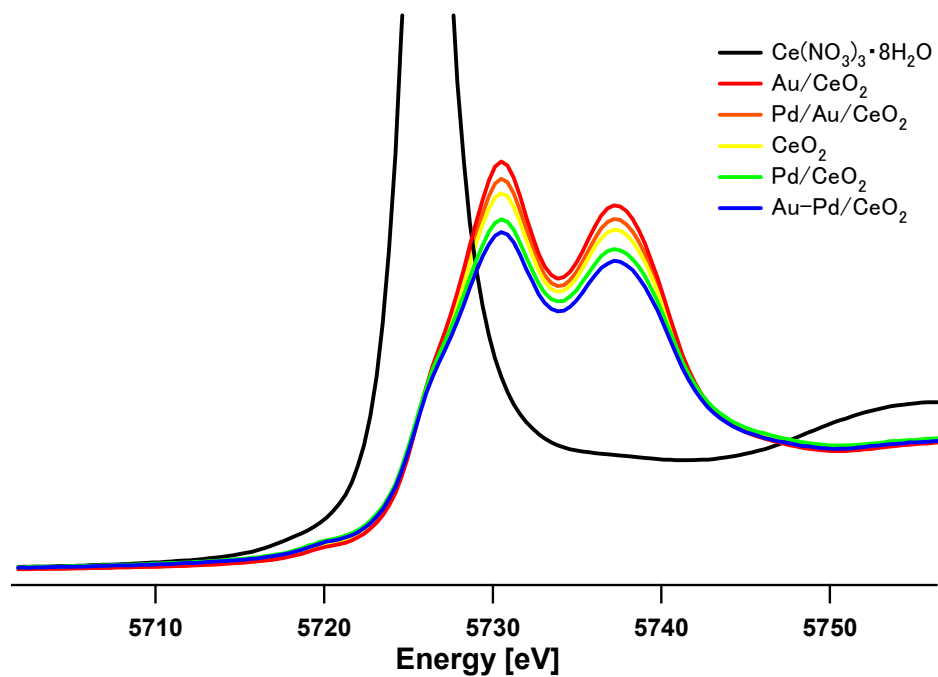


Figure 3-33. Ce L_{III}-edge XANES spectra of Pd/Au/CeO₂, Au-Pd/CeO₂, Au/CeO₂, Pd/CeO₂ and CeO₂. Ce(NO₃)₃·8H₂O was the reference of Ce(III).

3-2.3.2. Catalyst Design and Optimization of Reaction Conditions

I attempted the transformation from 2'-hydroxychalcone (**1a**) into aurone (**2a**) using various catalysts in butyl acetate (BuOAc) at 100 °C under an open air atmosphere (Table 3-5). Although homogeneous Pd species catalytically produced **2a**, the yield was not satisfactory (Table 3-5, entry 1); the production of **2a** stopped in the middle with the formation of Pd black (Figure 3-34), and the formation of flavanone (**4a**) was not be suppressed. To stabilize Pd species and to inhibit the 6-*endo-trig* cyclization, I prepared supported Pd catalysts (represented as Pd/support). Pd/Al₂O₃ and Pd/TiO₂ effectively increased the **2a** yield, although flavanone **4a** was still formed to some extent (Table 3-5, entries 3 and 4). Pd/CeO₂ effectively inhibited **4a** production; however, **2a** was obtained in a low yield (Table 3-5, entry 2 vs entry 11). The inhibition of **4a** was possibly due to the coordination of phenoxide species derived from **1a** toward Ce species, analogous to the typical aurone synthesis using stoichiometric reagents such as Hg(OAc)₂. In fact, when **1a** and the CeO₂ support were mixed under the same conditions described in Table 3-5, the CeO₂ support was colored, as revealed by both its appearance and its DR UV–Vis spectrum, suggesting that the phenoxide species derived from **1a** was adsorbed onto CeO₂ (Figure 3-35).^[27] When only the CeO₂ support was used, **2a** was not produced at all (Table 3-6, entry 1). Among the other metal catalysts (Au, Cu, Ru, Rh, and Ni) supported on CeO₂, only Au showed the catalytic activity toward the synthesis of **2a** (Table 3-5, entry 5 and Table 3-6, entries 2–5) whereas the selectivity toward **2a** was remarkably low because of the dominant formation of flavone (**3a**) catalyzed by Au (refer to section 3-1). Bimetallic nanoparticles composed of Pd and the other metal species (*i.e.* Pt–Pd, Cu–Pd, Rh–Pd, Ni–Pd, Pb–Pd, and Zn–Pd) supported on CeO₂ did not improve the **2a** yield (Table 3-6, entries 6–12). Exceptionally, Au–Pd bimetallic nanoparticles supported on CeO₂ (Au–Pd/CeO₂) boosted the production of **2a** concomitantly with considerable **3a** production by Au catalysis (Table 3-5, entry 6). The physical mixture of Au/CeO₂ and Pd/CeO₂ also promoted the production of **2a**; however, the yield was not comparable to that achieved using Au–Pd/CeO₂ and **3a** production was dominant because of the bare Au catalyst (Table 3-5, entry 7). Thus, the Pd-on-Au bimetallic nanoparticle catalyst supported on CeO₂ (Pd/Au/CeO₂) was designed to retain the Au promotion effect while inhibiting the Au catalysis toward **3a** production; this catalyst resulted in a high yield of and high

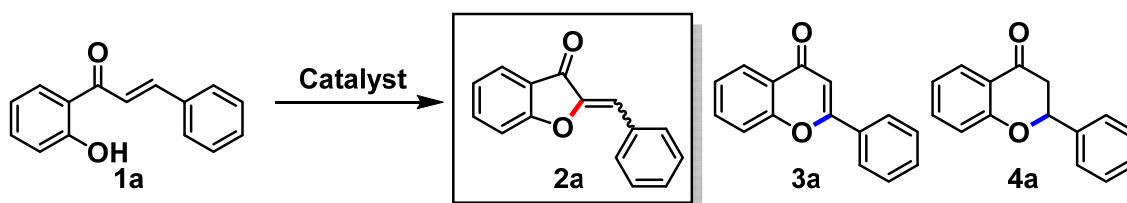
selectivity toward **2a** (Table 3-5, entry 8). The inhibition effect of Pd/Au/CeO₂ on the production of **3a** was also observed when the reaction was carried out starting from **4a** instead of **2a** (Figure 3-36).

When using Au/Pd/CeO₂, prepared through supporting Pd and Au species separately in this order, the yield of **2a** was no more than 2%, indicating Pd did not likely promote Au-catalyzed aurone synthesis (Table 3-6, entry 13). The result that Au/Pd/CeO₂ showed the low catalytic activity for flavone synthesis is probably related to that **3a** was hardly obtained in the presence of Au/CeO₂ prepared *via* calcination (Table 3-6, entry 14), possibly because the gold particle sizes were comparatively large.

The ratio of Au and Pd had an influence on the activity and selectivity for the transformation from **1a** to **2a** (Figure 3-37). In the case of Pd/Au/CeO₂, Pd-rich catalysts afforded high selectivity to and low yield of **2a** whereas Au-rich catalysts gave **3a** selectively in high yields (Figure 3-37a). Consequently, Pd/Au/CeO₂ with the Au/Pd ratio of 1/1 was the best catalyst in terms of the balance between activity and selectivity to **2a**. When Au–Pd/CeO₂ was used, the same tendency about Au/Pd ratio appeared possibly thanks to the ensemble effect diluting Au with Pd (Figure 3-37b); however, totally, the selectivity to **2a** was comparatively low because the covering of Au by Pd was more effective to suppress the Au catalysis to synthesize **3a**.

The effect of solvents was also very significant (Table 3-7). In low-polarity solvents such as toluene and diglyme, the production of **3a** and **4a** was substantially suppressed while the yields of **2a** were low. In polar solvents such as alcohols, *N,N*-dimethylacetamide (DMA), and *N,N*-dimethylformamide (DMF), the yields of **2a** were comparably high; however, considerable amounts of **3a** and **4a** were produced. BuOAc was the most suitable solvent for the efficient transformation into **2a** with simultaneous suppression of **3a** and **4a** production. With optimization of the reaction temperature (Table 3-8) and the amount of catalysts, the yield of **2a** reached 79% (Table 3-5, entry 9). Under an Ar atmosphere, **2a** was hardly obtained, which revealed that O₂ in air functioned as the sole oxidant in this system (Table 3-5, entry 10).

Table 3-5. Effect of catalysts on the transformation from 2'-hydroxychalcone (**1a**) into aurone (**2a**).^[a]

					
Entry	Catalyst	Conv. [%]	Yield [%]		
		1a	2a	3a	4a
1	Pd(TFA) ₂	38	12	2	16
2 ^[b]	Pd/CeO ₂	7	3	<1	4
3 ^[b]	Pd/TiO ₂	37	19	1	13
4 ^[b]	Pd/Al ₂ O ₃	47	16	3	25
5	Au/CeO ₂	>99	6	80	8
6	Au–Pd/CeO ₂	90	52	22	8
7	Au/CeO ₂ + Pd/CeO ₂	94	32	51	14
8	Pd/Au/CeO ₂	60	46	6	9
9 ^[c]	Pd/Au/CeO ₂	94	79	11	5
10 ^[c,d]	Pd/Au/CeO ₂	21	1	<1	13
11	None	16	<1	<1	16

[a] Reaction conditions: **1a** (0.3 mmol), catalyst (Au and/or Pd: 2 mol%), BuOAc (2 mL), open air (1 atm), 100 °C, 24 h. Yields and conversions were determined by GC.

[b] Supported Pd catalyst (50 mg, Pd: 1 mol%). [c] Catalyst (100 mg, Au: 5 mol%, Pd: 5 mol%). [d] Under Ar (1 atm). TFA = trifluoroacetate.



Figure 3-34. Pd black precipitation when the reaction to synthesize **2a** from **1a** proceeded for three hours using Pd(TFA)₂.

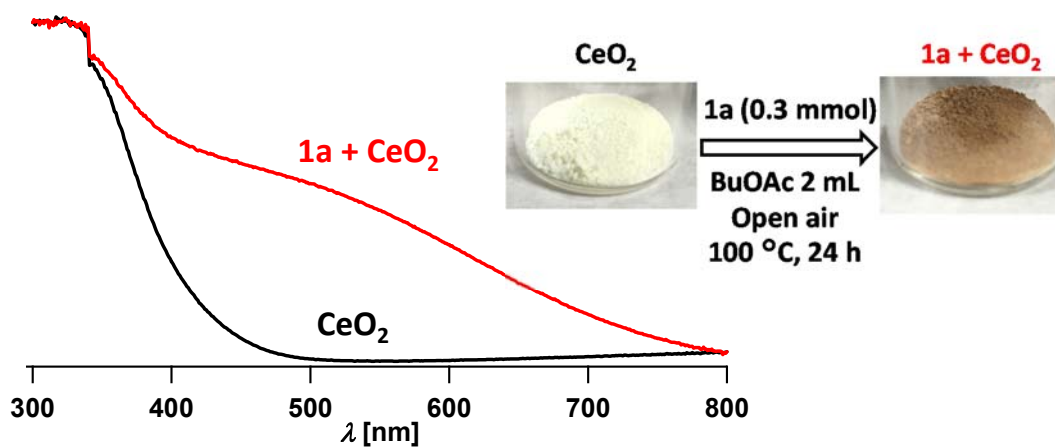
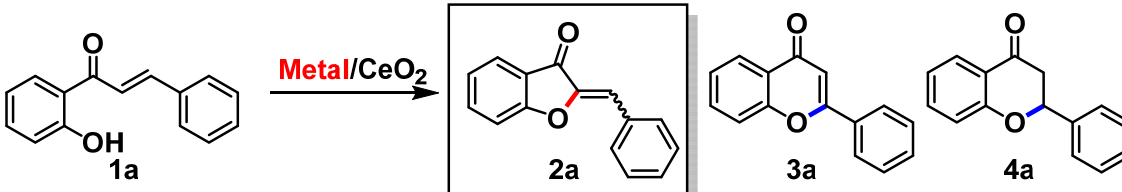


Figure 3-35. Change of CeO_2 color after mixing CeO_2 and **1a** on the reaction conditions of Table 3-6 shown as pictures and DR UV-Vis spectra.

Table 3-6. Effect of metal or bimetal supported CeO₂ catalysts on the transformation from 2'-hydroxychalcone (**1a**) into aurone (**2a**).^[a]

					
Entry	Catalyst	Conv. [%]	Yield [%]		
		1a	2a	3a	4a
1	CeO ₂	11	<1	<1	14
2	Cu/CeO ₂	9	<1	<1	4
3	Ru/CeO ₂	4	<1	<1	7
4	Rh/CeO ₂	4	<1	<1	6
5	Ni/CeO ₂	3	<1	<1	3
6	Pd/CeO ₂	17	8	<1	5
7	Pt–Pd/CeO ₂	17	6	2	3
8	Cu–Pd/CeO ₂	11	5	<1	3
9	Rh–Pd/CeO ₂	8	2	<1	4
10	Ni–Pd/CeO ₂	10	3	<1	3
11	Pb–Pd/CeO ₂	29	9	<1	4
12	Zn–Pd/CeO ₂	9	3	<1	2
13	Au/Pd/CeO ₂	16	2	<1	9
14 ^[b]	Au/CeO ₂	4	<1	6	7

[a] Reaction conditions: **1a** (0.3 mmol), metal supported catalyst (50 mg, metal: 2 mol% and/or Pd: 2 mol%), BuOAc (2 mL), open air (1 atm), 100 °C, 24 h. Conversions and yields were determined by GC analysis using biphenyl as an internal standard. [b] Au/CeO₂ was prepared through calcination at 300 °C for 2 h.

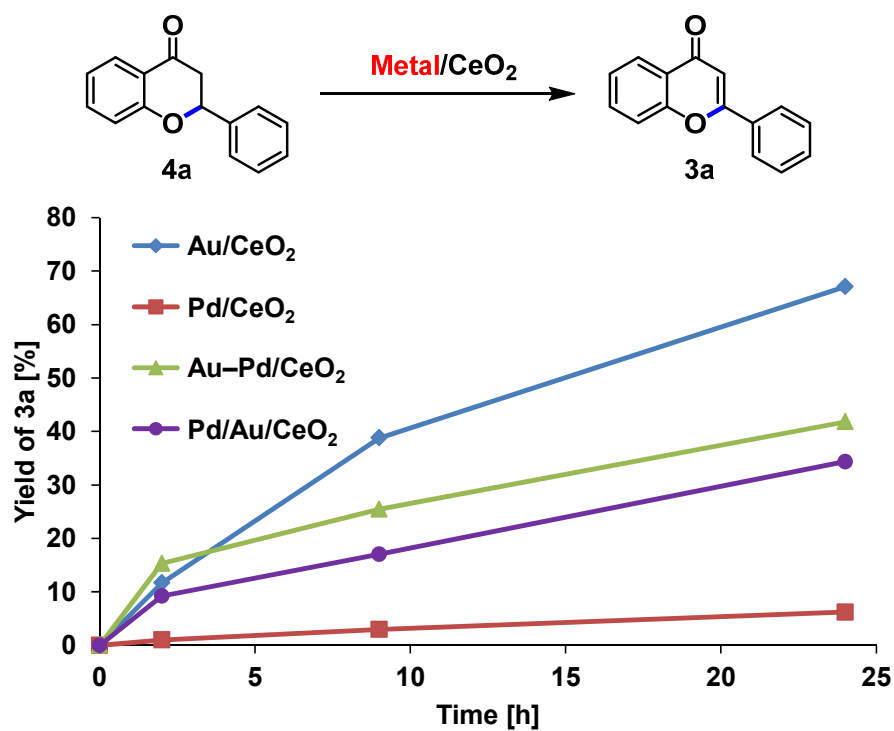


Figure 3-36. The reaction profiles in the synthesis of flavone (**3a**) from flavanone (**4a**). Reaction conditions: **4a** (0.3 mmol), catalyst (50 mg, Au and/or Pd: 2 mol%), BuOAc (2 mL), open air (1 atm), 100 °C. GC yields are shown here.

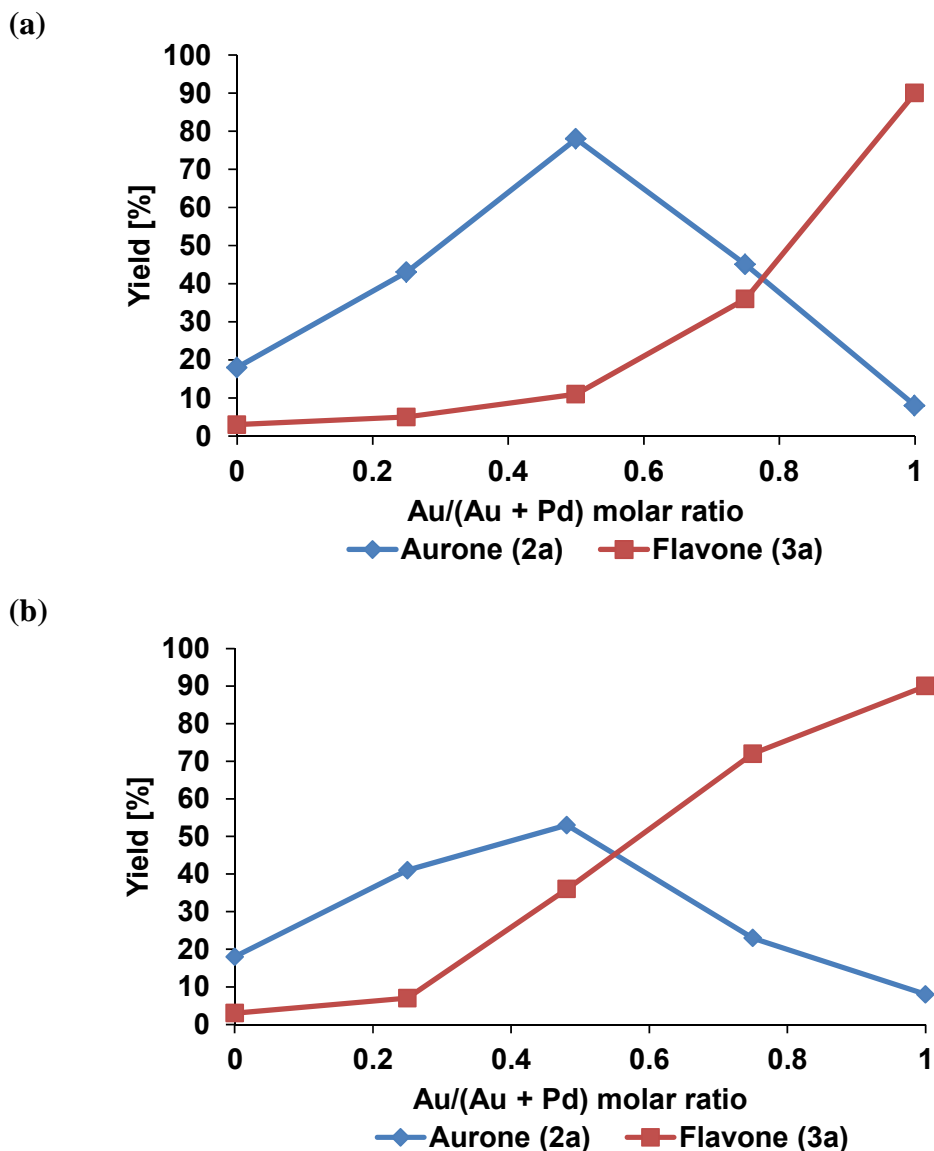


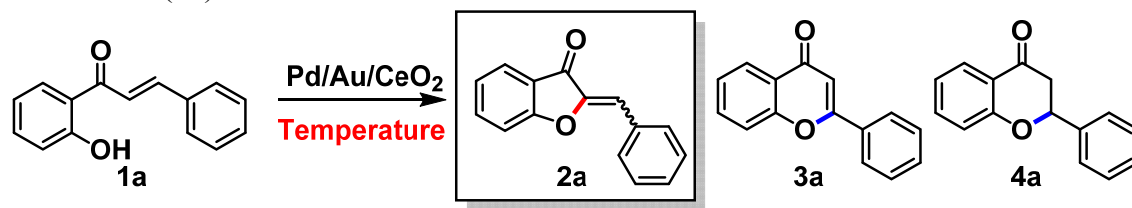
Figure 3-37. Effect of changing the ratio of Au and Pd on the synthesis of **2a** and **3a** using (a) Pd/Au/CeO₂ or (b) Au–Pd/CeO₂. Reaction conditions: **1a** (0.3 mmol), catalyst (100 mg, total metal of Au and/or Pd: 9 mol%), BuOAc (2 mL), open air (1 atm), 100 °C, 24 h. GC yields are shown here. In the case of (b), the ratios of 0.25 and 0.75 were calculated from the initial respective metal sources used for preparations.

Table 3-7. Effect of solvents on the transformation from 2'-hydroxychalcone (**1a**) into aurone (**2a**).^[a]

Entry	Solvent	Conv. [%]	Yield [%]		
		1a	2a	3a	4a
1	Toluene	11	2	3	6
2	Diglyme	17	17	3	3
3	1-Butanol	88	22	3	49
4	Cyclohexanol	85	24	6	55
5	DMA	95	39	23	20
6	DMF	95	48	22	12
7	BuOAc	60	46	6	9

[a] Reaction conditions: **1a** (0.3 mmol), Pd/Au/CeO₂ (50 mg, Au: 2 mol%, Pd: 2 mol%), solvent (2 mL), open air (1 atm), 100 °C, 24 h. Conversions and yields were determined by GC analysis using biphenyl as an internal standard.

Table 3-8. Effect of temperatures on the transformation from 2'-hydroxychalcone (**1a**) into aurone (**2a**).^[a]



Entry	Temperature [°C]	Conv. [%]	Yield [%]		
		1a	2a	3a	4a
1	90	37	30	5	4
2	100	60	46	6	9
3	110	65	46	8	13
4	120	17	3	<1	10

[a] Reaction conditions: **1a** (0.3 mmol), Pd/Au/CeO₂ (50 mg, Au: 2 mol%, Pd: 2 mol%), BuOAc (2 mL), open air (1 atm), 24 h. Conversions and yields were determined by GC analysis using biphenyl as an internal standard.

3-2.3.3. Heterogeneous Catalysis and Catalyst Reuse

To verify whether the observed catalytic reaction occurred on solid Pd/Au/CeO₂ or arose from leached metal species (Au and/or Pd) in the solution, Pd/Au/CeO₂ was removed by hot filtration during the reaction and the reaction was again carried out with the filtrate under the same conditions. The production of **2a** completely stopped with the removal of Pd/Au/CeO₂ (Figure 3-38). In addition, Au and Pd species in the filtrate after the reaction were not detected by inductively coupled plasma atomic emission spectroscopy (ICP-AES) (Au: <0.003%, Pd: <0.02%). Therefore, the observed catalysis to perform the current transformation into aurones is truly heterogeneous.

After the reaction under the optimized conditions, Pd/Au/CeO₂ can be readily retrieved from the reaction mixture by simple filtration. The retrieved Pd/Au/CeO₂ catalyst can be reused without a severe loss of its catalytic activity after calcination at 300 °C for 2 h, although the catalytic activity decreased when the calcination was not performed (Figure 3-39). TEM observations suggested that the size of the nanoparticles slightly increased during the reaction and was not affected by the calcination (Figures 3-40a and b). Thus, the activity loss without calcination in the second reaction was not caused by an increase in nanoparticle size, while the size of nanoparticles slightly affected the catalytic activity considering the results of the 3rd use (Figures 3-39 and 3-40c).

XRD patterns and FT-IR spectra revealed no change of the basic structure of CeO₂ (Figures 3-41 and 3-42). However, in the FT-IR spectra collected after the reaction, peaks were observed at 1456 cm⁻¹ and 1418 cm⁻¹, which are possibly attributable to phenyl-ring stretching vibrations. These peaks disappeared after the catalyst was calcined at 300 °C. On the basis of these results, the adsorption of organic compounds onto the catalyst was likely one of the reasons for the loss of catalytic activity when the recovered catalyst was not calcined.

XPS spectra exhibited that Pd(0) species considerably formed in Pd/Au/CeO₂ after the reaction, whereas no Pd(0) species were present before the reaction (Figures 3-43a and c). Moreover, the proportion of Pd(0) species gradually increased during the reaction (Figures 3-43b and c), and the Pd(0) species can be reoxidized to Pd(II) species by the calcination for regeneration. Thus, the decrease of Pd(II) species in Pd/Au/CeO₂ also possibly causes the aforementioned loss of its catalytic activity. It is difficult to

determine whether the adsorption of organic compounds or the decrease of active Pd(II) species is the main reason for the deactivation.

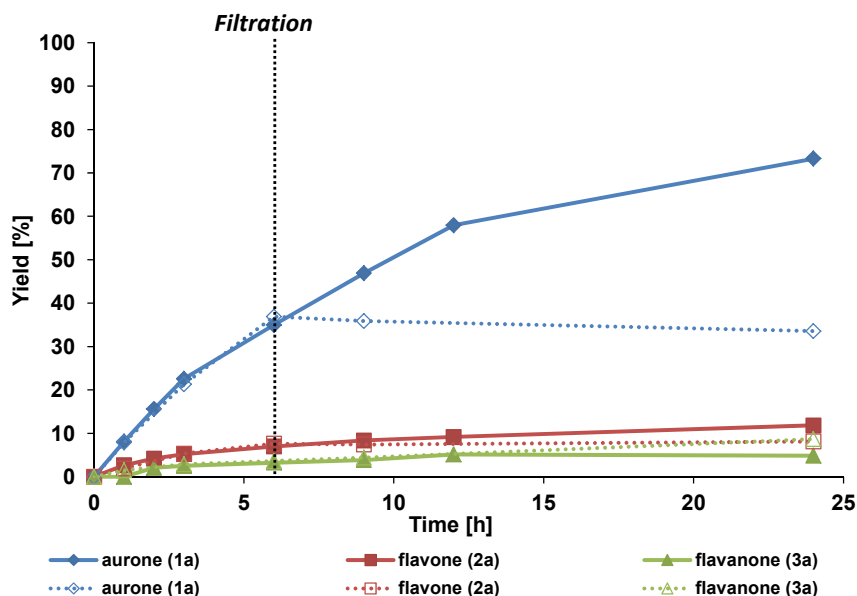


Figure 3-38. The reaction profile affected by removing Pd/Au/CeO₂ in the middle of the synthesis of the reaction starting from **1a** (verification of heterogeneous catalysis). Reaction conditions: **1a** (0.3 mmol), Pd/Au/CeO₂ (100 mg), BuOAc (2 mL), open air (1 atm), 24 h. GC yields are shown.

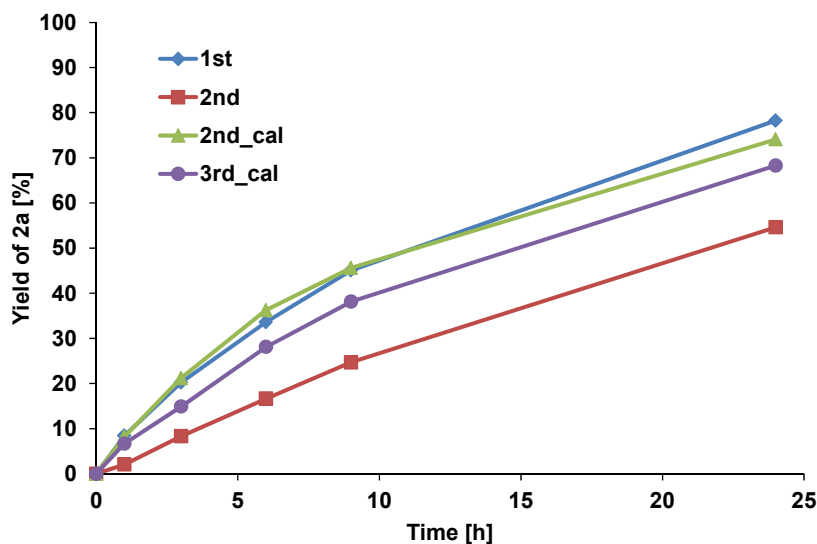


Figure 3-39. Reuse experiments.

Reaction conditions: **1a** (0.3 mmol), Pd/Au/CeO₂ (100 mg), BuOAc (2 mL), open air (1 atm), 24 h. Reaction profiles using Pd/Au/CeO₂ calcined for 2 h at 300 °C after the first and second reactions were showed as 2nd_cal and 3rd_cal respectively. Yields were determined by GC analysis using biphenyl as an internal standard.

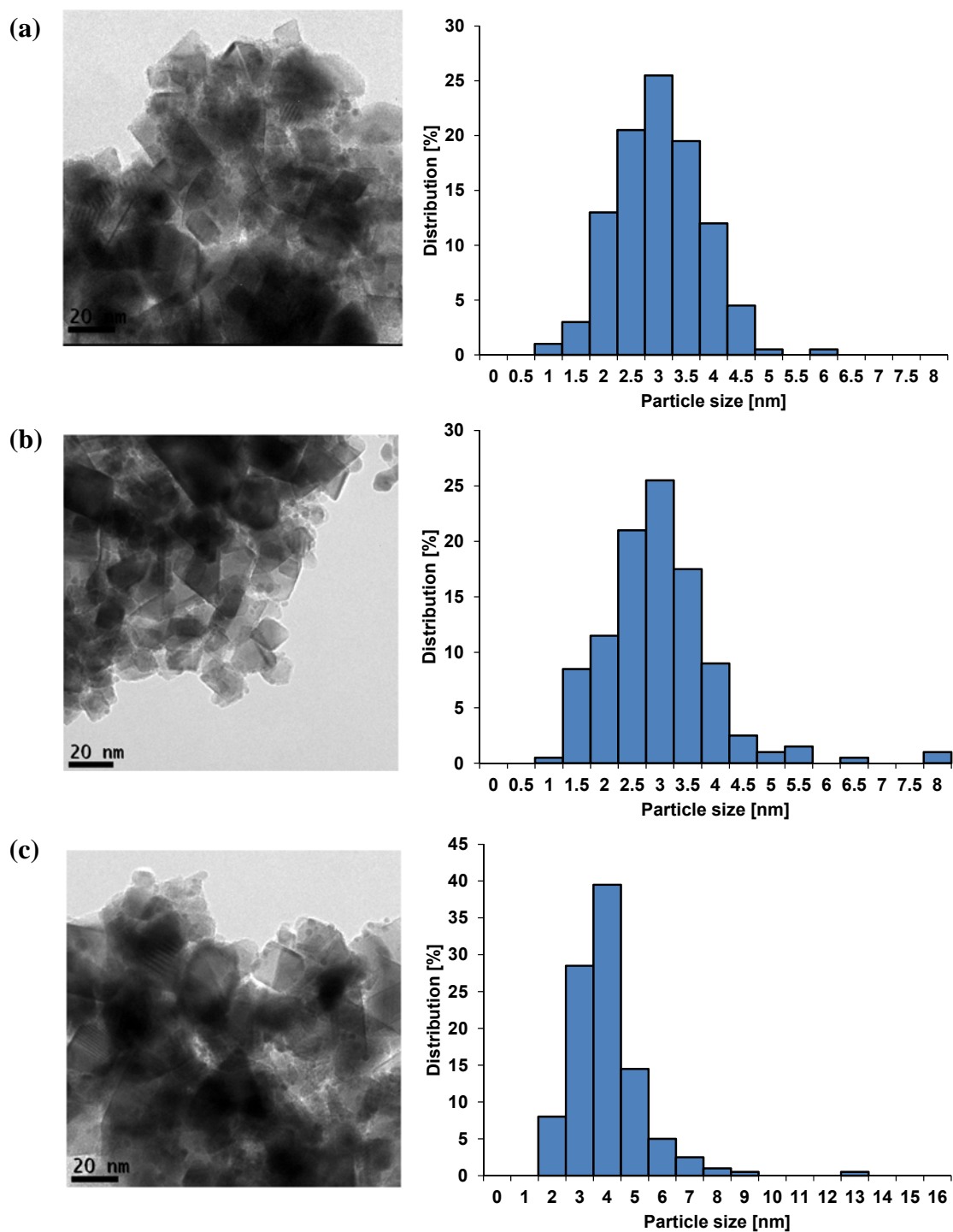


Figure 3-40. TEM images and nanoparticle size distributions of (a) Pd/Au/CeO₂ after the first reaction (mean diameter: 2.8 nm, $\sigma = 0.8$ nm), (b) Pd/Au/CeO₂ calcined for 2 h at 300 °C after the first reaction (mean diameter: 2.7 nm, $\sigma = 1.0$ nm) and (c) Pd/Au/CeO₂ after the third reaction (mean diameter: 3.5 nm, $\sigma = 1.3$ nm). The size distributions were determined using 200 particles.

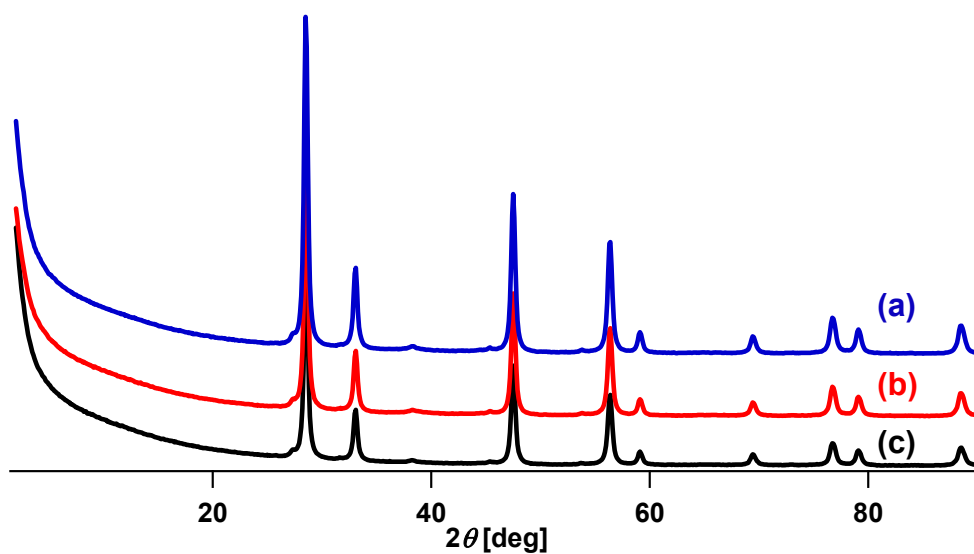


Figure 3-41. XRD patterns of (a) Pd/Au/CeO₂ calcined for 2 h at 300 °C after the first reaction, (b) Pd/Au/CeO₂ after the first reaction and (c) Pd/Au/CeO₂ before use.

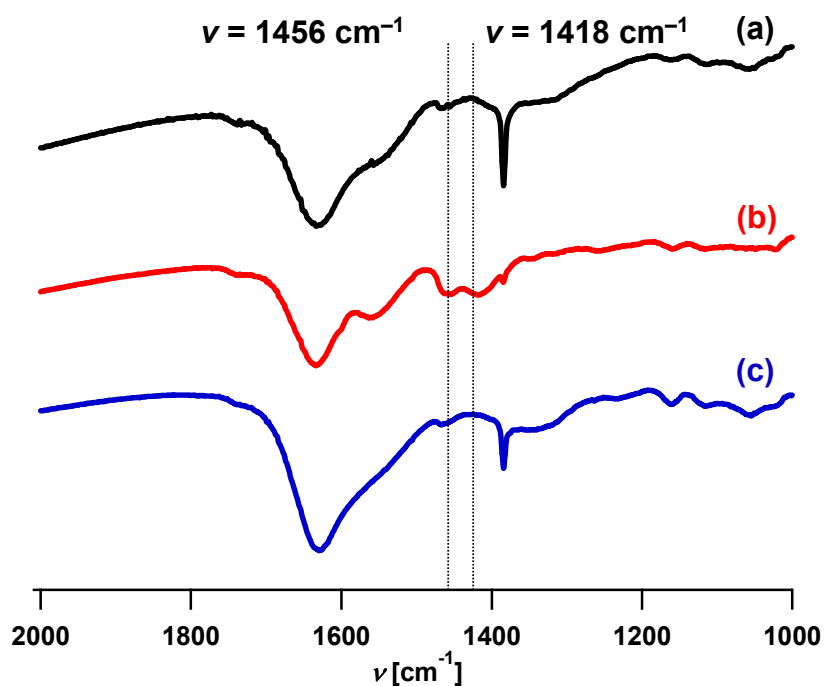


Figure 3-42. FT-IR spectra of (a) Pd/Au/CeO₂ before use, (b) Pd/Au/CeO₂ after the first reaction and (c) Pd/Au/CeO₂ calcined for 2 h at 300 °C after the first reaction.

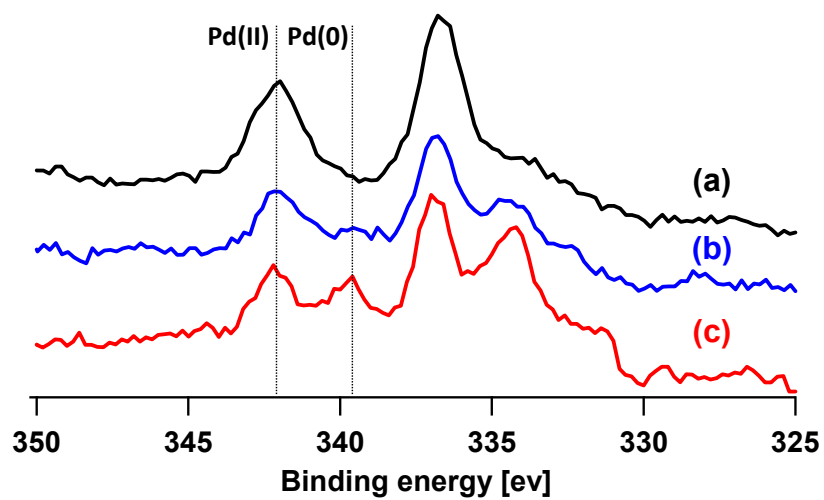
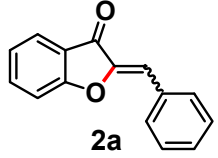
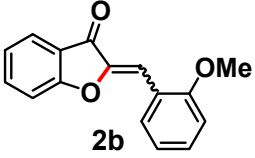
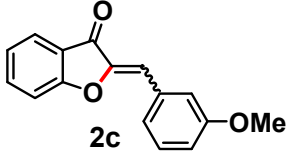
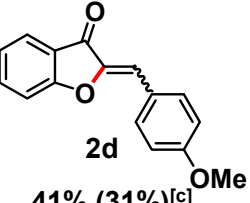
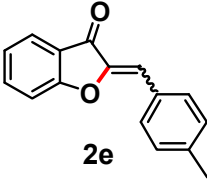
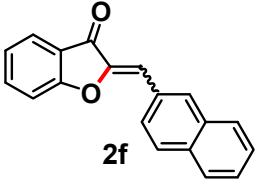
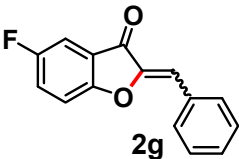
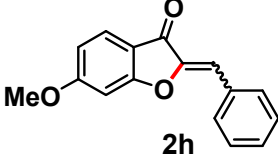
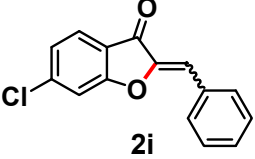
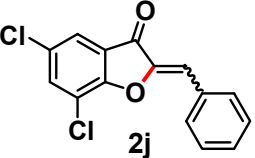
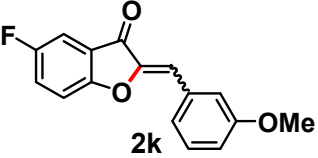
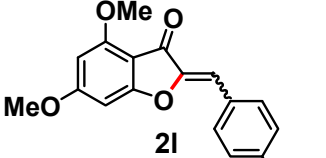
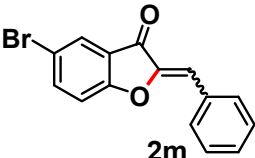
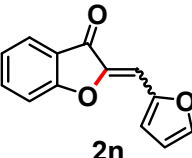
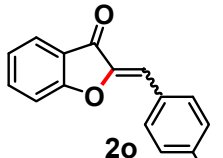


Figure 3-43. XPS spectra around 3d Pd region calibrated by C 1s (284.2 eV) of (a) Pd/Au/CeO₂ before use, (b) Pd/Au/CeO₂ as of 30 min after the reaction started (turnover number = ~1), and (c) Pd/Au/CeO₂ after the reaction.

3-2.3.4. Substrate Scope

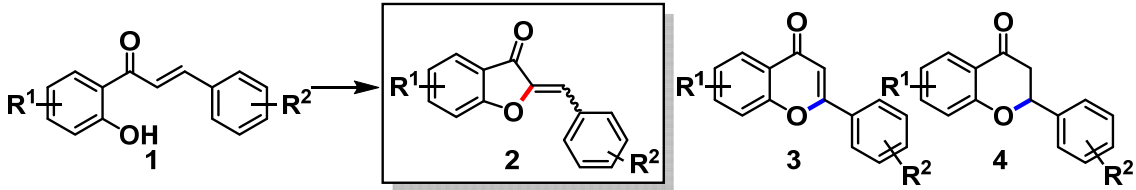
I examined the scope of the present Pd/Au/CeO₂-catalyzed transformation into aurones. Under the optimized reaction conditions, various aurones were successfully synthesized in a (*Z*)-selective fashion starting from simple chalcones (Table 3-9). The desired products were isolated by simple column chromatography on silica gel (When the separation of aurones and flavanones was quite difficult, especially using **1c**, **1g**, **1i**, or **1k** as substrates, a large part of aurones were lost during column chromatography operation). The conversions of chalcones (**1**) and the yields of aurones (**2**), flavones (**3**), and flavanones (**4**) determined by gas chromatography (GC) are summarized in Table 3-10. When 2'-hydroxychalcones substituted with a methoxy group at their 2-, 3-, or 4-position were used as the substrates, the corresponding aurones (**2b–2d**) were synthesized. In the case of 2'-hydroxy-4-methylchalcone, 4'-methylaurone (**2e**) was obtained without benzylic oxidation of the methyl group. The chalcone with a 2-naphthyl group as the B ring was converted into the corresponding aurone (**2f**). The use of chalcones with various substituents at these A-rings was also possible (**2g–2j**). In particular, 5'-fluoro-2'-hydroxychalcone was efficiently transformed into the corresponding aurone with a fluoro group (**2g**), which is an important group in the pharmaceutical field.^[28] Thus, a novel aurone with potential medicinal applications, *e.g.* 5-fluoro-3'-methoxyaurone (**2k**), was also successfully synthesized. In addition, as a demonstration of using plant-derived substrates, I used flavokavain A (2'-hydroxy-4,4',6'-trimethoxychalcone), which is a flavonoid extracted from kava plants, as the substrate to obtain the corresponding aurone efficiently (**2l**). However, this system was inapplicable to some substrates (**2m–2o**), possibly because their hydroxy groups could not easily access the Pd catalysts due to the preferential coordination of the other groups to Pd species.

Table 3-9. Scope of transformation from chalcones (**1**) into aurones (**2**)^[a]

 <p>2a</p> <p>79% (64%) Ratio: 83%, <i>E/Z</i> = 3/97</p>	 <p>2b</p> <p>46% (37%)^[b] Ratio: 67%, <i>E/Z</i> = 3/97</p>	 <p>2c</p> <p>61% (38%)^[b] Ratio: 67%, <i>E/Z</i> = 2/98</p>
 <p>2d</p> <p>41% (31%)^[c] Ratio: 45%, <i>E/Z</i> = 3/97</p>	 <p>2e</p> <p>29% (20%)^[b,c] Ratio: 44%, <i>E/Z</i> = 3/97</p>	 <p>2f</p> <p>45% (37%)^[c] Ratio: 70%, <i>E/Z</i> = <1/>99</p>
 <p>2g</p> <p>84% (39%) Ratio: 86%, <i>E/Z</i> = 1/99</p>	 <p>2h</p> <p>80% (60%)^[d] Ratio: 84%, <i>E/Z</i> = 3/97</p>	 <p>2i</p> <p>36% (16%)^[b,c] Ratio: 43%, <i>E/Z</i> = <1/>99</p>
 <p>2j</p> <p>28% (19%)^[b,e] Ratio: 45%, <i>E/Z</i> = <1/>99</p>	 <p>2k</p> <p>68% (36%) Ratio: 73%, <i>E/Z</i> = 1/99</p>	 <p>2l</p> <p>80% (72%)^[b,f] Ratio: 88%, <i>E/Z</i> = 7/93</p>
 <p>2m</p> <p><1%</p>	 <p>2n</p> <p>4%</p>	 <p>2o</p> <p>2%</p>

[a] Reaction conditions: **1** (0.3 mmol), Pd/Au/CeO₂ (100 mg, Au: 5 mol%, Pd: 5 mol%), BuOAc (2 mL), open air (1 atm), 100 °C, 24 h. Ratio of **2** = $2 \times 100 / (2 + 3 + 4)$ (%). The *E/Z* ratios were determined by GC analysis using biphenyl as an internal standard. The GC yields including the (*E*)-isomer are shown. The values in parentheses are the isolated yields of the (*Z*)-isomer. [b] 48 h. [c] Pd/Au/CeO₂ (200 mg, Au: 9 mol%, Pd: 9 mol%). [d] 50 h. [e] DMA (2 mL). [f] The isolated yield including the (*E*)-isomer.

Table 3-10. Details of substrate scope.^[a]



Substrate	Substituent	Conv. [%]	Yield [%]			Ratio of 2 [%]
		1	2	3	4	
1a	—	94	79	11	5	83
1b ^[b]	2-MeO	73	46	11	12	67
1c ^[b]	3-MeO	92	61	19	12	67
1d ^[c]	4-MeO	97	41	45	6	45
1e ^[b,c]	4-Me	91	29	24	12	44
1f ^[c]	B ring = 2-Naphthyl	68	45	5	14	70
1g	5'-F	>99	84	8	5	86
1h ^[d]	4'-MeO	>99	80	8	8	84
1i ^[b,c]	4'-Cl	89	36	7	41	43
1j ^[b,e]	3',5'-Cl	94	28	19	16	45
1k	5'-F, 3-MeO	94	68	15	11	73
1l ^[b]	4,4',6'-MeO	89	80	8	3	88
1m	5'-Br	49	<1	4	40	<1
1n	B ring = 2-furanyl	14	4	1	5	40
1o	4-Cl	41	2	4	24	5

[a] Reaction conditions: **1** (0.3 mmol), Pd/Au/CeO₂ (100 mg, Au: 5 mol%, Pd: 5 mol%), BuOAc (2 mL), open air (1 atm), 100 °C, 24 h. Ratio of **2** = $2 \times 100 / (2 + 3 + 4)$ (%). The conversions and yields were determined by GC analysis using biphenyl as an internal standard. [b] 48 h. [c] Pd/Au/CeO₂ (200 mg, Au: 9 mol%, Pd: 9 mol%). [d] 50 h. [e] DMA (2 mL).

3-2.3.5. Mechanistic Studies

The present transformation into aurones possibly proceeds through one of the following three paths (Figure 3-44): directed α -olefinic C–H activation/reductive elimination (Path A), migratory insertion/ β -hydride elimination (Path B), or single electron transfer (SET)/radical cyclization/hydrogen-atom transfer (HAT) (Path C). (note: Palladation directed by the OH of chalcones as a neutral ligand instead of the phenoxide can also possibly occur in this system, but it is difficult to determine which directing groups dominantly work. In Figure 3-44 and Figure 3-48, to simplify the mechanism, only anionic coordination modes by deprotonated chalcones are depicted.^[29]) The directed α -olefinic C–H activation included in Path A has rarely been reported,^[22] however, the reductive elimination from the 6-membered palladacycle was the major reaction mechanism proposed in reported aurone synthesis from ynones.^[14] The reaction in Path B is well known as the Wacker-type cyclization,^[20] however, a formal intramolecular α -olefinic C–H functionalization *via* Pd-catalyzed Wacker-type cyclization has, to my knowledge, never been reported. Path C was declared in previous reports for aurone synthesis using a stoichiometric oxidant such as Pb(OAc)₄ or Mn(OAc)₃.^[17d,e]

First, to verify whether a radical species is involved in this system, I carried out the reaction under the optimized conditions in the presence of an equimolecular amount of 2,2,6,6-tetramethylpiperidine 1-oxyl (TEMPO) or 2,6-di-*tert*-butyl-4-methylphenol (BHT) as a radical scavenger with respect to **1a** (Figure 3-45). The production rates of **2a** from **1a** did not decrease, indicating that radical species were irrelevant to this reaction; thus, Path C was excluded.

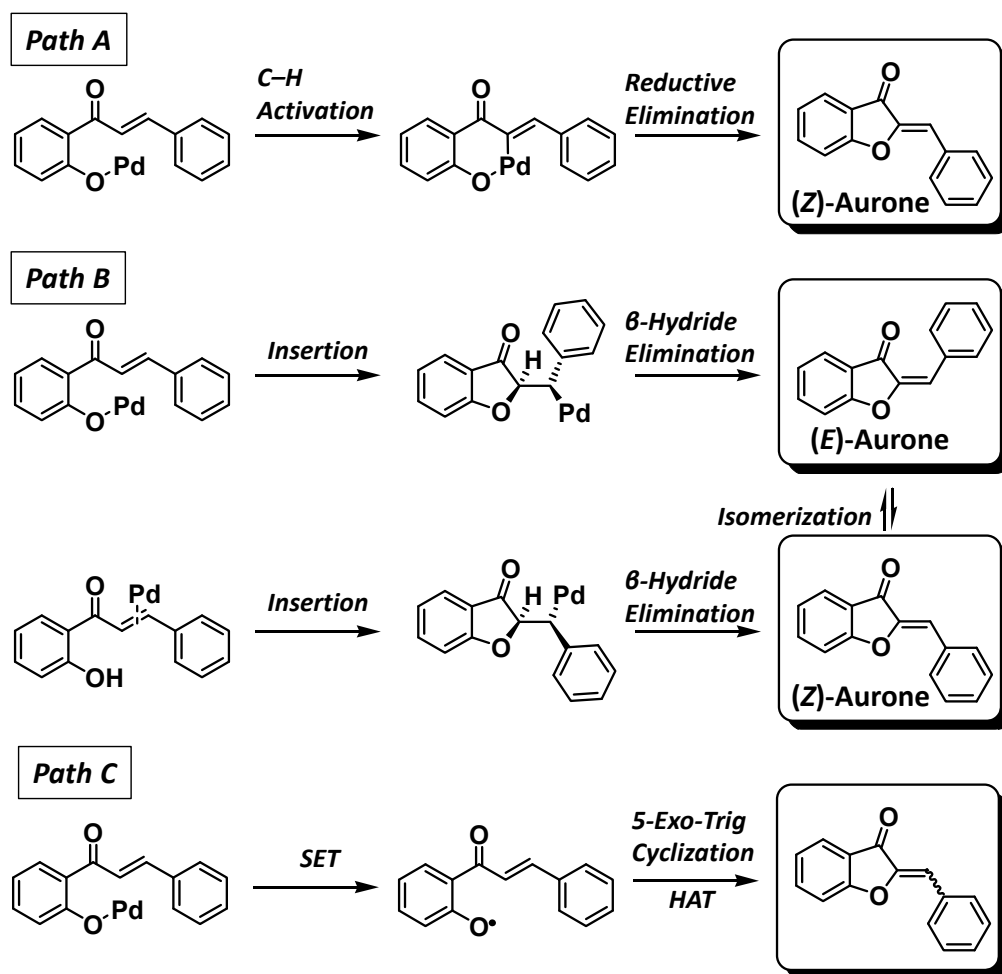


Figure 3-44. Possible paths of the transformation from chalcones into aurones.

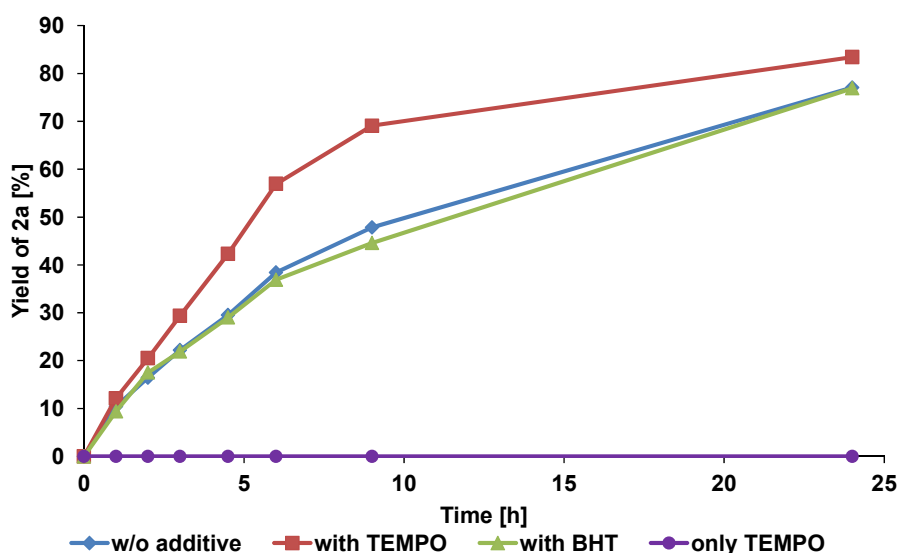


Figure 3-45. The effect of radical scavengers (BHT or TEMPO, 1 equivalent with respect to **1a**) on the transformation into **2a**. The reaction conditions were the same as those described in Figure 3-38. GC yields are shown here.

Next, to verify whether the reaction proceeds through Path A or Path B, I conducted the following control experiments (Figure 3-46): (a) the reaction using [α -D]-2'-hydroxychalcone ([α -D]-**1a**) or [β -D]-2'-hydroxychalcone ([β -D]-**1a**) as the substrate to confirm a scrambling of deuterium atoms; (b) isomerization of (*Z*)-aurone; (c) oxidative cyclization of 2-allyl phenol and the reaction of **1a** under the reported Wacker-type cyclization conditions;^[20a] and (d) oxidative cyclization of 2-allyl phenol and the reaction of **1a** under the present aurone synthesis conditions.

If the β -hydride elimination included in Path B occurs, the deuterium atoms would likely be scrambled between the aurones and Pd catalysts to produce partially D-labeled or non-labeled aurones when using [α -D]-**1a** or [β -D]-**1a**, respectively (Figure 3-46a). ¹H NMR analyses of the reaction solutions after the reactions indicated no scrambling of the deuterium atoms in this system (Figure 3-47)—hence, the existence of Path B cannot be confirmed. If reductive elimination included in Path A occurs, only (*Z*)-aurone should be produced. In the present system, the aurone was obtained in a (*Z*)-selective fashion, whereas small amounts of (*E*)-aurones were produced in the case of several substrates (*E/Z* = 1/99–7/93), which are derived from β -hydride elimination included in Path B or natural isomerization of (*Z*)-aurones.^[14d] The (*Z*)-isomer of **2a** was treated under the optimized reaction conditions for 24 h, resulting in isomerization into the (*E*)-isomer whose ratio was approximately the same as that of the product synthesized from **1a** (Figure 3-46b). Thus, the small amounts of (*E*)-isomers are possibly produced by isomerization after the (*Z*)-selective aurone formation through Path A. As previously reported,^[20a] the oxidative cyclization of 2-allyl phenol efficiently proceeded reproducibly under the Wacker-type cyclization conditions using PdCl₂. The production of **2a** from **1a**, however, did not proceed at all under the Wacker-type cyclization conditions (Figure 3-46c). By contrast, under the aurone synthesis conditions using Pd/Au/CeO₂ in DMA, **2a** was produced from **1a**, whereas the Wacker-type cyclization of 2-allyl phenol hardly proceeded (Figure 3-46d).

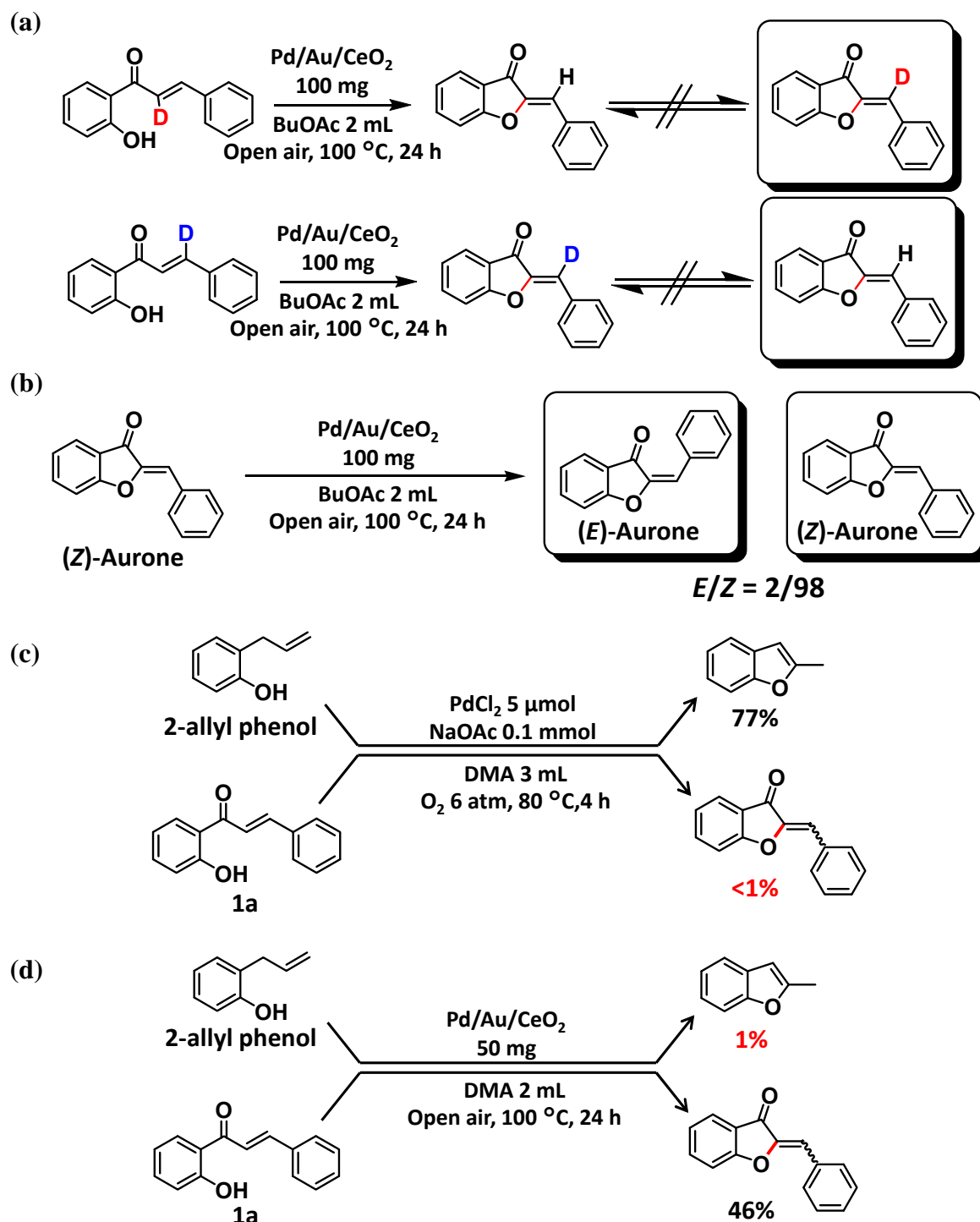


Figure 3-46. Overview of the mechanistic studies on the transformation into aurones: (a) Scrambling of deuterium using $[\alpha\text{-D}]\text{-1a}$ or $[\beta\text{-D}]\text{-1a}$ as a substrate under the optimized reaction conditions; (b) Isomerization of (Z)-aurone under the optimized reaction conditions; (c) Oxidative cyclization of 2-allyl phenol or **1a** under the reported Wacker-type cyclization conditions as shown in the figure; (d) Oxidative cyclization of 2-allyl phenol or **1a** on the aurone synthesis conditions as shown in the figure.

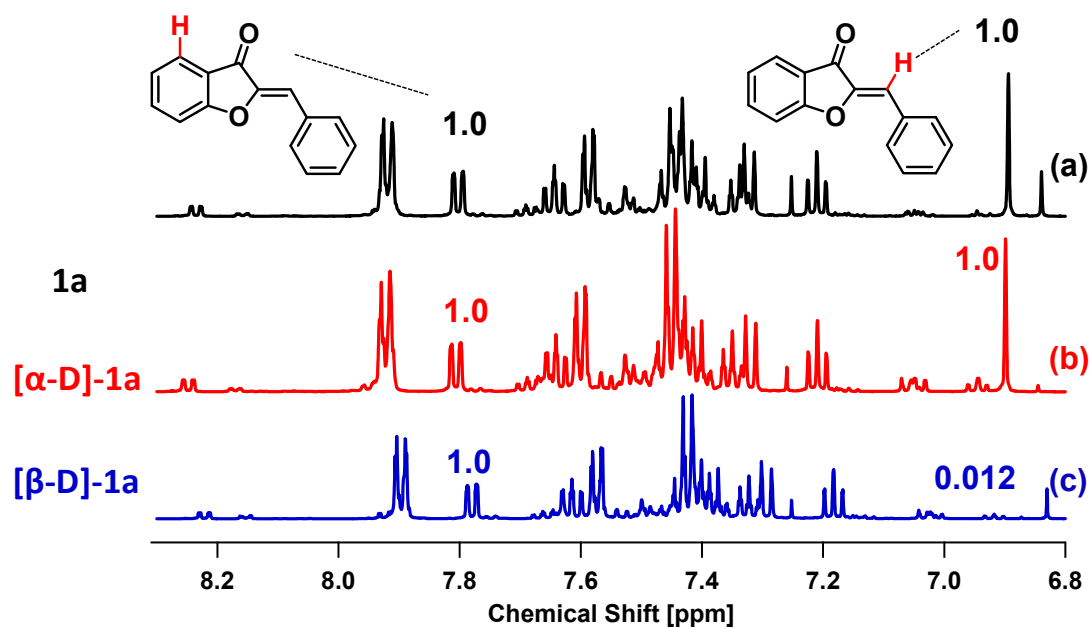


Figure 3-47. ^1H NMR (in CDCl_3) spectra of crude solution after the reaction on the optimized conditions using (a) 2'-hydroxychalcone (**1a**), (b) [α -D]-2'-hydroxychalcone, and (c) [β -D]-2'-hydroxychalcone as a substrate respectively. The numbers over peaks represent area ratios of the peaks.

On the basis of the aforementioned results, the present transformation from chalcones into aurones likely proceeds through Path A (Figure 3-48). After the coordination of deprotonated **1** to the Pd center, intramolecular olefinic α -C–H activation directed by the phenoxide group occurs to produce a 6-membered palladacycle. Then, **2** is produced through reductive elimination from the palladacycle with concomitant formation of a reduced Pd species, *e.g.*, Pd(0), which is then re-oxidized by O₂ in air to complete the catalytic cycle.

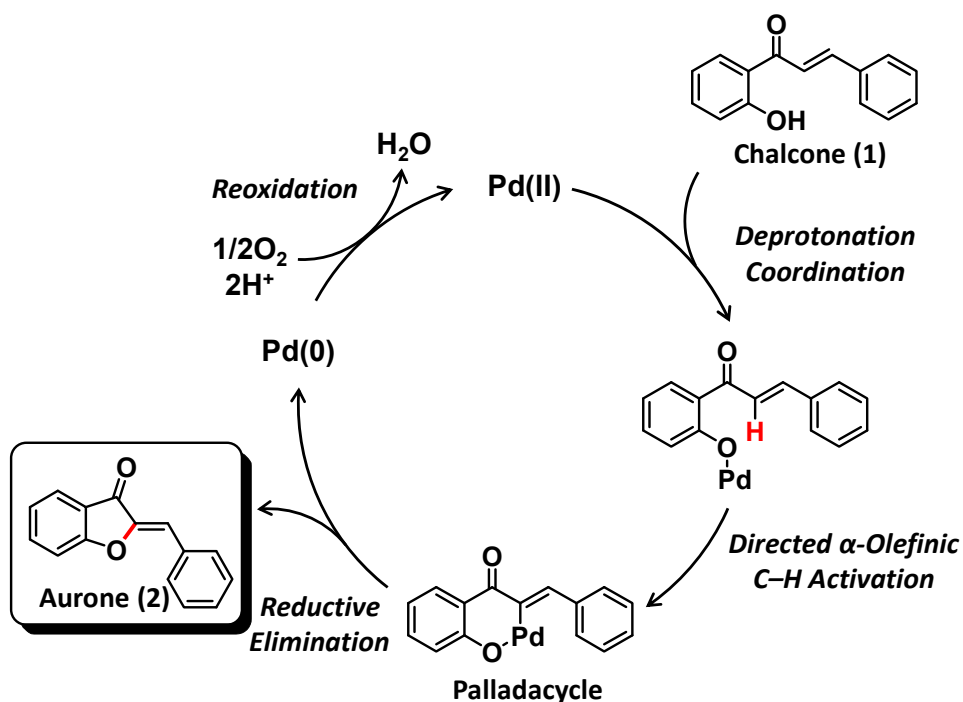


Figure 3-48. Proposed mechanism of transformation into aurones in this system.

Under an O₂ atmosphere instead of an open air atmosphere, the production rate of **2a** increased (Figure 3-49). Moreover, as shown in Figure 3-45, TEMPO worked as the re-oxidant of the reduced Pd species to promote the production rate of **2a**, although only TEMPO did not produce **2a** at all.^[12] These results suggest that the re-oxidation of the Pd species is probably included in the turnover-limiting step of the present transformation into aurones under an open air atmosphere. Furthermore, kinetic isotope effects were calculated based on the reaction results using **1a**, [α -D]-**1a**, or [β -D]-**1a** as the substrate; 1.45 for α -H and 1.08 for β -H, respectively (Figure 3-50). These small values indicate that the present directed α -olefinic C–H activation mechanism is not concerted metalation deprotonation (CMD) or σ -bond metathesis but electrophilic substitution.^[30]

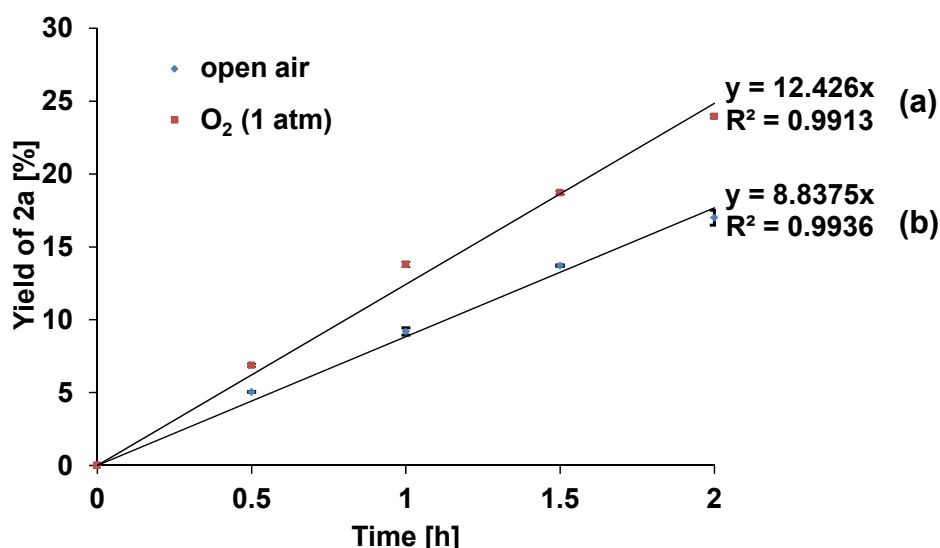


Figure 3-49. Reaction profiles and reaction rates of the transformation from **1a** into **2a** on the optimized conditions (a) under an O₂ atmosphere or (b) under an open air atmosphere. Error bars (\pm standard error) were calculated from the experiments conducted (a) twice and (b) four times, respectively. Reaction conditions: **1a** (0.3 mmol), Pd/Au/CeO₂ (100 mg), BuOAc (2 mL), open air or O₂ (1 atm), 100 °C. GC yields are shown.

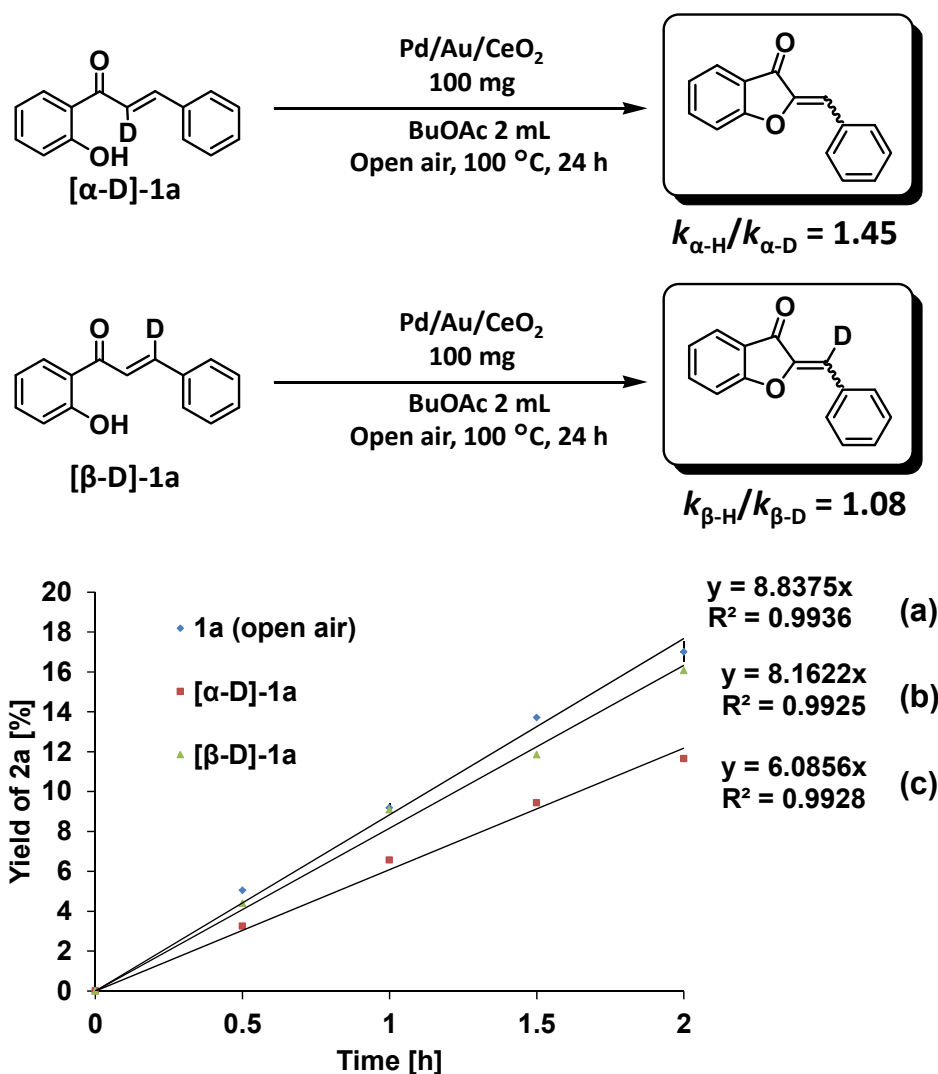


Figure 3-50. Kinetic isotope effects calculated based on reaction profiles and reaction rates of the transformation into **2a** on the optimized conditions starting from (a) **1a**, (b) $[\beta\text{-D}]\text{-1a}$, or (c) $[\alpha\text{-D}]\text{-1a}$. Regarding (a), error bars (\pm standard error) were calculated from the experiments conducted four times. Reaction conditions: substrate (0.3 mmol), Pd/Au/CeO₂ (100 mg), BuOAc (2 mL), open air (1 atm), 100 °C. GC yields are shown.

Finally, to demonstrate the effect of Au, I measured that the reaction profiles for the transformation from **1a** into **2a** using Pd/CeO₂ or Pd/Au/CeO₂ under an open air atmosphere or an O₂ atmosphere (Figure 3-51). Compared to the catalyst with only Pd, that with coexisting Pd and Au exhibited improved catalytic activity and catalyst longevity. Moreover, in the absence of Au, the production rate of **2a** was independent of the O₂ partial pressure. XPS spectra revealed that Pd(II) species were easily produced and stabilized in Pd/CeO₂ (Figure 3-52), which is consistent with previous reports.^[31] The stabilization of Pd(II) species can make it difficult for the reductive elimination step to induce. By contrast, when Pd/Au/CeO₂ was used, as previously mentioned, the re-oxidation of the reduced Pd species was included in the turnover-limiting step. Furthermore, as shown in XPS spectra of Figure 3-43, Pd(0) species, which did not appear before the reaction, substantially formed in Pd/Au/CeO₂ after the reaction. Several reports on Au–Pd bimetallic systems show that the resistance of Pd toward oxidation by O₂ is improved by Au (see the references of [17i,j] in Chapter I and section 1.1.4.4.) and that Au–Pd bond is more stable than Pd–Pd bond.^[32] Given the aforementioned results and previous reports, Au species likely contributed to the stabilization of Pd(0) during the reaction to inhibit the formation of inactive Pd oxides and/or promote the reductive elimination step.

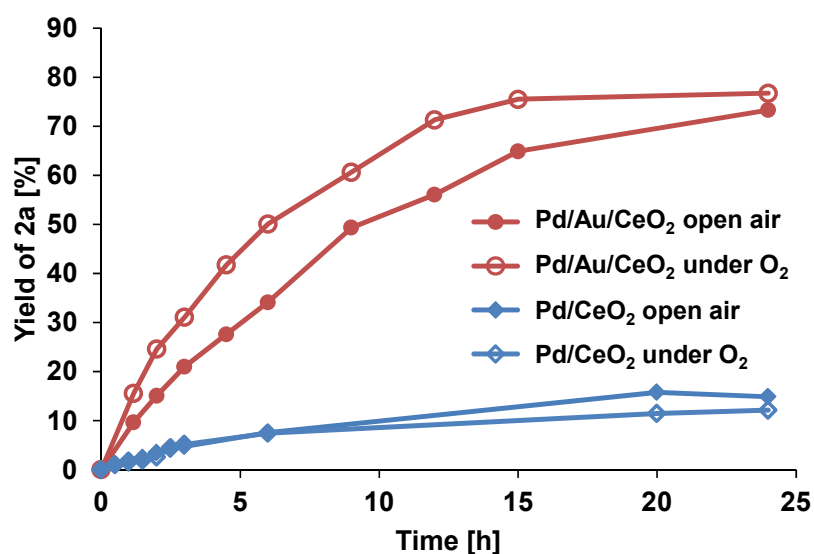


Figure 3-51. Reaction profiles of the transformation from **1a** into **2a** on the optimized conditions using Pd/CeO₂ or Pd/Au/CeO₂ in open air or under an O₂ atmosphere. Reaction conditions: **1a** (0.3 mmol), Pd/Au/CeO₂ or Pd/CeO₂ (100 mg), BuOAc (2 mL), open air or O₂ (1 atm), 100 °C, 24 h. GC yields are shown.

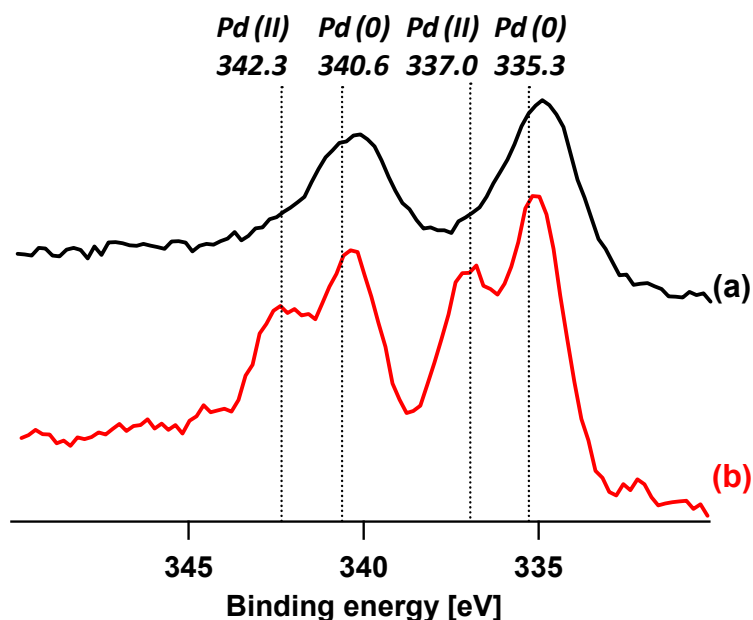


Figure 3-52. XPS spectra of (a) Pd/Al₂O₃ and (b) Pd/CeO₂ just after the reduction treatment around 3d Pd region calibrated by Al 2p (74.0 eV) and C 1s (284.2 eV), respectively.

3-2.4. Summary

I have achieved the first catalytic transformation from simple chalcones into various aurones over Pd-on-Au bimetallic nanoparticles supported on CeO₂ through the rational design of a function-integrated heterogeneous catalyst; the designed system included the following four roles indispensable for the catalytic transformation—a) a supported Pd species: a novel catalyst for aurone synthesis *via* rare directed α -olefinic C–H functionalization, b) an Au promoter: an improvement of catalytic activity as a result of stabilization of Pd(0), c) a CeO₂ support: the inhibition of the 6-*endo-trig* cyclization on the surface, and d) a Pd-on-Au structure: the inhibition of Au-catalyzed flavone synthesis. This catalysis was confirmed to be heterogeneous, and the catalysts can be reused. In addition, O₂ served as the sole oxidant and no additives were needed, making this system truly environmentally friendly. This system was also significantly useful as an aurone synthetic method; various aurones were synthesized starting from simple chalcones, including a natural compound extracted from plants, which will promote the pharmaceutical study of aurones. This study demonstrates the considerable potential of a heterogeneous catalyst design for novel difficult organic syntheses that have not yet been achieved using homogeneous catalysts or biocatalysts.

3.5. References

- [1] a) F. Ververidis, E. Trantas, C. Dauglas, G. Vollmer, G. Kretzschmar, N. Panopoulos, *Biotechnol. J.* **2007**, 2, 1235; b) I. Iwashina, *J. Plant Res.* **2000**, 113, 287; c) R. A. Dixon, *Annu. Rev. Plant Biol.* **2004**, 55, 225; d) R. J. Nijveldt, E. van Nood, D. E. C. van Hoorn, P. G. Boelens, K. van Norren, P. A. M. van Leeuwen, *Am. J. Clin. Nutr.* **2001**, 74, 418; e) R. E. Koes, F. Quattrocchio, J. N. M. Mol, *BioEssays* **1994**, 16, 123; f) B. Winkel-Shirley, *Plant Physiol.* **2001**, 126, 485; g) S. Martens, A. Mithöfer, *Phytochemistry* **2005**, 66, 2399; h) J. B. Harborne, C. A. Williams, *Phytochemistry* **2000**, 55, 481.
- [2] a) T. Yoshikawa, Y. Naito, *Japan Med. Assoc. J.* **2002**, 45, 271; b) C. A. Rice-Evans, N. J. Miller, G. Paganga, *Free Rad. Biol. Med.* **1996**, 20, 933.
- [3] a) M. Singh, M. Kaur, O. Silakari, *Eur. J. Med. Chem.* **2014**, 84, 206; b) T. B. Nguyen, O. Lozach, G. Surpateanu, Q. Wang, P. Retailleau, B. I. Iorga, L. Meijer, F. Guéritte, *J. Med. Chem.* **2012**, 55, 2811; c) E. Middleton, Jr., C. Kandaswami, T. C. Theoharides, *Pharmacol. Rev.* **2000**, 52, 673; d) A. K. Verma, R. Pratap, *Tetrahedron* **2012**, 68, 8523; e) R. Kshatriya, V. P. Jejurkar, S. Saha, *Tetrahedron* **2018**, 74, 811, and references cited therein.
- [4] a) B. Boucherle, M. Peuchmaur, A. Boumendjel, R. Haudecoeur, *Phytochemistry* **2017**, 142, 92; b) E. U. Mughal, A. Sadiq, S. Murtaza, H. Rafique, M. N. Zafar, T. Riaz, B. A. Khan, A. Hameed, K. M. Khan, *Bioorg. Med. Chem.* **2017**, 25, 100; c) H. M. Sim, K. Y. Loh, W. K. Yeo, C. Y. Lee, M. L. Go, *ChemMedChem* **2011**, 6, 713; d) A. Detsi, M. Majdalani, C. A. Kontogiorgis, D. Hadjipavlou-Litina, P. Kefalas, *Bioorg. Med. Chem.* **2009**, 17, 8073; e) N. J. Lawrence, D. Rennison, T. A. McGown, J. A. Hadfield, *Bioorg. Med. Chem. Lett.* **2003**, 13, 3759; f) N. Hadj-esfandiari, L. Navidpour, H. Shadnia, M. Amini, N. Samadi, M. A. Faramarzid, A. Shafiee, *Bioorg. Med. Chem.* **2007**, 17, 6354; g) O. Kayser, A. E. Kiderlen, *Tokai J. Exp. Clin. Med.* **1999**, 23, 423; h) M. P. Carrasco, A. S. Newton, L. Gonçalves, A. Góis, M. Machado, J. Gut, F. Nogueira, T. Hänscheid, R. C. Guedes, D. J. V. A. dos Santos, P. J. Rosenthal, R. Moreira, *Eur. J. Med. Chem.* **2014**, 80, 523.
- [5] a) W. Baker, *J. Chem. Soc.* **1933**, 1381; b) H. S. Mahal, K. Venkataraman, *J. Chem. Soc.* **1934**, 1767; c) J. Allan, R. Robinson, *J. Chem. Soc.* **1924**, 125, 2192; d) T. S. Wheeler, *Org. Synth.* **1952**, 32, 72; e) D. Nagarathnam, M. Cushman, *Tetrahedron* **1991**,

47, 5071; f) M. Kucukislamoglu, M. Nebioglu, M. Zengin, M. Arslan, N. Yayli, *J. Chem. Res.* **2005**, 9, 556; g) C. Jin, F. He, H. Wu, J. Chen, W. Su, *J. Chem. Res.* **2009**, 1, 27.

[6] a) T. Emilewicz, von Kostanecki, *Chem. Ber.* **1898**, 31, 696; b) H. S. Mahal, K. Venkataraman, *J. Chem. Soc.* **1936**, 569; c) W.-H. Huang, P.-Y. Chien, C.-H. Yang, A.-R. Lee, *Chem. Pharm. Bull.* **2003**, 51, 339; d) S. Alam, *J. Chem. Sci.* **2004**, 116, 325; e) P. D. Lokhande, S. S. Sakate, K. N. Taksande, B. Navghare, *Tetrahedron Lett.* **2005**, 46, 1573; f) N. Yao, A. Song, X. Wang, S. Dixon, K. S. Lam, *J. Comb. Chem.* **2007**, 9, 668; g) M. M. Naik, S. G. Tilve, V. B. Kamat, *Tetrahedron Lett.* **2014**, 55, 3340; h) Y. Hoshino, N. Takeno, *Bull. Chem. Soc. Japan* **1987**, 60, 4468; i) Y. K. Rao, S.-H. Fang, Y.-M. Tzeng, *Bioorg. Med. Chem.* **2005**, 13, 6850; j) H. S. Mahal, H. S. Rai, K. Venkataraman, *J. Chem. Soc.* **1935**, 866; k) Z. Du, H. Ng, K. Zhang, H. Zeng, J. Wang, *Org. Biomol. Chem.* **2011**, 9, 6930.

[7] Other synthetic procedures for flavones: a) Q. Yang, H. Alper, *J. Org. Chem.* **2010**, 75, 948; b) G. Maiti, R. Karmakar, R. N. Bhattacharya, U. Kayal, *Tetrahedron Lett.* **2011**, 52, 5610; c) M. Yoshida, Y. Fujino, K. Saito, T. Doi, *Tetrahedron* **2011**, 67, 9993; d) X.-F. Wu, H. Neumann, M. Beller, *Chem. Eur. J.* **2012**, 18, 12595; e) K. V. Sashidhara, M. Kumar, A. Kumar, *Tetrahedron Lett.* **2012**, 53, 2355.

[8] a) T. Diao, S. S. Stahl, *J. Am. Chem. Soc.* **2011**, 133, 14566; b) Y. Moon, D. Kwon, S. Hong, *Angew. Chem. Int. Ed.* **2012**, 51, 11333; c) Y. Izawa, C. Zheng, S. S. Stahl, *Angew. Chem. Int. Ed.* **2013**, 52, 3672; d) T. Diao, T. J. Wadzinski, S. S. Stahl, *Chem. Sci.* **2012**, 3, 887; e) W. Gao, Z. He, Y. Qian, J. Zhao, Y. Huang, *Chem. Sci.* **2012**, 3, 883; f) A. N. Campbell, S. S. Stahl, *Acc. Chem. Res.* **2012**, 45, 851; g) T. Diao, D. Pun, S. S. Stahl, *J. Am. Chem. Soc.* **2013**, 135, 8205; h) N. Gigant, J.-E. Bäckvall, *Chem. Eur. J.* **2014**, 20, 5890, and the references of [19f,g] in Chapter I.

[9] X. Jin, K. Yamaguchi, N. Mizuno, *Angew. Chem. Int. Ed.* **2014**, 53, 455.

[10] T. Oishi, K. Yamaguchi, N. Mizuno, *Angew. Chem. Int. Ed.* **2009**, 48, 6286.

[11] S. Sabatini, F. Gosetto, G. Manfroni, O. Tabarrini, G. W. Kaatz, D. Patel, V. Cecchetti, *J. Med. Chem.* **2011**, 54, 5722.

[12] M. Conte, H. Miyamura, S. Kobayashi, V. Chechik, *J. Am. Chem. Soc.* **2009**, 131, 7189.

[13] a) T. Nakayama, K. Yonekura-Sakakibara, T. Sato, S. Kikuchi, Y. Fukui, M. Fukuchi-Mizutani, T. Ueda, M. Nakao, Y. Tanaka, T. Kusumi, T. Nishino, *Science* **2000**,

290, 1163; b) T. Nakayama, *J. Biosci. Bioeng.* **2002**, 94, 487; c) C. Molitor, S. G. Mauracher, S. Pargan, R. L. Mayer, H. Halbwirth, A. Rompel, *Planta* **2015**, 242, 519; d) E. Wong, *Phytochemistry* **1966**, 5, 463; e) M. A. Farag, B. E. Deavours, Â. Fátima, M. Naoumkina, R. A. Dixon, L. W. Sumner, *Plant Physiol.* **2009**, 151, 1096.

[14] For aurone synthesis *via* 5-*exo-dig* cyclization of propargylic alcohol/ketone, see: a) C. M. Brennan, C. D. Johnson, P. D. McDonnell, *J. Chem. Soc. Perkin Trans. II* **1989**, 957; b) Z.-w. An, M. Catellani, G. P. Chiusoli, *J. Organomet. Chem.* **1990**, 397, 371; c) T.-T. Jong, S.-J. Leu, *J. Chem. Soc. Perkin. Trans. I* **1990**, 423; d) H. Harkat, A. Blanc, J.-M. Weibel, P. Pale, *J. Org. Chem.* **2008**, 73, 1620; e) K. Saito, M. Yoshida, T. Doi, *Chem. Lett.* **2015**, 44, 141; f) S. P. Chavan, G. B. B. Varadwaj, K. M. Parida, B. M. Bhanage, *ChemCatChem* **2016**, 8, 2649.

[15] For aurone synthesis *via* Claisen–Schmidt condensation of 3-coumaranones and benzaldehydes, see: a) R. S. Varma, M. Varma, *Tetrahedron Lett.* **1992**, 33, 5937; b) H. Sudhakar, N. Mulakayala, *Indian J. Adv. Chem. Sci.* **2016**, 4, 160.

[16] For 4-substituted aurone synthesis under the conditions of Algar–Flynn–Oyamada reaction, see: a) T. A. Geissman, D. K. Fukushima, *J. Am. Chem. Soc.* **1948**, 70, 1686; b) F. M. Dean, V. Podimuang, *J. Chem. Soc.* **1965**, 3978; c) T. R. Gormley, W. I. O’Sullivan, *Tetrahedron*, **1973**, 29, 369; d) X. Zhao, J. Liu, Z. Xie, Y. A. Li, *Synthesis*, **2012**, 44, 2217; e) S. Bhattacharyya, K. Hatua, *RSC Adv.* **2014**, 4, 18702; f) F. A. Ragab, T. A. A. Yahya, M. M. El-Naa, R. K. Arafa, *Eur. J. Med. Chem.* **2014**, 82, 506; g) A. L. Cole, S. Hossain, A. M. Cole, O. Phanstirl IV, *Bioorg. Med. Chem.* **2016**, 24, 2768.

[17] For aurone synthesis from chalcones using (super)stoichiometric amounts of metal oxidants, see: a) M. F. Grundon, D. Stewart, W. E. Watts, *J. C. S. Chem. Comm.* **1975**, 772; b) H. Sekizaki, *Bull. Chem. Soc. Jpn.* **1988**, 61, 1407; c) A. K. Patel, N. J. Patel, M. A. Patel, D. I. M. Brahmabhatt, *J. Heterocyclic Chem.* **2012**, 49, 504; d) K. Kurosawa, *Bull. Chem. Soc. Jpn.* **1969**, 42, 1456; e) K. Kurosawa, J. Higuchi, *Bull. Chem. Soc. Jpn.* **1972**, 45, 1132.

[18] A manuscript for catalytic aurone synthesis from simple chalcones using CuBr₂ in refluxed dimethyl sulfoxide has been reported; however, in my experiments according to the manuscript using **1a** as a substrate, the reproducibility could not be confirmed, mainly affording not aurone (**2a**), but flavone (**3a**); see: N. N. Agrawal, P. A. A. Soni, *Indian J. Chem.* **2006**, 45, 1301. Also, it is reported in another manuscript that aurones

can be produced from chalcones in the presence of catalytic amounts of CuBr₂; however, as results of my investigation, the reported NMR spectral data were not consistent with those of aurones but consistent with those of flavones; see: G. Priyadarshani, A. Nayak, S. M. Amrutkar, S. Das, S. K. Guchhait, C. N. Kundu, U. C. Banerjee, *ACS Med. Chem. Lett.* **2016**, 7, 1056. For the correct aurones' spectral data; see section 3-2.2.4. and the reference of [15b]. For the flavones' spectral data; see section 3-1.2.4. and the reference of [7a].

[19] C. D. Johnson, *Acc. Chem. Res.* **1993**, 26, 476.

[20] a) T. Mitsudome, T. Umetani, N. Nosaka, K. Mori, T. Mizugaki, K. Ebitani, K. Kaneda, *Angew. Chem. Int. Ed.* **2006**, 45, 481; b) G. Zeni, R. C. Larock, *Chem. Rev.* **2004**, 104, 2285; c) R. M. Trend, Y. K. Ramtohul, B. M. Stoltz, *J. Am. Chem. Soc.* **2005**, 127, 17778; d) V. Kotov, C. C. Scarborough, S. S. Stahl, *Inorg. Chem.* **2007**, 46, 1910; e) X. Ye, G. Liu, B. V. Popp, S. S. Stahl, *J. Org. Chem.* **2011**, 76, 1031; f) A. B. Weinstein, S. S. Stahl, *Angew. Chem. Int. Ed.* **2012**, 51, 11505; g) J. Doháňošová, T. Gracza, *Molecules* **2013**, 18, 6173.

[21] Z. Shi, N. Schröder, F. Glorius, *Angew. Chem. Int. Ed.* **2012**, 51, 8092.

[22] W.-J. Kong, Y.-J. Liu, H. Xu, Y.-Q. Chen, H.-X. Dai, J.-Q. Yu, *J. Am. Chem. Soc.* **2016**, 138, 2146.

[23] a) F. Kakiuchi, Y. Tanaka, T. Sato, N. Chatani, S. Murai, *Chem. Lett.* **1995**, 679; b) B. M. Trost, K. Imi, I. W. Davies, *J. Am. Chem. Soc.* **1995**, 117, 5371; c) Y. Hatamoto, S. Sakaguchi, Y. Ishii, *Org. Lett.* **2004**, 6, 4623; d) X. Shang, Z.-Q. Liu, *Chem. Soc. Rev.* **2013**, 42, 3253; e) R.-Y. Zhu, J. He, X.-C. Wang, J.-Q. Yu, *J. Am. Chem. Soc.* **2014**, 136, 13194.

[24] Y.-L. Zhang, Y.-Q. Wang, *Tetrahedron Lett.* **2014**, 55, 3255.

[25] L. Guo, F. Zhang, W. Hu, L. Li, Y. Jia, *Chem. Commun.* **2014**, 50, 3299.

[26] R. N. DeGuzman, Y.-F. Shen, E. J. Neth, S. L. Suib, C.-L. O'Young, S. Levine, J. M. Newsam, *Chem. Mater.* **1994**, 6, 815.

[27] a) E. Sharpe, T. Frasco, D. Andreescu, S. Andreescu, *Analyst* **2013**, 138, 249; b) N. C. Nelson, J. S. Manzano, A. D. Sadow, S. H. Overbury, I. I. Slowing, *ACS Catal.* **2015**, 5, 2051.

[28] S. Purser, P. R. Moore, S. Swallow, V. Gouverneur, *Chem. Soc. Rev.* **2008**, 37, 320.

[29] Y. Lu, D.-H. Wang, K. M. Engle, J.-Q. Yu, *J. Am. Chem. Soc.* **2010**, 132, 5916.

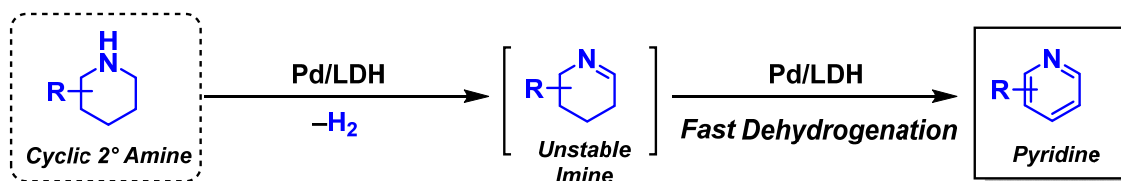
- [30] a) B. S. Lane, M. A. Brown, D. Sames, *J. Am. Chem. Soc.* **2005**, *127*, 8050; b) S. Würtz, S. Rakshit, J. J. Neumann, T. Dröge, F. Glorius, *Angew. Chem. Int. Ed.* **2008**, *47*, 7230.
- [31] a) Shen, W.-J.; Matsumura, Y. *Phys. Chem. Chem. Phys.* **2000**, *2*, 1519. b) Xiao, L.-h.; Sun, K.-p.; Xu, X.-l.; Li, X.-n. *Catal. Commun.* **2005**, *6*, 796; c) Y. Li, J. Hu, D. Ma, Y. Zheng, M. Chen, H. Wan, *ACS Catal.* **2018**, *8*, 1790.
- [32] J. Cai, Y. Y. Ye, *Phys. Rev. B* **1996**, *54*, 8398.

Chapter IV

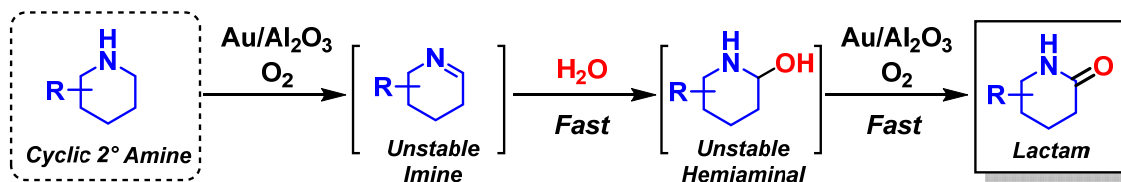
Selective Transformations of Secondary/Tertiary Amines Enabled by Supported Nanoparticle Catalysts

In this chapter, I describe my efforts aimed at the realization of challenging catalytic amine functionalizations that were informed by the specific oxidative abilities of metal nanoparticles discussed in Chapter I and Chapter III. These amine functionalizations include a) the selective transformations of cyclic secondary amines *via* the production of unstable imine intermediates and b) the α -methylene-selective functionalizations of tertiary amines. Regarding the first reaction type, I expected that the quick conversion of unstable imines to stable products would be an effective synthetic approach; in fact, the fast dehydrogenation of imines catalyzed by Pd nanoparticles afforded the acceptorless dehydrogenative aromatization of cyclic secondary amines (Figure 4-12a and section 4-1), and the quick hydration of imines to hemiaminals followed by the Au nanoparticle-catalyzed efficient oxidation of these hemiaminals led to the aerobic α -oxygenation of cyclic secondary amines (Figure 4-12b and section 4-2). Fortunately, the Au nanoparticle-catalyzed aerobic α -oxygenation was applicable to tertiary amines, and it was observed to proceed in an α -methylene-selective fashion (Figure 4-12c and section 4-2). Consequently, I expected that the novel catalytic amine oxidation with α -methylene-selectivity could be applied to the unprecedented regioselective α -functionalization of tertiary amines, in combination with suitable nucleophiles. Indeed, the hybrid catalytic system comprising supported Au nanoparticles and Zn salts enabled me to perform the unusual regioselective α -alkynylation of tertiary amines using molecular oxygen as the sole oxidant, leading to the formation of various propargylic amines, including some that are inaccessible through other procedures (Figure 4-12d and section 4-3). In the next section, I will discuss the hereby developed selective acceptorless dehydrogenative aromatization of cyclic secondary amines in the presence of supported Pd-based catalysts.

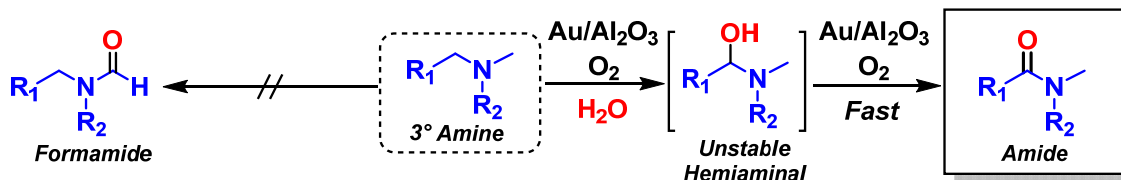
(a)



(b)



(c)



(d)

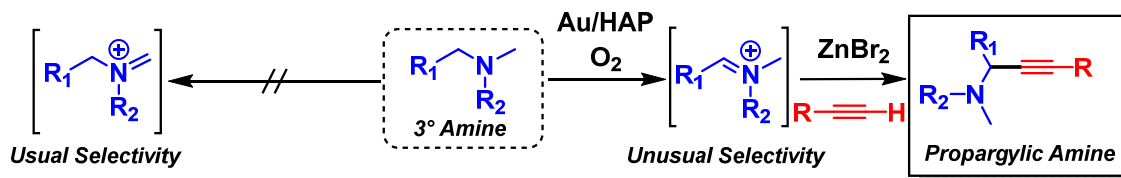


Figure 4-12. Overview of the reactions catalyzed by supported metal nanoparticles discussed in this chapter: (a) acceptorless dehydrogenative aromatization of cyclic secondary amines, (b) aerobic α -oxygenation of cyclic secondary amines, (c) aerobic α -oxygenation of tertiary amines, and (d) α -alkynylation of tertiary amines.

4-1 Selective Acceptorless Dehydrogenative Aromatization of Cyclic Secondary Amines Catalyzed by Supported Palladium Nanoparticles

Adapted with permission from *Chem. Lett.* **2019**, 48, 517–520. Copyright 2019 The Chemical Society of Japan.

4-1.1. Introduction

Catalytic dehydrogenation is one of the most fundamentally important reactions in both bulk and fine chemical productions.^[26] In industrial alkene productions, dehydrogenation has frequently been performed using heterogeneous catalysts under harsh reaction conditions.^[27] Several homogeneous complexes have been utilized for laboratory scale dehydrogenation-based fine chemical synthesis in the presence of appropriate hydrogen acceptors.^[28] In recent years, development of functional group transformation methods with low environmental load and high atom efficiency under mild reaction conditions is highly demanded, especially attention is focused on development of reactions based on catalytic acceptorless dehydrogenation.^[29] For example, considering alcohol oxidation, if the reaction can be realized as a highly efficient catalytic acceptorless dehydrogenation, H₂ gas can be taken out at the same time in addition to useful carbonyl compounds,^[30] as Fujita *et al.* developed Ir-catalyzed acceptorless dehydrogenation of alcohols with high turnover numbers using functional

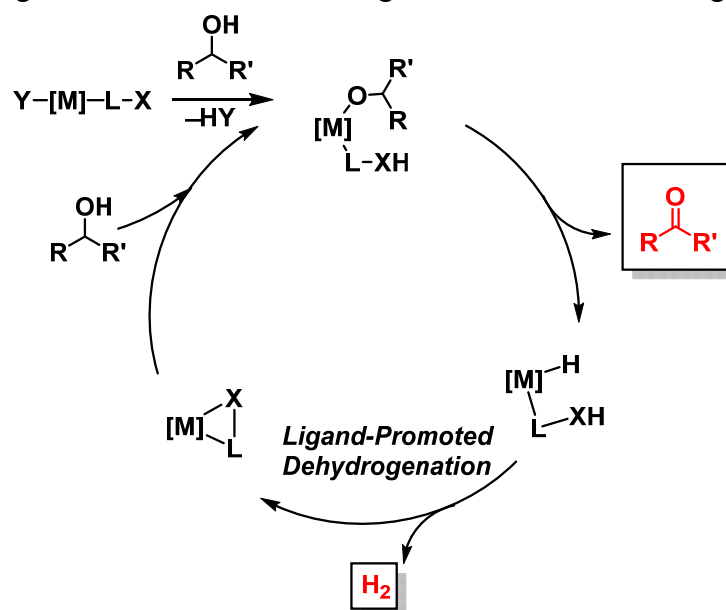


Figure 4-13. Ligand-promoted acceptorless alcohol dehydrogenation.^[30b-d]

ligands to promote a H₂ releasing step (Figure 4-13).^[30b-d] Therefore, the development of catalytic dehydrogenation systems plays an important role not only from a synthetic point of view but also in H₂ production and transportation.^[31]

From the above-mentioned viewpoint, in Mizuno group, several acceptorless dehydrogenative aromatization systems using supported palladium-nanoparticles-based catalysts have been recently developed; namely, dehydrogenation of cyclohexanols or cyclohexanones to phenols,^[32a] dehydrogenation of cyclohexylamines to anilines,^[32a] transformation of cyclohexanone oximes to anilines,^[32b] and synthesis of symmetrically^[32c] and unsymmetrically^[32d] substituted diarylamines (Figure 4-14). In some of the cases, supports possessing basic sites like LTH (Mg–Al–Ni layered triple hydroxide) and LDH (Mg–Al layered double hydroxide) can promote the acceptorless dehydrogenation^[32a,b] possibly *via* the systems as with the ligand-promoted dehydrogenation and/or the promotion of deprotonation steps. Based on these findings, I here aimed to develop a highly efficient catalytic system for acceptorless dehydrogenation of cyclic amines to produce heteroarenes. Heteroarenes are very important compounds, which are frequently seen in many pharmaceuticals.^[33] Dehydrogenative aromatization of cyclic amines is drawing attention as one of the methods for synthesizing heteroarenes, and many efficient catalytic systems using various kinds of oxidants (hydrogen acceptors) have been recently developed.^[34] Also,

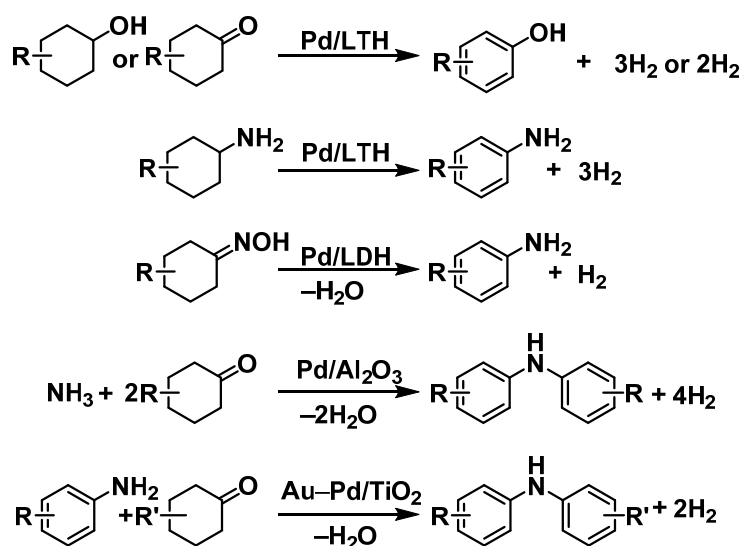


Figure 4-14. Recently developed acceptorless dehydrogenative aromatization reactions in Mizuno group.

many efficient catalytic systems for the acceptorless dehydrogenative aromatization of benzo-fused *N*-heterocycles, *e.g.*, tetrahydro(iso)quinolines and indolines, and piperazines have been reported until now.^[35] However, with respect to simple non-activated piperidines, there are almost no reports so far, including systems using hydrogen acceptors,^[36] partly because of the corresponding imine's instability as explained in section 4.1., although acceptorless amine dehydrogenation and transamination using palladium-doped hydrotalcites applicable to piperidine in a moderate yield have been reported very recently^[37]. Given the aforementioned background, there is still room for the development of acceptorless dehydrogenative aromatization applicable to a wide range of *N*-heterocycles.

In this section, an efficient acceptorless dehydrogenative aromatization of cyclic amines catalyzed by palladium nanoparticles supported on a layered double hydroxide ($\text{Mg}_6\text{Al}_2(\text{OH})_{16}\text{CO}_3 \cdot 4\text{H}_2\text{O}$) (Pd/LDH) has been reported (Figure 4-15). In the presence of Pd/LDH, dehydrogenative aromatization of various kinds of structurally diverse cyclic amines including piperidines, tetrahydro(iso)quinolines, and indolines efficiently proceeded to afford the corresponding heteroarenes in moderate to high yields under relatively mild conditions (80–125 °C). The choice of solvents was very important to allow the reaction to proceed under mild conditions, and aliphatic hydrocarbon solvents such as octane gave good results. The observed catalysis is truly heterogeneous in nature, and the Pd/LDH catalyst can be reused at least four times for the reaction of a model substrate (4-isopropylpiperidine, **1a**) though its catalytic activity gradually declined possibly due to the increase in the palladium particle size.

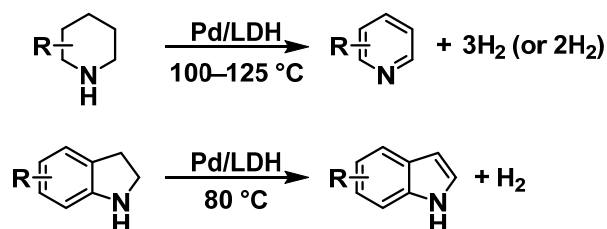


Figure 4-15. This work: Pd/LDH-catalyzed efficient acceptorless dehydrogenative aromatization of cyclic amines under mild conditions.

4-1.2. Experimental

4-1.2.1. Instruments and Reagents

GC analyses were performed on Shimadzu GC-2014 with a flame ionization detector (FID) equipped with a Rtx-1 capillary column (internal diameter = 0.25 mm, length = 30 m) or a Stabilwax capillary column (internal diameter = 0.25 mm, length = 30 m). GC-MS spectra were recorded on Shimadzu GCMS-QP2010 equipped with an InertCap 5 capillary column at an ionization voltage of 70 eV. XRD patterns were measured on a Rigaku SmartLab diffractometer ($\text{CuK}\alpha$, $\lambda = 1.5405 \text{ \AA}$, 45 kV, 200 mA). XPS measurements were carried out on JEOL JPS-9000 using $\text{Mg K}\alpha$ radiation ($h\nu = 1253.6 \text{ eV}$, 8 kV, 10 mA), and the binding energies were calibrated by using the Mg 2p signal at 49.5 eV. ^1H NMR spectra were measured on JEOL JHM-ECA 500 at 500 MHz, using tetramethylsilane (TMS) as an internal reference ($\delta = 0 \text{ ppm}$). ICP-AES analyses were performed on a Shimadzu ICPS-8100. TEM observations were performed on JEOL JEM-2010HC. Pd/C (Lot. No. 217-024030, N.E. CHEMCAT), $\text{Ru/Al}_2\text{O}_3$ (Lot. No. 437-000050, N.E. CHEMCAT), $\text{Pt/Al}_2\text{O}_3$ (Lot. No. 137-90020, N.E. CHEMCAT), LDH ($\text{Mg}_6\text{Al}_2(\text{OH})_{16}\text{CO}_3 \cdot 4\text{H}_2\text{O}$, BET surface area: $51 \text{ m}^2 \text{ g}^{-1}$, Tomita Pharmaceutical Co., Ltd.), Al_2O_3 (BET surface area: $160 \text{ m}^2 \text{ g}^{-1}$, Cat. No. KHS-24, Sumitomo Chemical), TiO_2 (BET surface area: $316 \text{ m}^2 \text{ g}^{-1}$, Cat. No. ST-01, Ishihara Sangyo Kaisya), and CeO_2 ($111 \text{ m}^2 \text{ g}^{-1}$, Cat. No. 544841-25G, Aldrich) were commercially available. Solvents, substrates, and metal sources were obtained from Kanto Chemical, TCI, Wako, Kojima Chemicals, Nacalai Tesque, Strem Chemicals, or Aldrich (reagent grade).

4-1.2.2. Preparation of Catalysts

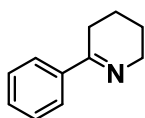
Preparation of Pd/LDH: An aqueous solution (30 mL) of K_2PdCl_4 (0.25 mmol), *in-situ* generated from PdCl_2 (0.25 mmol) and KCl (0.50 mmol), was vigorously stirred with LDH (1.0 g) at room temperature. After 15 min, the pH of the solution was adjusted to 10 by addition of an aqueous solution of NaOH (1 M), and the resulting slurry was further stirred for 18 h. The solid was then filtered off, washed with a large amount of water (3 L), and dried *in vacuo* to afford the supported Pd catalyst (Pd/LDH) as light brown powder. The content of Pd species in Pd/LDH was 0.2 mmol g^{-1} (2.2wt%). The Pd/LDH catalyst was directly utilized for the reaction without any pre-treatment. Other supported metal catalysts, such as $\text{Pd}/\text{Al}_2\text{O}_3$, Pd/TiO_2 , Pd/CeO_2 , Ru/LDH , Ir/LDH , and Au/LDH , were prepared *via* the same procedure.

The catalysts reduced with NaBH_4 were prepared as follows. The aforementioned supported metal catalyst (0.5 g) was dispersed into deionized water (30 mL). Then, NaBH_4 (20 mg) was added to the resulting slurry and stirred for 2 h at room temperature. After that, the reduced catalyst was filtered off, washed with large amount of water (2 L), and dried *in vacuo*, affording the desired catalyst.

4-1.2.3. Reactions and Synthesis

Catalytic Reaction: Into a Schlenk tube (volume: ~20 mL) connected to a balloon partially filled with Ar gas, Pd/LDH (75 mg, Pd: 3 mol %), a cyclic secondary amine (**1**, 0.5 mmol), decane (internal standard, 0.1 mmol), octane (2.0 mL), and a Teflon-coated magnetic stir bar were successively placed, and the reaction mixture was vigorously stirred at 120 °C, under 1 atm of Ar. After the reaction was completed, the conversions of **1** and the yields of *N*-heteroarenes (**2**) were determined by GC analysis using decane as an internal standard. The reactions of piperidine and 4-methylpiperidine were conducted in a test tube with an Ar balloon while the upper side of the test tube was cooled by refrigerant (−5 °C). The products were identified by GC-MS.

Synthesis of 2,3,4,5-tetrahydro-6-phenylpyridine (3e): Compound **3e** was prepared as follows according to the reference.^[38] Into a three-neck round bottom flask, 5-bromovaleronitrile (845 μ L, 7.3 mmol) in anhydrous THF (12.5 mL) was added under an Ar atmosphere. After the dropwise addition of a 1.6 M phenyllithium solution in dibutyl ether (5.2 mL, 8.3 mmol) to the mixture, the resulting solution was refluxed for 18 h with a condenser. Then, the reaction was quenched with a saturated aqueous solution of NaHCO₃ and extracted with dichloromethane (3 \times 50 mL). The combined organic layers were dried over Na₂SO₄, filtered off, and concentrated under reduced pressure. The crude residue was purified by silica gel column chromatography (dichloromethane/methanol 95:5) to provide the desired product.



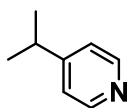
3e (CAS No. 57050-07-4)

2,3,4,5-tetrahydro-6-phenylpyridine (3e): ¹H NMR (500 MHz, CDCl₃, TMS): δ 1.65–1.70 (m, 2H), 1.81–1.86 (m, 2H), 2.61–2.65 (m, 2H), 3.82–3.86 (m, 2H), 7.36–7.38 (m, 3H), 7.75–7.77 (m, 2H). MS (70 eV, EI): *m/z* (%): 159 (87) [*M*⁺], 158 (100), 144 (19), 131 (14), 130 (31), 104 (41), 103 (83), 91 (28), 77 (30), 76 (13), 51 (16).

Leaching Test: To establish whether the catalytic reaction occurred on solid Pd/LDH or not, the catalyst was removed by hot filtration 90 min after the reaction started under the optimized conditions and the reaction was again carried out with the filtrate under the same conditions. The reactions were conducted in a glove box filled with Ar. When the amount of leached metals was measured, the filtrate after the reaction proceeded for 3 h was evaporated *in vacuo*, treated with concentrated aqua regia (1 mL), and sonicated. Then, Pd species in the filtrate were analyzed by ICP-AES after the filtrate was moved into a 10 mL volumetric flask.

Reuse Test: After the reaction, Pd/LDH was retrieved from the reaction mixture by simple filtration using a PTFE membrane filter. The retrieved catalyst was washed with EtOH (150 mL) and dried *in vacuo*. Then, the catalyst was used for the reuse experiment under the optimized conditions.

4-1.2.4. Spectral Data of Products



2a (CAS No. 696-30-0): 95% yield, >99% substrate conversion (Table 4-4, entry 1)

4-isopropylpyridine (2a): MS (70 eV, EI): m/z (%): 121 (66) [M^+], 120 (18), 106 (100), 79 (20), 78 (20), 77 (21), 51 (20).



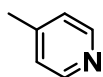
2b (CAS No. 109-06-8): 74% yield, 83% substrate conversion (Table 4-4, entry 2)

2-methylpyridine (2b): MS (70 eV, EI): m/z (%): 93 (100) [M^+], 92 (27), 78 (19), 67 (17), 66 (60), 65 (23), 52 (11), 51 (21), 50 (12).



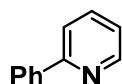
2c (CAS No. 108-99-6): 58% yield, 83% substrate conversion (Table 4-4, entry 3)

3-methylpyridine (2c): MS (70 eV, EI): m/z (%): 93 (100) [M^+], 92 (37), 67 (20), 66 (51), 65 (38), 63 (12).



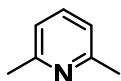
2d (CAS No. 108-89-4): 48% yield, 71% substrate conversion (Table 4-4, entry 4)

4-methylpyridine (2d): MS (70 eV, EI): m/z (%): 93 (100) [M^+], 92 (29), 67 (16), 66 (44), 65 (26), 51 (11).



2e (CAS No. 1008-89-5): 84% yield, 86% substrate conversion (Table 4-4, entry 5)

2-phenylpyridine (2e): MS (70 eV, EI): m/z (%): 156 (13), 155 (100) [M^+], 154 (85), 128 (12), 127 (19), 77 (20), 51 (12).



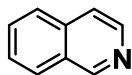
2f (CAS No. 108-48-5): >99% yield, >99% substrate conversion (Table 4-4, entry 6)

2,6-dimethylpyridine (2f): MS (70 eV, EI): m/z (%): 108 (10), 107 (100) [M^+], 106 (43), 92 (20), 79 (13), 66 (33), 65 (21).



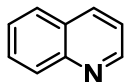
2g (CAS No. 110-86-1): 54% yield, 92% substrate conversion (Table 4-4, entry 7)

pyridine (2g): MS (70 eV, EI): m/z (%): 79 (100) [M^+], 78 (13), 52 (74), 51 (34), 50 (26).



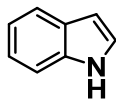
2h (CAS No. 119-65-3): 85% yield, 93% substrate conversion (Table 4-4, entry 8)

isoquinoline (2h): MS (70 eV, EI): m/z (%): 130 (10), 129 (100) [M^+], 128 (20), 102 (34), 76 (12), 75 (11), 51 (16), 50 (10).



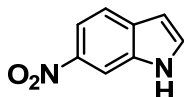
2i (CAS No. 91-22-5): 58% yield, 70% substrate conversion (Table 4-4, entry 9)

quinoline (2i): MS (70 eV, EI): m/z (%): 130 (10), 129 (100) [M^+], 128 (20), 102 (31), 76 (12), 51 (15).



2j (CAS No. 120-72-9): 79% yield, 98% substrate conversion (Table 4-4, entry 10)

indole (2j): MS (70 eV, EI): m/z (%): 118 (9), 117 (100) [M^+], 116 (9), 90 (47), 89 (34), 63 (13).



2k (CAS No. 4769-96-4): 53% yield, 82% substrate conversion (Table 4-4, entry 11)

6-nitroindole (2k): MS (70 eV, EI): m/z (%): 162 (100) [M^+], 132 (31), 116 (75), 104 (19), 89 (62), 63 (25), 62 (12).

4-1.3. Results and Discussion

4-1.3.1. Effect of Catalysts and Optimization of Reaction Conditions

To begin with, the acceptorless dehydrogenative aromatization of **1a** to 4-isopropylpyridine (**2a**) was conducted in the presence of various supported Pd catalysts prepared by a deposition-precipitation method (denoted as Pd/support, support = LDH, Al₂O₃, CeO₂, or TiO₂) (Table 4-1) because in the previous studies it was found that only palladium-based catalysts exhibited high performance for dehydrogenative aromatization reactions.^[32] In particular, the Pd/LDH-catalyzed reaction in octane efficiently proceeded under relatively milder conditions (120 °C) than those of previously reported dehydrogenation systems including Mizuno and co-workers' systems,^[32] giving the desired **2a** in 95% yield for 2 h without detectable by-products (Table 4-1, entry 1).

Within a few minutes after the start of the reaction, the color of Pd/LDH was changed from initial light brown to black. To elucidate what occurs during the reaction, fresh Pd/LDH and used Pd/LDH were examined in detail. The X-ray photoelectron spectroscopy (XPS) spectrum of the freshly prepared Pd/LDH catalyst showed that the binding energies of Pd 3d_{3/2} and Pd 3d_{5/2} were 341.1 eV and 335.9 eV, respectively (Figure 4-16a), indicating that the oxidation state of the palladium species was +2. The X-ray diffraction (XRD) pattern of Pd/LDH was almost the same as that of the parent LDH support, and no obvious signals due to palladium oxides and hydroxides were detected (Figure 4-17a, b). Thus, Pd(II) hydroxide species are likely highly dispersed on LDH. Next, after completion of the reaction, the catalyst was recovered, and its XPS spectrum was measured. The peaks due to the binding energies of Pd 3d_{3/2} and Pd 3d_{5/2} were observed at 339.9 eV and 334.5 eV, respectively (Figure 4-16b). Therefore, the Pd(II) species in the freshly prepared catalyst was reduced to Pd(0) species during the reaction. The XRD pattern of the used Pd/LDH indicated that the structure of LDH was maintained and no large palladium particles were formed during the reaction (Figure 4-17c). The transmission electron microscopy (TEM) analysis of the used catalyst revealed that palladium nanoparticles were formed on the surface of LDH (average particle size (d_{av}) = 3.9 nm, standard deviation (σ) = 1.1 nm, Figure 4-18). Based on the above experimental results, it was revealed that *in situ* generated Pd(0)

nanoparticles were the active species for the present acceptorless dehydrogenative aromatization.

For the reaction of **1a**, supported palladium catalysts such as Pd/Al₂O₃, Pd/CeO₂, Pd/TiO₂, and commercially available Pd/C also gave the desired **2a** in moderate to high yields (Table 4-1, entries 8–11). The average particle sizes of the catalysts used were almost the same, and the initial yields of **2a** produced by the Pd-supported catalysts were not much different (Table 4-2). These results suggested that the effect of supports was not so significant—in this system, the acceptorless dehydrogenation promoted by basic sites of LDH was not observed.

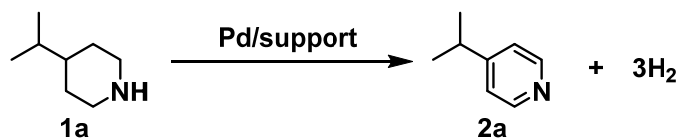
The effect of solvents on the reaction of **1a** appeared markedly. Among the solvents examined such as octane, cyclooctane, *p*-xylene, mesitylene, *N,N*-dimethylacetamide (DMA), diethyleneglycol dimethyl ether (diglyme), *N,N*-dimethylformamide (DMF), a linear aliphatic hydrocarbon solvent octane showed the best result (Table 4-1, entry 1). The reaction in a cyclic alkane solvent cyclooctane gave **2a** in only 19% yield (Table 4-1, entry 2). When the reaction of **1a** was carried out under the conditions described in Table 1 using aromatic solvents such as *p*-xylene and mesitylene, the yields of **2a** were 24% and 20%, respectively (Table 4-1, entries 3 and 4). For several reported functional group transformations by palladium nanoparticle catalysts, aromatic solvents have been utilized so far,^[39] and Mizuno group has also often used aromatic solvents previously (see the references of [11f] and [17k] in Chapter I).^[32d] However, aromatic solvents are not suitable for reactions by palladium nanoparticle catalysts from the results of the above-mentioned solvent effect and the fact that the addition of an aromatic compound such as naphthalene completely inhibited the reaction of **1a**. Moreover, in other palladium-nanoparticles-catalyzed acceptorless dehydrogenative aromatization reported by Mizuno *et al.* (see the references of [11f] and [17k] in Chapter I), it was confirmed that the addition of an aromatic compound strongly inhibited the reactions (unpublished data). Also, polar solvents such as DMA, diglyme, and DMF were not effective for the reaction of **1a** (Table 4-1, entries 5–7).

Ru/LDH, Rh/LDH, Ir/LDH, and Au/LDH were also prepared according to the similar procedure as above and the reactions of **1a** were performed using these catalysts; however, **2a** was not produced at all (Table 4-3, entries 2 and 4–9). To date, Pt(0)

nanoparticle catalysts have been often utilized for acceptorless dehydrogenative aromatization of organic hydrides such as methylcyclohexane under harsh conditions (typically >300 °C).^[40] Thus, the reaction of **1a** was examined in the presence of a commercially available supported Pt(0) catalyst (Pt/Al₂O₃); however, **2a** was not produced at all (Table 4-3, entry 10). In addition, commercially available Ru/Al₂O₃ was not effective (Table 4-3, entry 3). Therefore, it is due to the specific catalysis of Pd(0) nanoparticles that acceptorless dehydrogenative aromatization of cyclic amines can be realized under relatively mild conditions like this system.

It was confirmed by volumetric measurement and MS analysis of the evolved gas that three equivalents of H₂ gas with respect to **2a** was produced during the reaction using Pd/LDH. Naturally, under the present conditions, the reaction did not proceed in the absence of the catalysts or the presence of just LDH (Table 4-1, entry 12).

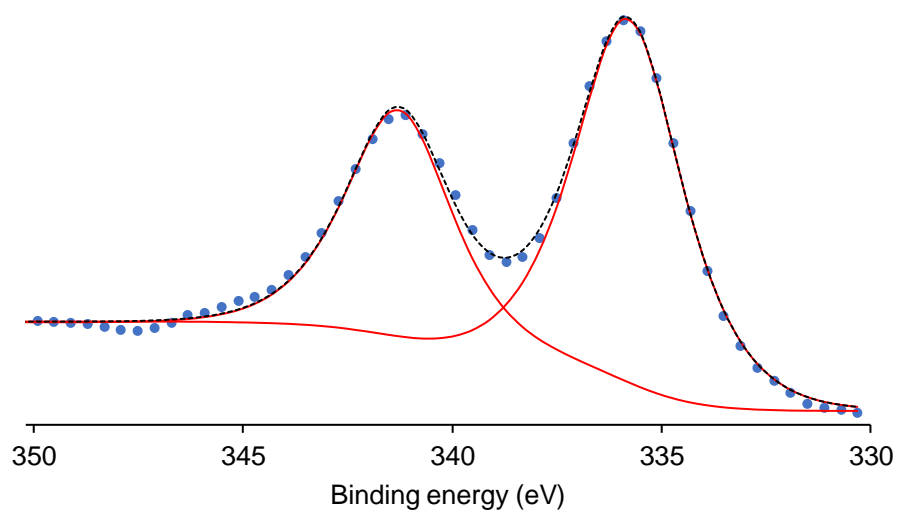
Table 4-1. Effect of catalysts and solvents on the dehydrogenative aromatization of **1a**.^[a]



Entry	Catalyst	Solvent	Time [h]	Yield [%]
1	Pd/LDH	Octane	2	95
2	Pd/LDH	Cyclooctane	2	19
3	Pd/LDH	<i>p</i> -Xylene	2	24
4	Pd/LDH	Mesitylene	2	17
5	Pd/LDH	DMA	2	20
6	Pd/LDH	Diglyme	2	3
7	Pd/LDH	DMF	2	1
8	Pd/Al ₂ O ₃	Octane	2	88
9	Pd/CeO ₂	Octane	2	73
10	Pd/TiO ₂	Octane	2	58
11	Pd/C	Octane	2	82
12 ^[b]	LDH	Octane	3	<1

[a] Reaction conditions: **1a** (0.5 mmol), catalyst (Pd: 3 mol%), solvent (2 mL), 120 °C, Ar atmosphere (1 atm). Yields were determined by GC analysis using decane or biphenyl as the internal standard. [b] LDH (75 mg).

(a)



(b)

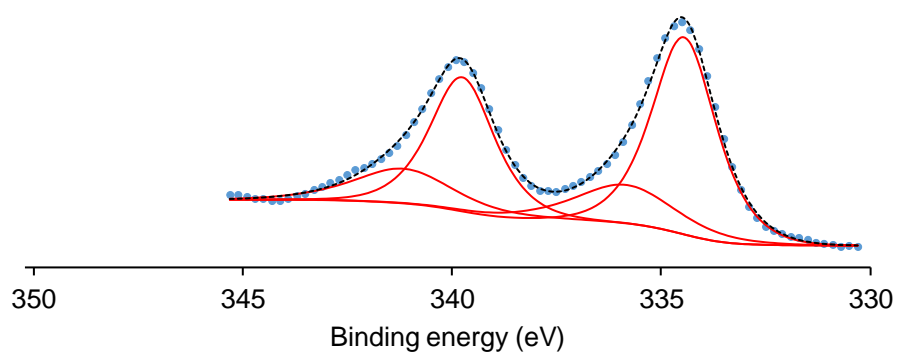


Figure 4-16. XPS spectra of around Pd 3d components: (a) freshly prepared Pd/LDH and (b) Pd/LDH after the used for the dehydrogenative aromatization of **1a**. The red lines and black broken line indicate the deconvoluted signals and the sum of these lines, respectively. The blue dots indicate the data plots. The binding energies were calibrated by using the Mg 2p signal at 49.5 eV.

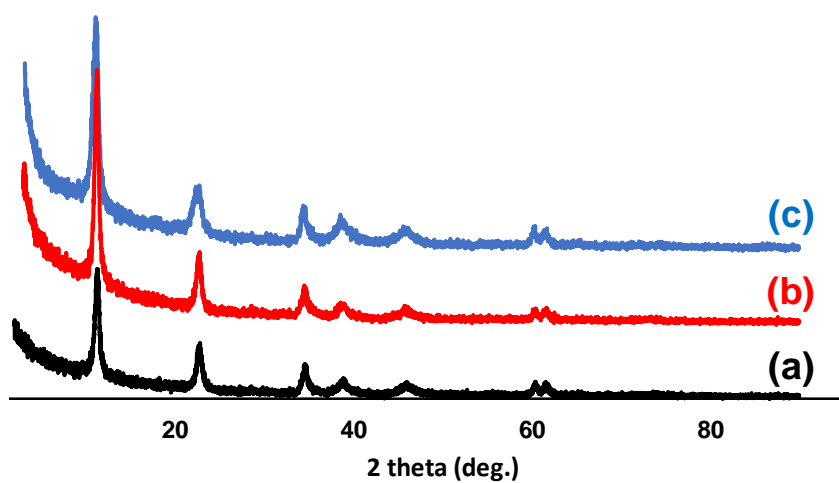


Figure 4-17. XRD patterns of (a) LDH, (b) freshly prepared Pd/LDH, and (c) Pd/LDH after the used for the dehydrogenative aromatization of **1a**.

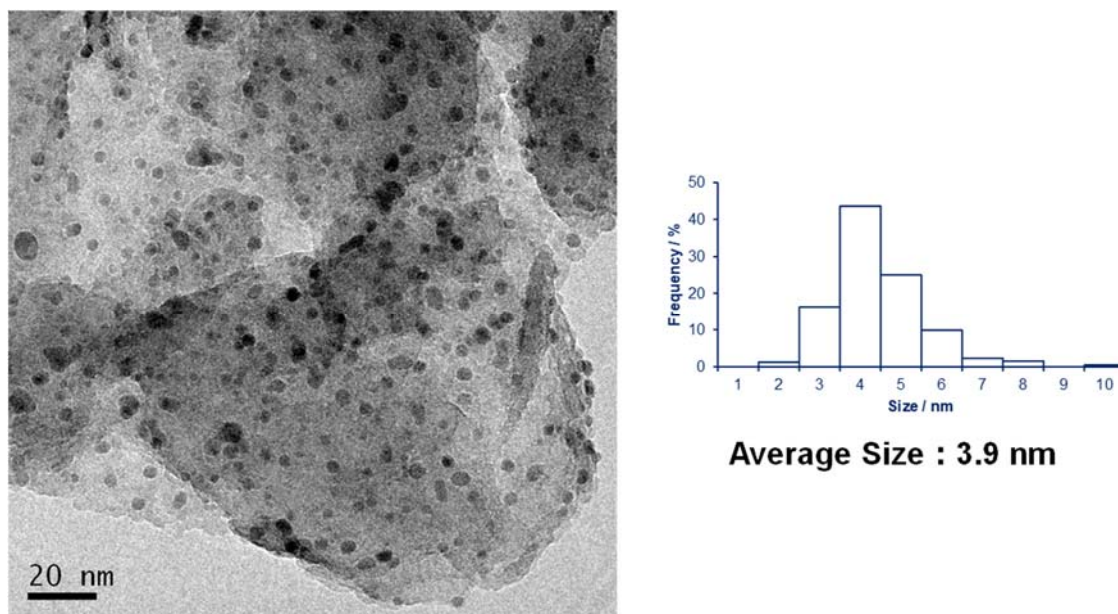
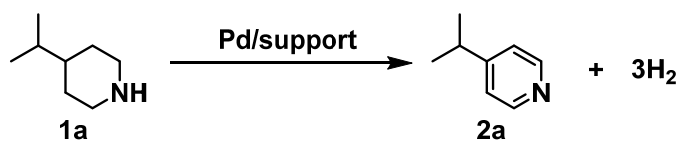


Figure 4-18. TEM image and Pd nanoparticle distribution of Pd/LDH after the first use.

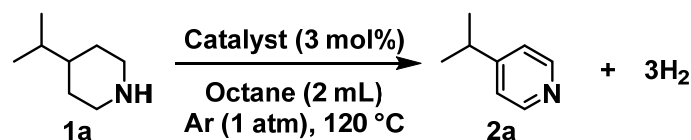
Table 4-2. Effect of supports on the dehydrogenative aromatization of **1a**.^[a]



Entry	Catalyst	Yield of 2a [%]	Average Pd size [nm]
1 ^[b]	Pd/LDH	20	3.9
2	Pd/Al ₂ O ₃	24	3.0
3	Pd/CeO ₂	15	2.2
4	Pd/TiO ₂	20	3.0

[a] Reaction conditions: **1a** (0.5 mmol), catalyst (Pd: 3 mol%), octane (2 mL), 120 °C, Ar atmosphere (1 atm), 30 min. Yields were determined by GC analysis using decane as the internal standard. Pd/Al₂O₃, Pd/CeO₂, and Pd/TiO₂ were prepared by deposition-precipitation followed by NaBH₄ treatment. [b] Pd/LDH was prepared by deposition-precipitation method and directly utilized for the reaction without any pre-treatment.

Table 4-3. Effect of metals on the dehydrogenative aromatization of **1a**.^[a]

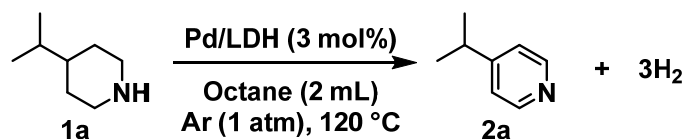


Entry	Catalyst	Remark	Time [h]	Yield of 2a [%]
1 ^[b]	Pd/LDH	As-prepared	2	95
2 ^[b]	Ru/LDH	As-prepared	3	<1
3 ^[c]	Ru/Al ₂ O ₃	Commercially available	3	<1
4 ^[b]	Rh/LDH	As-prepared	3	<1
5 ^[d]	Rh/LDH	NaBH ₄ reduction	3	<1
6 ^[b]	Ir/LDH	As-prepared	3	<1
7 ^[d]	Ir/LDH	NaBH ₄ reduction	3	<1
8 ^[b]	Au/LDH	As-prepared	3	<1
9 ^[d]	Au/LDH	NaBH ₄ reduction	3	<1
10 ^[c]	Pt/Al ₂ O ₃	Commercially available	3	<1

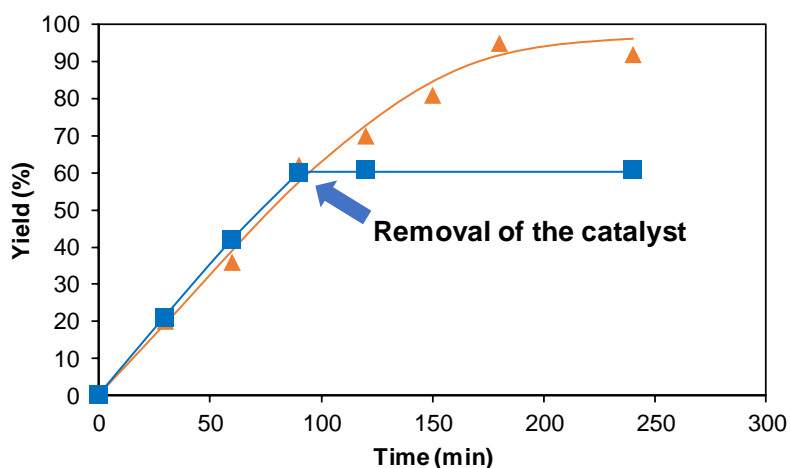
[a] Reaction conditions: **1a** (0.5 mmol), catalyst (metal: 3 mol%), octane (2 mL), 120 °C, Ar atmosphere (1 atm). Yields were determined by GC analysis using decane as the internal standard. [b] The catalysts were prepared by deposition-precipitation method and directly utilized for the reaction without any pre-treatment. [c] Obtained from N.E. CHEMCAT. [d] The catalysts were prepared by deposition-precipitation method and utilized for the reaction after the treatment with NaBH₄.

4-1.3.2. Heterogeneous Catalysis and Catalyst Reuse

To establish whether the observed catalysis for the acceptorless dehydrogenative aromatization of **1a** occurred heterogeneously on Pd/LDH or was a result of the presence of leached palladium species in the reaction solution, the catalyst was removed by hot filtration 1.5 h after the reaction was started (at ~60% conversion of **1a**) under the conditions described in Figure 4-19, and the reaction was restarted with the filtrate under the same conditions. The production of **2a** immediately ceased upon the removal of Pd/LDH (Figure 4-19a). Additionally, after the reaction, the filtrate was analyzed using inductively coupled plasma atomic emission spectroscopy (ICP-AES), and it was observed that the palladium species was barely detectable (below 0.01%). Consequently, the observed catalysis for the reaction was determined to be truly heterogeneous.¹⁵ After the reaction was completed, Pd/LDH can easily be retrieved from the reaction mixture by simple filtration with more than 90% recovery. The repeated reuse experiments were performed using the retrieved catalyst. Although Pd/LDH can be reused at least four times for the reaction of **1a**, its catalytic activity unfortunately gradually declined; 92% yield of **2a** with the fresh catalyst and 72% yield for the fourth reuse under the conditions described in Figure 4-19b. It was confirmed by the TEM analyses that the average palladium particle size gradually increased during the repeated reuse experiments; the average particle size after the first run was 3.9 nm and increased up to 6.7 nm ($\sigma = 2.6$ nm) after the third reuse experiment (Figure 4-20). Therefore, the deactivation is likely caused by the increase in the palladium particle size.



(a)



(b)

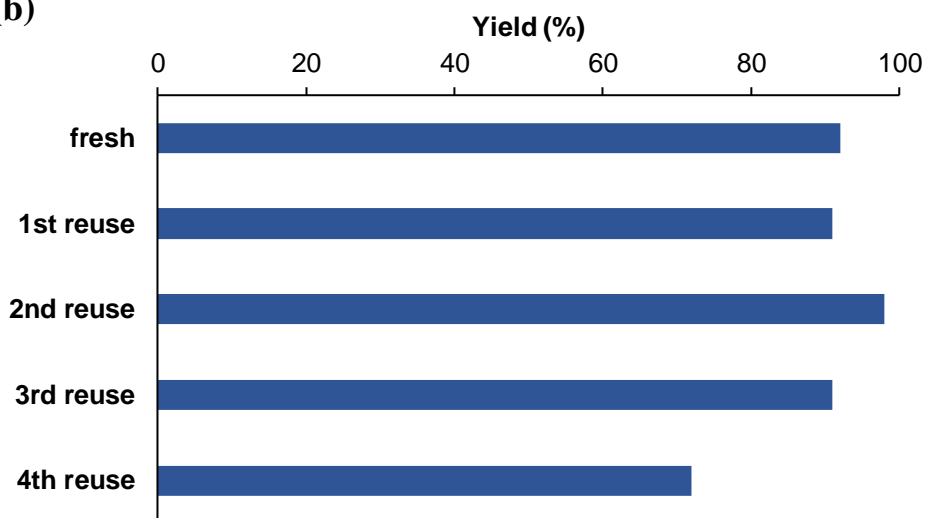


Figure 4-19. (a) Effect of removal of Pd/LDH on the dehydrogenative aromatization of **1a**. Symbol "▲" indicates the profile of **2a** yield without removal of the catalyst, and symbol "■" indicates the profile of **2a** yield when the catalyst was removed at 90 min. (b) The results of reuse experiments. Reaction conditions: **1a** (0.5 mmol), Pd/LDH (3 mol%), octane (2 mL), Ar (1 atm), 120 °C, 3 h (for reuse experiments). Yields were determined by GC analysis.

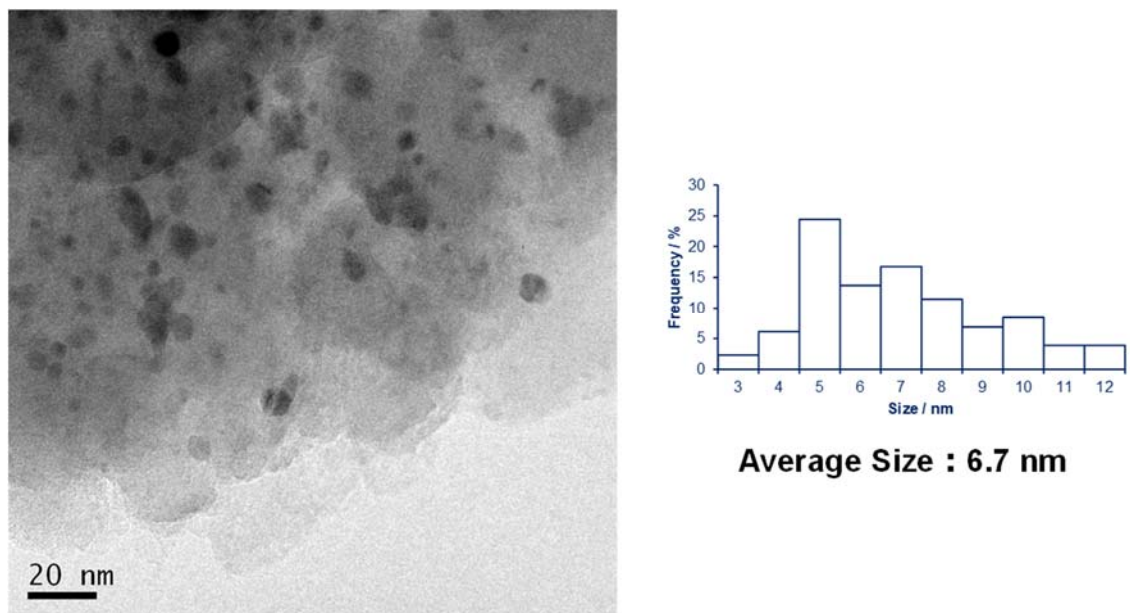
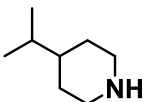
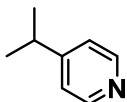
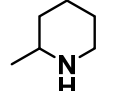
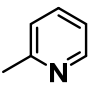
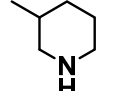
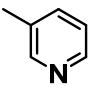
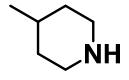
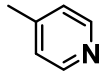
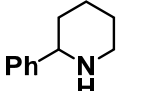
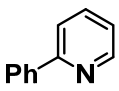
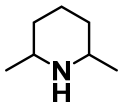
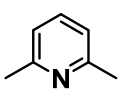
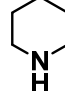
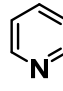
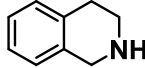
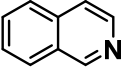
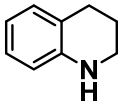
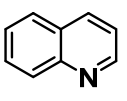
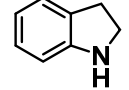
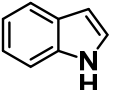
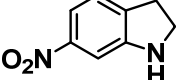
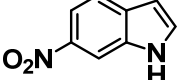


Figure 4-20. TEM images and distribution of Pd nanoparticles on LDH after the third reuse experiment.

4-1.3.3. Substrate Scope

With the optimized reaction conditions, the substrate scope for the proposed Pd/LDH-catalyzed acceptorless dehydrogenative aromatization was investigated. As shown in Table 4-4, various cyclic amines including piperidine, tetrahydro(iso)quinoline, and indoline derivatives can be converted into the corresponding heteroarenes under relatively mild conditions (80–125 °C). When piperidines substituted with an alkyl group at the 2-, 3-, or 4-position (**1a–1d**) were used as the substrates, the reaction proceeded efficiently to give the corresponding monoalkylated pyridines in moderate to high yields (Table 4-4, entries 1–4). 2-Phenylpiperidine (**1e**) also gave the corresponding pyridine in a good yield (Table 4-4, entry 5). The reaction of 2,6-dimethylpiperidine (**1f**) also proceeded efficiently to afford a quantitative yield of 2,6-dimethylpyridine (Table 4-4, entry 6), indicating that the influence of the steric crowding around the nitrogen atom is not significant. It is noteworthy that this reaction system was also applicable to the reaction of non-substituted piperidine (**1g**) (Table 4-4, entry 7). The reaction of benzo-fused piperidines such as tetrahydroisoquinoline (**1h**) and tetrahydroquinoline (**1i**) gave isoquinoline and quinoline, respectively (Table 4-4, entries 8 and 9). The reaction of indolines (**1j** and **1k**) smoothly proceeded even at 80 °C (Table 4-4, entries 10 and 11). In the case of 6-nitroindoline (**1k**), 6-nitroindole was obtained as the major product with concomitant formation of 6-aminoindole as the by-product (Table 4-4, entry 11).

Table 4-4. Substrate scope of Pd/LDH-catalyzed acceptorless dehydrogenative aromatization of cyclic amines.^[a]

Entry	Substrate	Product	<i>T</i> [°C], <i>t</i> [h]	Yield [%]
1	 1a	 2a	120, 2	95
2 ^[b]	 1b	 2b	100, 18	74
3 ^[b]	 1c	 2c	100, 18	58
4 ^[b]	 1d	 2d	100, 18	48
5 ^[c]	 1e	 2e	120, 2	84
6	 1f	 2f	120, 18	>99
7	 1g	 2g	125, 24	54
8 ^[b]	 1h	 2h	100, 3	85
9	 1i	 2i	120, 18	58
10	 1j	 2j	80, 18	79
11 ^[d]	 1k	 2k	80, 18	53 ^[e]

[a] Reaction conditions: substrate (0.5 mmol), Pd/LDH (Pd: 3 mol%), octane (2 mL), Ar atmosphere (1 atm). Yields were determined by GC analysis using decane as the internal standard. [b] Heptane (2 mL) was used as the solvent. [c] Substrate (0.2 mmol). [d] DMA (2 mL) was used as the solvent, and the yield was determined using biphenyl added to the solution after the reaction as the internal standard. [e] 6-Aminoindole was formed as the by-product (~20%).

4-1.3.4. Mechanistic Studies

Finally, the reaction pathway for the Pd/LDH-catalyzed acceptorless dehydrogenative aromatization of piperidines was investigated. The reaction profile for the Pd/LDH-catalyzed reaction of **1e** exhibited that an imine 2,3,4,5-tetrahydro-6-phenylpyridine (**3e**) was detected during the reaction albeit in only small amounts (Figure 4-21), suggesting that the reaction proceeds through the imine intermediate. In the previous reports of palladium nanoparticles-catalyzed dehydrogenative aromatization of cyclohexanones or cyclohexylamines, the reactions were composed of the rate-limiting substrate dehydrogenation followed by the fast disproportionation (see the references of [11f] and [17k] in Chapter I).^[32] I considered that the present Pd/LDH-catalyzed aromatization of cyclic amines also proceeded through such a dehydrogenation-disproportionation sequence. Thus, **3e** was prepared according to the reported procedure,^[38] and the reaction of **3e** was carried out under the standard conditions. As shown in Figure 4-22, it was confirmed that the corresponding pyridine **2e** was formed by the imine disproportionation. However, the production rate of **2e** starting from **3e** was significantly smaller than that starting from **1e** (Figure 4-22 vs Figure 4-21). In a separate experiment, it was confirmed that the presence of an excess of an imine relative to the catalyst strongly inhibited the amine dehydrogenation; the addition of **3e** (1.3 equivalents to **1a**) in the reaction starting from **1a** totally inhibited the dehydrogenation while the disproportionation of **3e** preferentially occurred (Table 4-5). I interpret these experimental results as follows. Firstly, acceptorless dehydrogenation of an amine proceeds to afford an imine intermediate (Figure 4-23a). Then, the corresponding pyridine is immediately formed through disproportionation (Figure 4-23b-1) before the imine accumulates onto Pd nanoparticles and/or converts into the trimer as shown in Figure 4-5.^[5c,d,20g-i] However, the possibility of a direct fast dehydrogenation pathway (Figure 4-23b-2) cannot be completely denied.

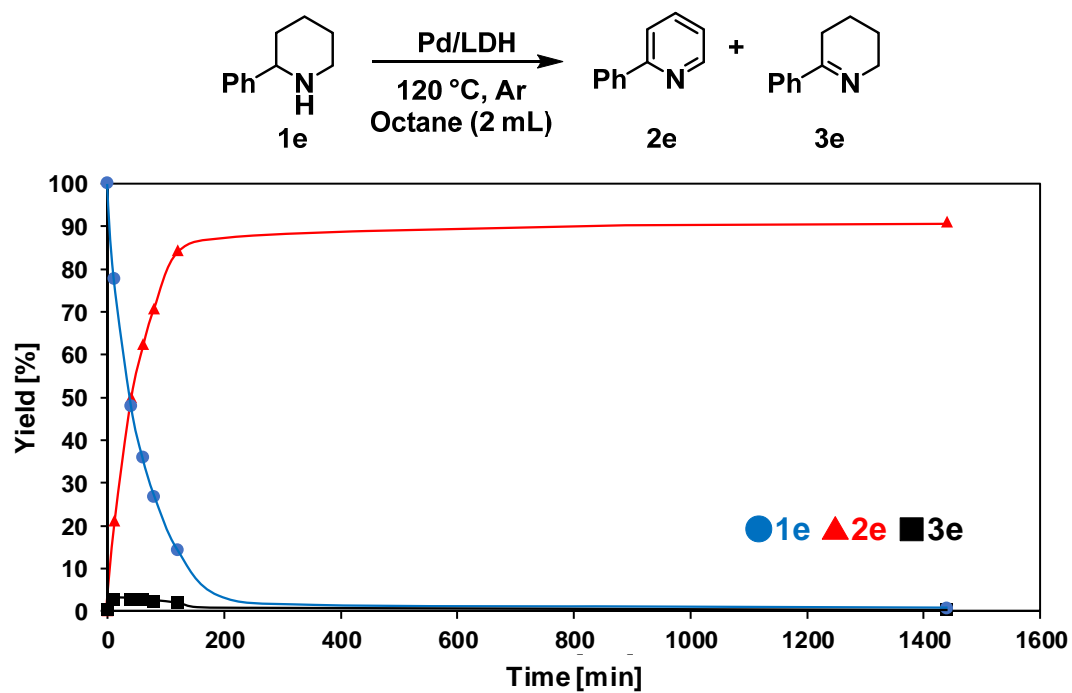


Figure 4-21. Reaction profile for the dehydrogenative aromatization of **1e**. Reaction conditions: **1e** (0.5 mmol), Pd/LDH (3 mol%), octane (2 mL), Ar (1 atm), 120 °C. Yields were determined by GC analysis.

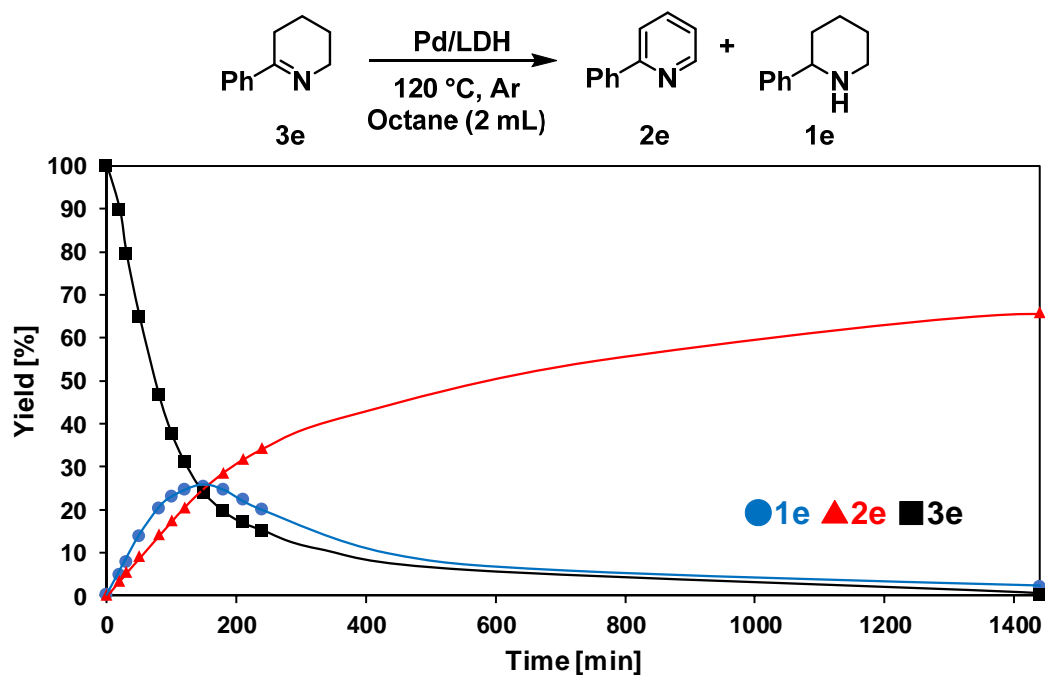
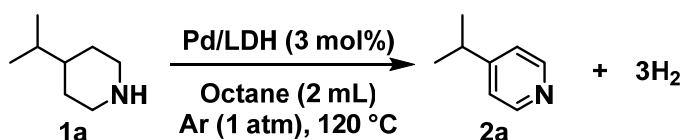


Figure 4-22. Reaction profile for the dehydrogenative aromatization of **3e**. Reaction conditions: **3e** (0.5 mmol), Pd/LDH (3 mol%), octane (2 mL), Ar (1 atm), 120 °C. Yields were determined by GC analysis.

Table 4-5. Effect of imine **3e** on the aromatization of **1a**^[a]



Entry	Additive	Conv. of 1a [%]	Yield of 2a [%]
1	None	>99	93
2	3e (0.2 mmol)	5	<1

[a] Reaction conditions: **1a** (0.15 mmol), Pd/LDH (Pd: 3 mol%), octane (2 mL), 120 °C, Ar atmosphere (1 atm), 90 min. Conversions and yields were determined by GC analysis using decane as the internal standard.

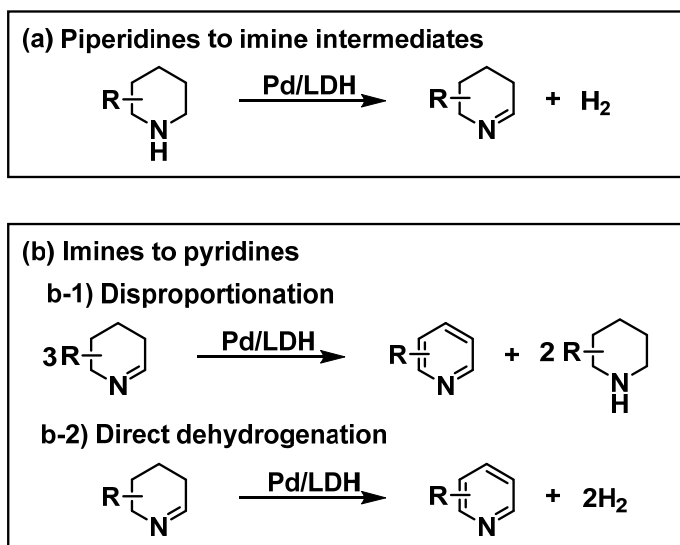


Figure 4-23. Plausible reaction paths for the Pd/LDH-catalyzed acceptorless dehydrogenative aromatization of cyclic amines.

4-1.4. Summary

In summary, in the presence of Pd nanoparticle catalysts, such as Pd/LDH, the acceptorless dehydrogenative aromatization of versatile cyclic amines including non-activated piperidines has been developed under mild conditions for the first time. Only palladium catalysts can promote this dehydrogenative aromatization among the examined supported precious metal catalysts, *i.e.*, Pd, Ru, Rh, Ir, Au, and Pt. The present catalysis is truly heterogeneous and the catalyst can be reused at least four times without a severe loss of its catalytic activity. This transformation was enabled by Pd nanoparticles-catalyzed fast dehydrogenation of an unstable intermediate imine before it converted into byproducts such as trimers.

In the next section, as another useful functionalization of amines including cyclic secondary amines, α -oxygenation catalyzed by supported nanoparticles will be developed through amine oxidation/hydration/hemiaminal oxidation—unstable imines produced *via* amine oxidation will be fast hydrated into hemiaminals followed by the fast oxidation toward amides.

4-2 Selective Formal α -Oxygenation of Secondary/Tertiary Amines Catalyzed by Supported Gold Nanoparticles

Adapted with permission from *Angew. Chem. Int. Ed.* **2016**, 55, 7212–7217. Copyright 2016 John Wiley and Sons and Copyright Clearance Center.

4-2.1. Introduction

Amides are very important compounds in both bulk and fine chemical industries given their widespread applications as intermediates in organic synthesis, raw materials for engineering plastics, intensifiers for perfumes, color pigments for ink, anti-block reagents, detergents, and lubricants.^[41] Among the various synthetic methods developed for amide preparation to date, nucleophilic substitution of carboxylic acid derivatives (such as acid chlorides, anhydrides, and esters) with amines (including NH_3) is one of the most commonly utilized methods.^[1b] Hydration of nitriles and the Beckmann rearrangement have found utility in the production of large scale industrial chemicals, such as acrylamide^[42] and ϵ -caprolactam.^[43] However, these traditional methods often employ stoichiometric amounts of toxic reagents and/or produce large amounts of waste. Therefore, the development of novel, green procedures for amide synthesis with high atom economy is of paramount importance. An approach pioneered by Milstein and co-workers, involving acylation of primary and secondary amines using alcohols or aldehydes instead of carboxylic acid derivatives, and with generation of H_2 or water (when using O_2 as the terminal oxidant) as the sole byproduct, has recently emerged as an attractive environmentally friendly alternative for amide synthesis.^[44] Although this method provides a powerful tool for accessing linear amides, synthesis of cyclic amides with a wide variety of substituted patterns is somewhat problematic.

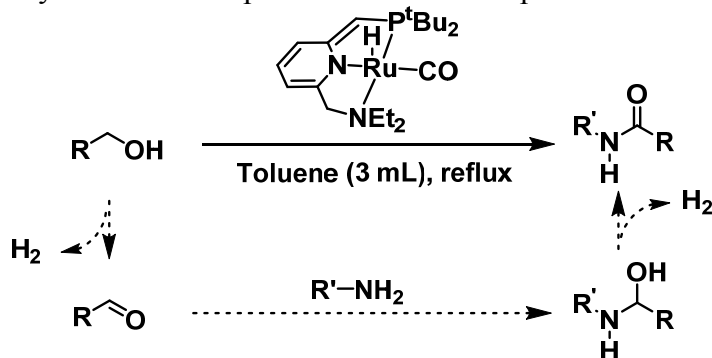


Figure 4-24. Green synthesis of amides from alcohols and amines with liberation of H_2 pioneered by Milstein *et al.*^[45a]

Selective α -oxygenation of amines using O_2 as the terminal oxidant would provide another powerful green synthetic method for amides, given 1) the easy accessibility of amines through a wide variety of chemical transformations, 2) use of O_2 as the green terminal oxidant, and 3) generation of water as the sole by-product. However, as shown in section 4.1., the α -oxygenation of amines has been generally carried out using stoichiometric organic or inorganic oxidants, such as mercury complex,^[24a] hypervalent iodine,^[24b] RuO_4 ,^[24c] and I_2 .^[24d] Therefore, the α -oxygenation of a variety of amines using O_2 as the terminal oxidant is highly attractive, yet challenging.

Recently, Mizuno *et al.* developed an efficient method for α -oxygenation of primary amines into primary amides by ruthenium hydroxide supported on alumina, $Ru(OH)_x/Al_2O_3$,^[45a] and manganese oxide-based octahedral molecular sieves, OMS-2 (Figure 4-25).^[45b] Although these procedures are highly efficient for the α -oxygenation of primary amines, secondary and tertiary amines cannot be converted into the corresponding secondary and tertiary amides.

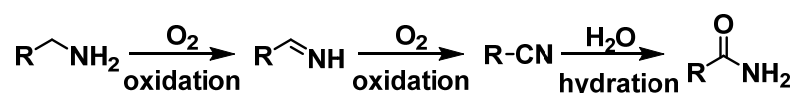


Figure 4-25. $Ru(OH)_x/Al_2O_3$ or OMS-2-catalyzed α -oxygenation of primary amines developed by Mizuno *et al.*^[45]

As a continuation of the development of efficient amide synthetic methods,^[45, 46] the development of a method for α -oxygenation of secondary and tertiary amines has been focused on. To date, several homogeneous^[20g, 24e, f, k-n] and heterogeneous catalysts^[25] are reported to catalyze α -oxygenation of secondary and tertiary amines using O_2 as the terminal oxidant. However, substrate scopes for these procedures are generally limited to tetrahydro(iso)quinoline or aniline derivatives. Quite recently, Milstein and co-workers reported an “acceptorless” homogeneous ruthenium-catalyzed oxygenation of secondary amines into amides.^[24h, i] However, in this case the substrate scope was limited to cyclic secondary amines. To the best of my knowledge, there is no precedent for the α -oxygenation of aliphatic linear secondary and tertiary amines using O_2 as the terminal oxidant. Therefore, the development of novel catalysts for amine α -oxygenation with a wide substrate scope; especially for the selective α -oxygenation of unsymmetrical secondary and tertiary amines; is highly desirable.

In this section, for the first time, a highly selective and widely applicable route for heterogeneous α -oxygenation of secondary and tertiary amines is disclosed. The method uses O_2 as the oxidant and is catalyzed by gold nanoparticles supported on alumina (Au/Al_2O_3 , with an average particle size of $Au = 4.9$ nm). The present reaction proceeds through the following oxidation/hydration/oxidation sequence; a) oxidation of secondary/tertiary amines into imine/iminium intermediates (Figure 4-26, step 1), b) hydration of the imine/iminium intermediates to form hemiaminals (Figure 4-26, step 2), and c) oxidation of the hemiaminals into the desired amide products (Figure 4-26, step 3). In the presence of Au/Al_2O_3 , a wide range of cyclic and linear secondary and tertiary amines can be converted into the corresponding amides in moderate to high yields. The catalysis in the present reaction is truly heterogeneous, and the Au/Al_2O_3 catalyst can be reused several times without a severe loss of its catalytic activity. This reaction is an efficient green method for the α -oxygenation of secondary and tertiary amines when it is considered that 1) water is used as the oxygen atom source in the amide group, 2) O_2 is employed as the terminal oxidant, and 3) water is the only theoretical byproduct. Additionally, ^{18}O -labeled amides were readily synthesized using $H_2^{18}O$ as the oxygen source.

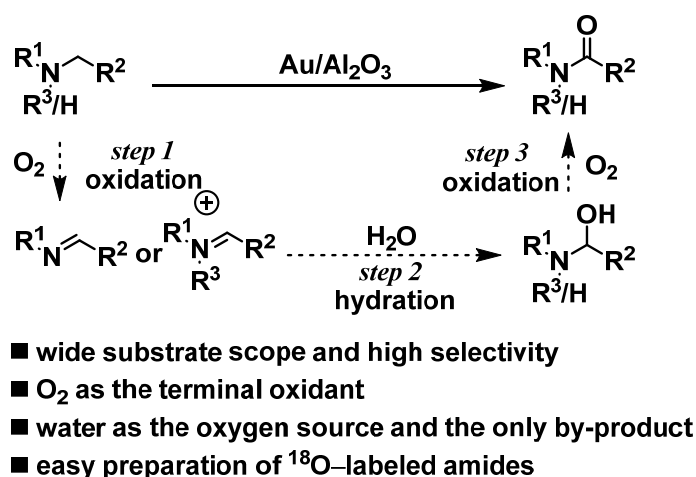


Figure 4-26. This work: Au/Al_2O_3 -catalyzed selective α -oxygenation of secondary and tertiary amines to the corresponding amides.

4-2.2. Experimental

4-2.2.1. Instruments and Reagents

Instruments and Reagents: Gas Chromatography (GC) analyses were performed on a Shimadzu GC-2014 equipped with a flame ionization detector (FID) and an InertCap-5 capillary column. GC mass spectrometry (GC-MS) spectra were recorded on a Shimadzu GCMS-QP2010 equipped with an InertCap-5 capillary column at an ionization voltage of 70 eV. Liquid-state NMR spectra were recorded on JEOL JNM-ECA-500 spectrometer. ^1H and ^{13}C NMR spectra were measured at 500 and 125 MHz, respectively, using tetramethylsilane (TMS) as an internal reference ($\delta = 0$ ppm). ICP-AES analyses were performed on a Shimadzu ICPS-8100. TEM observations were performed on JEOL JEM-2010HC. CeO_2 (BET: $111 \text{ m}^2 \text{ g}^{-1}$, Cat. No. 544841-25G, Aldrich), Al_2O_3 (BET: $160 \text{ m}^2 \text{ g}^{-1}$, Cat. No. KHS-24, Sumitomo Chemical), TiO_2 (BET: $316 \text{ m}^2 \text{ g}^{-1}$, Cat. No. ST-01, Ishihara Sangyo Kaisya), ZrO_2 (BET: $9 \text{ m}^2 \text{ g}^{-1}$, Cat. No. 37022, Nacalai Tesque), and ZnO (BET: $37 \text{ m}^2 \text{ g}^{-1}$, Cat. No. 260-01261, Wako) were acquired from commercial sources. Solvents and substrates were obtained from Kanto Chemical, TCI, Wako, or Aldrich (reagent grade), and purified prior to the use (if required).^[47]

4-2.2.2. Preparation of Catalysts

Preparation of Au/Al₂O₃: An aqueous solution of H₂AuCl₄·4H₂O (8.3 mM, 60 mL) containing Al₂O₃ (2.0 g) was vigorously stirred at room temperature. After 15 min, the pH of the solution was quickly adjusted to 10 by addition of an aqueous solution of NaOH (1.0 M), and the resulting slurry was further stirred for 24 h. The solid was then filtered off, washed with a large amount of water (3 L), and dried *in vacuo* to afford the supported hydroxide catalyst precursor. Then, the hydroxide precursor was calcined at 400 °C for 2 h, giving Au/Al₂O₃ as a purple powder (Au content: 4.1wt%). Various supported gold catalysts were prepared in the same method used to prepare Au/Al₂O₃.

Pd/Al₂O₃ (Pd: 2.5wt%), Ru/Al₂O₃ (Ru: 2.1wt%), and Rh/Al₂O₃ (Rh: 2.1wt%) were prepared using K₂PdCl₄, RuCl₃·*n*H₂O, and RhCl₃·3H₂O as the respective metal sources in the almost same procedures—the adjusted pH was 12 and the hydroxide precursors were reduced under a H₂ atmosphere for 30 min at 150 °C.^[48] Cu/Al₂O₃ (Cu: 2.5wt%) was prepared using CuCl₂·2H₂O as the metal source through the pH adjustment of 12 without the reduction.^[49]

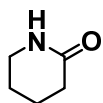
4-2.2.3. Reactions and Synthesis

Catalytic Reaction: Au/Al₂O₃ (4 mol %, 100 mg), amine (**1**, 0.5 mmol), H₂O (2 mL), and a Teflon-coated magnetic stir bar were successively placed in a Pyrex glass reactor (volume: ~20 mL) and the reaction mixture was purged with O₂ and vigorously stirred at 60–100 °C. After the reaction was completed, a large quantity of acetone and an internal standard (diphenyl) was added to the reaction mixture, and the conversions of **1** and the amide yields were determined by GC analysis. As for isolation of amide products, an internal standard was not added. After the reaction, the catalyst was filtered off (>95 % recovery), and then the filtrate was dried with Na₂SO₄ and concentrated by evaporation. The crude product was subjected to column chromatography on silica gel (typically using hexane/acetone as an eluent), giving the pure amides. The products were identified by GC-MS and NMR (¹H and ¹³C) analyses. The retrieved catalyst was washed with water and acetone, and calcined at 400 °C for 2 h before being used in the reuse experiment. Caution: the reaction using pure O₂ as the oxidant can be dangerous. Thus, the reactions should be conducted carefully.

Leaching Test: To establish whether the catalytic reaction occurred on solid Au/Al₂O₃ or not, the catalyst was removed by hot filtration 3 h after the reaction started under the optimized conditions and the reaction was again carried out with the filtrate under the same conditions. When the amount of leached metals was measured, the filtrate after the reaction proceeded for 24 h was evaporated *in vacuo*, treated with concentrated aqua regia (1 mL), and sonicated. Then, Au and Al species in the filtrate were analyzed by ICP-AES after the filtrate was moved into a 100 mL volumetric flask.

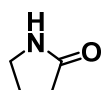
Reuse Test: After the reaction, Au/Al₂O₃ was retrieved from the reaction mixture by simple filtration using a PTFE membrane filter. The retrieved catalyst was washed with acetone (200 mL) and deionized water (100 mL), dried *in vacuo*, and calcined at 400°C for 2 h. Then, the catalyst was used for the reuse experiment using piperidine as the substrate under the optimized conditions.

4-2.2.4. Spectral Data of Products



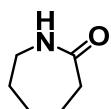
2a (CAS No. 675-20-7)

2-Piperidone (2a): ^1H NMR (500 MHz, CDCl_3 , TMS): δ 1.73–1.83 (m, 4H), 2.35 (t, J = 6.8 Hz, 2H), 3.30–3.32 (m, 2H), 7.18 (brs, 1H). ^{13}C – $\{^1\text{H}\}$ NMR (125 MHz, CDCl_3 , TMS): δ 20.90, 22.29, 31.52, 42.24, 172.94. MS (70 eV, EI): m/z (%): 99 (100) [M^+], 98 (18), 71 (11), 70 (23), 56 (13), 55 (31).



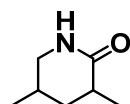
2b (CAS No. 616-45-5)

2-Pyrrolidone (2b): MS (70 eV, EI): m/z (%): 85 (100) [M^+], 84 (21), 56 (14).



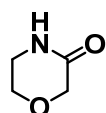
2c (CAS No. 105-60-2)

ε-Caprolactam (2c): MS (70 eV, EI): m/z (%): 113 (82) [M^+], 85 (53), 84 (47), 67 (12), 56 (78), 55 (100).



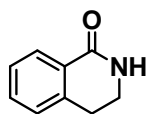
2d (CAS No. 179683-97-7)

3,5-Dimethyl-2-piperidone (*cis/trans* mixture, *cis:trans* = 2.5:1) (2d): MS (70 eV, EI): *cis*: m/z (%): 127 (55) [M^+], 112 (45), 98 (10), 85 (14), 84 (62), 70 (22), 69 (30), 57 (37), 56 (100), 55 (35); *trans*: 127 (56) [M^+], 112 (43), 85 (12), 84 (54), 70 (21), 69 (26), 57 (35), 56 (100), 55 (33).



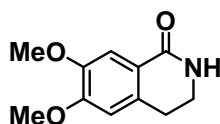
2e (CAS No. 109-11-5)

Morpholin-3-one (2e): MS (70 eV, EI): m/z (%): 101 (100) [M^+], 71 (44).



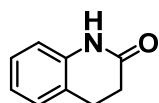
2f (CAS No. 1196-38-9)

3,4-Dihydroisoquinolin-1(2H)-one (2f): ^1H NMR (500 MHz, CDCl_3 , TMS): δ 2.95–2.98 (m, 2H), 3.54–3.58 (m, 2H), 7.19–7.21 (m, 1H), 7.32–7.36 (m, 1H), 7.41–7.45 (m, 1H), 7.78 (brs, 1H), 8.04–8.06 (m, 1H). ^{13}C – $\{^1\text{H}\}$ NMR (125 MHz, CDCl_3 , TMS): δ 28.24, 40.04, 127.02, 127.29, 127.79, 129.02, 132.11, 139.01, 166.95. MS (70 eV, EI): m/z (%): 147 (76) [M^+], 118 (100), 91 (13), 90 (68), 89 (27), 63 (11).



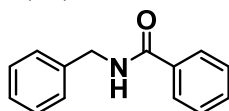
2g (CAS No. 493-49-2)

3,4-Dihydro-6,7-dimethoxyisoquinolin-1(2H)-one (2g): MS (70 eV, EI): m/z (%): 207 (100) [M^+], 208 (13), 179 (11), 178 (64), 163 (10), 150 (64), 135 (15).



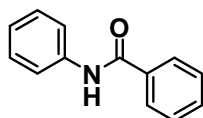
2h (CAS No. 553-03-7)

3,4-Dihydroquinolin-2(1H)-one (2h): MS (70 eV, EI): m/z (%): 147 (100) [M^+], 148 (10), 119 (75), 118 (89), 117 (11), 104 (18), 92 (31), 91 (25), 78 (16), 77 (16), 59 (13), 51 (13).



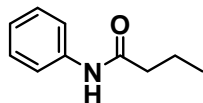
2i (CAS No. 1485-70-7)

N-Benzylbenzamide (2i): MS (70 eV, EI): m/z (%): 211 (58) [M^+], 210 (22), 106 (27), 105 (100), 91 (11), 77 (68), 51 (21).



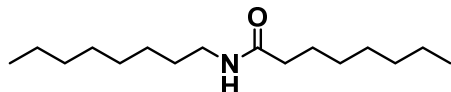
2j (CAS No. 93-98-1)

N-Phenylbenzamide (2j): MS (70 eV, EI): m/z (%): 197 (19) [M^+], 105 (95), 77 (100), 65 (20), 51 (33).



2k (CAS No. 1129-50-6)

N-Phenylbutanamide (2k): MS (70 eV, EI): m/z (%): 163 (4) [M^+], 94 (7), 93 (100), 92 (8), 77 (9), 71 (6), 66 (8), 65 (13), 51 (7).



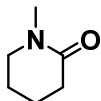
2l (CAS No. 42886-89-5)

N-Octyloctanamide (2l): MS (70 eV, EI): m/z (%): 255 (21) [M^+], 226 (17), 212 (19), 198 (21), 185 (11), 184 (81), 171 (61), 157 (17), 156 (55), 144 (11), 142 (16), 128 (33), 127 (41), 115 (13), 114 (65), 101 (23), 100 (41), 87 (33), 86 (55), 73 (76), 72 (23), 71 (21), 69 (13), 60 (12), 58 (19), 57 (100), 56 (12), 55 (37).



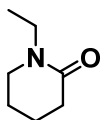
2m (CAS No. 872-50-4)

1-Methyl-2-pyrrolidone (2m): MS (70 eV, EI): m/z (%): 99 (100) [M^+], 98 (63), 70 (11).



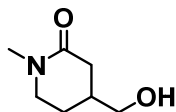
2n (CAS No. 931-20-4)

1-Methyl-2-piperidone (2n): MS (70 eV, EI): m/z (%): 113 (81) [M^+], 112 (23), 70 (31), 58 (14), 57 (100), 56 (20), 55 (49).



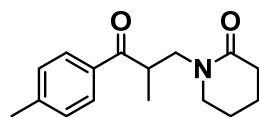
2o (CAS No. 4789-07-5)

1-Ethyl-2-piperidone (2o): MS (70 eV, EI): m/z (%): 127 (100) [M^+], 112 (56), 99 (17), 98 (45), 85 (15), 84 (81), 71 (19), 70 (11), 58 (23), 56 (40), 55 (31).



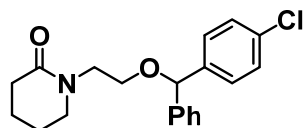
2p (CAS No. 20845-32-3)

4-(Hydroxymethyl)-1-methyl-2-piperidinone (2p): MS (70 eV, EI): m/z (%): 143 (89) [M^+], 126 (3), 115 (47), 113 (11), 112 (15), 100 (6), 84 (11), 82 (14), 74 (19), 70 (6), 58 (20), 57 (100), 55 (34).



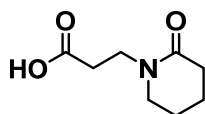
2q (CAS No. 1919899-17-4)

1-[2-Methyl-3-(4-methylphenyl)-3-oxopropyl]-2-piperidinone (2q): ^1H NMR (500 MHz, CDCl_3 , TMS): δ 1.18 (d, $J = 7.5$ Hz, 3H), 1.43–1.52 (m, 1H), 1.53–1.59 (m, 1H), 1.62–1.70 (m, 1H), 2.21–2.27 (m, 1H), 2.28–2.35 (m, 1H), 2.41 (s, 3H), 3.18–2.26 (m, 2H), 3.29–3.33 (dd, $J = 13.5$ and 6.0 Hz, 1H), 3.66–3.70 (dd, $J = 13.0$ and 8.5 Hz, 1H), 4.13–4.20 (m, 1H), 7.27 (d, $J = 8.0$ Hz, 2H), 7.92 (d, $J = 8.0$ Hz, 2H). ^{13}C – $\{^1\text{H}\}$ NMR (125 MHz, CDCl_3 , TMS): δ 15.74, 21.15, 21.72, 23.24, 32.44, 38.79, 50.56, 52.51, 128.66, 129.43, 134.32, 144.21, 170.50, 203.57. MS (70 eV, EI): m/z (%): 259 (16) [M^+], 160 (11), 140 (100), 119 (76), 112 (64), 100 (26), 99 (11), 91 (46), 84 (55), 65 (19), 56 (22), 55 (22).



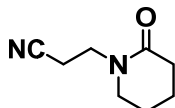
2r (CAS No. 1919899-18-5)

1-[2-[(4-Chlorophenyl)phenylmethoxy]ethyl]-piperidinone (2r): ^1H NMR (500 MHz, CDCl_3 , TMS): δ 1.74–1.80 (m, 4H), 2.34–2.36 (m, 2H), 3.43–3.46 (m, 2H), 3.57–3.63 (m, 4H), 5.31 (s, 1H), 7.24–7.33 (m, 9H). ^{13}C – $\{^1\text{H}\}$ NMR (125 MHz, CDCl_3 , TMS): δ 21.47, 23.51, 32.45, 47.72, 50.01, 67.56, 83.26, 126.94, 127.85, 128.28, 128.63, 128.67, 133.30, 140.91, 141.77, 170.01. MS (70 eV, EI): m/z (%): 201 (12), 166 (13), 165 (19), 142 (47), 128 (8), 127 (100), 112 (50), 99 (7), 98 (6), 84 (18), 77 (1), 56 (6), 55 (5).



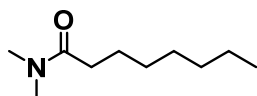
2s (CAS No. 117705-04-1)

3-(2-Oxopiperidin-1-yl)propanoic acid (2s): MS (70 eV, EI): m/z (%): 171 (41) [M^+], 126 (28), 125 (16), 124 (11), 115 (42), 112 (34), 99 (22), 98 (49), 97 (10), 84 (100), 82 (14), 71 (13), 70 (17), 69 (10), 56 (61), 55 (61), 54 (11), 53 (11).



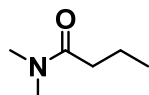
2t (CAS No. 73186-30-8)

2-Oxo-1-piperidinepropanenitrile (2t): ^1H NMR (500 MHz, CDCl_3 , TMS): δ 1.81–1.88 (m, 4H), 2.40 (t, $J = 6.5$ Hz, 2H), 2.70 (t, $J = 6.3$ Hz, 2H), 3.48 (t, $J = 5.8$ Hz, 2H), 3.59 (t, $J = 6.3$ Hz, 2H). ^{13}C - $\{^1\text{H}\}$ NMR (125 MHz, CDCl_3 , TMS): δ 16.05, 21.13, 23.26, 32.26, 44.22, 49.74, 118.46, 170.49. MS (70 eV, EI): m/z (%): 152 (84) [M^+], 112 (80), 99 (13), 98 (25), 84 (100), 83 (12), 56 (25), 55 (26).



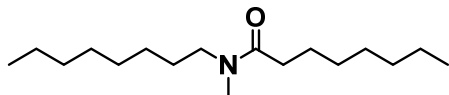
2u (CAS No. 1118-92-9)

***N,N*-Dimethyloctanamide (2u):** MS (70 eV, EI): m/z (%): 171 (2) [M^+], 100 (20), 87 (100), 72 (33), 57 (14).



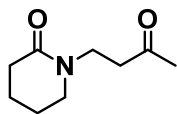
2v (CAS No. 1118-92-9)

***N,N*-Dimethylbutanamide (2v):** MS (70 eV, EI): m/z (%): 115 (81) [M^+], 100 (28), 87 (100), 72 (73), 71 (20), 58 (10), 55 (10).



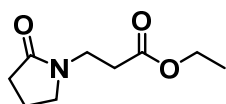
2w (CAS No. 76058-03-2)

***N*-Methyl-*N*-octyloctanamide (2w):** MS (70 eV, EI): m/z (%): 269 (1) [M^+], 198 (17), 171 (12), 170 (100), 114 (12), 100 (16), 87 (40), 73 (14), 58 (25), 57 (54), 55 (17).



2x (CAS No. 1339447-48-1)

1-(3-Oxobutyl)-2-piperidinone (2x): MS (70 eV, EI): m/z (%): 169 (25) [M^+], 127 (10), 126 (100), 112 (16), 99 (11), 98 (37), 84 (25), 56 (13), 55 (13).



2y (CAS No. 61930-87-8)

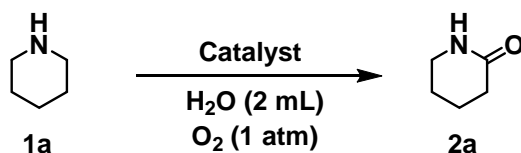
1-(2-Oxopyrrolidine)propanoic acid ethylester (2y): MS (70 eV, EI): m/z (%): 185 (44) [M^+], 157 (3), 140 (35), 139 (15), 129 (3), 128 (4), 112 (34), 111 (40), 98 (100), 84 (20), 83 (11), 70 (56), 69 (16), 56 (13).

4-2.3. Results and Discussion

4-2.3.1. Effect of Catalysts

Initially, various supported metal catalysts (designated as metal/support) were prepared and applied to the α -oxygenation of piperidine (**1a**) into 2-piperidone (**2a**) (Table 4-6). The reaction was carried out in water at 100 °C in O₂ (1 atm). Under these conditions, it was confirmed that **2a** was not obtained in the presence of pure Al₂O₃ or in the absence of catalysts (Table 4-6, entries 14 and 15). In the presence of Pd/Al₂O₃, only a trace amount of **2a** was obtained (Table 4-6, entry 1). Other supported metal catalysts, such as Ru/Al₂O₃, Rh/Al₂O₃, and Cu/Al₂O₃ did not show any catalytic activity for the present transformation (Table 4-6, entries 2–4). Notably, Au/Al₂O₃ promoted the reaction significantly (Table 4-6, entry 5), and a quantitative yield of **2a** was obtained after 24 h (Table 4-6, entry 6). Among the various supports examined, Al₂O₃ was the best (Table 4-6, entries 5–10). The gold amount determined by ICP-AES and mean size of gold nanoparticles calculated from TEM images (Figure 4-27) on each support are summarized in Table 4-7. The reaction using Au/Al₂O₃ in air (1 atm) only gave a trace amount of **2a** (Table 4-6, entry 11), while a 57% yield of **2a** was obtained in pressurized air (5 atm; Table 4-6, entry 12). The reaction did not proceed at all under an Ar atmosphere (Table 4-6, entry 13), which indicates that O₂ is the terminal oxidant in the oxygenation reaction.

Table 4-6. α -Oxygenation of piperidine (**1a**) to piperidone (**2a**) with various supported metal catalysts.^[a]



Entry	Catalyst	Conv. [%]	Yield [%]
1	Pd/Al ₂ O ₃	30	3
2	Ru/Al ₂ O ₃	26	<1
3	Rh/Al ₂ O ₃	23	<1
4	Cu/Al ₂ O ₃	24	<1
5	Au/Al ₂ O ₃	83	63
6 ^[b]	Au/Al ₂ O ₃	>99	>99
7	Au/ZnO	66	52
8	Au/ZrO ₂	57	40
9	Au/CeO ₂	54	34
10	Au/TiO ₂	38	10
11 ^[c]	Au/Al ₂ O ₃	7	6
12 ^[d]	Au/Al ₂ O ₃	>99	57
13 ^[b,e]	Au/Al ₂ O ₃	4	<1
14 ^[f]	Al ₂ O ₃	<1	<1
15	none	<1	<1

[a] Reaction conditions: **1a** (0.5 mmol), catalyst (4 mol%), H₂O (2 mL), O₂ (1 atm), 100 °C, 3 h. Conversions and yields were determined by GC analysis. [b] 24 h. [c] Air (1 atm). [d] Air (5 atm). The low carbon balance is likely due to volatilization of **1a** during the reaction. [e] Ar (1 atm). [f] Al₂O₃ (100 mg).

Table 4-7. Au content and average particle sizes of various supported Au nanoparticle catalysts.

Catalyst	Metal content [mmol g ⁻¹]	Average size [nm]	Standard deviation [nm]
Au/Al ₂ O ₃	0.208	4.9	1.4
Au/ZnO	0.183	3.3	0.9
Au/ZrO ₂	0.112	9.5	3.0
Au/CeO ₂	0.234	3.5	1.3
Au/TiO ₂	0.147	2.2	0.5

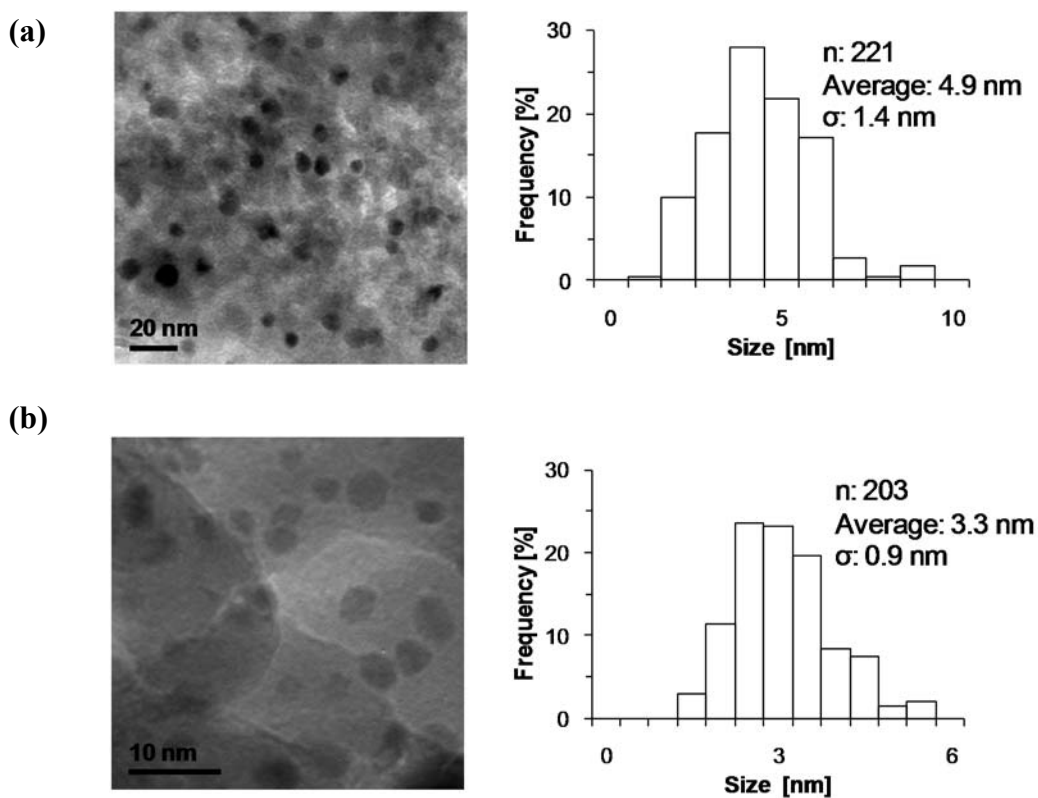


Figure 4-27. TEM images and Au particle size distributions of (a) Au/Al₂O₃ (average: 4.9 nm, σ : 1.4 nm) and (b) Au/ZnO (average: 3.3 nm, σ : 0.9 nm).

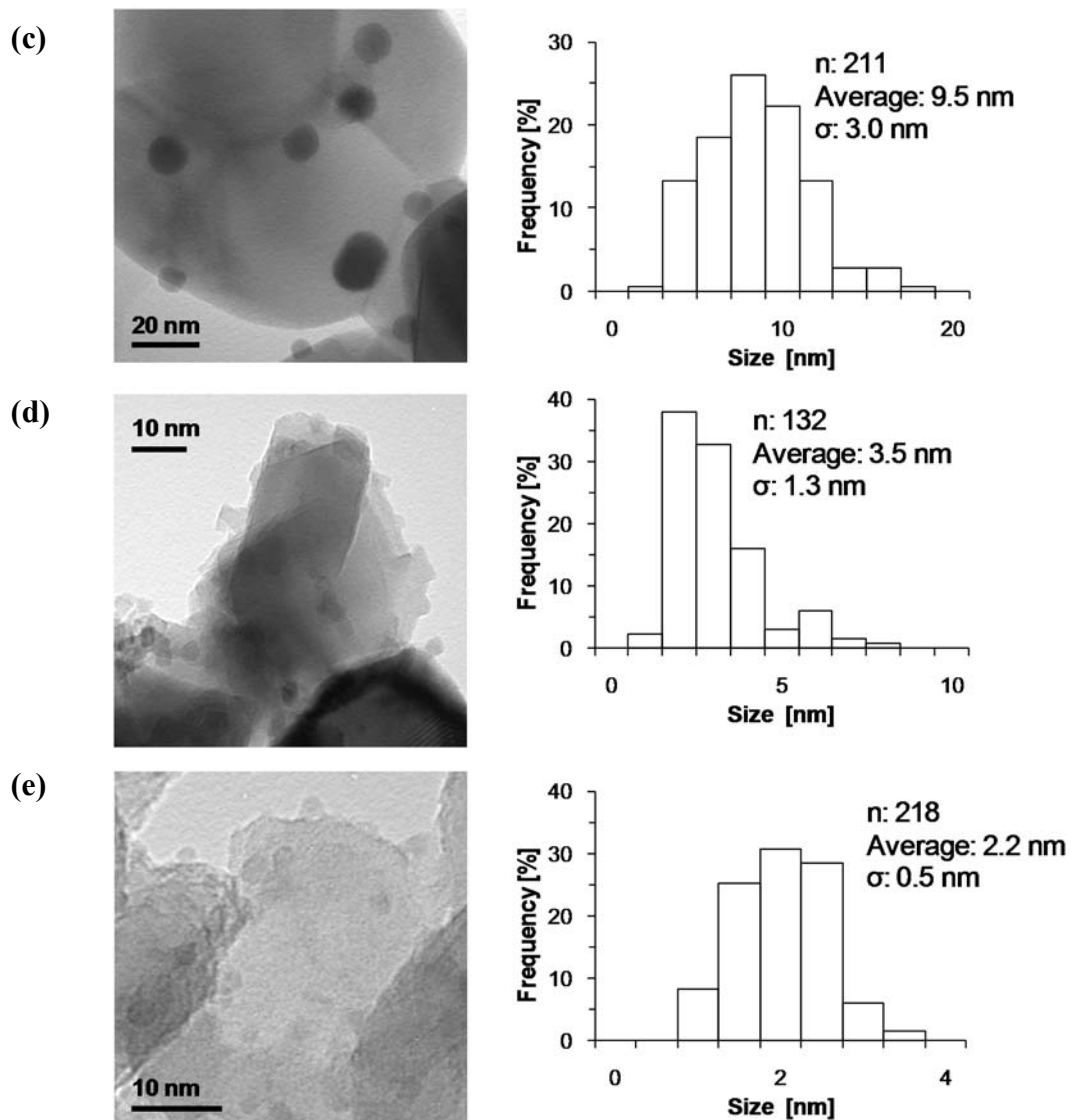


Figure 4-27 (continued). TEM images and Au particle size distributions of (c) Au/ZrO₂ (average: 9.5 nm, σ : 3.0 nm), (d) Au/CeO₂ (average: 3.5 nm, σ : 1.3 nm), and (e) Au/TiO₂ (average: 2.2 nm, σ : 0.5 nm).

4-2.3.2. Heterogeneous Catalysis and Catalyst Reuse

To verify whether the observed catalysis for the present reaction was truly heterogeneous, Au/Al₂O₃ was removed by hot filtration when the yield of **2a** reached approximately 60%, and the reaction then carried out with the filtrate under the same reaction conditions. As shown in Figure 4-28, the reaction completely stopped upon removal of Au/Al₂O₃. Furthermore, the analysis of the filtrate by inductively coupled plasma atomic emission spectroscopy (ICP-AES) revealed that gold species were hardly present in the filtrate (that is, gold was not present in quantities above the instrumental detection limit: Au <0.008%). These experimental results indicate that catalysis did not originate from gold species leached from the catalyst, and thus, the described catalyst is deemed intrinsically heterogeneous. After the reaction, Au/Al₂O₃ can be easily retrieved by simple filtration, achieving >95% recovery. The retrieved catalyst can be reused several times, though the yields of the desired product (**2a**) gradually decreased after repeated reuse experiments (Figure 4-29). This is likely because of the aggregation of gold nanoparticles; the average particle size of gold increased from 4.9 nm (fresh catalyst) to 7.3 nm (1st use) and to 9.9 nm after the third reuse experiment (Figure 4-30).

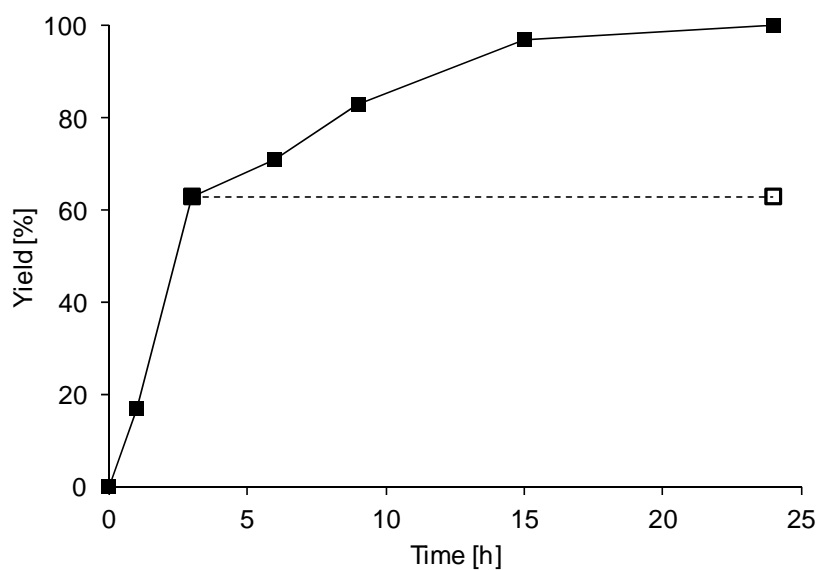


Figure 4-28. Effect of removal of the Au/Al₂O₃ catalyst on α -oxygenation of piperidine (**1a**) to 2-piperidone (**2a**). Reaction conditions are the same as those described in Table 4-6. GC yields are shown here.

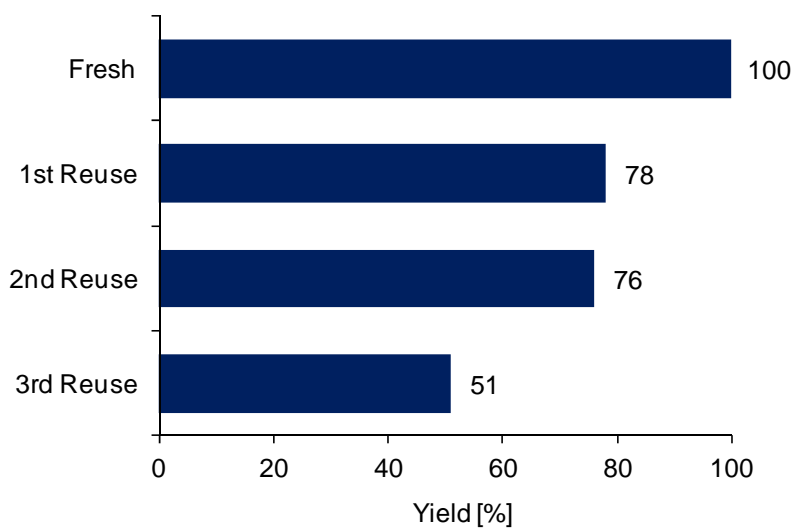


Figure 4-29. Au/Al₂O₃ reuse experiments for α -oxygenation of piperidine (**1a**) to 2-piperidone (**2a**). Reaction conditions are the same as those described in Table 4-6. GC yields are shown here.

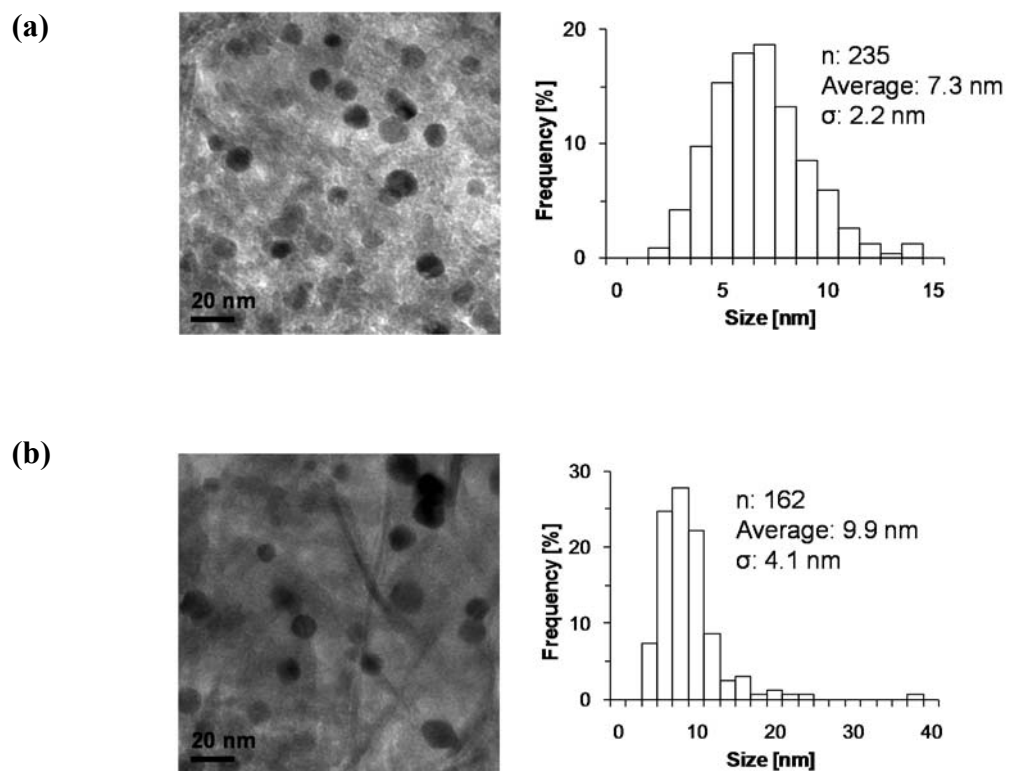


Figure 4-30. TEM images and Au particle size distributions of (a) Au/Al₂O₃ after the 1st use (average: 7.3 nm, σ : 2.2 nm) and (b) Au/Al₂O₃ after the 3rd reuse experiment (average: 9.9 nm, σ : 4.1 nm).

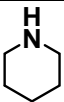
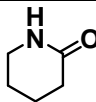
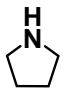
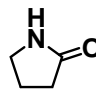
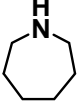
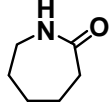
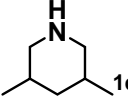
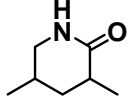
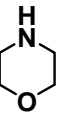
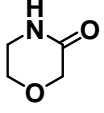
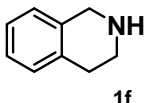
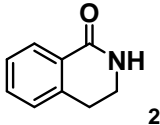
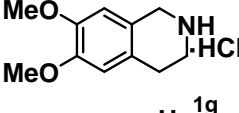
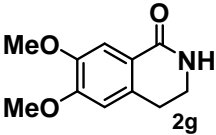
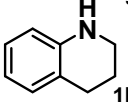
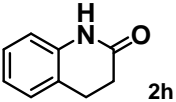
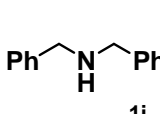
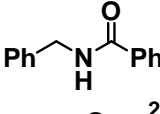
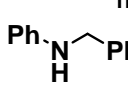
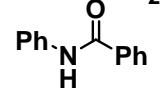
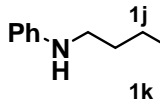
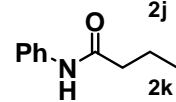
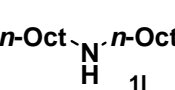
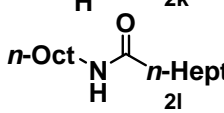
4-2.3.3. Substrate Scope

With the optimized reaction conditions in hand, the substrate scope for α -oxygenation was examined. As shown in Table 4-8, various secondary cyclic and linear amines can be oxygenated to produce the corresponding amides in moderate to high yields. The α -oxygenation of five-, six-, and seven-membered cyclic amines efficiently proceeded to give the corresponding lactams (Table 4-8, entries 1–8). When morpholine (**1e**) was used as a substrate, it was exclusively oxygenated in the 3-position to give the corresponding amide, and oxygenation did not occur at the 2-position (Table 4-8, entry 5). Furthermore, the α -oxygenation of tetrahydroisoquinoline derivatives (**1f** and **1g**) effectively proceeded at the benzylic positions (Table 4-8, entries 6 and 7). Although tetrahydroquinoline (**1h**) was oxygenated to afford the corresponding amide (34%), quinoline (51%) was a major product in this case (Table 4-8, entry 8). Various linear amines were oxygenated to give the corresponding amides in moderate yields (Table 4-8, entries 9–12). The relatively low yields are mainly due to the formation of aldehydes, carboxylic acids, and amines as the by-products (Figure 4-31). Specifically, the imine or iminium intermediates formed by the oxidation of secondary or tertiary amines are hydrolyzed to give amines and aldehydes. The aldehydes formed are further oxidized to the corresponding carboxylic acids. The primary amines are oxidized to aldimines followed by hydrolytic decomposition/oxidation, giving the corresponding carboxylic acids.

The present catalytic system was also applicable to the α -oxygenation of tertiary amines. As shown in Table 4-9, various kinds of cyclic and linear tertiary amines were efficiently oxygenated to give the corresponding amides. The present α -oxygenation method was especially powerful for the selective synthesis of lactams from cyclic tertiary amines. The five- and six-membered tertiary cyclic amines were all exclusively oxygenated at cyclic *N*-methylene positions to give the corresponding lactams in high yields (Table 4-9, entries 1–8). A cyclic tertiary amine with an alcohol group reacted well, and the hydroxy group in **2p** remained intact (Table 4-9, entry 4). Tolperisone, a well-known muscle relaxant,^[50] was also a suitable substrate, and selectively oxygenated at the ring position (Table 4-9, entry 5). Cloperastine, a cough suppressant,^[51] was also selectively oxygenated to give the corresponding amide, leaving chloride and ether functional groups intact (Table 4-9, entry 6). As for the ester

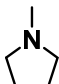
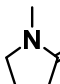
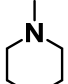
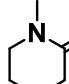
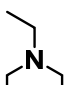
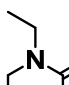
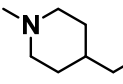
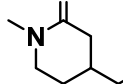
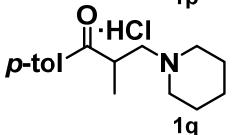
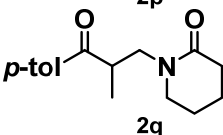
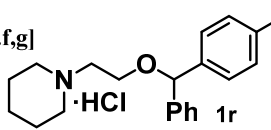
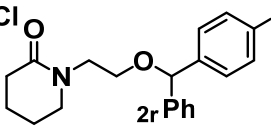
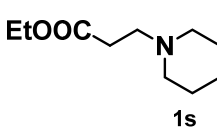
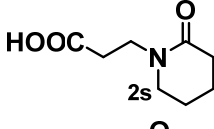
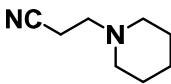
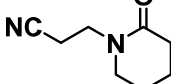
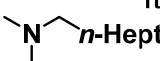
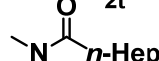
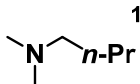
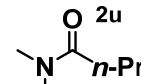
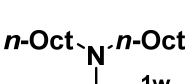
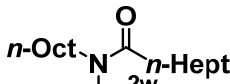
group substituted amine **1s**, the oxygenation proceeded efficiently, although the ester group was hydrolyzed into the corresponding carboxylic acid functional group (Table 4-9, entry 7). A cyclic tertiary amine substituted with a nitrile group reacted smoothly without hydrolysis or hydration of the nitrile group (Table 4-9, entry 8). Linear tertiary amines were also oxygenated in moderate to high yields (Table 4-9, entries 9–11). It should be noted that the aforementioned α -oxygenation of tertiary amines proceeded in a highly regioselective manner and exclusively gave one regioisomer. Such high regioselectivity is likely derived from the high stability of iminium and/or hemiaminal intermediates compared with the counterparts, but kinetic reasons like steric effects cannot be excluded. Furthermore, **2t** was successfully synthesized starting from **1a** and acrylonitrile through an aza-Michael addition/ α -oxygenation one-pot sequential reaction (Figure 4-32a). Methylvinylketone and ethylacrylate can also be applied to the sequential reaction (Figure 4-32b and c). In the case of methylvinylketone used as the substrate, an enaminone by-product (ethyl (*E*)-3-(pyrrolidin-1-yl)acrylate) was formed in 9% yield.

Table 4-8. Scope of the α -oxygenation of “secondary” amines.^[a]

Entry	Substrate	Product	Conv. [%]	Yield [%]
1	 1a	 2a	>99	>99(80)
2	 1b	 2b	>99	>99
3	 1c	 2c	>99	52
4 ^[b,c]	 1d	 2d	98	40(41)
5 ^[b,c]	 1e	 2e	52	51
6	 1f	 2f	>99	94(77)
7 ^[d]	 1g	 2g	>99	>99
8 ^[e]	 1h	 2h	85	34
9 ^[c,f,g]	 1i	 2i	>99	63
10 ^[f,g]	 1j	 2j	>99	51
11 ^[b,c,f,g]	 1k	 2k	>99	57
12 ^[b,c,f,h]	 1l	 2l	99	75

[a] Reaction conditions: **1** (0.5 mmol), Au/Al₂O₃ (4 mol%), H₂O (2 mL), O₂ (1 atm), 100 °C, 24 h. Conversions and yields were determined by GC analysis. The values in the parentheses are the isolated yields. For entry 6, the average isolated yield for two runs (containing $\pm 4\%$ error) is shown. [b] 80 °C. [c] Au/Al₂O₃ (8 mol%). [d] NaOH (1.5 mmol). [e] Quinoline was formed in 51% yield. [f] 1,4-dioxane/H₂O (0.1 mL/1.9 mL). [g] NaOH (1.0 mmol). [h] 48 h.

Table 4-9. Scope of the α -oxygenation of “tertiary” amines.^[a]

Entry	Substrate	Product	Conv. [%]	Yield [%]
1	 1m	 2m	>99	>99
2	 1n	 2n	>99	96
3 ^[b]	 1o	 2o	>99	86(75)
4 ^[c]	 1p	 2p	99	73(72)
5 ^[b,d,e]	 1q	 2q	98	85(66)
6 ^[c,f,g]	 1r	 2r	99	99(93)
7 ^[b,d,f]	 1s	 2s	>99	94(91)
8 ^[c]	 1t	 2t	>99	>99(98)
9 ^[b,c,h]	 1u	 2u	99	87(78)
10 ^[b,c,h]	 1v	 2v	>99	71
11 ^[b,c,h,i]	 1w	 2w	95	49(45)

[a] Reaction conditions: **1** (0.5 mmol), Au/Al₂O₃ (4 mol%), H₂O (2 mL), O₂ (1 atm), 80 °C, 24 h. Conversions and yields were determined by GC analysis. The values in the parentheses are the isolated yields. For entry 9, the average isolated yield for two runs (containing $\pm 3\%$ error) is shown. [b] Au/Al₂O₃ (8 mol%). [c] 60 °C. [d] 1,4-dioxane/H₂O (0.1 mL/1.9 mL). [e] NaOH (1.5 mmol). [f] NaOH (1.0 mmol). [g] THF/H₂O (0.5 mL/1.5 mL). [h] THF/H₂O (1.7 mL/0.3 mL). [i] 48 h.

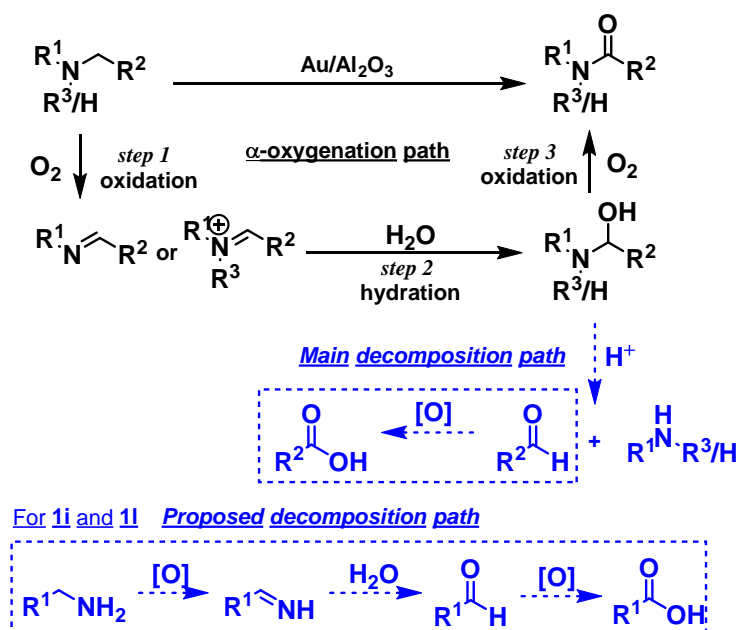


Figure 4-31. Possible paths for the by-product formation.

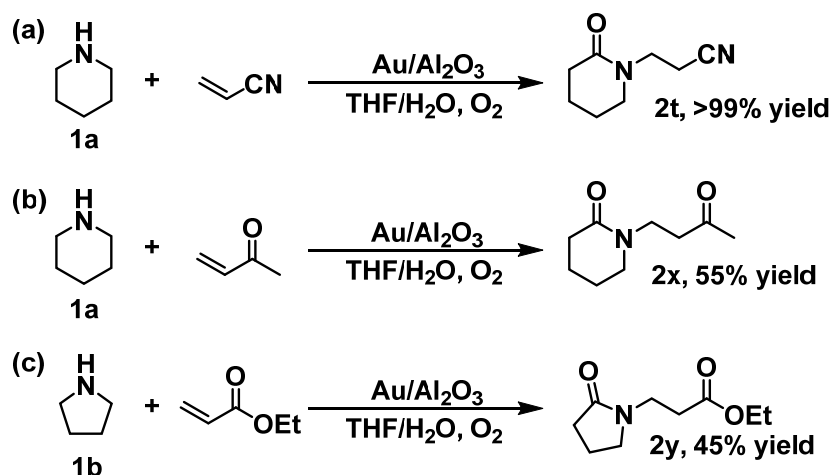


Figure 4-32. The sequential aza-Michael addition/ α -oxygenation reactions. Reaction conditions: **1** (0.5 mmol), acrylonitrile, methylvinylketone or ethylacrylate (0.5 mmol), Au/Al₂O₃ (4 mol%), THF/H₂O (1 mL/1 mL), O₂ (1 atm), 50 °C, 24 h. Yields were determined by GC analysis.

4-2.3.4. Mechanistic Studies

When the oxidation of dibenzylamine (**1i**) by Au/Al₂O₃ was performed in 1,4-dioxane in the absence of water, *N*-benzylidenebenzylamine (**3i**) was obtained in 46% yield (Figure 4-33a). Additionally, the reaction of **3i** in water afforded the corresponding amide **2i** in 63% yield. These results suggest the involvement of imines as intermediates in the α -oxygenation of secondary amines (Figure 4-33b). Similarly, for the α -oxygenation of tertiary amines, iminium intermediates are likely formed through the oxidation of tertiary amines by Au/Al₂O₃. It was observed that aldehydes, carboxylic acids, and amines were formed as by-products during the reaction. Consequently, it is possible that the present α -oxygenation reaction proceeds through an initial hydrolysis of imine or iminium intermediates into aldehydes and amines, followed by the reaction of these decomposed intermediates to afford the amide products. To confirm this hypothesis, the reaction of benzylamine and benzaldehyde was carried out. In this case, **2i** was indeed formed in 33% yield, together with 54% of benzoic acid (Figure 4-33c). The oxygenation of **3i** in the presence of [2,3,4,5,6-D₅]-benzaldehyde gave a 66% yield of **2i**, and the [D₅]-phenyl group content in the product was 36% (Figure 4-33d). Therefore, the present α -oxygenation reaction mainly proceeds through the pathway shown in Figure 4-26, but partly through the aforementioned hypothetical pathway.

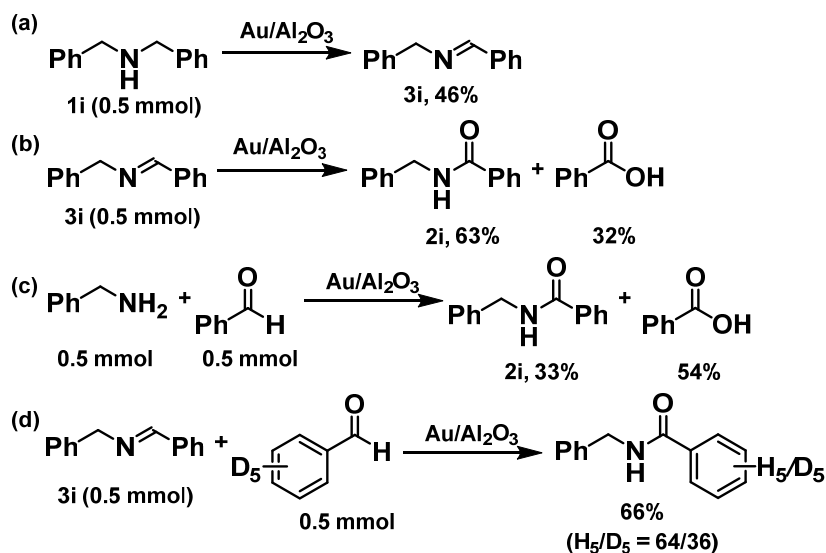
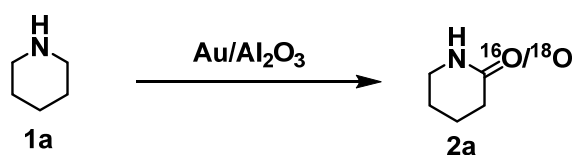


Figure 4-33. Mechanistic studies. Reaction conditions for (a): Au/Al₂O₃ (4 mol%), 1,4-dioxane (2 mL), O₂ (1 atm), 100 °C, 24 h; for (b)–(d): Au/Al₂O₃ (8 mol%), NaOH (1 mmol), H₂O (2 mL), O₂ (1 atm), 100 °C, 24 h. GC yields are shown here.

The α -oxygenation of **1a** in H₂¹⁸O, using ¹⁶O₂ (1 atm) as the oxidant, resulted in a 93% ¹⁸O incorporation at the amide carbonyl group (Table 4-10, entry 2). This high labeling ratio of ¹⁸O in **2a** demonstrates the potential utility of the present α -oxygenation method for the preparation of ¹⁸O-labeled amides. Indeed, several ¹⁸O-labeled amides were successfully synthesized by the present method using H₂¹⁸O (Figure 4-34). In contrast, the α -oxygenation of **1a** in H₂¹⁶O using ¹⁸O₂ (1 atm) as the oxidant gave **2a** with only 1% ¹⁸O labeling at the amide carbonyl group (Table 4-10, entry 3). These results suggest that the oxygen atom in the amide group was derived from water rather than O₂, thus supporting the involvement of hemiaminal intermediates formed by hydration of imine or iminium intermediates. Finally, the oxidation of the hemiaminal intermediates by Au/Al₂O₃ gave the corresponding amide products.

Table 4-10. α -oxygenation of piperidine (**1a**) using H₂¹⁸O or ¹⁸O₂.^[a]



Entry	Solvent	Atmosphere	Conv. [%]	Yield [%]	2a (¹⁶ O)/ 2a (¹⁸ O)
1	H ₂ ¹⁶ O	¹⁶ O ₂	>99	83	>99/<1
2	H ₂ ¹⁸ O	¹⁶ O ₂	>99	81	7/93
3	H ₂ ¹⁶ O	¹⁸ O ₂	95	52	99/1

[a] Reaction conditions: **1a** (0.5 mmol), Au/Al₂O₃ (4 mol%), H₂O (1 g), O₂ (1 atm), 100 °C, 24 h. Conversions and yields were determined by GC analysis.

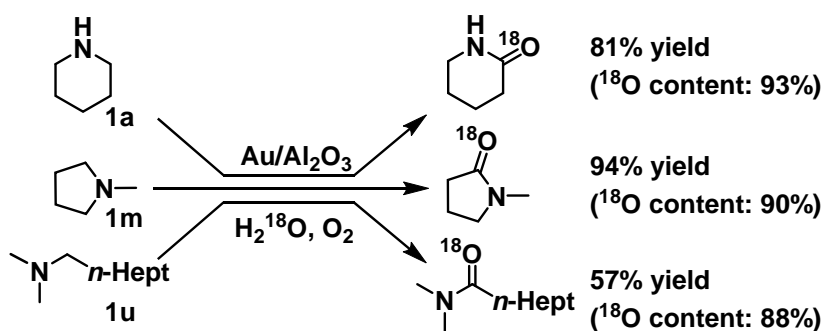


Figure 4-34. Syntheses of ^{18}O -labeled amides. Reaction conditions: for **1a**: **1a** (0.5 mmol), $\text{Au}/\text{Al}_2\text{O}_3$ (4 mol%), H_2^{18}O (0.9 mL), O_2 (1 atm), 100 $^\circ\text{C}$, 24 h. For **1m**: **1m** (0.5 mmol), $\text{Au}/\text{Al}_2\text{O}_3$ (4 mol%), THF (0.5 mL), H_2^{18}O (0.5 mL), O_2 (1 atm), 60 $^\circ\text{C}$, 24 h. For **1u**: **1u** (0.5 mmol), $\text{Au}/\text{Al}_2\text{O}_3$ (8 mol%), THF (1.7 mL), H_2^{18}O (0.3 mL), O_2 (1 atm), 60 $^\circ\text{C}$, 24 h. Yields were determined by GC analysis.

The oxygenation of **1n** in the presence of a stoichiometric amount of 2,2,6,6-tetramethylpiperidine 1-oxyl (TEMPO) in O₂ (1 atm) was 2.4 times faster than the oxygenation without TEMPO, and the formation of 1-hydroxy-2,2,6,6-tetramethylpiperidine (TEMPOH) was observed (Figure 4-35). The reaction in the presence of TEMPO in O₂ without Au/Al₂O₃ did not give **2n**. Furthermore, the acceleratory effect of TEMPO was also observed for the oxygenation of a secondary amine **1a** (Figure 4-36). Additionally, the oxygenation of **1n** using 1 equiv. of TEMPO (with respect to **1n**) as the terminal oxidant in Ar (1 atm), proceeded to give **2n** in 25% yield together with TEMPOH (96% yield based on TEMPO; Figure 4-35). Under the same reaction conditions, the oxygenation of **1a** also gave **2a** in 11% yield, concomitant with TEMPOH (41% yield; Figure 4-36). This 1:4 amide/TEMPOH stoichiometry is consistent with that of the overall reaction shown in Figure 4-37. It has been reported that TEMPO can work as a one-electron oxidant to abstract a hydrogen atom from Au–H species, where TEMPO itself is reduced to TEMPOH (refer to section 3-1.3.4. and the reference of [12] in Chapter III). Thus, the above experimental results indicate the involvement of Au–H species during the reaction, and suggest that an Au–H species is likely formed during the oxidation of amines and the hemiaminal intermediates. Specifically, β -H elimination after coordination of amines and hemiaminals to gold would generate Au–H species. TEMPO acts as a one-electron oxidant to effectively regenerate the active gold species through the oxidation of Au–H species. In contrast, two electron oxidants, such as pyridine *N*-oxide, hardly promoted the oxygenation of **1n** and **1a** (Figures 4-35 and 4-36), suggesting that this type of oxidant is not suitable for the oxidation of Au–H species. The substantial promotional effect of TEMPO on the reaction indicates that the oxidation of Au–H species is likely involved in the turnover-limiting step. The aforementioned reaction is faster in O₂ (1 atm) than in air (1 atm), which also supports the involvement of the oxidation of Au–H species by O₂ in the turnover-limiting step. The slow oxidation of Au–H species retards the oxidation of hemiaminal intermediates, which results in the competing hydrolytic decomposition of imine or iminium intermediates.

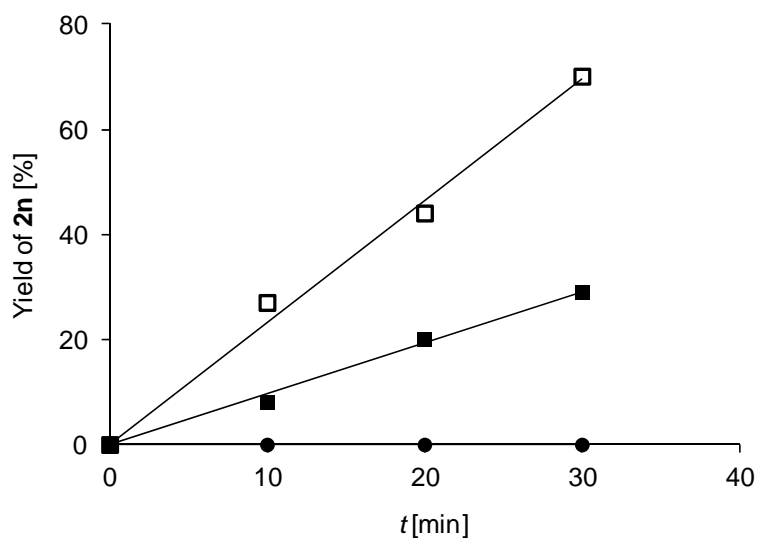
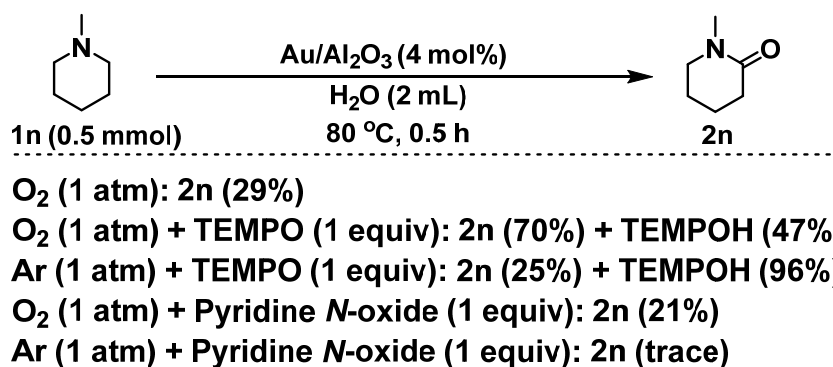


Figure 4-35. Effect of various oxidants on the present α -oxygenation of a tertiary amine. Reaction conditions: **1n** (0.5 mmol), Au/Al₂O₃ (4 mol%), H₂O (2 mL), 80 °C, 0.5 h. Yields were determined by GC analysis. Open squares indicate the reaction profile in the presence of TEMPO (0.5 mmol) in O₂ (1 atm), line fit: Yield = 2.32*t* (*R*² = 0.99); closed squares indicate the reaction profile without TEMPO in O₂ (1 atm), line fit: Yield = 0.96*t*, (*R*² = 0.99); closed circles indicate the reaction profile in the presence of TEMPO (0.5 mmol) in O₂ (1 atm) without Au/Al₂O₃.

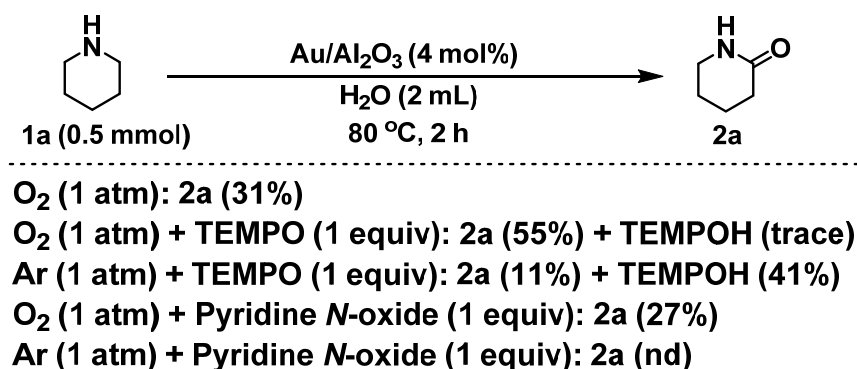


Figure 4-36. Effect of various oxidants on the present α -oxygenation of a secondary amine. Reaction conditions: **1a** (0.5 mmol), Au/Al₂O₃ (4 mol%), H₂O (2 mL), 80 °C, 2 h. Yields were determined by GC analysis.

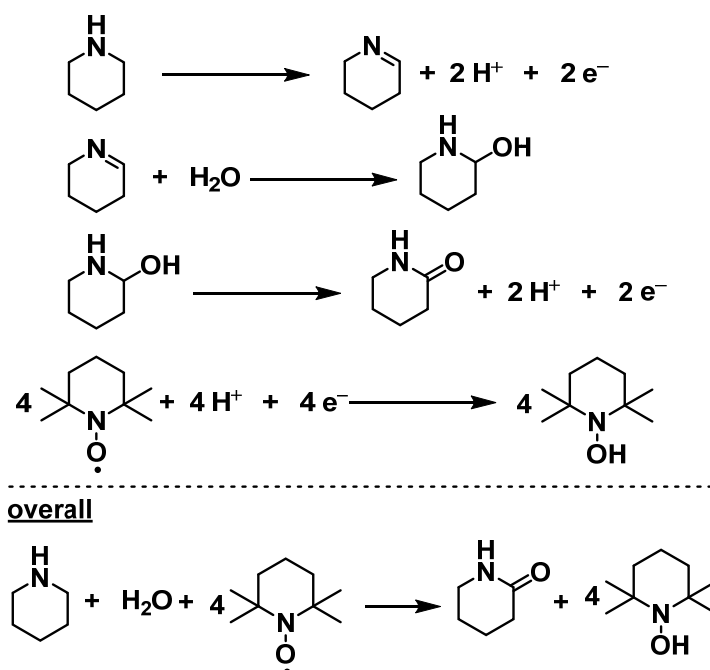


Figure 4-37. Reaction stoichiometry for the oxygenation using TEMPO as the oxidant.

On the basis of the aforementioned experimental results, the overall mechanism of the present Au-catalyzed α -oxygenation of amines to amides is shown in Figure 4-38 (in the case of tertiary amines). Firstly, amines coordinate to gold nanoparticles, followed by β -hydride elimination to produce iminium cations concomitant with an Au–H species. The iminium cations are hydrated toward hemiaminals, which adsorb onto Au nanoparticles *via* deprotonation by the basic sites of supports. Finally, β -hydride elimination occurs to give the desired amides and Au–H species. The Au–H species are oxidized to Au and H₂O using O₂ as the terminal oxidant, leading to the achievement of the catalytic cycle.

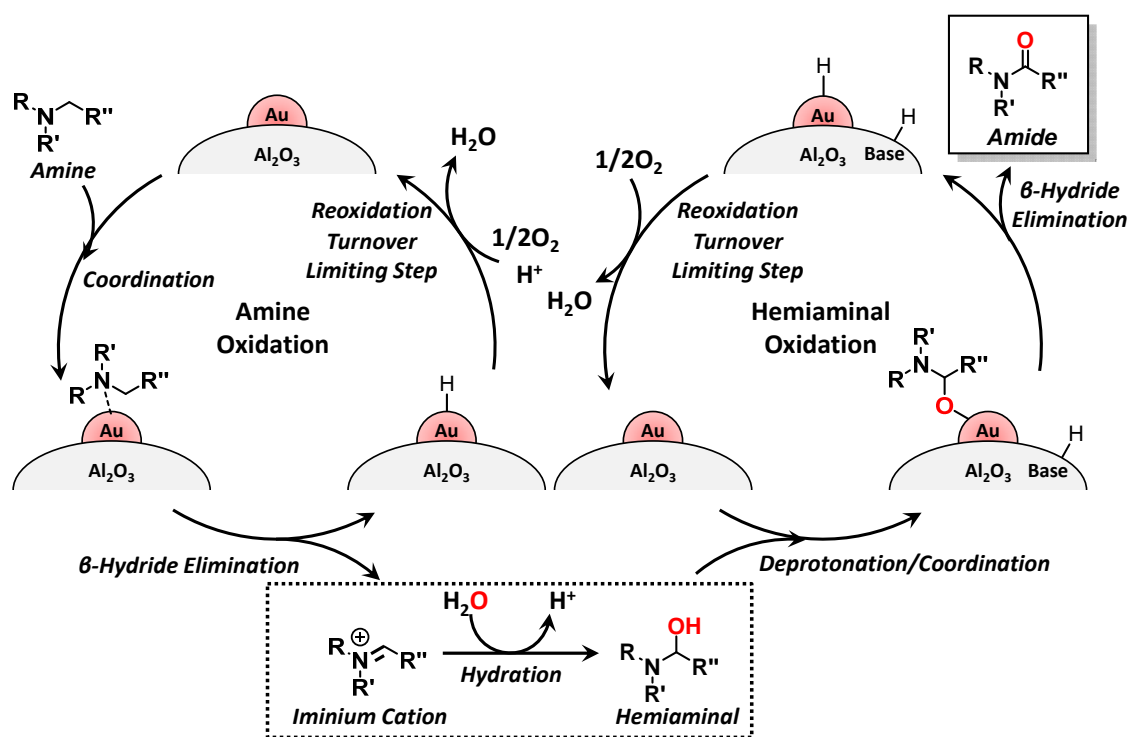


Figure 4-38. Overall plausible reaction mechanism of the present α -oxygenation.

4-2.4. Summary

In summary, an efficient heterogeneously Au/Al₂O₃-catalyzed α -oxygenation of secondary and tertiary amines has been successfully developed for the first time using O₂ as the sole oxidant. Additionally, this reaction provides a convenient method for the synthesis of ¹⁸O-labeled amides when H₂¹⁸O is used for the reaction media. Owing to the practicality of the reaction conditions, I hope that this α -oxygenation method will find wide application in the synthesis of amide derivatives and related compounds.

In addition, remarkably, I discovered the unusual selectivity to tertiary amine oxidation catalyzed by Au nanoparticles—a cyclic *N*-methylene position is preferentially oxidized to produce the corresponding iminium cation. This non-*N*-methyl selective amine oxidation can be applied to unprecedented transformations. In the next section, I will focus on α -alkynylation of tertiary amines by utilizing the Au-catalyzed unusual selective tertiary amine oxidation.

4.5. References

- [1] a) B. R. Brown, *The Organic Chemistry of Aliphatic Nitrogen Compounds*, Oxford University Press, New York, **1994**; b) M. B. Smith, J. March, *March's Advanced Organic Chemistry: Reactions, Mechanisms, and Structure*, 6th Edition, Wiley, Hoboken, New Jersey, **2007**.
- [2] a) F.-X. Felpin, J. Lebreton, *Eur. J. Chem.* **2003**, 3693; b) H. Sun, D.O. Scott, *ACS Med. Chem. Lett.* **2011**, 2, 638; c) S. Löber, H. Hübner, N. Tschammer, P. Gmeiner, *Trends Pharmacol. Sci.* **2011**, 32, 148; d) J. Genovino, S. Lütz, D. Sames, B. Touré, *J. Am. Chem. Soc.* **2013**, 135, 12346; e) E. Vitaku, D. T. Smith, J. T. Njardarson, *J. Med. Chem.* **2014**, 57, 10257; f) R. D. Taylor, M. MacCoss, A. D. G. Lawson, *J. Med. Chem.* **2014**, 57, 5845; g) C.-V. T. Vo, J. W. Bode, *J. Org. Chem.* **2014**, 79, 2809; h) C. M. Marson, *Adv. Heterocycl. Chem.* **2017**, 121, 13; i) Y.-Y. Wang, J. W. Bode, *J. Am. Chem. Soc.* **2019**, 10.1021/jacs.9b05074; j) L. R. E. Pantaine, J. A. Milligan, J. K. Matsui, C. B. Kelly, G. A. Molander, *Org. Lett.* **2019**, 10.1021/acs.orglett.9b00602.
- [3] a) T. Cernak, K. D. Dyksta, S. Tyagarajan, P. Vachal, S. W. Krska, *Chem. Soc. Rev.* **2016**, 45, 546; b) J. He, L. G. Hamann, H. M. L. Davies, R. E. J. Beckwith, *Nat. Commun.* **2015**, 6, 5943.
- [4] For reviews on α -functionalization of cyclic amines, see: a) K. R. Campos, *Chem. Soc. Rev.* **2007**, 36, 1069; b) E. A. Mitchell, A. Pesciulli, N. Lefevre, L. Meerpoel, B. U. W. Maes, *Chem. Eur. J.* **2012**, 18, 10092.
- [5] a) P. Beak, W.-K. Lee, *Tetrahedron Lett.* **1989**, 30, 1197; b) P. Beak, A. Basu, D. J. Gallagher, Y. S. Park, S. Thayumanavan, *Acc. Chem. Res.* **1996**, 29, 552; c) W. Chen, L. Ma, A. Paul, D. Seidel, *Nat. Chem.* **2018**, 10, 165; d) A. Paul, D. Seidel, *J. Am. Chem. Soc.* **2019**, 141, 8778.
- [6] a) P. R. Payne, P. Garcia, P. Eisenberger, J. C.-H. Yim, L. L. Schafer, *Org. Lett.* **2013**, 15, 2182; b) A. J. J. Lennox, S. L. Goes, M. P. Webster, H. F. Koolman, S. W. Djuric, S. S. Stahl, *J. Am. Chem. Soc.* **2018**, 140, 11227. Ru-catalyzed non-directed C–H activation of cyclic secondary amines was also reported although the selectivity was low, see: c) C. S. Yi, S. Y. Yun, I. A. Guzei, *Organometallics*, **2004**, 23, 5392. For directed α -C–H activation examples, see: d) Y. Ishii, N. Chatani, F. Kakiuchi, S. Murai, *Organometallics* **1997**, 16, 3615; e) N. Chatani, T. Asaumi, T. Ikeda, S. Yorimitsu, Y. Ishii, F. Kakiuchi, S. Murai, *J. Am. Chem. Soc.* **2000**, 122, 12882; f) N. Chatani, T.

- Asaumi, S. Yorimitsu, T. Ikeda, F. Kakiuchi, S. Murai, *J. Am. Chem. Soc.* **2001**, *123*, 10935; g) S. J. Pastine, D. V. Gribkov, D. Sames, *J. Am. Chem. Soc.* **2006**, *128*, 14220.
- [7] a) H. M. L. Davies, *J. Mol. Catal. A Chem.* **2002**, *189*, 125; b) H. M. L. Davies, C. Venkataramani, T. Hansen, D. W. Hopper, *J. Am. Chem. Soc.* **2003**, *125*, 6462.
- [8] For reviews related to oxidative α -functionalization of tertiary amines, see: a) Z. Li, S. Bohle, C.-J. Li, *Proc. Natl. Acad. Sci.* **2006**, *103*, 8928; b) C.-J. Li, *Acc. Chem. Res.* **2009**, *42*, 335; c) C. J. Scheuermann, *Chem. Asian J.* **2010**, *5*, 436; d) C. S. Yeung, V. M. Dong, *Chem. Rev.* **2011**, *111*, 1215; e) W. Shi, C. Liu, A. Lei, *Chem. Soc. Rev.* **2011**, *40*, 2761; f) C. Liu, H. Zhang, W. Shi, A. Lei, *Chem. Rev.* **2011**, *111*, 1780; g) S. A. Girard, T. Knauber, C.-J. Li, *Angew. Chem. Int. Ed.* **2014**, *53*, 74; h) C. Liu, J. Yuan, M. Gao, S. Tang, W. Li, R. Shi, A. Lei, *Chem. Rev.* **2015**, *115*, 12138; i) J. W. Beatty, C. R. J. Stephenson, *Acc. Chem. Res.* **2015**, *48*, 1474.
- [9] a) Z. Li, C.-J. Li, *J. Am. Chem. Soc.* **2004**, *126*, 11810; b) Z. Li, C.-J. Li, *Org. Lett.* **2004**, *6*, 4997; c) M. Niu, Z. Yin, H. Fu, Y. Jiang, Y. Zhao, *J. Org. Chem.* **2008**, *73*, 3961; d) C. M. R. Volla, P. Vogel, *Org. Lett.* **2009**, *11*, 1701; e) X. Xu, X. Li, *Org. Lett.* **2009**, *11*, 1027; f) M. Rueping, R. M. Koenigs, K. Poscharny, D. C. Fabry, D. Leonori, C. Vila, *Chem. Eur. J.* **2012**, *18*, 5170; g) Q. Shen, L. Zhang, Y.-R. Zhou, J.-X. Li, *Tetrahedron Lett.* **2013**, *54*, 6725; h) X. Jin, K. Yamaguchi, N. Mizuno, *RSC Adv.* **2014**, *4*, 34712; i) F. Alonso, A. Arroyo, I. Martín-García, Y. Moglie, *Adv. Synth. Catal.* **2015**, 357, 3549; j) S. P. Teong, D. Yu, Y. N. Sum, Y. Zhang, *Green Chem.* **2016**, *18*, 3499; k) M. Odachowski, M. F. Greaney, N. J. Turner, *ACS Catal.* **2018**, *8*, 10032.
- [10] a) Y. Shen, M. Li, S. Wang, T. Zhan, Z. Tan, C.-C. Guo, *Chem. Commun.* **2009**, 953; b) A. Sud, D. Sureshkumar, M. Klusmann, *Chem. Commun.* **2009**, 3169; c) F. Yang, J. Li, J. Xie, Z.-Z. Huang, *Org. Lett.* **2010**, *12*, 5214; d) J. Xie, Z.-Z. Huang, *Angew. Chem. Int. Ed.* **2010**, *49*, 10181; e) M. Rueping, C. Vila, R. M. Koenigs, K. Poscharny, D. C. Fabry, *Chem. Commun.* **2011**, *47*, 2360; f) J. Xie, H. Li, J. Zhou, Y. Cheng, C. Zhu, *Angew. Chem. Int. Ed.* **2012**, *51*, 1252; g) C. Huo, M. Wu, X. Jia, H. Xie, Y. Yuan, J. Tang, *J. Org. Chem.* **2014**, *79*, 9860.
- [11] a) S.-I. Murahashi, N. Komiya, H. Terai, T. Nakae, *J. Am. Chem. Soc.* **2003**, *125*, 15312; b) M. North, *Angew. Chem. Int. Ed.* **2004**, *43*, 4126; c) S.-I. Murahashi, N. Komiya, H. Terai, *Angew. Chem. Int. Ed.* **2005**, *44*, 6931; d) S.-I. Murahashi, T. Nakae, H. Terai, N. Komiya, *J. Am. Chem. Soc.* **2008**, *130*, 11005; e) S.-I. Murahashi, D. Zhang,

Chem. Soc. Rev. **2008**, *37*, 1490; f) M. Rueping, S. Zhu, R. M. Koenigs, *Chem. Commun.* **2011**, *47*, 12709; g) Y. Pan, S. Wang, C. W. Kee, E. Dubuisson, Y. Yang, K. P. Loh, C.-H. Tan, *Green Chem.* **2011**, *13*, 3341; h) A. M. Nauth, E. Schechtel, R. Dören, W. Tremel, T. Opatz, *J. Am. Chem. Soc.* **2018**, *140*, 14169; i) C.-K. Chen, A. G. Hortmann, M. R. Marzabadi, *J. Am. Chem. Soc.* **1988**, *110*, 4829; j) O. Yilmaz, M. S. Oderinde, M. H. Emmert, *J. Org. Chem.* **2018**, *83*, 11089; k) M.-X. Sun, Y.-F. Wang, B.-H. Xu, X.-Q. Ma, S.-J. Zhang, *Org. Biomol. Chem.* **2018**, *16*, 1971.

[12] a) Z. Li, C.-J. Li, *J. Am. Chem. Soc.* **2005**, *127*, 6968; b) A. J. Catino, J. M. Nichols, B. J. Nettles, M. P. Doyle, *J. Am. Chem. Soc.* **2006**, *128*, 5648; c) P. Liu, C.-Y. Zhou, S. Xiang, C.-M. Che, *Chem. Commun.* **2010**, *46*, 2739; d) M. O. Ratnikov, X. Xu, M. P. Doyle, *J. Am. Chem. Soc.* **2013**, *135*, 9475.

[13] a) Z. Li, C.-J. Li, *J. Am. Chem. Soc.* **2005**, *127*, 3672; b) A. G. Condie, J. C. González-Gómez, C. R. J. Stephenson, *J. Am. Chem. Soc.* **2010**, *132*, 1464.

[14] a) Z. Li, C.-J. Li, *Eur. J. Org. Chem.* **2005**, 3173; b) O. Baslé, C.-J. Li, *Green Chem.* **2007**, *9*, 1047.

[15] a) D. P. Hari, B. König, *Org. Lett.* **2011**, *13*, 3852; b) M. Rueping, S. Zhu, R. M. Koenigs, *Chem. Commun.* **2011**, *47*, 8679.

[16] O. Baslé, C.-J. Li, *Org. Lett.* **2008**, *10*, 3661.

[17] a) A. McNally, C. K. Prier, D. W. C. MacMillan, *Science* **2011**, *334*, 1114; b) Y. Miyake, K. Nakajima, Y. Nishibayashi, *J. Am. Chem. Soc.* **2012**, *134*, 3338; c) Z. Zuo, D. T. Ahneman, L. Chu, J. A. Terrett, A. G. Doyle, D. W. C. MacMillan, *Science* **2014**, *345*, 437; d) C. L. Joe, A. G. Doyle, *Angew. Chem. Int. Ed.* **2016**, *55*, 4040; e) S. M. Thullen, T. Rovis, *J. Am. Chem. Soc.* **2017**, *139*, 15504; f) I. B. Perry, T. F. Brewer, P. J. Sarver, D. M. Schultz, D. A. DiRocco, D. W. C. MacMillan, *Nature* **2018**, *560*, 70.

[18] a) F. Kienzle, *Tetrahedron Lett.* **1983**, *24*, 2213; b) C.-K. Chen, A. G. Hortmann, M. R. Marzabadi, *J. Am. Chem. Soc.* **1988**, *110*, 4829; c) M. L. Deb, S. S. Dey, I. Bento, M. T. Barros, C. D. Maycock, *Angew. Chem. Int. Ed.* **2013**, *52*, 9791; d) S. Mahato, S. Halder, C. K. Jana, *Chem. Commun.* **2014**, *50*, 332; e) A. Shahrissa, R. Teimuri-Mofrad, M. Gholamhosseini-Nazari, *Synlett* **2015**, *26*, 1031; f) N. A. Waghmode, A. H. Kalbandhe, P. B. Thorat, N. N. Karade, *Tetrahedron Lett.* **2016**, *57*, 680.

[19] Instead of α -functionalization, C–N bond cleavages of tertiary amines *via* the oxidation have been also reported, see: a) K. Ouyang, W. Hao, W.-X. Zhang, Z. Xi,

Chem. Rev. **2015**, *115*, 12045; b) Y. Liu, B. Yao, C.-L. Deng, R.-Y. Deng, R.-Y. Tang, X.-G. Zhang, J.-H. Li, *Org. Lett.* **2011**, *13*, 2184; c) X. Zhang, W. Yang, L. Wang, *Org. Biomol. Chem.* **2013**, *11*, 3649; d) Y.-S. Bao, B. Zhaorigetu, B. Agula, M. Baiyin, M. Jia, *J. Org. Chem.* **2014**, *79*, 803; e) I. C. Yoon, T. G. Kim, C. S. Cho, *Organometallics* **2014**, *33*, 1890; f) J. Roque, Y. Kuroda, L. T. Göttemann, R. Sarpong, *Science* **2018**, *361*, 171; g) J. Roque, Y. Kuroda, L. T. Göttemann, R. Sarpong, *Nature* **2018**, *564*, 244, and references of 23b and 23f.

[20] a) B. Zhu, R. J. Angelici, *Chem. Commun.* **2007**, 2157; b) R. J. Angelici, *J. Organomet. Chem.* **2008**, *693*, 847; c) R. D. Patil, S. Adimurthy, *Adv. Synth. Catal.* **2011**, *353*, 1695; d) E. R. Klobukowski, M. L. Mueller, R. J. Angelici, L. K. Woo, *ACS Catal.* **2011**, *1*, 703; e) A. Feula, J. S. Fossey, *RSC Adv.* **2013**, *3*, 5370; f) T. O. Dairo, N. C. Nelson, I. I. Slowing, R. J. Angelici, L. K. Woo, *Catal. Lett.* **2016**, *146*, 2278; g) S. Minakata, Y. Ohshima, A. Takemiya, I. Ryu, M. Komatsu, Y. Ohshiro, *Chem. Lett.* **1997**, *26*, 311; h) E. Gravel, E. Poupon, R. Hocquemiller, *Tetrahedron* **2006**, *62*, 5248; i) D. R. Fandrick, C. A. Hart, I. S. Okafor, M. A. Mercadante, S. Sanyal, J. T. Masters, M. Sarvestani, K. R. Fandrick, J. L. Stockdill, N. Grinberg, N. Gonnella, H. Lee, C. H. Senanayake, *Org. Lett.* **2016**, *18*, 6192.

[21] a) L. A. Hull, G. T. Davis, D. H. Rosenblatt, H. K. R. Williams, R. C. Weglein, *J. Am. Chem. Soc.* **1967**, *89*, 1163; b) J. R. L. Smith, L. A. V. Mead, *J. Chem. Soc. Perkin. Trans. 2* **1973**, 206; c) Y. L. Chow, W. C. Danen, S. F. Nelsen, D. H. Rosenblatt, *Chem. Rev.* **1978**, *78*, 243; d) Y. Moro-oka, T. Ikawa, *J. Am. Chem. Soc.* **1980**, *102*, 1751; e) F. D. Lewis, T.-I. Ho, J. T. Simpson, *J. Org. Chem.* **1981**, *46*, 1077; f) F. D. Lewis, *Acc. Chem. Res.* **1986**, *19*, 401; g) S. B. Karki, J. P. Dinnocenzo, J. P. Jones, K. R. Korzekwa, *J. Am. Chem. Soc.* **1995**, *117*, 3657; h) J. I. Manchester, J. P. Dinnocenzo, L. Higgins, J. P. Jones, *J. Am. Chem. Soc.* **1997**, *119*, 5069; i) Y. Goto, Y. Watanabe, S. Fukuzumi, J. P. Jones, J. P. Dinnocenzo, *J. Am. Chem. Soc.* **1998**, *120*, 10762; j) M. Bietti, A. Cuppoletti, C. Dagostin, C. Florea, C. Galli, P. Gentili, H. Petride, C. R. Caia, *Eur. J. Org. Chem.* **1998**, 2425; k) A. Cuppoletti, C. Dagostin, C. Florea, C. Galli, P. Gentili, O. Lanzalunga, A. Petride, H. Petride, *Chem. Eur. J.* **1999**, *5*, 2993.

[22] a) M. Polonovski, M. Polonovski, *Bull. Soc. Chim. Fr.* **1927**, *41*, 1190.; b) A. Cave, C. Kan-Fan, P. Potier, J. Le Men, *Tetrahedron* **1967**, *23*, 4681; c) J. P. Ferris, R. D. Gerwe, G. R. Gapski, *J. Am. Chem. Soc.* **1967**, *89*, 5270; d) J. P. Ferris, R. D. Gerwe, G.

R. Gapski, *J. Org. Chem.* **1968**, *33*, 3493; e) T. Kametani, M. Ihara, *J. Chem. Soc. Perkin. Trans. I* **1980**, 629; f) T. Tamminen, R. Jokela, B. Tirkkoken, M. Lounasmaa, *Tetrahedron* **1989**, *45*, 2683; g) A.-C. Carbonnelle, V. Gott, G. Roussi, *Heterocycles* **1993**, *36*, 1763; h) G. Rousselet, P. Capdevielle, M. Maumy, *Tetrahedron Lett.* **1995**, *36*, 4999; i) D.-R. Hwang, B.-J. Uang, *Org. Lett.* **2002**, *4*, 463; j) J. Royer, M. Bonin, L. Micouin, *Chem. Rev.* **2004**, *104*, 2311; k) Z. Xu, X. Yu, X. Feng, M. Bao, *J. Org. Chem.* **2011**, *76*, 6901; l) K. M. Jones, P. Karier, M. Klusmann, *ChemCatChem* **2012**, *4*, 51.

[23] a) S.-I. Murahashi, T. Hirano, T. Yano, *J. Am. Chem. Soc.* **1978**, *100*, 348; b) S.-I. Murahashi, T. Watanabe, *J. Am. Chem. Soc.* **1979**, *101*, 7429; c) X. Zhang, A. Fried, S. Knapp, A. S. Goldman, *Chem. Commun.* **2003**, 2060; d) C. C. Lu, J. C. Peters, *J. Am. Chem. Soc.* **2004**, *126*, 15818; e) J. P. Collman, H. J. H. Wang, R. A. Decreau, T. A. Eberspacher, C. J. Sunderland, *Chem. Commun.* **2005**, 2497; f) Z. Ling, L. Yun, L. Liu, B. Wu, X. Fu, *Chem. Commun.* **2013**, *49*, 4214; g) I. Jovel, S. Prateptongkum, R. Jackstell, N. Vogl, C. Weckbecker, M. Beller, *Chem. Commun.* **2010**, *46*, 1956.

[24] a) E. Wenkert, E. C. Angell, *Synth. Commun.* **1988**, *18*, 1331; b) R. M. Moriarty, R. K. Vaid, M. P. Duncan, *Tetrahedron Lett.* **1988**, *29*, 6913; c) H. Petride, C. Drăghici, C. Florea, A. Petride, *Cent. Eur. J. Chem.* **2004**, *2*, 302; d) R. J. Griffiths, G. A. Burley, E. P. A. Talbot, *Org. Lett.* **2017**, *19*, 870; e) S. Murata, M. Miura, M. Nomura, *J. Org. Chem.* **1989**, *54*, 4700; f) S. Murata, M. Miura, M. Nomura, *J. Chem. Soc. Chem. Commun.* **1989**, 116; g) M. M. Al-Subu, W. J. Jondi, A. A. Amer, M. Hannoun, M. J. Musmar, X.-F. Wu, C. B. Bheeter, H. Neumann, P. H. Dixneuf, M. Beller, *Chem. Commun.* **2012**, *48*, 12237; h) J. R. Khusnutdinova, Y. Ben-David, D. Milstein, *J. Am. Chem. Soc.* **2014**, *136*, 2998; i) U. Gellrich, J. R. Khusnutdinova, G. M. Leitus, D. Milstein, *J. Am. Chem. Soc.* **2015**, *137*, 4851; j) C. J. Legacy, A. Wang, B. J. O'Day, M. H. Emmert, *Angew. Chem. Int. Ed.* **2015**, *54*, 14907; k) Y. Liu, C. Wang, D. Xue, M. Xiao, J. Liu, C. Li, J. Xiao, *Chem. Eur. J.* **2017**, *23*, 3062; l) S. Yang, P. Li, Z. Wang, L. Wang, *Org. Lett.* **2017**, *19*, 3386; m) T. Thatikonda, S. K. Deepake, U. Das, *Org. Lett.* **2019**, *21*, 2532; n) Y. Zhang, D. Riemar, W. Schilling, J. Kollmann, S. Das, *ACS Catal.* **2018**, *8*, 6659.

[25] For the papers containing Au-catalyzed α -oxygenation despite of quite limited scopes, see: a) M.-H. So, Y. Liu, C.-M. Ho, C.-M. Che, *Chem. Asian J.* **2009**, *4*, 1551; b) P. Preedasuriyachai, W. Chavasiri, H. Sakurai, *Synlett* **2011**, *8*, 1121; c) H. Miyamura,

- M. Morita, T. Inasaki, S. Kobayashi, *Bull. Chem. Soc. Jpn.* **2011**, *84*, 588; d) T. Amaya, T. Ito, T. Hirao, *Heterocycles* **2012**, *86*, 927, and the references of [20d] and [20f].
- [26] G. E. Dobereiner, R. H. Crabtree, *Chem. Rev.* **2010**, *110*, 681.
- [27] D. E. Resasco, in *Encyclopedia of catalysis*, I. T. Horváth, Ed.; Wiley, New York, **2003**; Vol. 3.
- [28] a) J. Choi, A. H. R. MacArthur, M. Brookhart, A. S. Goldman, *Chem. Rev.* **2011**, *111*, 1761; b) C. M. Jensen, *Chem. Commun.* **1999**, 2443.
- [29] C. Gunanathan, D. Milstein, *Science*, **2013**, *341*, 1229712.
- [30] a) J. Zhang, G. Leitus, Y. B.-David, D. Milstein, *J. Am. Chem. Soc.* **2005**, *127*, 10840; b) K. Fujita, N. Tanino, R. Yamaguchi, *Org. Lett.* **2007**, *9*, 109; c) J. Zhang, E. Balaraman, G. Leitus, D. Milstein, *Organometallics*, **2011**, *30*, 5716; d) K. Fujita, T. Yoshida, Y. Imori, R. Yamaguchi, *Org. Lett.* **2011**, *13*, 2278.
- [31] H. Crabtree, *Chem. Rev.* **2017**, *117*, 9228.
- [32] a) X. Jin, K. Taniguchi, K. Yamaguchi, K. Nozaki, N. Mizuno, *Chem. Commun.* **2017**, *53*, 5267; b) X. Jin, Y. Koizumi, K. Yamaguchi, K. Nozaki, N. Mizuno, *J. Am. Chem. Soc.* **2017**, *139*, 13821; c) Y. Koizumi, K. Taniguchi, X. Jin, K. Yamaguchi, K. Nozaki, N. Mizuno, *Chem. Commun.* **2017**, *53*, 10827; d) K. Taniguchi, X. Jin, K. Yamaguchi, K. Nozaki, N. Mizuno, *Chem. Sci.* **2017**, *8*, 2131.
- [33] M. Kojima, M. Kanai, *Angew. Chem. Int. Ed.* **2016**, *55*, 12224.
- [34] S. Hati, U. Holzgrabe, S. Sen, *Beilstein J. Org. Chem.* **2017**, *13*, 1670, and references cited therein.
- [35] a) S. Chakraborty, W. W. Brennessel, W. D. Jones, *J. Am. Chem. Soc.* **2014**, *136*, 8564; b) J. Wu, D. Talwar, S. Johnston, M. Yan, J. Xiao, *Angew. Chem. Int. Ed.* **2013**, *52*, 6983; c) Y. Wu, H. Yi, A. Lei, *ACS Catal.* **2018**, *8*, 1192. d) K.-H. He, F.-F. Tan, C.-Z. Zhou, G.-J. Zhou, X.-L. Yang, Y. Li, *Angew. Chem. Int. Ed.* **2017**, *56*, 3080; e) C. Deraedt, R. Ye, W. T. Ralston, F. D. Toste, G. A. Somorjai, *J. Am. Chem. Soc.* **2017**, *139*, 18084; f) Y. Mikami, K. Ebata, T. Mitsudome, T. Mizugaki, K. Jitsukawa, K. Kaneda, *Heterocycles*, **2011**, *82*, 1371; g) S. K. Moromi, S. M. A. H. Siddiki, K. Kon, T. Toyao, K. Shimizu, *Catal. Today* **2017**, *281*, 507; h) T. Hara, K. Mori, T. Mizugaki, K. Ebitani, K. Kaneda, *Tetrahedron Lett.* **2003**, *44*, 6207; i) K. Fujita, T. Wada, T. Shiraishi, *Angew. Chem. Int. Ed.* **2017**, *56*, 10886; j) K. Fujita, Y. Tanaka, M. Kobayashi, R. Yamaguchi, *J.*

- Am. Chem. Soc.* **2014**, *136*, 4829; k) D. Forberg, T. Schwob, M. Zaheer, M. Friedrich, N. Miyajima, R. Kempe, *Nat. Commun.* **2016**, *7*, 13201.
- [36] For a rare example of dehydrogenation applicable to non-substituted piperidine with a hydrogen acceptor, see: W. Yao, Y. Zhang, X. Jia, Z. Huang, *Angew. Chem. Int. Ed.* **2014**, *53*, 1390.
- [37] D. Ainembabazi, N. An, J. C. Manayil, K. Wilson, A. F. Lee, A. M. Voutchkova-Kostal, *ACS Catal.* **2019**, *9*, 1055.
- [38] C. Matera, M. Quadri, M. Sciacaluga, D. Y. Pomè, F. Fasoli, M. D. Amici, S. Fucile, C. Gotti, C. Dallanocce, G. Grazioso, *Eur. J. Med. Chem.* **2016**, *108*, 392.
- [39] a) S. Pang, Y. Zhang, Y. Huang, H. Yuan, F. Shi, *Catal. Sci. Technol.* **2017**, *7*, 2170; b) Y. Shimomoto, R. Matsubara, M. Hayashi, *Adv. Synth. Catal.* **2018**, *360*, 3297.
- [40] a) F. Alhumaidan, D. Cresswell, A. Garforth, *Energy Fuels*, **2011**, *25*, 4217; b) C. Zhang, X. Liang, S. Liu, *Int. J. Hydrogen Energy*, **2011**, *36*, 8902; c) Y. Wang, N. Shah, G. P. Huffman, *Energy Fuels*, **2004**, *18*, 1429; d) N. Kariya, A. Fukuoka, M. Ichikawa, *Appl. Catal. A*, **2002**, *233*, 91.
- [41] a) C. E. Mabermann in *Encyclopedia of Chemical Technology*, J. I. Kroschwitz, Ed.; Wiley, New York, **1991**, 251–266; Vol. 1; b) D. Lipp in *Encyclopedia of Chemical Technology*, J. I. Kroschwitz, Ed.; Wiley, New York, **1991**, 266–287; Vol. 1; c) R. Opsahl in *Encyclopedia of Chemical Technology*, J. I. Kroschwitz, Ed.; Wiley, New York, **1991**, 346–356; Vol. 1.
- [42] a) C. E. Habermann, *Acrylamide: Kirk-Othmer Encyclopedia of Chemical Technology*, John Wiley&Sons, New York, **2002**, *1*, 288; b) T. Ohara, T. Sato, N. Shimizu, G. Prescher, H. Schwind, O. Weiberg, K. Marten, H. Greim, *Acrylic Acid and Derivatives: Ullmann's Encyclopedia of Industrial Chemistry*, Wiley-VCH, Weinheim, **2012**.
- [43] a) J. Ritz, H. Fuchs, H. Kieczka, W. C. Moran, *Caprolactam: Ullmann's Encyclopedia of Industrial Chemistry*, Wiley-VCH, Weinheim, **2012**; b) W. B. Fisher, L. Crescentini, *Caprolactam: Kirk-Othmer Encyclopedia of Chemical Technology*, John Wiley&Sons, New York, **2015**.
- [44] a) C. Gunanathan, Y. Ben-David, D. Milstein, *Science* **2007**, *317*, 790; b) L. U. Nordstrøm, H. Vogt, R. Madsen, *J. Am. Chem. Soc.* **2008**, *130*, 17672; c) S. C. Ghosh, S. Muthaiah, Y. Zhang, X. Xu, S. H. Hong, *Adv. Synth. Catal.* **2009**, *351*, 2643; d) N. D.

Schley, G. E. Dobereiner, R. H. Crabtree, *Organometallics* **2011**, *30*, 4174; e) N. Ortega, C. Richter, F. Glorius, *Org. Lett.* **2013**, *15*, 1776; f) P. P. M. Schleker, R. Honeker, J. Klankermayer, W. Leitner, *ChemCatChem* **2013**, *5*, 1762; g) K. Shimizu, K. Ohshima, A. Satsuma, *Chem. Eur. J.* **2009**, *15*, 9977; h) H. Miyamura, H. Min, J.-F. Soulé, S. Kobayashi, *Angew. Chem. Int. Ed.* **2015**, *54*, 7564, and the references of [19b] and [19c] in Chapter I.

[45] a) J. W. Kim, K. Yamaguchi, N. Mizuno, *Angew. Chem. Int. Ed.* **2008**, *47*, 9249; b) Y. Wang, H. Kobayashi, K. Yamaguchi, N. Mizuno, *Chem. Commun.* **2012**, *48*, 2642.

[46] a) K. Yamaguchi, H. Kobayashi, T. Oishi, N. Mizuno, *Angew. Chem. Int. Ed.* **2012**, *51*, 544; b) H. Fujiwara, Y. Ogasawara, M. Kotani, K. Yamaguchi, N. Mizuno, *Chem. Asian J.* **2008**, *3*, 1715; c) Y. Wang, K. Yamaguchi, N. Mizuno, *Angew. Chem. Int. Ed.* **2012**, *51*, 7250; d) K. Yamaguchi, H. Kobayashi, Y. Wang, T. Oishi, Y. Ogasawara, N. Mizuno, *Catal. Sci. Technol.* **2013**, *3*, 318; e) H. Fujiwara, Y. Ogasawara, K. Yamaguchi, N. Mizuno, *Angew. Chem. Int. Ed.* **2007**, *46*, 5202; f) K. Yamaguchi, M. Matsushita, N. Mizuno, *Angew. Chem. Int. Ed.* **2004**, *43*, 1576.

[47] *Purification of Laboratory Chemicals, 3rd Edition*, D. D. Perrin, W. L. F. Armarego, Eds.; Pergamon Press, Oxford, **1988**.

[48] K. Taniguchi, S. Itagaki, K. Yamaguchi, N. Mizuno, *Angew. Chem. Int. Ed.* **2013**, *52*, 8420.

[49] K. Sakagami, X. Jin, K. Suzuki, K. Yamaguchi, N. Mizuno, *Chem. Lett.* **2015**, *45*, 173.

[50] a) P. Kocsis, S. Farkas, L. Fodor, N. Bielik, M. Thán, S. Kolok, A. Gere, M. Csejtej, I. Tarnawa, *J. Pharmacol. Exp. Ther.* **2005**, *315*, 1237; b) P. Stamenova, R. Koytchev, K. Kuhn, C. Hansen, F. Horvath, S. Ramm, D. Pongratz, *Eur. J. Neurol.* **2005**, *12*, 453.

[51] M. A. Catania, S. Cuzzocrea, *Ther. Clin. Risk. Manag.* **2011**, *7*, 83.

[52] a) K. Lauder, A. Toscani, N. Scalacci, D. Castagnolo, *Chem. Rev.* **2017**, *117*, 14091; b) J. J. Chen, D. M. Swope, *J. Clin. Pharmacol.* **2005**, *45*, 878; c) K. Wessel, I. Szelenyi, *Clin. Investig.* **1992**, *70*, 459; d) J. W. Langston, I. Irwin, E. B. Langston, L. S. Forno, *Science* **1984**, *225*, 1480; e) L. W. Elmer, J. M. Bertoni, *Expert Opin. Pharmacother.* **2008**, *9*, 16; f) I. Bolea, A. Gella, M. Unzeta, *J. Neural Transm.* **2013**, *120*, 893; g) M. L. Schmitt, A.-T. Hauser, L. Carlino, M. Pippel, J. Schulz-Fincke, E. Metzger, D. Willmann, T. Yiu, M. Barton, R. Schüle, W. Sippl, M. Jung, *J. Med. Chem.*

2013, 56, 7334; h) P. B. Huleatt, M. L. Khoo, Y. Y. Chua, T. W. Tan, R. S. Liew, B. Balogh, R. Deme, F. Göloncsér, K. Magyar, D. P. Sheela, H. K. Ho, B. Sperlágh, P. Mátyus, C. L. L. Chai, *J. Med. Chem.* **2015**, 58, 1400; i) M. Baranyi, P. F. Porceddu, F. Göloncsér, S. Kulcsár, L. Otrokocsi, A. Kittel, A. Pinna, L. Frau, P. B. Huleatt, M.-L. Khoo, C. L. L. Chai, P. Dunkel, P. Mátyus, M. Morelli, B. Sperlágh, *Mol. Neurodegener.* **2016**, 11, 6.

[53] a) G. Abbiati, A. Arcadi, G. Bianchi, S. D. Giuseppe, F. Marinelli, E. Rossi, *J. Org. Chem.* **2003**, 68, 6959; b) W. S. Bremner, M. G. Organ, *J. Comb. Chem.* **2008**, 10, 142; c) V. A. Peshkov, O. P. Pereshivko, S. Sharma, T. Meganathan, V. S. Parmer, D. S. Ermolat'ev, E. V. Van der Eycken, *J. Org. Chem.* **2011**, 76, 5867; d) G. Bartoli, C. Cimarrelli, R. Cipolletti, S. Diomedi, R. Giovannini, M. Mari, L. Marsili, E. Marcantoni, *Eur. J. Org. Chem.* **2012**, 630; e) T. S. Symeonidis, I. N. Lykakis, K. E. Litinas, *Tetrahedron* **2013**, 69, 4612; f) B. Alcaide, P. Almendros, J. M. Alonso, I. Fernández, G. Gómez-Campikkos, M. R. Torres, *Chem. Commun.* **2014**, 50, 4567; g) J. Chen, R. Properzi, D. P. Uccello, J. A. Young, R. G. Dushin, J. T. Starr, *Org. Lett.* **2014**, 16, 4146; h) S. Tong, Q. Wang, M.-X. Wang, J. Zhu, *Angew. Chem. Int. Ed.* **2015**, 54, 1293.

[54] a) G. F. Hennion, R. S. Hanzel, *J. Am. Chem. Soc.* **1960**, 82, 4908; b) I. E. Kopka, Z. A. Fataftah, M. W. Rathke, *J. Org. Chem.* **1980**, 45, 4616; c) A. Chevalier, C. Massif, P.-Y. Renard, A. Romieu, *Chem. Eur. J.* **2013**, 19, 1686.

[55] a) K. E. Rodriques, A. Basha, J. B. Summers, *Tetrahedron Lett.* **1988**, 29, 3455; b) P. Merino, S. Anoro, E. Castillo, F. Merchan, T. Tejero, *Tetrahedron: Asymmetry* **1996**, 7, 1887; c) S. N. Osipov, A. S. Golubev, N. Sewald, K. Burger, *Tetrahedron Lett.* **1997**, 38, 5965; d) P. Merino, S. Franco, J. M. Gascon, F. L. Merchan, T. Tejero, *Tetrahedron: Asymmetry* **1999**, 10, 1867; e) Y. Ma, E. Lobkovsky, D. B. Collum, *J. Org. Chem.* **2005**, 70, 2335; f) M. Benaglia, D. Negri, G. Dell'Anna, *Tetrahedron Lett.* **2004**, 45, 8705; g) J.-X. Ji, J. Wu, A. S. C. Chan, *Proc. Natl. Acad. Sci. U. S. A.* **2005**, 102, 11196; h) Z. Shao, J. Wang, K. Ding, A. S. C. Chan, *Adv. Synth. Catal.* **2007**, 349, 2375; i) Y. Lu, T. C. Johnstone, B. A. Arndtsen, *J. Am. Chem. Soc.* **2009**, 131, 11284; j) D. E. Frantz, R. Fässler, E. M. Carreira, *J. Am. Chem. Soc.* **1999**, 121, 11245; k) S. Pinet, S. U. Pandya, P. Y. Chavant, A. Ayling, Y. Vallee, *Org. Lett.* **2002**, 4, 1463; l) B. Jiang, Y.-G. Si, *Tetrahedron Lett.* **2003**, 44, 6767; m) K. Y. Lee, C. G. Lee, J. E. Na, J. N. Kim, *Tetrahedron Lett.* **2005**, 46, 69; n) L. Zani, S. Alesi, P. G. Cozzi, C. Bolm, *J. Org. Chem.*

2006, 71, 1558; o) G. Huang, Z. Yin, X. Zhang, *Chem. Eur. J.* **2013**, 19, 11992; p) J.-X. Ji, T. T.-L. Au-Yeung, J. Wu, C. W. Yip, A. S. C. Chan, *Adv. Synth. Catal.* **2004**, 346, 42; q) M. Rueping, A. P. Antonchick, C. Brinkmann, *Angew. Chem. Int. Ed.* **2007**, 46, 6903; r) C. Fischer, E. M. Carreira, *Synthesis* **2004**, 2004, 1497; s) L. Rubio-Pérez, M. Iglesias, J. Munárriz, V. Polo, *Chem. Commun.* **2015**, 51, 9860; t) J. F. Traverse, A. H. Hoveyda, M. L. Snapper, *Org. Lett.* **2003**, 5, 3273.

[56] a) Z. Li, C. Wei, L. Chen, R. S. Varma, C.-J. Li, *Tetrahedron Lett.* **2004**, 45, 2443; b) B. M. Choudary, C. Sridhar, M. L. Kantam, B. Sreedhar, *Tetrahedron Lett.* **2004**, 45, 7319; c) M. L. Kantam, B. V. Prakash, C. R. V. Reddy, B. Sreedhar, *Synlett* **2005**, 15, 2329; d) M. Kidwai, V. Bansal, A. Kumar, S. Mozumdar, *Green Chem.* **2007**, 9, 742; e) X. Zhang, A. Corma, *Angew. Chem. Int. Ed.* **2008**, 47, 4358; f) W.-W. Chen, R. V. Nguyen, C.-J. Li, *Tetrahedron Lett.* **2009**, 50, 2895; g) K. Layek, R. Chakravarti, M. L. Kantam, H. Maheswaran, A. Vinu, *Green Chem.* **2011**, 13, 2878; h) B. Sreedhar, P. S. Reddy, C. S. V. Krishna, P. V. Babu, T. Zeng, L. Yang, R. Hudson, G. Song, A. R. Moores, C.-J. Li, *Org. Lett.* **2011**, 13, 442; i) Z. Lin, D. Yu, Y. N. Sum, Y. Zhang, *Chemsuschem* **2012**, 5, 625; j) L. Lili, Z. Xin, G. Jinsen, X. Chunming, *Green Chem.* **2012**, 14, 1710; k) K. V. V. Satyanarayana, P. A. Ramaiah, Y. L. N. Murty, M. R. Chandra, S. V. N. Pammi, *Catal. Commun.* **2012**, 25, 50; l) G. Villaverde, A. Corma, M. Iglesias, F. Sánchez, *ACS Catal.* **2012**, 2, 399; m) B. J. Borah, S. J. Borah, L. Saikia, D. K. Dutta, *Catal. Sci. Technol.* **2014**, 4, 1047; n) M. H.-Sarvari, F. Moeini, *New J. Chem.* **2014**, 38, 624.

[57] M. Yamaguchi, I. Hirao, *Tetrahedron Lett.* **1983**, 24, 1719; b) B. M. Trost, S.-F. Chen, *J. Am. Chem. Soc.* **1986**, 108, 6053; c) H. Takahata, K. Takahashi, E.-C. Wang, T. Yamazaki, *J. Chem. Soc. Perkin. Trans. I* **1989**, 1211; d) M. Perscheid, D. Schollmeyer, U. Nubbemeyer, *Eur. J. Org. Chem.* **2011**, 5250; e) M. Jäkel, J. Qu, T. Schnitzer, G. Helmchen, *Chem. Eur. J.* **2013**, 19, 16746; f) W. H. Pearson, P. Stoy, Y. Mi, *J. Org. Chem.* **2004**, 69, 1919; g) T. Murai, Y. Mutoh, Y. Ohta, M. Murakami, *J. Am. Chem. Soc.* **2004**, 126, 5968.

[58] N. Cabello, J. C. Kizirian, S. Gille, A. Alexakis, G. Bernardinelli, L. Pinchard, J. C. Caille, *Eur. J. Org. Chem.* **2005**, 2005, 4835.

[59] For many reports on Zn-alkynyl species to promote nucleophilic addition of alkynes, see a) H. Sasaki, D. Boyall, E. M. Carreira, *Helv. Chim. Acta* **2001**, 84, 964; b)

R. Fässler, C. S. Tomooka, D. E. Frantz, E. M. Carreira, *Proc. Natl. Acad. Sci.* **2004**, *101*, 5843; c) M. Yamashita, K. Yamada, K. Tomioka, *Adv. Synth. Catal.* **2005**, *347*, 1649; d) X.-F. Wu, H. Neumann, *Adv. Synth. Catal.* **2012**, *354*, 3141; e) S. Tang, L. Zeng, Y. Liu, A. Lei, *Angew. Chem. Int. Ed.* **2015**, *54*, 15850; f) J. Yuan, J. Wang, G. Zhang, C. Liu, X. Qi, Y. Lan, J. T. Miller, A. J. Kropf, E. E. Bunel, A. Lei, *Chem. Commun.* **2015**, *51*, 576; g) X. Qi, Y. Li, G. Zhang, Y. Li, A. Lei, C. Liu, Y. Lan, *Dalton Trans.* **2015**, *44*, 11165; h) X. Yue, X. Qi, R. Bai, A. Lei, Y. Lan, *Chem. Eur. J.* **2017**, *23*, 6419, and the references of [55j–o].

[60] a) C. Glaser, *Chem. Ber.* **1869**, *2*, 422; b) C. Glaser, *Ann. Chem. Pharm.* **1870**, *154*, 137; c) A. S. Hay, *J. Org. Chem.* **1962**, *27*, 3320; d) T. Oishi, T. Katayama, K. Yamaguchi, N. Mizuno, *Chem. Eur. J.* **2009**, *15*, 7539.

[61] F. S. Fawcett, *Chem. Rev.* **1950**, *47*, 219.

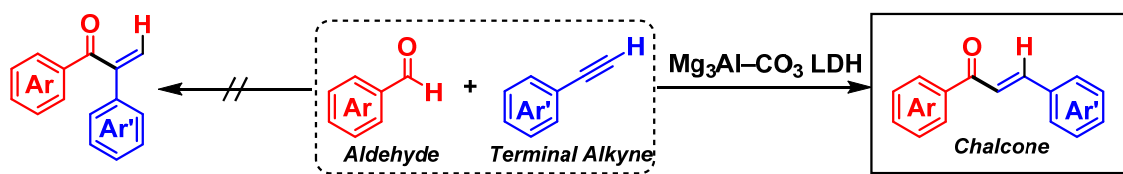
[62] a) A. Grirrane, I. Resa, A. Rodriguez, E. Carmona, E. Alvarez, E. Gutierrez-Puebla, A. Monge, A. Galindo, D. del Rio, R. A. Andersen, *J. Am. Chem. Soc.* **2007**, *129*, 693; b) P. Jochmann, D. W. Stephan, *Chem. Commun.* **2014**, *50*, 8395; c) K. Budny-Godlewski, D. Kubicki, I. Justyniak, J. Lewiński, *Organometallics* **2014**, *33*, 5093.

Chapter V

General Conclusions and Future Perspectives

Through the research work described in this doctoral dissertation, which is based on the rational construction of systems specific to solid catalysts, I demonstrated various kinds of unprecedented catalytic selective molecular transformations (Figure 5-1): a) transition-metal-free selective formal hydroacylation of terminal alkynes catalyzed by $\text{Mg}_3\text{Al-CO}_3$ LDH (Chapter II), b) one-pot selective flavone synthesis starting from aldehydes and ketones catalyzed by Au particles supported on $\text{Mg}_3\text{Al-CO}_3$ LDH (Chapter III), c) selective aurone synthesis from simple chalcones catalyzed by Pd-on-Au nanoparticles supported on CeO_2 (Chapter III), d) selective acceptorless dehydrogenative aromatization of cyclic secondary amines catalyzed by Pd nanoparticles supported on $\text{Mg}_3\text{Al-CO}_3$ LDH (Chapter IV), e) selective formal α -oxygenation of secondary and tertiary amines catalyzed by Au nanoparticles supported on Al_2O_3 (Chapter IV), and f) unusual regioselective α -alkynylation of tertiary amines catalyzed by a hybrid system comprising Au nanoparticles supported on HAP and ZnBr_2 (Chapter IV).

a) $\text{Mg}_3\text{Al-CO}_3$ LDH-catalyzed selective formal hydroacylation



b) Au/LDH-catalyzed selective flavone synthesis

c) Pd/Au/ CeO_2 -catalyzed selective aurone synthesis

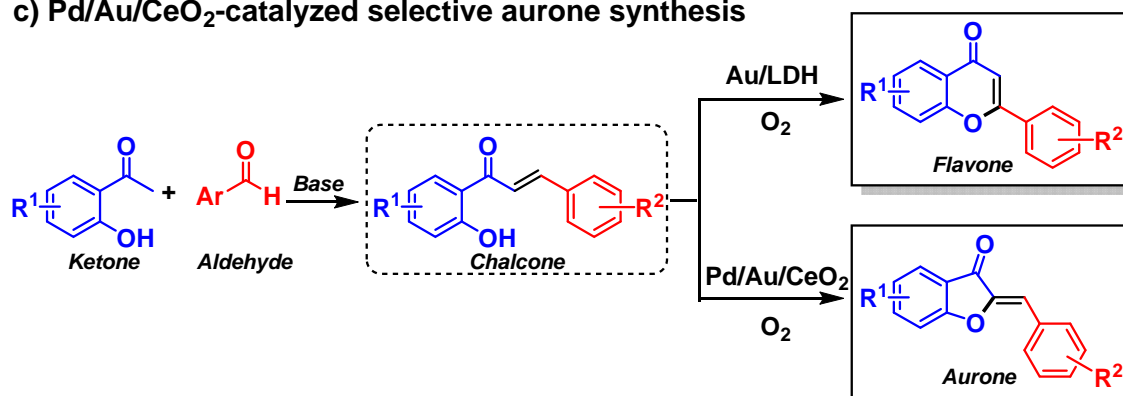
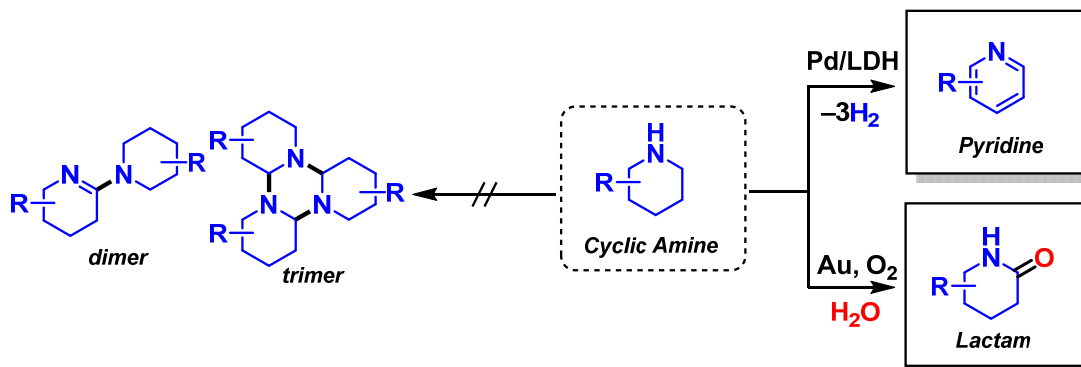


Figure 5-1. Unprecedented catalytic selective molecular transformations developed as part of the research work detailed in this dissertation. a) $\text{Mg}_3\text{Al-CO}_3$ LDH-catalyzed selective formal hydroacylation. b) Au/LDH-catalyzed selective flavone synthesis. c) Pd/Au/ CeO_2 -catalyzed selective aurone synthesis.

d) Pd/LDH-catalyzed selective dehydrogenative aromatization of cyclic amines

e) Au/Al₂O₃-catalyzed selective α -oxygenation of cyclic secondary amines



e) Au/Al₂O₃-catalyzed selective α -oxygenation of tertiary amines

f) Au/HAP and ZnBr₂-catalyzed selective α -alkynylation of tertiary amines

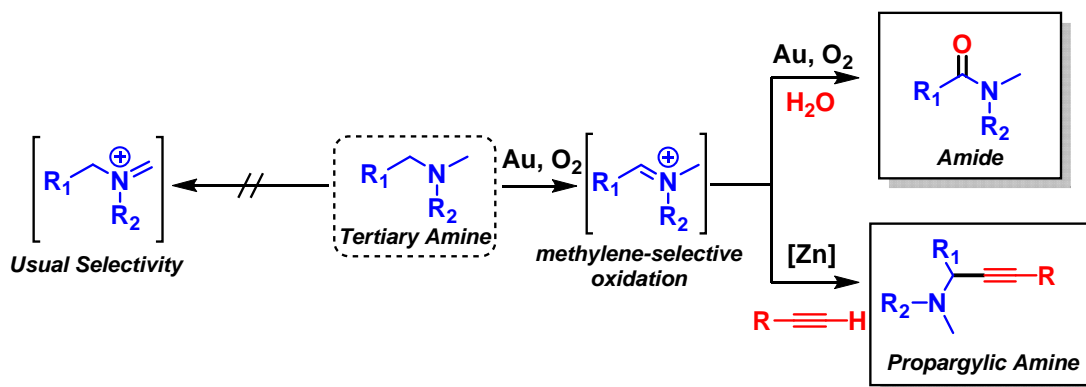


Figure 5-1 (continued). Unprecedented catalytic selective molecular transformations developed as part of the research work discusses in this doctoral dissertation. d) Pd/LDH-catalyzed selective acceptorless dehydrogenative aromatization of cyclic secondary amines. e) Au/Al₂O₃-catalyzed selective α -oxygenation of secondary and tertiary amines. f) Au/HAP and ZnBr₂-catalyzed unusual regioselective α -alkynylation of tertiary amines.

In Chapter I, I discussed the general design of catalysts and the systems specific to solid catalysts. In that chapter, I also introduced the practical liquid-phase organic reactions developed to date that are heterogeneously catalyzed. On the basis of this background, I detailed an original strategy to establish heterogeneously catalyzed organic syntheses: the rational construction of systems specific to solid catalysts for the development of unprecedented catalytic selective molecular transformations (Figure 5-2). In particular, the strategy consists in the stepwise design of

function-integrated solid catalysts that can be used to promote target elementary reactions, an approach that can be subdivided into the following steps: I) identification of a support possessing unique surface/bulk chemical properties, II) identification of support-immobilized nanoparticles acting as the main catalyst exhibiting multiple catalysis activity and/or engaging in concerted catalysis alongside the support, III) identification of support-immobilized bimetallic nanoparticles whereby the second metallic species is a catalysis promoter whose activity is controlled by ligand effects and ensemble effects, and IV) identification of structure-controlled bimetallic nanoparticles immobilized on a support consisting of an alloy, a core-shell, or a cluster-in-cluster.

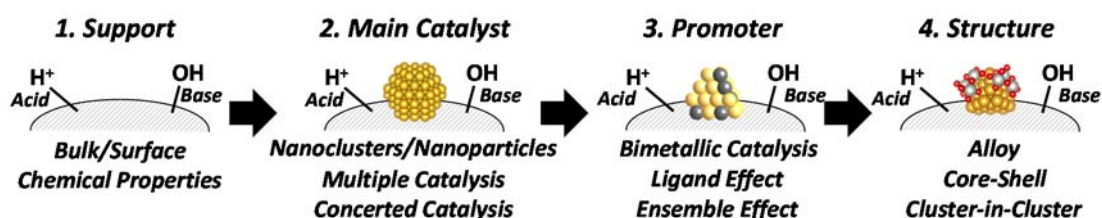


Figure 5-2. Rational construction of systems specific to solid catalysts.

In Chapter II, I described my efforts whereby, using only $\text{Mg}_3\text{Al}-\text{CO}_3$ LDH as catalyst, I successfully developed the first transition-metal-free formal hydroacylation of terminal alkynes that is applicable to various substrates, including those having cyano or ester moieties (Figure 5-3). This transformation was made possible by the unique chemical properties of $\text{Mg}_3\text{Al}-\text{CO}_3$ LDH, that is this catalyst's ionicity and basicity, which effectively promote both the nucleophilic addition of terminal alkynes and prototropy of propargylic alcohols to hydroacylated products. The successful development of this formal hydroacylation reaction will promote the utilization of solid materials' own specific chemical properties for novel organic reactions.

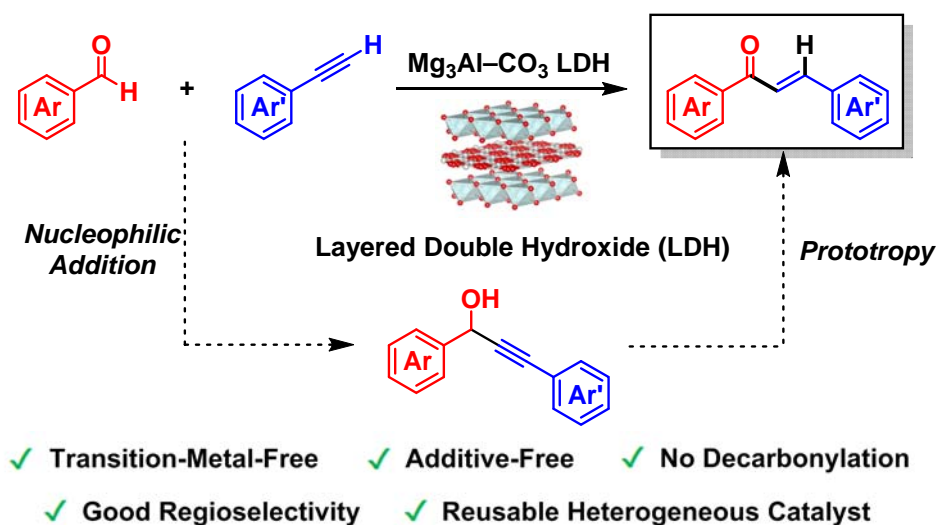


Figure 5-3. Overview of the reactivity detailed in Chapter II.

In Chapter III, I detailed my efforts aimed at realizing the selective synthesis of flavonoids, including flavones and aurones, *via* chalcones by utilizing function-integrated heterogeneous catalysts.

In section 3-1, I described the development of a catalyst consisting of Au nanoparticles supported on $\text{Mg}_2\text{Al-CO}_3$ LDH; using this catalytic system, I realized the first one-pot selective synthesis of flavones that relied on benzaldehydes (or benzyl alcohols) and 2'-hydroxyacetophenones as starting materials and that used molecular oxygen in atmospheric air as the sole oxidant (Figure 5-4). This flavone synthesis proceeds through multiple catalysis by Au nanoparticles and Claisen–Schmidt condensation catalyzed by LDH, intramolecular oxa-Michael addition catalyzed by LDH, and aerobic oxidative dehydrogenation catalyzed by Au nanoparticles. Notably, the key dehydrogenation reaction, which was hitherto unknown to be gold-catalyzed, was found to be the result of concerted catalysis between gold and LDH *via* the system whereby Au nanoparticles were dispersed on the surface of the LDH support. This system is a good example of novel efficient selective transformations made possible by nanoparticle-based specific catalysis, multiple catalysis, and concerted catalysis.

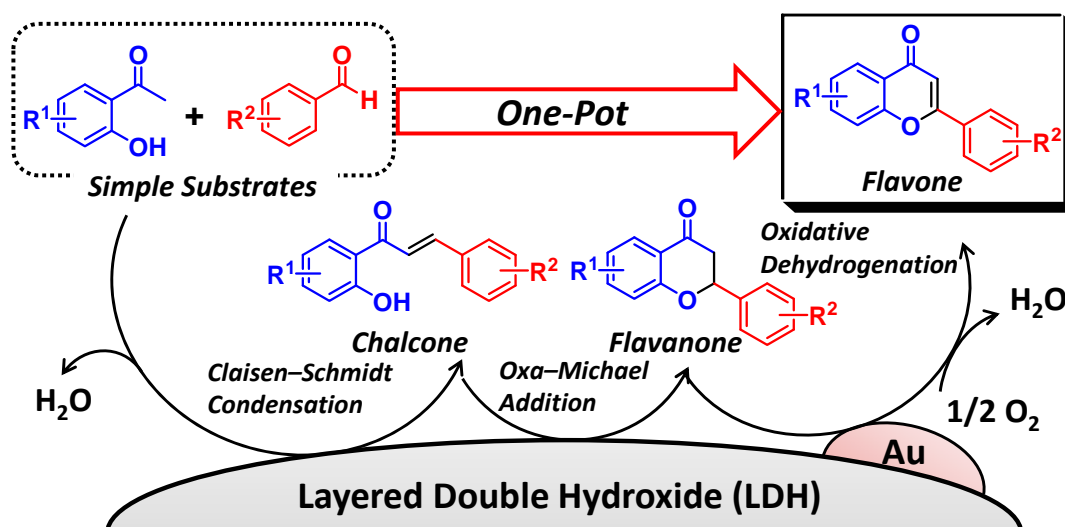


Figure 5-4. Overview of the reactivity discussed in section 3-1.

In section 3-2, I described the design of Pd-on-Au bimetallic nanoparticle catalysts supported on CeO_2 ; using this catalytic system, for the first time was achieved the catalytic transformation of simple chalcones into various aurones (Figure 5-5). The design of this catalyst was based on the aforementioned rational construction of systems specific to solid catalysts from a support to a structure. In particular, step I): a CeO_2 support was chosen for its ability to inhibit the 6-*endo-trig* cyclization of the substrate on its surface. Step II): a support-immobilized Pd-based species was chosen as the main catalyst for aurone synthesis *via* rare directed α -olefinic C–H functionalization. Step III): an Au promoter was chosen, as it improved the system’s catalytic activity as a result of stabilization of Pd(0). Step IV): a Pd-on-Au structure was chosen for its inhibition of Au-catalyzed flavone synthesis. In spite of the same route as the biosynthetic one which requires B ring oxidation, the catalytic transformation of simple chalcones into aurones through a route that does not involve B ring oxidation had not yet been reported. Thus, results from the investigations described in this doctoral dissertation indicate that it is possible to rationally design heterogeneous catalysts able to realize selective organic reactions that have not yet been achieved using homogeneous catalysts or biocatalysts.

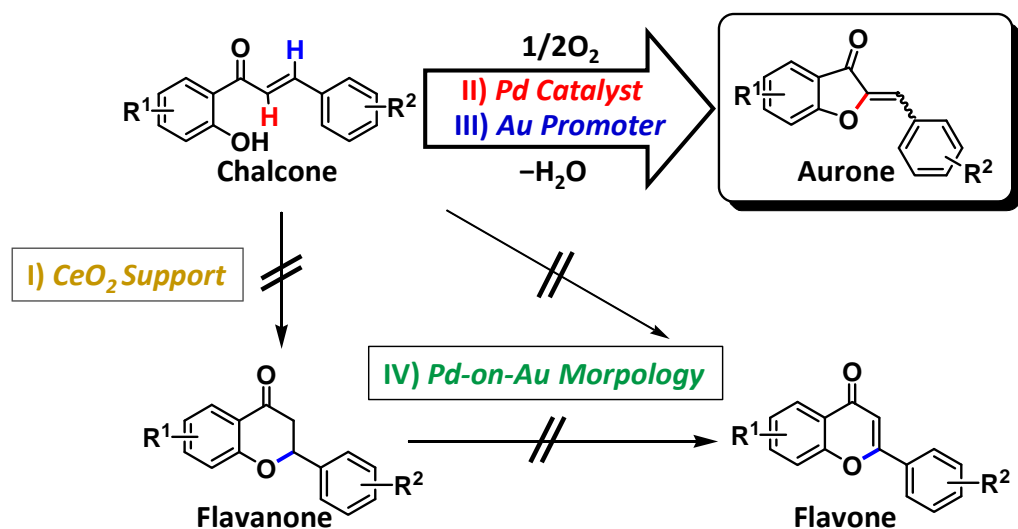


Figure 5-5. Overview of the reactivity discussed in section 3-2.

In Chapter IV, I discussed my efforts aimed at realizing challenging amine transformations (including selective transformations of cyclic secondary amines and α -methylene-selective functionalizations of tertiary amines) by focusing on a unique oxidation catalyzed by support-immobilized metal nanoparticles.

In section 4-1 is discussed the development of an unprecedented selective acceptorless dehydrogenative aromatization of cyclic amines applicable to piperidines that relies on the use of Pd nanoparticle catalysts supported on Mg₃Al-CO₃ LDH and proceeds in mild conditions without producing the corresponding dimers or trimers (Figure 5-6). This transformation was made possible *via* catalysis by support-immobilized Pd nanoparticles of the fast dehydrogenation of unstable imines leading to the formation of aromatic products, preventing the conversion of the said imines into the corresponding dimers and/or trimers. Notably, this reaction did not proceed at all in the presence of the other precious metal nanoparticles, indicating the specificity of Pd nanoparticles for the catalysis of dehydrogenative aromatization reactions.

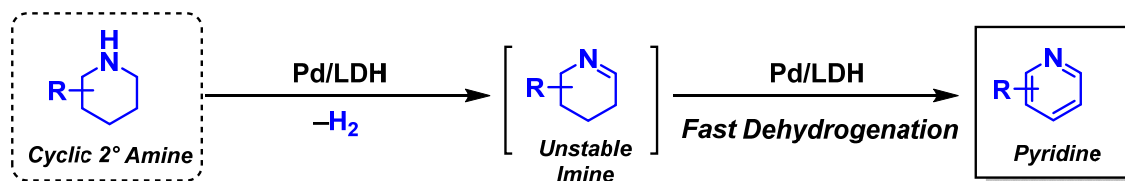


Figure 5-6. Overview of the reactivity described in section 4-1.

In section 4-2, I detailed the novel aerobic α -oxygenation of a variety of amines, which is applicable to both secondary and tertiary amines, relies on a catalyst consisting of Au nanoparticles immobilized on an Al_2O_3 support, and comprises the following sequence of reactions: amine oxidation, imine (iminium cation) hydration, and hemiaminal oxidation (Figure 5-7). In this system, cyclic secondary amines like piperidines and pyrrolidines can be transformed into stable lactams *via* fast hydration of unstable imines followed by efficient hemiaminal oxidation. Importantly, the present Au nanoparticle-catalyzed aerobic α -oxygenation of tertiary amines was not α -methyl selective but α -methylene-selective; no formamides were observed to form, even when tertiary amines comprising *N*-methyl groups were utilized as substrates. To the best of my knowledge, this reactivity represents the first example of catalytic α -oxygenation of tertiary amines displaying the mentioned α -methylene selectivity.

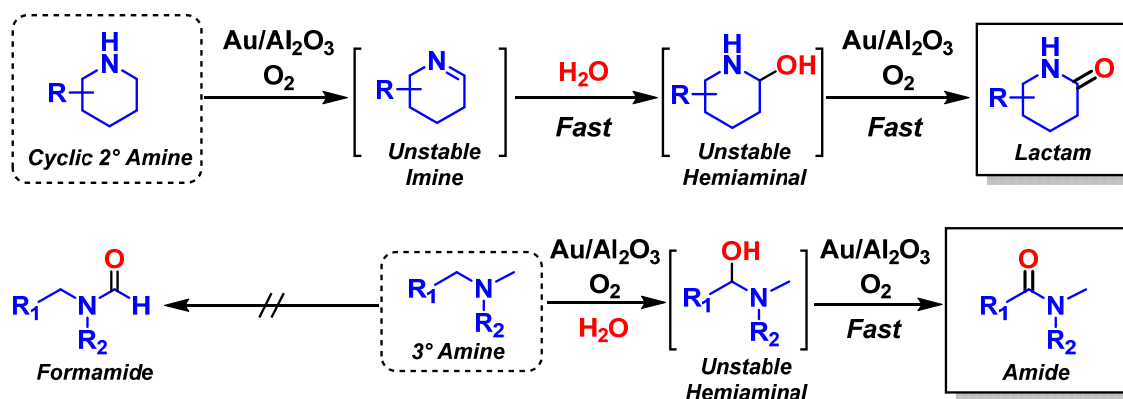


Figure 5-7. Overview of the reactivity discussed in section 4-2.

In section 4-3 is described the development of a novel and unusual regioselective α -alkynylation of tertiary amines that is applicable to the synthesis of a wide range of cyclic propargylic amines, including simple yet unprecedented ones (Figure 5-8). This system relies on a hybrid catalytic system comprising Au nanoparticles supported on

hydroxyapatite (Au/HAP) and Zn salts. This α -alkynylation proceeds *via* α -methylene-selective amine oxidation to produce iminium cations, followed by Zn-catalyzed nucleophilic addition of alkynes to the said iminium cations, possibly through the *in situ* formation of Zn–alkynyl species. I would like to emphasize that this transformation is the first general α -functionalization of tertiary amines *via* unusual α -methylene selectivity achieved in the absence of directing groups or carbenoids. The introduction of this reactivity will drastically change amine-based organic synthesis.

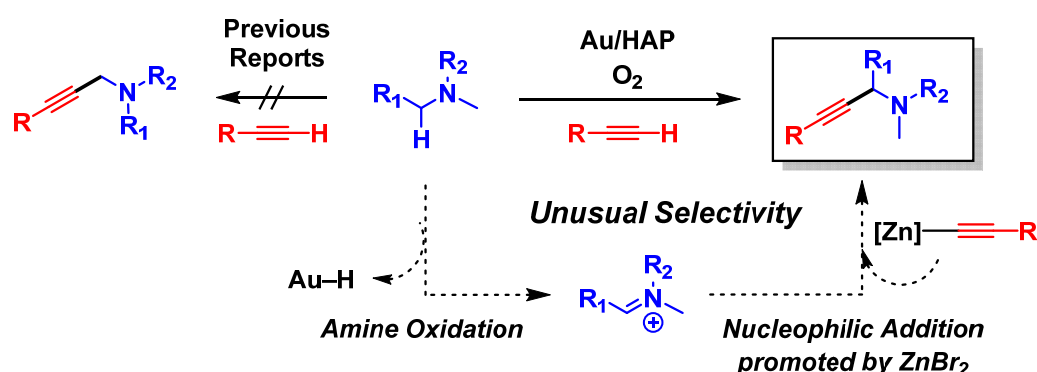


Figure 5-8. Overview of the reactivity discussed in section 4-3.

All of the catalytic systems developed as part of the research work detailed in this doctoral dissertation were heterogeneous in nature (except for the Zn-based catalysis described in section 4-3). Furthermore, the solid catalysts obtained can be reused. Moreover, all the reactions described rely on molecular oxygen as the sole oxidant or on no oxidants at all. Therefore, the selective molecular transformations I have developed are not only unprecedented but also environmentally-friendly.

In terms of future perspectives, I believe that a number of the unique catalytic systems developed in this study will be utilized to expand the use and promote the development of novel advanced organic reactions. In the section of the dissertation that follows, I will discuss in detail the basis of the mentioned predictions.

In Chapter II, I observed the hitherto unknown catalysis by LDH of the nucleophilic addition of alkynes and prototropy of propargylic alcohols, which would be applicable to an aldehyde–alkyne cross-dehydrogenative coupling (CDC) performed using other metal-substituted and/or supported LDHs and a suitable hydrogen acceptor

(Figure 5-9). If the present intramolecular electron/proton transfer of prototropy occurs through LDH-based catalysis, a hydrogen acceptor can receive the electron and proton from the substituent and/or supported metals to produce propargylic ketones. Moreover, if the CDC efficiently proceeds even in the presence of amine substrates, the sequence of aldehyde–alkyne CDC and hydroamination of propargylic ketones will take place to produce enaminones, although propargylic amines can be normally obtained *via* A³-coupling. Naturally, LDH-catalyzed alkyne nucleophilic addition will also be applicable to reactions with the other electrophiles.

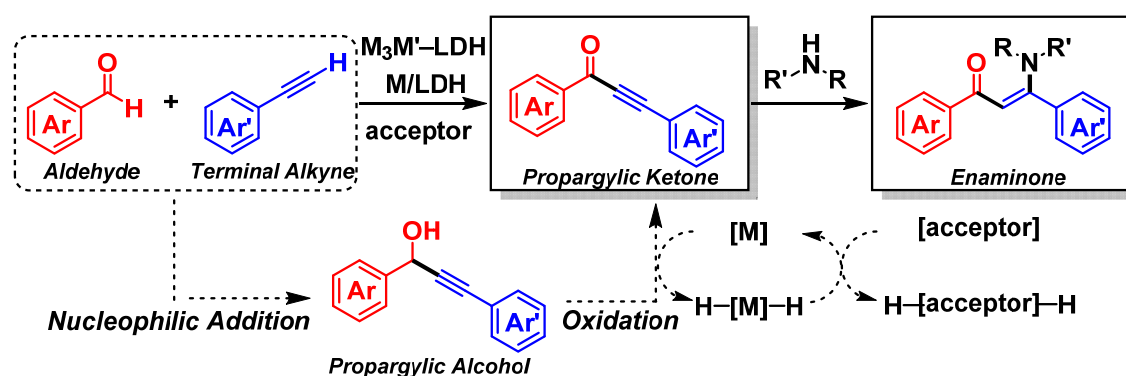


Figure 5-9. Potential future applications of the reactivity discussed in Chapter II. Aldehyde–alkyne cross-dehydrogenative coupling and enaminone synthesis, which is opposite to A³-coupling, using other metal-substituted and/or layered double hydroxide-supported catalysts and a hydrogen acceptor. A³-coupling: aldehyde–alkyne–amine coupling.

In section 3-1, I described a one-pot flavone synthesis heterogeneously catalyzed by Au/LDH that constitutes a green method for the synthesis of β -substituted, α,β -unsaturated carbonyl compounds starting from simple substrates *via* aldol condensation/1,4-addition/aerobic oxidative dehydrogenation (Figure 5-10, top). If the 1,4-addition proceeds intermolecularly using a range of nucleophiles, useful compounds like enaminones can easily be accessed. Additionally, starting from saturated carbonyl compounds, the sequential reactions consisting of oxidative dehydrogenation, 1,4-addition, and oxidative dehydrogenation will provide the same kinds of carbonyl compounds with the original skeletons retained (Figure 5-10, bottom).

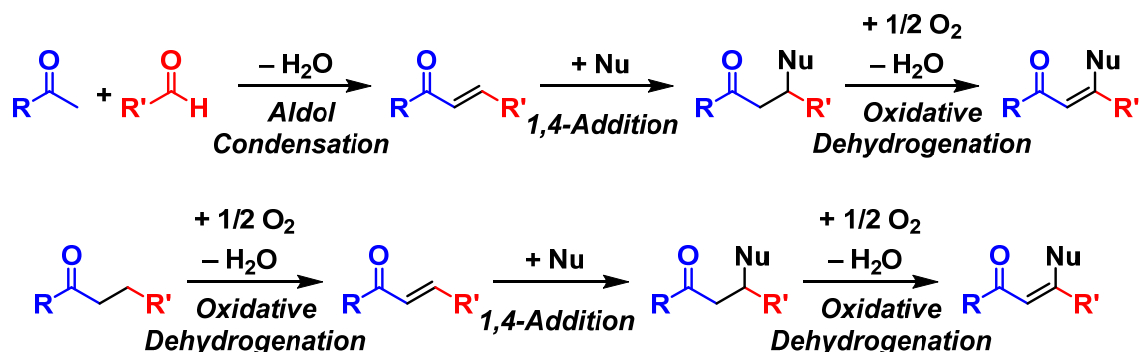


Figure 5-10. Future perspective applications of the reactivity described in section 3-1: green synthesis of β -substituted α,β -unsaturated carbonyl compounds made possible by a novel Au nanoparticle-based catalysis of the aerobic oxidative dehydrogenation of carbonyl compounds. Nu: nucleophile.

In section 3-1, the turnover-limiting-step of the Au-catalyzed aerobic oxidative dehydrogenation was suggested to be the reoxidation of the Au-H species. In fact, in a related publication (*Chem. Commun.* **2016**, 52, 14314), an Au nanoparticle-based catalyst supported on manganese oxide octahedral molecular sieves (OMS-2) exhibited a high catalytic activity in the aerobic oxidative dehydrogenation, thanks to the promotion of the reoxidation step by OMS-2 working as an electron mediator between substrate and molecular oxygen. In this study, the substrate scope of Au nanoparticle-catalyzed oxidative dehydrogenation turned out to be limited to β -heteroatom-substituted carbonyl compounds (heteroatom = N, O, or S). For instance, a cyclohexanone cannot be converted to a cyclohexenone using the mentioned Au nanoparticle-based catalysts. If the above limitation were to be overcome, on the other hand, a wider range of useful α,β -unsaturated carbonyl compounds could be easily synthesized by aerobic oxidative dehydrogenation systems, including the ones reported in Figure 5-10. At the present time, the heterogeneously catalyzed aerobic oxidative dehydrogenation of various non- β -heteroatom-substituted carbonyl compounds has been achieved for the first time using Au-Pd bimetallic nanoparticle catalysts supported on CeO₂ (Figure 5-11). To my surprise, the dehydrogenative aromatization of cyclohexenones to phenol, which is normally quite fast in the presence of Pd nanoparticles, did not proceed in this system. By contrast, the selective oxidative

α,β -dehydrogenation of cyclohexanones to cyclohexenones did take place. I believe that further investigation of this reaction system will expand its substrate scope.

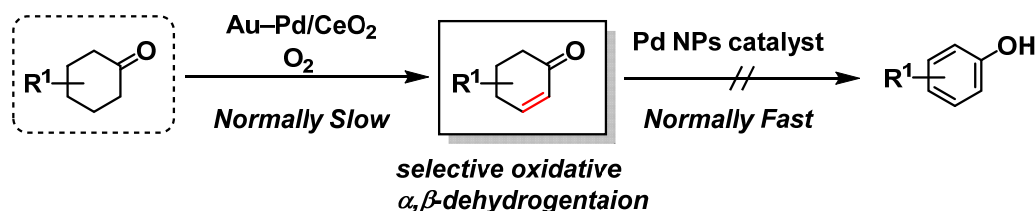


Figure 5-11. Potential future applications of the reactivity discussed in section 3-1: the catalytic aerobic oxidative dehydrogenation performed in the presence of Au-Pd/CeO₂ developed as part of the research work described in this dissertation may in the future be applicable to non- β -heteroatom-substituted carbonyl compounds, including cyclohexanones.

In section 3-2, I described my finding that the novel Pd-catalyzed C-H functionalization probably proceeded *via* phenol-directed olefinic C-H activation and reductive elimination. Thus, it can be assumed that this catalytic system can be utilized for the synthesis of aromatic heterocycles like dibenzofurans, carbazoles, and dibenzothiophenes *via* directed aryl C(sp²)-H bond activation and reductive elimination (Figure 5-12). In addition, the mechanistic investigations conducted on the role of the Au nanoparticles in the present aurone synthetic system suggested that Au contributed to the stabilization of Pd(0). An Au-containing catalytic system of this type will render possible other heterogeneously Pd-catalyzed aerobic reactions like the reaction depicted in Figure 5-11, although it is not clear at this point whether or not Pd(0) stabilization is effective for the oxidative dehydrogenation.

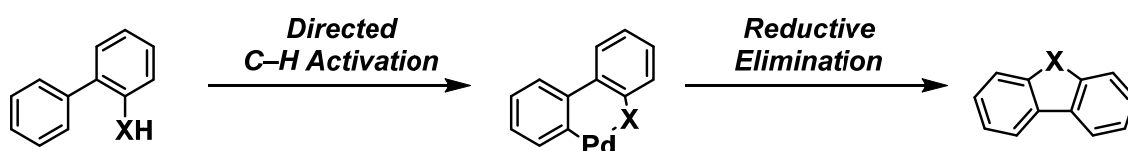


Figure 5-12. Potential future applications of the reactivity discussed in section 3-2: the synthesis of aromatic heterocycles like dibenzofurans, carbazoles, and dibenzothiophenes *via* directed aryl C(sp²)-H bond activation and reductive elimination catalyzed by Pd-based species.

In section 4-1 was described the newly developed acceptorless dehydrogenative aromatization of cyclic amines to pyridines catalyzed by support-immobilized Pd and proceeding through the production of imine intermediates. If some nucleophiles attack *in situ*-generated imines, novel 2-substituted pyridine syntheses can be developed in the presence of Pd catalysts, even though the aromatization of imines is a very fast process. Moreover, if the synthesis of amides from cyclic secondary amines discussed in section 4-2 were to occur in concomitance with H₂ release and in the absence of oxidants, the relevant system would prove invaluable in terms of the simultaneous production of useful compounds and H₂. In fact, by utilizing the findings reported in sections 4-1 and 4-2, the acceptorless α -oxygenation of cyclic secondary amines to lactams has been achieved using as catalysts Au–Pd nanoparticles supported on Al₂O₃ (Figure 5-13). These transformations will lead to more kinds of cyclic amine functionalizations.

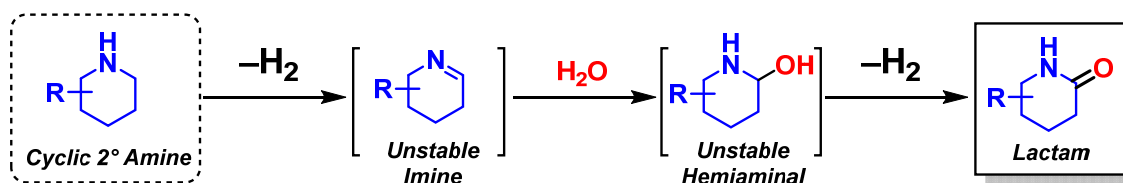


Figure 5-13. Future potential applications of the reactivity described in sections 4-1 and 4-2: the hereby developed acceptorless α -oxygenation of cyclic secondary amines to lactams using Au–Pd nanoparticles supported on Al₂O₃ as catalyst.

In section 4-3 was discussed the Au-catalyzed α -methylene-selective α -functionalization of tertiary amines with nucleophiles; the use of a wider range of nucleophiles will expand the applicability of the present high-impact transformation. In the mentioned section, I also reported the observation that hybrid catalytic systems consisting of both heterogeneous and homogeneous catalysts proved effective in rendering possible unprecedented efficient molecular transformations. As the novel reaction enabled by the other hybrid system comprising heterogeneous and homogeneous catalysts, the one-pot two-step synthesis of unsymmetrical triarylamine *via* acceptorless dehydrogenative aromatization has been developed presently using Pd/C and *p*-toluenesulfonic acid as catalysts (Figure 5-14). Moreover, as an example of

the utilization of stoichiometric homogeneous reagents' characteristics for heterogeneous catalysts, the Pd-catalyzed selective synthesis of primary anilines from NH_3 and cyclohexanones relying on the preferential adsorption of styrenes on Pd nanoparticles has recently been reported (Figure 5-15, related publication: *Angew. Chem. Int. Ed.* **2019**, 58, 10893). The introduction of the homogeneous/heterogeneous hybrid catalytic systems I developed will accelerate the development of unprecedented reactions by utilizing the specific features of the individual components of the catalytic system.

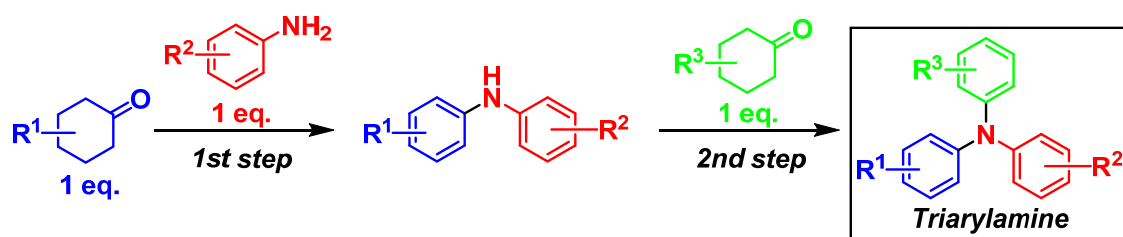


Figure 5-14. Potential future applications of the reactivity described in section 4-3: currently, the one-pot two-step synthesis of unsymmetrical triarylamines *via* acceptorless dehydrogenative aromatization using a hybrid catalytic system comprising Pd/C and *p*-toluenesulfonic acid has been achieved.

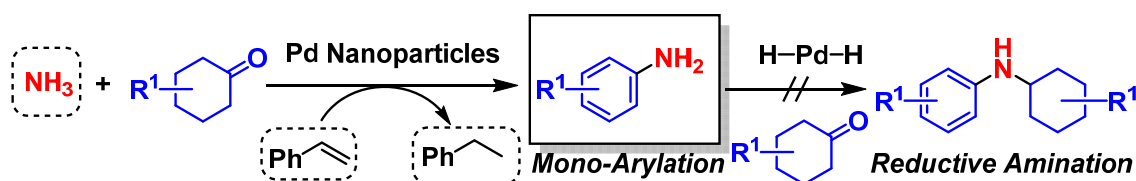


Figure 5-15. Future potential applications of the reactivity discussed in section 4-3: Pd-catalyzed selective primary aniline synthesis from NH_3 and cyclohexanones using the preferential adsorption of styrenes onto Pd nanoparticles (related publication).

In conclusion, throughout the research work described in this doctoral dissertation, the development of unprecedented catalytic selective molecular transformations was made possible by the rational construction of systems specific to solid catalysts; the stepwise design of function-integrated solid catalysts that promoted target elementary reactions required to be achieved in the order of a support, a main catalyst, a promoter, and a structure. This strategy proved helpful not just for the practical realization of target reactions but also for the discovery of unexpected catalytic activities, as described

in this chapter in terms of the future perspectives of the present work. The realization of various transformations in this study from specific ones like flavonoid synthesis till general ones like unusual α -functionalization of amines will promote the use of heterogeneous catalysts in a wide range of chemical fields. I hope that this dissertation will afford a general guideline for the development of unprecedented catalytic selective molecular transformations rendered possible by heterogeneous catalysts.

List of Publications

Main Publications

1. “Gold Nanoparticles Supported on a Layered Double Hydroxide as Efficient Catalysts for the One-Pot Synthesis of Flavones”
Takafumi Yatabe, Xiongjie Jin, Kazuya Yamaguchi, Noritaka Mizuno
Angew. Chem. Int. Ed. **2015**, 54, 13302–13306.
2. “Supported Gold Nanoparticles for Efficient α -Oxygenation of Secondary and Tertiary Amines into Amides”
Xiongjie Jin, Kengo Kataoka, Takafumi Yatabe, Kazuya Yamaguchi, Noritaka Mizuno
Angew. Chem. Int. Ed. **2016**, 55, 7212–7217.
3. “Unusual Olefinic C–H Functionalization of Simple Chalcones Toward Aurones Enabled by the Rational Design of a Function-Integrated Heterogeneous Catalyst”
Takafumi Yatabe, Xiongjie Jin, Noritaka Mizuno, Kazuya Yamaguchi
ACS Catal. **2018**, 8, 4969–4978.
4. “Transition-Metal-Free Catalytic Formal Hydroacylation of Terminal Alkynes”
Takafumi Yatabe, Noritaka Mizuno, Kazuya Yamaguchi
ACS Catal. **2018**, 8, 11564–11569.
5. “Heterogeneously Palladium-catalyzed Acceptorless Dehydrogenative Aromatization of Cyclic Amines”
Takashi Oyama, Takafumi Yatabe, Xiongjie Jin, Noritaka Mizuno, Kazuya Yamaguchi
Chem. Lett. **2019**, 48, 517–520.

Related Publications

1. “Gold nanoparticles on OMS-2 for heterogeneously catalyzed aerobic oxidative α,β -dehydrogenation of β -heteroatom-substituted ketones”

Daichi Yoshii, Xiongjie Jin, Takafumi Yatabe, Kazuya Yamaguchi, Noritaka Mizuno
Chem. Commun. **2016**, 52, 14314–14317.

2. “Selective Synthesis of Primary Anilines from NH_3 and Cyclohexanones by Utilizing Preferential Adsorption of Styrene on the Pd Nanoparticle Surface”

Yu Koizumi, Xiongjie Jin, Takafumi Yatabe, Ray Miyazaki, Jun-ya Hasegawa, Kyoko Nozaki, Noritaka Mizuno, Kazuya Yamaguchi
Angew. Chem. Int. Ed. **2019**, 58, 10893–10897.

Acknowledgement

First of all, I deeply thank Professor Kazuya Yamaguchi, my supervisor, for giving overall guidance on my research since I was an undergraduate student. I could not complete my doctoral dissertation without a lot of his invaluable comments and suggestions. He also kindly accepted my ideas on a variety of topics and my participation in many kinds of activities such as domestic/international conferences, coursework of MERIT (Materials Education program for the future leaders in Research, Industry, and Technology), the internship at National Institute of Advanced Industrial Science and Technology, *etc.*, leading to my fulfilling research life and broadening my vision.

I am also grateful to Professor Noritaka Mizuno for accepting me in this laboratory and providing valuable and impressive comments. Thanks to the wonderful research environment he constructed, I have been concentrating on tackling my research without inconvenience.

I wish to express my gratitude to the judging committee members of this doctoral dissertation, Professor Kazuyuki Ishii, Professor Tetsuya Shishido, Associate Professor Yusuke Sunada, Associate Professor Tomohisa Sawada, and Professor Kazuya Yamaguchi. Their valuable questions, comments, and suggestions improved my doctoral dissertation.

I would like to give special thanks to Assistant Professor Xiongjie Jin for giving me profound advices and helping numerous things with me from my undergraduate days. Without his helpful comments, I could not achieve some of my researches.

I am deeply indebted to the present staff members of Yamaguchi laboratory, Associate Professor Kosuke Suzuki and Assistant Professor Tomohiro Yabe, and the previous staff members, Dr. Mitsuhiro Hibino and Dr. Yoshiyuki Ogasawara, for their precious suggestions, discussions, and much kind help.

Also, I would like to thank Ms. Chizu Umezu for her kind support to my office work in daily lives.

Special thanks also go to the present and previous students in the laboratory. I spent much fulfilling time and talked about a lot of things with the members. In particular, regarding the contents of 4-1 section and 4-2 section, I appreciate very much the works of Mr. Oyama and Mr. Kataoka, respectively.

I show deep gratitude to the Advanced Characterization Nanotechnology Platform of the University of Tokyo, supported by “Nanotechnology Platform” of the Ministry of Education, Culture, Sports, Science and Technology (MEXT), Japan, for TEM, STEM, and XPS analyses, and the Photon Factory Program Advisory Committee for XANES measurements.

I also would like to thank Enago (www.enago.jp) for the English language review.

I owe MERIT and JSPS (Japan Society for the Promotion of Science) for the financial support during the master course and doctoral course, respectively.

In closing, I express my deepest gratitude to my family and my wife for continuously supporting what I want to do and encouraging me at any time.

Takafumi Yatabe

August, 2019